Author:
Mejia Estrada, Iskra

Title:
Hydrometeorological characterisation of urban flash floods

Hydrometeorological characterisation of urban flash floods

By

Pamela Iskra Mejía Estrada

School of Geographical Sciences

A dissertation submitted to the University of Bristol in accordance with the requirements for award of the degree of

Doctor of Philosophy

in the Faculty of Science

November 2019

Word count: 61395

Abstract

Under a climate change scenario, the frequency and intensity of hydrometeorological extremes is likely to increase. Amongst current natural hazards, floods account for the largest and costliest events and these have caused significant economical and societal losses which sometimes taken years to recover from. Flash floods in particular have a greater potential for damage given their associated quick onset and inefficient response from the population. From their many causes, flash flooding from intense, localised rainfall in urban areas represents a major challenge to forecasters and this is reflected in the insufficient adaptation and mitigation strategies in terms of awareness and preparedness.

A crucial step towards flash flood risk reduction is the improvement of current numerical modelling capabilities. Given that there are many approaches to simulate and link the physical processes that lead to an urban flash flood, there is a pressing need to define strengths and weaknesses of the current numerical modelling tools to select the most efficient models and approaches that facilitate a quantitative assessment on hazard and exposure.

The research presented here introduces a methodology for the hydrometeorological characterisation of urban flash floods at sub-daily and catchment scales (i.e. less than 100 km^2), which focuses on the parameterisation of cities to determine the influence of the urban canopy on atmospheric processes and in the response to intense rainfall. It aims to provide information on the capabilities and limitations of the numerical tools involved while identifying how to improve their efficiency and accuracy. It also accounts for the specific layout of a given city (thus potentially transferrable to any urban environment), proposing an advance towards the accurate numerical representation of these events.

This study presents, for the first time in the context of flash flooding, the use of a widely applied numerical weather prediction tool that has the capabilities to account for urban areas in the atmospheric processes during the origin of intense rainfall. It replaces the use of satellite-derived, remote-sensed and ground-based rainfall information (and the uncertainty associated) and instead provides information on the degree of contribution of model structure and parameters to capture the critical development and magnitude of intense rainfall. Outputs of this meteorological tool are used as climatological forcing for a hydrological model. A recent benchmark study consolidated its robustness as a highly flexible numerical tool for rainfall-runoff simulation at daily scale, so the inclusion of urban areas and the evaluation of hourly variations of river flows represents a novelty.

Two major flash flood events in the United Kingdom in the past 20 years were selected as case studies given the magnitude of damages and losses in major English cities. The proposed methodology evaluates the impact of the parameterisation of cities in the meteorological and hydrological models on the simulated rainfall and flows, respectively, and pinpoints the most suitable configuration for further applications via the quantification of the error propagation.

The results provide information on the effectiveness of the novel framework proposed and areas for its improvement, while opening the discussion on its potential to be applied to further case studies. This shows that the framework proposed contributes to the improvement of numerical tools to reproduce and map urban flash floods, therefore strengthening the basis of strategies for flash flood risk reduction.

Acknowledgements

I was supposed to come to Bristol only to do some science and -just like in Kraków- I ended up in a maelstrom of emotions and life-changing experiences along with the work that I'm presenting here.

Firstly, I'd like to thank my supervisor, Prof. Paul Bates, for your unbreakable commitment to keep developing my strengths as a hydrologist. A meeting with you always meant an opportunity to single out the relevant ideas and openly discuss their suitability, I always left your office hugely motivated and focused. You have set a decidedly high bar when it comes to being and outstanding lecturer, supervisor and researcher. To Prof. Jim Freer and Gemma Coxon, for the thorough review of my work and the room you gave me to test the hydrological model in two demanding case studies. To Dr. Miguel Rico Ramírez, for the brilliant comments and detailed questions that always pushed me to spot the good, the bad and the ugly of the results I was presenting.

To the National Council of Science and Technology in Mexico (CONACyT) for scholarship awarded for the completion of my doctoral studies under the CVU no. 490283.

My loving gratitude to my mum from your no. 1 fan, with great love and admiration, for being cornerstone of my determination to achieve my dreams and to fly high. To my brother, the most intelligent and resourceful man and an outstanding biologist during a pandemic that is currently shaking the world.

My sincerest recognition of the role that my friends have played in this adventure. Mónica, my sister and wonder woman, I'd be honoured to follow your accomplishments as we get old. Chucho, I'm truly grateful to learn from your fearlessness and determination to make your voice heard. Oscar, your life lessons are the foundation of my self-confidence and sense of adventure.

A heartfelt "thank you" to fellow Mexicans and friends in Bristol for the immense support, life-changing talks and endless pints. To Ale, Marco, Daniel and Jessica, you are my family away from my family, thank you for your unconditional love. Jess, I wish you could see through my eyes for you to see the treasure you are and how proud I am to be your friend. To Fee, for those wine evenings and for your exceptional and continuous generosity.

Back in Mexico, there's a breathtakingly extensive group of people, blood-related and not, who have always meant joy, humour and strength. Your love has built a bridge over the ocean and has made me feel close to you, despite the accumulated hugs I haven't been able to deliver

(yet). My incredibly unswerving and affectionate grandma, Lucina. The Estrada Moreno, Calzada Estrada, Navarro Estrada, Estrada Albino, Sánchez Estrada and Pozo Estrada families. My cousins Alejandro, Alfonso, Alicia, Jorge and Lorena, your passion stands out with every milestone you reach. Everyone from the Estrada Flores family. All the magnificent people that always had me in their thoughts, despite me not being there to enjoy your company.

Pursuing the PhD dream in a country different that the one I'm proud to belong to has allowed me to know other cultures and mindsets as well as ways of thinking, cooking and drinking! For that I'm greatly indebted to the researchers in Browns with whom I've shared laughs and successes over a cup of tea. Starting for my favourite Norwegian scientist, Synne Brustad. You always top the list of hard-working students. Erik Mackie, for making my first Browns Weekend Away the milestone of my confidence to make friends. Alan, Ale, Amy, Bea, Gaz, Guillaume, Markus, Mike, Philip and Rory, you've taken care of me in one way or another at some point, I will always be grateful for that. To Louisa, Pete, Simbi and Tom, your relevant comments greatly enhanced the quality of the final draft of this thesis. Nik and Orestis, despite the stupendous amount of beer and rakya we shared, I will always remember your jokes, advice, time shared and games played.

These acknowledgements would be incomplete without the mention of the Trevers family. My profound gratitude to Krys and Martin for your remarkable and affectionate support, for embracing the cultural differences and being immeasurable part of the reason why I call the United Kingdom my home. And of course, to Matt. Your passion to learn and to pursue constant improvement are qualities I deeply admire in you as a scientist and climber. You are the brilliant man who has opened my eyes and my best friend who has opened my heart. I'm incredibly indebted to you for your patience and that unbounded love you have shown me in a hundred ways is buoyantly reciprocated. You've taught me so much and I can't wait to learn more from you.

Finally, I'll always be in debt to the hydrologists that I found and found me over these last years of academic work. For your help with coding, methods and knowledge. You've left a long-lasting impression on what it takes to be a successful and respectable researcher.

Author’s declaration

I declare that the work in this dissertation was carried out in accordance with the requirements of the University's Regulations and Code of Practice for Research Degree Programmes and that it has not been submitted for any other academic award. Except where indicated by specific reference in the text, the work is the candidate's own work. Work done in collaboration with, or with the assistance of, others, is indicated as such. Any views expressed in the dissertation are those of the author.

SIGNED:  DATE: 1 November 2019

Contents

Abstract ii
Acknowledgements iv
Author's declaration vi
Contents vii
List of Figures xv
List of Tables xxiii
List of Abbreviations xxv
Chapter 1. Introduction 1
1.1 Motivation of the study 1
1.1.1 Economical losses due flooding and flash flooding 1
1.1.2 Impact of urbanisation on flooding 2
1.1.3 Characterisation of flash floods: difficulties and relevance 4
1.2 Definition of flash flood 5
1.2.1 Definition given by previous research. 5
1.2.2 Definition used in the present research and criteria to choose case studies 7
1.3 Aim and contribution of the study 8
1.4 Thesis outline 10
Chapter 2. The hydrometeorological cascade 12
2.1 Introduction 12
2.1.1 Description of the cascade 13
2.1.2 Application of the cascade to urban areas: relevant physical processes 16
2.1.1.1 Microclimate of urban areas 16
2.1.1.2 Urban riverine response to flash floods 17
2.2 Stage 1: Estimation of precipitation 19
2.2.1 Point rainfall measurement 19
2.2.2 Remote-sensed rainfall data 20

2.2.2.1 Radar 20
2.2.2.2 Satellite 22
2.2.3 Merged products 23
2.2.3.1 Satellite + gauge 23
2.2.3.2 Radar + gauge 23
2.2.4 Downscaling of Global Climate Models 24
2.2.4.1 Definition of downscaling 24
2.2.4.2 Statistical downscaling 24
2.2.4.3 Dynamical downscaling 25
Convection-permitting modelling 26
Ensemble Prediction System 28
2.2.5 Data assimilation 29
2.2.6 Reanalysis 30
2.3 Stage 2: Estimating flash flood flows 30
2.3.1 Introduction 30
2.3.2 Parameterisation of urban areas in hydrological models 31
2.3.2.1 The Hydrological Response Unit 32
2.3.2.2 Diversion of flow within a cell to storage/river 33
2.3.3 Numerical models used to characterise the hydrology of flash floods 34
2.3.3.1 Lumped models 35
2.3.3.2 Semi-distributed models 36
2.3.3.3 Distributed models 37
2.4 Applications of the cascade in flood characterisation and forecasting projects 38
2.4.1 Projects on flood characterisation 38
2.4.1.1 HYdrological cycle in the Mediterranean EXperiment 38
2.4.1.2 IMproving Predictions and management of hydrological Extreme 39
2.4.1.3 Flooding From Intense Rainfall 39
2.4.2 Projects on flood forecasting 40
2.4.2.1 Global Flood Awareness System and European Flood Awareness System 40

2.4.2.3 Met Office Global and Regional Ensemble Prediction System 41
2.5 Conclusion 42
Chapter 3. Hydrometeorological modelling framework 44
3.1 Meteorological modelling 45
3.1.1 Model selection 45
3.1.2 Description of the meteorological model 47
3.1.3 WRF preprocessing 48
3.1.4 WRF solver 49
3.1.3.1 Vertical interpolation of atmospheric data 49
3.1.3.2 Physics parameterisations 50
Microphysics 50
Cumulus 51
Land Surface 52
Urban Surface 52
Planetary Boundary Layer 52
Surface Layer 53
Radiation 53
3.2 Hydrological modelling 54
3.2.1 Model selection 54
3.2.2 Description of the hydrological tool 55
3.2.3 Digital Terrain Analysis 55
3.2.3.1 Catchment discretisation 57
Inputs 57
Process 57
Outputs 57
3.2.3.1 Obtaining Hydrological Response Units 57
Inputs 57
Process 58
Outputs 58

3.2.4 Rainfall-runoff modelling 59
Inputs 59
Model initialisation 59
Flow routing 61
Channel routing scheme 61
Outputs 64
3.3 Experimental set-up 65
3.3.1 Meteorological modelling 66
3.3.1.1 Model set-up and boundary conditions 66
Atmospheric input data 66
Number and ratio of nested domains 66
Vertical levels 66
Length of the simulation and spin-up time 67
3.3.1.2 Model parameterisations 67
Microphysics 68
Cumulus 69
Land surface 69
Urban surface 71
Planetary Boundary Layer 72
Surface Layer 73
Radiation 73
Physics parameterisations interaction and implementation 73
3.3.2 Hydrological modelling 75
3.3.2.1 Information used for Digital Terrain Analysis 75
3.3.2.2 Databases used for rainfall-runoff modelling 76
3.4 Evaluation of model outputs 77
3.4.1 Meteorological modelling verification metrics 77
3.4.1.1 Evaluation of model outputs at synoptic scale using satellite-derived data 78
3.4.1.2 Evaluation of model outputs at meso-scale using weather radar data 78

3.4.1.2 Evaluation of model outputs at local scale using rain gauge data 79
3.4.2 Hydrological model calibration and validation 80
3.5 Conclusions 81
Chapter 4. Meteorological modelling case 1. Newcastle 2012 flash flood event 83
4.1 Introduction 83
4.1.1 Justification of choice of the event 83
4.2 Meteorological setting 85
4.2.1 Historical context of flash floods in the Tyneside region 85
4.2.2 Antecedent conditions 85
4.2.3 The event 87
4.3 Meteorological model set-up 90
4.3.1 Domains and boundary conditions 90
4.3.2 Building height distribution 91
4.4 Results and discussion 92
4.4.1 Synoptic scale analysis 92
4.4.2 Mesoscale analysis 97
4.4.3 Local scale analysis 103
4.4.5 Overall model performance 109
4.5 Final remarks 111
Chapter 5. Meteorological modelling case 2. Birmingham 2007 flash flood event 112
5.1 Introduction 112
5.1.1 Justification of choice of event 112
5.2 Meteorological setting 114
5.2.1 Historical context of flash floods in the Midlands 114
5.2.2 Antecedent conditions 114
5.2.2 The event 115
5.3 Meteorological model set-up 119
5.3.1 Domains and boundary conditions 119
5.3.2 Building height distribution 120

5.4 Results and discussion 121
5.4.1 Synoptic scale analysis 121
5.4.2 Mesoscale analysis 125
5.4.3 Local scale analysis 131
5.4.4 Overall model performance 139
5.5 Final remarks 141
5.5.1 On the Birmingham 2007 case study 141
5.5.2 On the comparison of simulated rainfall between the Newcastle 2012 and the Birmingham 2007 events 142
Chapter 6. Hydrological modelling 144
6.1. Case 1. Newcastle 2012 flash flood event 145
6.1.1 Hydrology of the event 145
6.1.1.1 Antecedent conditions 145
6.1.1.2 River level and discharge during the event 146
6.1.2 Site description 148
6.1.2.1 Catchment characteristics 148
6.1.2.2 River gauge 150
6.1.2.3 The Ouse Burn Interceptor and Trunk Sewer system 150
6.1.3 Digital Terrain Analysis 151
6.1.4. Model calibration 153
6.1.4.1 Assessment of the simulated flow 154
During peaks in runoff 154
During low runoff periods 155
Influence of the Ouse Burn Interceptor and Trunk Sewer System 158
6.1.4.2 Performance statistics 159
6.1.5 Model validation 162
6.1.5.1 Impact of the urban canopy layer parameterisations in runoff simulations. . 167
6.2 Case 2. Birmingham 2007 flash flood event 168
6.2.1 Hydrology 168

6.2.1.1 Antecedent conditions 168
6.2.1.2 River level and discharge during the event 169
6.2.2 Site description 171
6.2.2.1 Catchment characteristics 171
6.2.2.2 River gauge 174
6.2.3 Digital Terrain Analysis 175
6.2.4 Model calibration 176
6.2.4.1 Assessment of the simulated flow 177
During peaks in runoff 177
During low runoff periods 178
External influences on the river flow 178
6.2.4.2 Performance statistics 182
6.2.5. Model validation 184
6.2.5.1 Impact of the urban canopy layer parameterisations in runoff simulations. . 190
6.3 Final remarks 191
Chapter 7. Conclusions 193
7.1 Summary 193
7.2 Novelty of the research 195
7.3 On the error propagation through the hydrometeorological modelling framework 197
7.3.1 Considering the Newcastle 2012 flash flood event 197
7.3.2 Considering the Birmingham 2007 flash flood event 198
7.3.3 Final remarks 200
7.4 Critique of the modelling framework 200
7.4.1 On the choice of microphysics schemes 200
7.4.2 On the calibration and validation of the hydrological model 201
7.4.2.1 Use of rainfall datasets with different spatial resolution 201
7.4.2.2 Split time for calibration and validation 201
7.4.3 On the hydrological uncertainty evaluation 202
7.4.4 On the hydrological model structure 203

7.4.5 On the number of case studies 204
7.5 Future lines of research 204
Appendix A. Tests that helped shaping the meteorological modelling set-up implemented 207
A.1 Testing an additional microphysics scheme 207
A.2 Testing model spin-up time 210
A.3 Testing resolution of the innermost domain 211
References 213

List of Figures

Figure 2.1. Conceptualisation of the modelling cascade given propagation, bounds and reduction of uncertainty at each step as proposed by (Smith et al., 2018). Figure adapted under the Creative Commons licence 15

Figure 2.2. Radar snapshots before and after the vertical correction scheme for the Crug-y-Gorllwyn radar in southwest Wales, as presented by Harrison et al. (2000) 22

Figure 2.3. Conceptualisation of the convective processes within a cloud as solved by Convection-Permitting Models (adapted from Brisson et al., 2017) 28

Figure 2.4. Conceptualisation of the elements and configuration of a catchment discretised in Hydrological Response Units 33

Figure 2.5. Conceptualisation of the generation of surface runoff in an urban pixel according to Cuo et al. (2008) 34

Figure 3.1. Workflow of the hydrometeorological modelling framework. For a detailed description of each stage, refer to the corresponding sections of this Chapter 45

Figure 3.2. Horizontal grid structure of the Arakawa-C grid in the WRF model. Adapted from (Kang et al., 2014) 47

Figure 3.3. Location of the overlap of theta points of parent and nested domain with nesting ratio 1:3 49

Figure 3.4. Representation of the physics schemes considered for meteorological modelling 50

Figure 3.5. Flowchart of the Digital Terrain Analysis to determine the Hydrological Response Units using simulated rainfall (green) and observed rainfall (purple) 56

Figure 3.6. Conceptualisation of the structure of DECIPHeR. Model parameters are highlighted in yellow 62

Figure 3.7. Conceptualisation of the interaction of the relevant physics schemes considered for the meteorological modelling 74

Figure 4.1. Top row: national scale map highlighting the north-east area of interest (left), location of Newcastle city centre in reference to the coast and Hartlepool (centre), places where the event photographs were taken (right). Bottom row: a) Newgate Street on 28th June 2012 (Glenis et al., 2018), b) The Quayside, north bank, viewing the Gateshead Millennium Bridge (Summers, 2012) 84

Figure 4.2. Location of the rain gauges for which the Long-Term-Average values for the Newcastle 2012 event is shown 86

Figure 4.3. Surface pressure chart showing the location of the fronts and the troughs (thin, black lines), valid 00:00 UTC on 28th June 2012 (as shown in Allan, 2012) 87

Figure 4.4. Radar imagery of the June 2012 event showing the storm track over the Tyne catchment (top left), 15-minute accumulated values for 15:00 UTC (top right), 16:15 UTC (middle), 17:15 UTC (bottom). Newcastle city centre is marked with a red dot 89

Figure 4.5. Location and extent of the nested domains for the meteorological simulation of the Newcastle 2012 case study 90

Figure 4.6. Visual distribution of building heights in the innermost domain of the Newcastle case study. Green outline corresponds to domain 4 92

Figure 4.7. Histogram of the building height distribution for domain 4 of the Newcastle case study 92

Figure 4.8. Accumulated rainfall maps from 15:00 UTC to 17:00 UTC on the 28th June 2012 using GPM IMERG data (top panel) and for simulations 1-9 (see Table 4.4 for the specific combination of the physics schemes) 94

Figure 4.9. Comparison of accumulated rainfall maps from 15:00 UTC to 17:00 UTC on the 28th June 2012 using information from domains 1-4 (top to bottom, left to right) for simulation 2, across the innermost domain 97

Figure 4.10a. Hourly time evolution of the rainfall on 28th June 2012 (15:00, 16:00 and 17:00 UTC). Observed radar values (top row) and rainfall patterns for WRF simulations 1, 2 and 3 100

Figure 4.10b. Hourly time evolution of the rainfall on 28th June 2012 (15:00, 16:00 and 17:00 UTC). Observed radar values (top row) and rainfall patterns for WRF simulations 4, 5 and 6 101

Figure 4.10c. Hourly time evolution of the rainfall on 28th June 2012 (15:00, 16:00 and 17:00 UTC). Observed radar values (top row) and rainfall patterns for WRF simulations 7, 8 and 9 102

Figure 4.11. Spatial extent of the Tyne catchment (top left), location of the rain gauges used in the local scale analysis of the June 2012 event (top right) and land cover processed by the WRF model (bottom) 103

Figure 4.12. Simulated rainfall for the nine WRF scenarios (see Table 4.4), grouped by urban canopy model scheme, for two gauges in the Tyne catchment. See Figure 4.11 for location of gauges 106

Figure 4.13. Simulated rainfall for the nine WRF scenarios (see Table 4.4), grouped by urban canopy model scheme, for two gauges in the Tyne catchment. See Figure 4.11 for location of gauges 107

Figure 4.14. Simulated rainfall for the nine WRF scenarios (see Table 4.4), grouped by urban canopy model scheme, for two gauges in the Tyne catchment. See Figure 4.11 for location of gauges 108

Figure 4.15. WRF simulations ranked by performance for the June 2012 case study, showing bar length as the contribution of each metric to the overall performance 110

Figure 5.1. Photographs of disruption across the Midlands during 20 July 2007. Top row, left: reference map, a) Flooding in Old Birmingham Road, where sandbags could not prevent internal flooding of the houses along said road (Hughes, 2007), b) Damages on 20th July ("Church Street Tewkesbury 2007 Flood", (Tewkesbury-Museum, 2007), c) Flooding outside Thatcham Railway Station (Flaschen, 2007) 113

Figure 5.2. Positions of the Polar Front Jet Stream for July 2006 and 2007 (taken from Pitt, 2008) 115

Figure 5.3. Synoptic chart for 06:00 UTC 20 July 2007 (taken from Brown, 2016) 116

Figure 5.4. Precipitation levels for England and Wales during 19–20 July 2007 (Prior et al., 2008) 117

Figure 5.5. Location of the gauges with the highest recorded values on 19-20 July (see Table 5.1), located in the south Midlands region 118

Figure 5.6. Radar imagery of the Summer 2007 event showing the storm track over the Trent catchment (top left), 15-minute accumulated values for 13:00 UTC (top right), 14:00 UTC (middle), 16:00 UTC (bottom). Birmingham city centre is marked with a red dot 119

Figure 5.7. Location and extent of the nested domains for the meteorological simulation of the Birmingham 2007 case study 120

Figure 5.8. Visual distribution of building heights in the innermost domain of the Birmingham case study. Green outline corresponds to domain 4 121

Figure 5.9. Histogram of the building height distribution [m] for domain 4 of the Birmingham case study 121

Figure 5.10. Accumulated rainfall maps from 12:00 UTC to 18:00 UTC on the 20th July 2007 using GPM IMERG data (top panel) and for simulations 1-9 (see Table 5.3 for the specific combination of the physics schemes) 124

Figure 5.11a. Hourly time evolution of the rainfall on 20th July 2007 (13:00, 14:00 and 16:00 UTC). Observed radar values (top row) and rainfall patterns for WRF simulations 1, 2 and 3 128

Figure 5.11b. Hourly time evolution of the rainfall on 20th July 2007 (13:00, 14:00 and 16:00 UTC). Observed radar values (top row) and rainfall patterns for WRF simulations 4, 5 and 6 129

Figure 5.11c. Hourly time evolution of the rainfall on 20th July 2007 (13:00, 14:00 and 16:00 UTC). Observed radar values (top row) and rainfall patterns for WRF simulations 7, 8 y 9 130

Figure 5.12. Spatial extent of the Trent catchment (left), location of the rain gauges used in the local scale analysis of the July 2007 event (middle) and land cover processed by the WRF model (right) 131

Figure 5.13. Simulated rainfall for the nine WRF scenarios, grouped by urban canopy model scheme, for two gauges in the Trent catchment 134

Figure 5.14. Simulated rainfall for the nine WRF scenarios, grouped by urban canopy model scheme, for two gauges in the Trent catchment. See Figure 5.12 for location of gauges 135

Figure 5.15. Simulated rainfall for the nine WRF scenarios, grouped by urban canopy model scheme, for two gauges in the Trent catchment. See Figure 5.12 for location of gauges 136

Figure 5.16. Simulated rainfall for the nine WRF scenarios, grouped by urban canopy model scheme, for two gauges in the Trent catchment. See Figure 5.12 for location of gauges 137

Figure 5.17. Simulated rainfall for the nine WRF scenarios, grouped by urban canopy model scheme, for a gauge in the Trent catchment. See Figure 5.12 for location of gauges 138

Figure 5.18. WRF simulations ranked by performance for the June 2012 case study, showing bar length as the contribution of each metric to the overall performance 141

Figure 6.1. Location of the river gauges for which a flow comparison is made to highlight the severity of the June 2012 event, within the Tyne catchment 146

Figure 6.2. River level and discharge for gauging stations 23007, 23016, 23017 and 23018 during the 28th June 2012 147

Figure 6.3. Location and physical characteristics of the Ouse Burn catchment 149

Figure 6.4. Photographs of the station 23016 (Source: Author) 150

Figure 6.5. Spatial configuration of the observed and simulated gridded climatological inputs for the Ouse Burn catchment discretisation 152

Figure 6.6. Hourly calibrated flow for the two-month period a) 26 August 2008 to 24 October 2008, b) 20 October 2009 to 19 December 2009, c) 17 February 2010 to 18 April 2010, d) 7 April 2012 to 31 May 2012. Spread of the 5th and 95th percentiles of the behavioural ensemble defined using the GLUE methodology is shown in grey, 50th percentile is shown as a dotted line, observed flow is shown as a red line. Right column= subset of left column 156

Figure 6.7. Hourly calibrated flow for the two-month period a) 25 October 2008 to 23 December 2008, b) 24 December 2008 to 21 February 2009, c) 14 December 2010 to 11 February 2011 and d) 9 December 2011 to 6 February 2012. Spread of the 5th and 95th percentiles of the behavioural ensemble defined using the GLUE methodology is shown in grey, 50th percentile is shown as a dotted line, observed flow is shown as a red line. Right column= subset of left column 157

Figure 6.8. Hourly calibrated flow for the two-month period a) 19 December 2008 to 16 February 2010, b) 24 December 2008 to 21 February 2009, c) 14 December 2010 to 11 February 2011 and d) 9 December 2011 to 6 February 2012. Spread of the entire ensemble is shown as dark grey, 5th and 95th percentiles of the behavioural ensemble defined using the GLUE methodology is shown in light grey, 50th percentile is shown as a dotted line, observed flow is shown as a red line. Right column= subset of left column 159

Figure 6.9. Scatter plots of the parameter space after the calibration period of the June 2012 event 161

Figure 6.10. Scatter plot of the obtained values of the channel velocity during the calibration process of the June 2012 case study 162

Figure 6.11a. Hourly simulated flow for the validation period of hydrological simulation of the June 2012 event using observed rainfall (top panel) and simulations 1-6 (left to right, top to bottom) 163

Figure 6.11b. Hourly simulated flow for the validation period of hydrological simulation of the June 2012 event using observed rainfall (top panel) and simulations 1-9 (left to right, top to bottom) 164

Figure 6.12. Simulated hydrological scenarios ranked by performance for the June 2012 case study, showing bar length as the contribution of each metric to the overall performance 166

Figure 6.13. Some of the counties and cities affected during the summer 2007 floods 170

Figure 6.14. Long-term daily maxima (lower bound of blue envelope) and minima (upper bound of green envelope) during 1961-2006, estimated daily outflows (grey line) and daily hydrograph with recorded values for 2007 for England and Wales 171

Figure 6.15. Spatial extent of the hydrometric area 28 “Trent” and river reaches within the catchment 172

Figure 6.16. Location and physical characteristics of the Rea catchment: elevation, binary map of land cover (urban/non-urban) and river network 173

Figure 6.17. Photographs of the station 28039 “Rea al Calthorpe Park” (Source: National River Flow Archive) 175

Figure 6.18. Comparison of the spatial configuration of the observed and simulated gridded rainfall inputs, and map of the Hydrological Response Units obtained for the Rea catchment 176

Figure 6.19. Hourly calibrated flow for the two-month period a) 27 July 2004 to 24 September 2004, b) 25 September 2004 to 23 November 2004, c) 20 September 2005 to 18 November 2005, d) 14 November 2006 to 12 January 2007. Spread of the 5th and 95th percentiles of the behavioural ensemble defined using the GLUE methodology is shown in grey, 50th percentile is shown as a dotted line, observed flow is shown as a red line. Right column= subset of left column 180

Figure 6.20. Hourly calibrated flow for the two-month period a) 24 November 2009 to 22 January 2005, b) 24 March 2005 to 22 May 2005, c) 18 January 2006 to 18 March 2006, d) 18 May 2006 to 16 July 2006. Spread of the 5th and 95th percentiles of the behavioural ensemble defined using the GLUE methodology is shown in grey, 50th percentile is shown as a dotted line, observed flow is shown as a red line. Right column= subset of left column 181

Figure 6.21. Hourly calibrated flow for the two-month period a) 19 November 2011 to 27 January 2006, b) 13 January 2007 to 13 March 2007. Right column= subset of left column 182

Figure 6.22. Scatter plots of the parameter space after the calibration period of the July 2008 event 184

Figure 6.23a. Hourly simulated flow for the validation period of hydrological simulation of the July 2007 event using observed rainfall (top panel) and simulations 1-3 (left to right, top to bottom) 185

Figure 6.23b. Hourly simulated flow for the validation period of hydrological simulation of the July 2007 event using observed rainfall (top panel) and simulations 4-9 (left to right, top to bottom) 186

Figure 6.24. Simulated hydrological scenarios ranked by performance for the July 2007 case study, showing bar length as the contribution of each metric to the overall performance 189

Figure A.1. Accumulated rainfall map from 15:00 UTC to 17:00 UTC on the 28th June 2012 from GPM data (left) and for the WRF simulation using the Eta microphysics (right) 208

Figure A.2. Simulated rainfall using the Eta microphysics scheme for six gauges in the Tyne catchment. See Figure 4.11 for location of gauges 209

Figure A.3. Accumulated rainfall map from 15:00 UTC to 17:00 UTC on the 28th June 2012 for the WRF simulations a) with 6 hours of spin-up time, b) with 24-hours of spin-up time 211

List of Tables

Table 1.1. Thesis content by chapter 11

Table 2.1. Impacts of urbanisation in flash flood-related environmental variables 19

Table 2.2. Overview of the main characteristics of the numerical models for hydrological simulations (after Sitterson et al., 2018) 35

Table 3.1. Model parameters and variables in DECIPHeR 63

Table 3.2. USGS 24-category Land Use Categories 70

Table 3.3. WRF physics parameterisation for the present study 75

Table 4.1. Total rainfall recorded in the Tyneside region in several stations, shown as totals and as percentage of the monthly Long-Term Average 86

Table 4.2. Rainfall accumulations and return periods of recorded values in five stations in the Tyneside region during the 2012 flash flood event 88

Table 4.3. Grid cell size and area of the WRF model set-up for the Newcastle 2012 case study 90

Table 4.4. Urban canopy models and microphysics parameterisations used in the nine WRF scenarios to simulate rainfall for the Newcastle 2012 event 93

Table 4.5. Skill scores and accumulated rainfall for the nine WRF simulations of the June 2012 event 110

Table 5.1. Accumulated rainfall values in [mm] for the wettest rain gauges in the Midlands region on 19-20 July 117

Table 5.2. Grid cell size and area of the WRF model set-up for the Birmingham 2007 case study 120

Table 5.3. Urban canopy models and microphysics parameterisations used in the nine WRF scenarios to simulate rainfall for the Birmingham 2007 event 122

Table 5.4. Skill scores and accumulated rainfall for the nine WRF simulations of the July 2007 event 140

Table 6.1. Mean daily and Long-Term Average flow for three river gauges in the Tyne catchment on two dates before the June 2012 flood 146

Table 6.2. Rank order of peak levels in [m] for some of the gauges in the Tyne catchment. Values from the June 2012 event are highlighted in blue 147

Table 6.3. Physical characteristics and hydrological descriptors of the Ouse Burn catchment 149

Table 6.4. Hydrological model parameter ranges for urban areas for the June 2012 case study 153

Table 6.5. Hydrological model parameter ranges for rural areas for the June 2012 case study 154

Table 6.6. Performance metrics for the calibration period 160

Table 6.7. Performance metrics for the calibration period of the hydrological modelling of the June 2012 event 165

Table 6.8. Rank of the ten highest June-July recorded runoff values for England and Wales 169

Table 6.9. Physical characteristics and hydrological descriptors of the Rea catchment 174

Table 6.10. Hydrological model parameter ranges for the urban areas for the July 2008 case study 177

Table 6.11. Hydrological model parameter ranges for the rural areas for the July 2008 case study 177

Table 6.12. Performance metrics for the calibration period 183

Table 6.13. Performance metrics for the calibration period of the hydrological modelling of the July 2008 event 187

Table A.1. Skill scores for the WRF simulation using the Eta microphysics 210

Table A.2. Skill scores for the WRF simulations using 6 and 24 hours of spin-up time 211

List of Abbreviations

AET	Actual evapotranspiration
BEM	Building Energy Model urban canopy scheme
BEP	Building Effect Parameterisation urban canopy scheme
BFIHOST	Base Flow Index from the 29-class Hydrology Of Soil Types dataset
CEH	Centre for Ecology and Hydrology
CEH-GEAR	Centre for Ecology and Hydrology Gridded estimates of hourly areal rainfall for Great Britain
CHV	Channel routing velocity
CPM	Convection-Permitting Model
CSI	Critical Success Index
DECIPHeR	Dynamic Fluxes and Connectivity for Predictions in Hydrology
DEM	Digital Elevation Model
DTA	Digital Terrain Analysis
DUD	Dudhia shortcoming radiation parameterisation
EA	Environment Agency
ECMWF	European Centre for Medium-Range Weather Forecasts
EFAS	European Flood Awareness System
FFIR	Flooding From Intense Rainfall
FNL	National Centers for Environmental Prediction Final Analysis
GCM	Global Circulation Model
GFS	Global Forecast System
GLUE	Generalised Likelihood Uncertainty Estimation
GLoFAS	Global Flood Awareness System
GPM	Global Precipitation Measurement
HRU	Hydrological Response Unit
HyMeX	HYdrological cycle in the Mediterranean EXperiment
IMERG	Integrated Multi-satEllite Retrieval for GPM algorithm
IMPREX	IMproving Predictions and management of hydrological Extreme
IPCC	Intergovernmental Panel on Climate Change
KF	Kain-Fritsch cumulus scheme
$Ln(T_0)$	Lateral saturated hydraulic transmissivity
LSM	Land-surface model
LTA	Long-Term Average
mAOD	Meters Above Ordnance Datum
MBE	Mean Bias Error
MO	Monin-Obukhov surface layer parameterisation

MOGREPS	Met Office Global and Regional Ensemble Prediction System
MORR	Morrison microphysics scheme
MYJ	Mellor-Yamada-Janjic Planetary Boundary parameterisation
NCEP	National Centers for Environmental Prediction
NoahLSM	Noah Land Surface Model
NRFA	National River Flow Archive
NSE	Nash-Sutcliffe Efficiency
NWP	Numerical Weather Prediction
P	Precipitation
PBL	Planetary Boundary Layer
PET	Potential evapotranspiration
PROPWET	Catchment Wetness Index
Q95	95th percentile of the Nash-Sutcliffe Efficiency index
QC	Quality Control
Q_{EX}	Precipitation excess flow from Root Zone
Q_{IN}	Flow from upslope Hydrological Response Unit
Q_{OF}	Overland flow
Q_{SZ}	Saturated excess flow from Saturated Zone
RCM	Regional Circulation Model
RMSE	Root Mean Square Error
RRTM	Rapid Radiative Transfer Model longwave radiation scheme
RZ_s	Root zone storage
SEPA	Scottish Environment Protection Agency
SFFS	Scottish Flood Forecasting Service
SLUCM	Single Layer Urban Canopy Model
S_{max}	Maximum effective deficit of saturated zone
SR_{ini}	Root zone storage initially occupied
SR_{max}	Maximum root zone storage
STEPS	Short-Term Ensemble Prediction System
SZM	Form of exponential decline in conductivity
SZ_s	Saturated zone storage
TBR	Tipping-Bucket Rainfall
T_d	Unsaturated zone drainage delay
THOM	Thompson microphysics scheme
UCM	Urban Canopy Model
UHI	Urban Heat Island
USGS	United States Geological Survey
UTC	Coordinated Universal Time
UZ_s	Unsaturated zone storage
WPS	Weather Research and Forecasting Model Preprocessing System

WRF	Weather Research and Forecasting
WSM6	Weather Research and Forecasting Model Single-Moment 6-class microphysics scheme

Chapter 1

Introduction

1.1 Motivation of the study

1.1.1 Economical losses due flooding and flash flooding

Worldwide, the most dangerous non-geophysical, climate-related hydrometeorological hazard are floods (Gaume et al., 2008; Shrestha et al., 2019a; UNESCO, 2017). Their frequency and intensity are being modified by climate change, and every year considerable economical and societal losses have been reported (Kelsch et al., 2001; Ma et al., 2018). According to the Centre for Research on the Epidemiology of Disasters (CRED), from 1994 to 2013 these events caused damage to 2.4 billion people, which is 55% of the total population affected (CRED, 2015). In Europe alone, floods in the period 1991-1995 accounted for €99 billion. Summer floods in China in 1998 caused nearly 30 billion USD in damages; a year later, Bangladesh reported its highest number of fatalities during April (approximately 140 000). The record of annual losses related to flooding in Europe was reported in 2002, when the historical cities of Prague and Dresden were severely inundated, and damages exceeded €20 billion. During 2013, floods parts of Europe, Asia, Canada and Australia accounted for 47% of the losses worldwide, and 45% of the insurance claims (Svetlana et al., 2015). Every year between 2007 and 2016, nearly 85 million people have been affected by these events.

In the United Kingdom, flooding represents the greatest natural risk, a condition that is often worsened for the development of new habitable properties in flood plains (Surminski et al., 2014). One in six properties (nearly 5.2 million properties) is vulnerable to flood risk, from which 2.4 million are at risk of fluvial or coastal flooding and 2.8 million are at risk of flash flooding from surface water flows (Ramsbottom et al., 2012). Regarding wastewater infrastructure in cities, more than 55% of the sewage networks are located in flood prone areas. The areas at risk of flooding constitute nearly 13% of the United Kingdom's gross domestic product generating £1.1 billion in losses due to inland and coastal flooding. As example, the cost of the 2013–14 United Kingdom winter floods is estimated at £600 million (Pidcock, 2014). On the other hand, the damages during storm Desmond (fourth storm of the 2015-2016 season) are estimated at £870 million, from which £600 million were losses in Cumbria alone but that could have been as high as £2.2 billion in an undefended scenario (FloodRe, 2019). Finally, according to the Synthesis Report (SYR) of the IPCC Fifth Assessment Report,

population growth, an increase in the value of buildings and -more pressingly- climate change can cause the total annual cost of flooding in the United Kingdom to rise up to 15 times by 2080s “under high emission scenarios” (IPCC, 2014).

From all the types of floods accounted for, flash floods in particular have particularly high economical and societal impacts and losses associated (Kelsch et al., 2001), making them the world’s costliest and deadliest natural hazard (World Meteorological Organization, 2019). In the last decade of the 20th Century, over 1.4 billion people were affected (Karbasi et al., 2018). In Europe, flash floods account for 56% of the records of inundation from 1870 to 2016 (Paprotny et al., 2018) and they are the most destructive hazard in the western Mediterranean region. Some events have had outstanding losses associated with them, such as the Gard 2002 flash flood (when 250 mm of rainfall was recorded in 5-6 hours) with damages estimated at €1.2 billion, and the Aude 1999 flash flood (during which 70 mm, 400 mm and 600 mm of rainfall were recorded during 1 hour, 7 hours and 24 hours, respectively) with losses that reached €3.3 billion (Gaume et al., 2009).

1.1.2 Impact of urbanisation on flooding

Climate change, rapid and unplanned urbanisation as well as the disruption to natural recharge processes in urban areas exacerbate the responsiveness of a catchment, thus modifying the frequency and magnitude and impacts of flash floods (Şen, 2018). According to the United Nations, nearly 55% of the global population lives in urban areas, and projections estimate a change to 68% by 2050; this rapid change in land cover also has a huge impact in flood trends, as the percentage of urban coverage increases the likelihood of surface runoff, a major component of flash floods, with studies positively correlating urbanisation and river flows (Pitt, 2008). Urban coverage refers to impervious surfaces, compacted land areas and the alteration of natural water paths that modify the hydraulic properties of the soil, reducing its infiltration and storage capabilities, thus enhancing the occurrence of high-peak flows, surface runoff and flooding from a given rainfall event (Sharif et al., 2006), so a flash flood is more likely to occur in a city than in an area with natural coverage of similar extent (Doswell, 2015).

Atmospheric dynamics in cities greatly vary from those in non-urban areas regarding rainfall, temperature and air quality so their pattern and trends must be considered in climate projections. (Barlage et al., 2016; Zhang et al., 2018). In cities, wind speed and direction are modified by buildings, which act as vertical obstacles, enhancing the location of “isolated connective initiation events”, which result in an increase in the number of storm events (Haberlie et al., 2015). Liu et al. (2019) carried out a meta-analysis on the effect of urbanization

on rainfall and found that, given a storm direction, precipitation over cities is enhanced 2% and 4% to the left and right of the storm path, respectively; 16% over the city and 18% downwind of the city. Precipitation maxima is also affected in urban clusters, specially over and downwind of a city These changes in regional climatology are thought to result from diurnal activities or urbanised regions on the atmosphere (Ganeshan et al., 2013; Shepherd et al., 2002). Another major change in local climatology is the presence of Urban Heat Islands (UHI), a phenomenon that clearly distinguishes higher temperatures in urban areas than in surrounding or rural regions. An increase in surface roughness length (lower layer of the atmosphere where heat fluxes, dispersion and ventilation paths are modified due to the presence up high-rise buildings) also plays an important role in the atmospheric conditions that favour precipitation (Shepherd, 2005) or the longevity of precipitation clouds, despite having no impact on originating a storm (Stallins et al., 2013).

Given that the overall vulnerability of an urban area stems from the interaction of “physical, sociocultural, economic, and institutional conditions” (Acosta-Coll et al., 2018), flash floods in urban areas might not be historically unique, but they can result in great damages and losses to properties (such as internally flooded houses and businesses), transport network (including the erosive potential of high flows on bridges) and human welfare (Archer et al., 2018) as detailed in Section 1.1.1. The magnitude of the consequences is often exacerbated by the inherent quick response of the catchment that hinders the effective response from the population (a more comprehensive definition of “quick response of the catchment” is given in Section 1.2.1, where the duration of the onset of a flash flood is discussed).

Finally, the urbanisation on flood prone areas and highly dynamic changes in land use invariably modify the patterns of hazard, resulting in a increment in exposure at global level (Handmer et al., 2001), with some studies placing urban flash floods as hydrometeorological phenomena that requires prioritisation of risk reduction strategies (Alfieri et al., 2011). Common consequences of the impact of urbanisation in flash flood extremes include an increase in peak discharge values, annual maximum discharge and flood frequency. Although sometimes these changes are not directly attributed to urbanisation due to the influence of yearly variation in storm behaviour, there have been reported cases of an increase in the frequency of discharge peak exceedance during urbanisation periods, compared to measurements in the 1950s (Konrad, 2016). The study by Miller et al. (2017) gathers evidence of the impacts of urbanisation on climate and water resources in the United Kingdom and evaluates the confidence in the direction of the changes, where the confidence is expressed as high, medium and low under the same concept as the IPCC Assessment Report 5. In general, they found that there will be an increase in several environmental scenarios triggered by either urbanisation or climate change. For example, there is a high level of confidence that

an increase in population, rainfall amounts and wetter winters will lead to an increase in pluvial flooding, which in turn will cause a marked rise in property flooding, sewer flooding and thus population affected. They also document a low confidence in the rise impervious land cover, winter events, rainfall intensity and extreme summer precipitation that will enhance pluvial flooding. Similarly, they also report low confidence in the rise of flood risk and flood frequency due to climate change, but they state with high confidence that this is rather due to urbanisation and the combined effect of urbanisation and climate change.

1.1.3 Characterisation of flash floods: difficulties and relevance

There is currently extensive research on the development of fluvial floods and water quality, but several in-depth studies that review the latest tools of modelling and forecasting flash floods agree that these events and their impacts are understudied, specifically un urban areas (Cutter et al., 2018; Hapuarachchi et al., 2011; Miller et al., 2017), despite the significant losses associated with their occurrence due to their exceptional magnitude or non-familiarity with the area. In the United Kingdom there is abundant literature on the impacts of climate change in future flooding scenarios, although analyses that address specific consequences of flash flooding in urban areas are less abundant. In particular, there have been studies on the influence of urbanisation on fluvial flood hazard for other countries (Salvadore et al., 2015; Sheng et al., 2009). Therefore, the need to study fluvial flooding in areas that are particularly prone to events with a quick onset becomes more complicated with the spatial scale, however, it is urban settlements that require a detailed analysis given the complexity of a building layout (Miller et al., 2017).

Another difficulty that arises from high flood peaks in a short period of time is that conventional stage measurements are commonly damaged or swept away during the event, leaving the rivers ungauged (Marchi et al., 2010). Measuring capacity of rain gauges is also often exceeded by the spatial and temporal scale or the originating storm, even in catchments with a dense rain gauge network (Anagnostou et al., 2006). Flash floods also require a deep process understanding for forecasting and risk management, a task that cannot be done by learning from moderate floods (given that the surface runoff processes change with the severity of the storm and antecedent conditions) but from past flash flood events despite the inherent observational difficulties (Borga et al., 2011).

Flash floods are multi-scale phenomena as they develop across several spatial and temporal scales. The first catchments to react to intense rainfall are the small ones (a few km^2). Catchments with low infiltration capacity, as explained in section 1.1.2, cause sudden overland flow, a reaction that can be absorbed by larger streams, even if the runoff is caused by an

intense, localised rainfall. However, at larger scales, these rives with high capacity have a different behaviour. The contribution of smaller catchments mentioned earlier is combined into the larger stream, so the overland flow takes place a few hours after the rainfall has started. Hence, there is a question of scales to be addressed (Lutoff et al., 2018).

The analysis of the progression of processes that lead to a flash flood facilitates establishing a link between catchment conditions previous and during the event, and the severity of the flood. Furthermore, the inherent nature of flash floods requires an analysis at hourly or even sub-hourly scale, so the processes are looked at in great detail, compared to floods with a slower evolution, where regional controls play a more important role (Merz et al., 2008).

Numerical simulation of past flash flood events delivers valuable information on the hydrological response of catchment given a meteorological forcing. It also provides insights into the behaviour of a river that might have been anticipated but not observed. A comprehensive record of historical flash floods constitutes the foundation information to validate analyses on flood susceptibility. This inventory can comprise field data, an archiv of past flash flood events, crowd-sourced information, interviews to the locals and satellite imagery (Doswell, 2015). On the other hand, indirect estimations of peak rainfall values and highest discharges is also useful to document an event, therefore reconstructing a past flash flood is crucial in risk assessment studies (Ali et al., 2017). Given the documented short onset and significant flash flood events in the United Kingdom in the past 20 years, the Met Office (the United Kingdom's national weather service), the Environment Agency (responsible for "protection and enhancement of the environment in England") and other emergency response bodies must meet the challenge of establishing appropriate prediction, preparedness and reaction policies (Cave et al., 2008). Characterisation studies that address the catchment response to intense, localised rainfall, such as the present one, are therefore a key tool in climate and hydrological sciences that facilitate local forecasts and improve flood risk management (Collier, 2007; Marchi et al., 2010).

1.2 Definition of flash flood

1.2.1 Definition given by previous research.

Flash floods are present in both inland and coastal environments, and regardless of the location, the name of the event implies a rapid evolution that is usually associated with low response time (usually less than one hour) between recognising potential flood risk and the occurrence of water levels that pose a threat to livelihood and properties.

When associated with inland events, flash floods develop depending on catchment characteristics -such as land cover, antecedent soil conditions and stream conditions. A thorough study of significant flash floods events in the United Kingdom identifies two major categories depending on the environment in which they are present (Archer et al., 2018).

- Fluvial flash floods refer to a sudden rise of water levels in a river channel and is often reported in the media as a “wall of water”. However, this can be rapid enough to produce an actual breaking wavefront that can occur in steep upland catchments as well lowland areas. The wavefront steepens as it travels downstream, and this is reflected in abrupt discharge peaks in the hydrograph of the event. Fluvial flash floods can also occur as a result of the failure of a defence structure, melting snow that increases the runoff, and due to the sudden release of water from an ice jam (accumulation of broken blocks of ice formed in cold conditions), usually formed against bridges or other structures (NOAA, 2019).
- Pluvial floods (or ponding) occur where the soil infiltration capacity is surpassed by the precipitation -a common phenomenon in chalk streams-, so all excess rainfall contributes to overland flow. Poor infiltration capacity is also observed in urban areas, where the impervious land cover leads to surface water flooding that can overwhelm sewage networks, which then in turn results in flash flooding even before the precipitation has reached the river. In addition to this, there is the urban riverine response, where watercourses respond similar to fluvial floods, producing downstream-moving waterfronts and record peak discharges.

For both cases, the exact definition of flash flood is still a topic of discussion (Braud et al., 2014). An initial effort by the IAHS-UNESCO-WMO defines a flash flood as an event “of short duration with a relatively high peak discharge” (IAHS-UNESCO-WMO, 1974), highlighting that a "suitable break point between a flash flood and a normal flood" is a duration of six hours or less between the causative event and the flood. This duration of flash floods comes from the limitations to manual data collection and numerical modelling at the time of the first definition by WMO, which in turn at this time required different forecasting techniques than a “normal flood” (Hall, 1981). Despite the apparently outdated definitions, this six-hour attribute is still applied to Mediterranean and Continental areas of Europe (European-Commission, 2013) and by the US National Oceanic and Atmospheric Administration (NOAA, 2019).

A further definition of flash flood was built by Braud et al. (2014) upon the comparison of the duration of the event to the catchment concentration time. This interpretation therefore allows the inclusion of flash floods with longer durations, up to 24 hours in catchments of approximately 1000 km^2.

Another vague but easily communicable definition of a flash flood is given by the United States Geological Survey (USGS), which characterises a flash flood as the result of a “rapid rise in (stream) water height” after a rainfall event. The concept also entails the lack of soil infiltration capacity (enhanced by “dry climate and rocky terrain”) as one of the major underlying causes of a flash flood. The USGS, following the statement by the World Meteorological Organisation, places flash floods over river floods as the main cause of the loss of life (USGS, 2020; World Meteorological Organization, 2019).

On the other hand, in their study on historical flash floods in Britain, Archer et al. (2018) compile relevant features of the events and propose a definition based on the national climate and landscape, stating that flash floods are the consequence of intense rainfall as a result of both synoptic and meso-scale convective features, that causes accumulations of more than 40 mm of rain in one hour. They also point out that the precipitation totals or peak discharge values are not by definition the source of danger for flash floods, but that it is the quickness of the onset that poses the key risk.

Finally, the Environment Agency in England defines a flash flood as events with an extremely quick occurrence and immense force, capable of carrying heavy debris such as natural landscape features (rocks, trees), vehicles and bridges. It specifies that the most common type of flash floods occur as a consequence of intense rainfall: in rivers, it causes streams to swell; in cities, it can cause the sewage network to be overwhelmed and produce surface runoff. This organisation also points out the key characteristics of a flash flood: intense rainfall, short onset between the start of the rain event and the flooding, large volumes of fast moving water, damage to urban structures, further destruction caused by debris and critical threats to life (Environment-Agency, 2013b).

1.2.2 Definition used in the present research and criteria to choose case studies

The definition of flash flood that will be considered in this thesis refers to events as a result of intense, localised rainfall and follows the IAHS-UNESCO-WMO suggested lapse of six hours or less between the peak of the storm and the rise in river levels. Furthermore, the present research deals with the hydrometeorological aspect of inland flash floods in urban areas.

In the context of the present research, hydrometeorology of urban flash floods refers to the study of the meteorology of intense storms and the consequent urban riverine response; surface water flooding is not analysed.

The choice of case studies began with a search of historic flash floods in the United Kingdom more recent than 2000 and up to 2012 that are associated with great losses, or that occurred in one of the major cities in the country. This time frame ensures that the studied events would be no more than 20 years old, and that the databases of climatic and hydrological variables for the study (hourly discharge, potential evapotranspiration and rainfall) would cover the chosen events. A list of events was retrieved from search engines and studies such as the one carried out by Archer et al. (2018).

The location of the selected flash floods was checked against the location and length of record of the river gauges in the United Kingdom's National River Flow Archive. Outflows of the catchments are monitored by stations that a) are no more than 10 km upstream from where the major impacts of the flash flood were recorded so that the modelling is relevant for a given case, b) are not affected by hydropower production generation nor reservoirs as both represent a source of significant changes to average flow, c) correspond to catchments with at least 40% of urbanised cover according to the Land Cover Map 2000 (CEH, 2002), the dataset that the NRFA uses as valid catchment information, so that two land uses (urban and non-urban) are clearly present, and d) that would not exceed 100 km^2 to avoid compromising the available computational capabilities for numerical modelling.

Most of the aforementioned criteria are based on the availability of the data and computational resources at the moment of the modelling. If those constraints were lifted, more test cases could certainly be considered.

1.3 Aim and contribution of the study

The research presented here proposes a hydrometeorological modelling framework to characterise the physical processes associated with an urban flash flood, namely intense, localised rainfall and urban catchment response under said scenario. It comprises two stages: modelling of intense, localised rainfall that preceded a flash flood and simulation of river runoff during the event. Simulated rainfall (the output of interest of the meteorological model) will be used as climatological input to simulate discharge, and this will be compared against that produced using observed rainfall.

The present study involves the use of a publicly available, well documented numerical weather prediction tool that has been successfully applied in the characterisation of meteorological drivers and forecasting of flash floods, as well as urban meteorology studies worldwide; and a highly flexible, fully distributed hydrological numerical tool that is based on the core concept of an established hydrological model.

The numerical weather prediction tool implemented in this research has been the model of choice for many flash flood and urban meteorology studies. However, they focus mostly on alpine and forest environments, or on the effects of the urban canopy on air quality, so none of them has explored the capabilities of the model to reproduce intense, localised rainfall in urban areas. On the other hand, the implementation of the chosen hydrological tool at hourly scale, along with a simple but efficient representation of the urban landscape is being done for the first time, providing useful information on model performance to reproduce sub-daily flow variations. The integration of the two numerical tools is also another novelty of the present study. Both components of the hydrometeorological framework are freely available, which allows assessment of their uncertainty in model structure and facilitates the reproducibility of its outcomes.

A complete description of the cascade methodology, the numerical tools involved, the databases used to run the simulations and validate the results, including the rationale behind the choice of model, description of model structure, identified strengths and research opportunities is detailed in Chapter 3.

This research will therefore demonstrate a methodology for error propagation from a weather model to a hydrological model in a downscaling framework. It aims to bridge the gap between the current documented abilities of the cascade and its potential at local scale in urban areas. The research also aims at proposing a suitable approach for the characterisation of urban flash floods and parameterisation of key components of flood risk. Specific research questions include: How to integrate the urban landscape in the simulation of the atmospheric and hydrological processes during a flash flood? What is the optimal configuration of the modelling framework to reproduce other past flash flood events?

The knowledge gathered from this study aims at contributing to the archive of historical events used to define the pattern of events and increase the ability to identify and predict them. It also allows benchmarking of the performance of the numerical tools, providing a clear path to improve the modelling framework and setting the foundation for the feasibility of future forecasting applications.

1.4 Thesis outline

This research study is organised in seven chapters that describe the theoretical basis, results and outcomes of the hydrometeorological characterisation of two flash flood events in urbanised catchments in the United Kingdom. Chapter 2 introduces the state of the art regarding developments that lead to the current understanding and practices of hydrometeorological modelling of flash floods. Once this update on methods has been presented, Chapter 3 outlines the proposed methodology, including a comprehensive description of the numerical tools used and justification of use. This Chapter also includes the procedure to evaluate the meteorological and hydrological model outputs and justifies the robustness of the performance metrics implemented. Chapter 4 deals with the numerical modelling and discussion of the outputs of the meteorological modelling for the first case study, highlighting the importance of considering the urban canopy in the vertical discretisation of the atmosphere. Here, additional model sensitivity tests that helped defining an optimal model set-up are documented. Chapter 5 presents the meteorological modelling and results for the second case study, following the recommendations and main findings on model performance presented in the previous Chapter. Moving on to the following stage of the research, Chapter 6 presents the hydrological modelling for both case studies, grouped in a single Chapter given the common core assumptions in the numerical representation of hydrological response of the urban catchments. Finally, Chapter 7 contains the main findings of the study, including limitations of the study and future lines of research, and summarises the applicability of the modelling framework as a characterisation tool. Further details on the content of each chapter are presented in Table 1.2, which summarises the key points addressed

Table 1.1. Thesis content by chapter

Chapter 1	Introduction
	- Overview of the magnitude of impacts of flash floods - Importance of improving the understanding of these hydrometeorological hazards as motivation for the present study. - Main and specific objectives and research questions.
Chapter 2	Characterisation of urban flash floods in context
	- State of the art on the methods to characterise 1) intense, localised rainfall associated to flash floods, and 2) the rapid response of urban catchments - Identified research gap
Chapter 3	Hydrometeorological modelling framework
	- Outline of the numerical modelling framework. - Description of the proposed numerical tools to reproduce the intense rainfall and of river discharge during a flash flood in an urban catchment. - Description of the rationale behind model set-up and databases used as boundary and initial conditions. - Performance metrics for meteorological model evaluation, and methodology for hydrological model calibration and validation.
Chapter 4	Meteorological modelling case 1. Newcastle 2012 flash flood event
	- Overview of the severity of the impacts of the first flash flood event that lead to its choice as case study. - Description of the development of the antecedent atmospheric conditions. - Description of the atmospheric conditions and measured rainfall on the day of the event in the Tyneside region of the United Kingdom, highlighting its magnitude with respect of historical records - Analysis of results at three spatial scales. - Evaluation of model performance given the implementation of urban canopy models. - Sensitivity tests on use of microphysics scheme and spin-up time, and justification of current meteorological model set-up.
Chapter 5	Meteorological modelling case 2. Birmingham 2007 flash flood event
	- Overview of the severity and extent of the impacts of the series of flash flood events that include the second case study. - Description of the development of the antecedent atmospheric conditions. - Description of the atmospheric conditions and measured rainfall on the day of the event for gauges across the Midlands region of the Unite Kingdom. - Analysis of results at three spatial scales. - Evaluation of model performance given the implementation of urban canopy models.
Chapter 6	Hydrological modelling
	- Description of the core assumptions behind the hydrological model parameter range to represent the urban land cover for both case studies. For each case study: - Outline of soil moisture deficit and river flows prior to the event, - River levels and discharge during the flash flood recorded at several stations, stressing the magnitude of the rapid response of the urban catchment. - Model calibration considering hydrological model parameters that control soil saturation conditions for the urban hydrological response units. - Model validation and performance metrics when using observed (from databases) and simulated rainfall (from meteorological model outputs), considering the impact of the choice of urban canopy parameterisations from the meteorological modelling.
Chapter 7	Conclusions
	- Summary of the existing efforts on hydrometeorological characterisation of flash floods, highlighting the contribution of the study. - Limitation of the study regarding the numerical tools implemented. - Potential of the proposed hydrometeorological modelling framework. - Future lines of research.

Chapter 2

The hydrometeorological cascade as urban flash flood risk reduction tool

2.1 Introduction

Ahmadalipour et al. (2019) classified existing flash flood studies aimed at reducing flood risk depending on their objective into several categories. This classification, outlined below, pinpoints the main pathways that are currently being followed when undertaking research aimed at managing and reducing flash flood risk:

1. Assessing and improving forecasting skill, including the definition of indices to quantify hazard.
2. Analysing the impact of climatological variables and human-made environmental changes on flash flood hazard, including the understanding and social perceptions of the flood risk components.
3. Numerical modelling of flash flood hazard and risk, including characterisation of relevant physical processes, patterns and regimes.
4. Post-flash flood analyses, including field measurements and analysis of damages consequences.

From these streams of research, the present work is placed in Category 3. The objective is aligned with the work from several authors who agree on the pressing need to optimise and develop modelling techniques and frameworks that help understanding and characterising the hazard and impacts of flash flood events (Amengual et al., 2007; Amponsah et al., 2016; Archer et al., 2018; Borga et al., 2011; Marchi et al., 2010) that, as outlined in the previous chapter, account for considerable losses at global level.

One of the numerical tools used for this is the hydrometeorological cascade. In a nutshell, this modelling framework procures the seamless modelling of the atmospheric and hydrological processes that precede an event, such as a flash flood (Kelsch, 2001) or a drought (Vu et al., 2015). The rationale behind the choice of this framework, including its components, applications, strengths and weaknesses are outlined in this chapter.

2.1.1 Description of the cascade

The hydrometeorological cascade is a numerical tool for the modelling, estimation, analysis and interaction of the relevant physical atmospheric and hydrological processes that are linked to the occurrence of a flood event. The cascade should represent the evolution and connexion of the natural processes that lead to a flood event. Implementing and linking different models to simulate the stages of the even provides crucial information on the effects of parameter uncertainty given that an end-to-end modelling framework allows its propagation (Rodríguez-Rincón et al., 2015), where end-to-end represents the context of study in which there is a continuous analysis from the meteorological level (rainfall as a driver of floods) to the consideration of warnings and impacts.

The end-to-end concept as the result of numerical modelling and the application of its outcomes normally involves the meteorological and hydrological stages for the development of operational forecasting products. As stated by Hapuarachi et al., (2014), the first step in effective flash flood forecasting begins with the correct representation of the precedent rainfall, and the natural following step is the modelling of the hydrologic processes. In these studies, the climate scenarios are used as drivers of rainfall-runoff models that allow the simulations of past (hindcasting) and future (forecasting) scenarios. Hence, the hydrometeorological cascade involves two main steps: the preparation of atmospheric settings and the numerical modelling of streamflow (Khazaei et al., 2012). Some studies also include the analysis of hydraulic processes. In this last step, flood depths and extents are analysed, and warnings on flood occurrence can be issued (Flack et al., 2019).

Application of a hydrometeorological cascade must be done at sub-daily scale, so that the generation of weather forcings as boundary conditions for hydrological modelling are sufficient to produce the quick variations of stream conditions (Caldwell et al., 2013). Quantification of simulated runoff peaks needs to be done at hourly scale to account for the sub-daily variations as a result of intense rainfall (Amponsah et al., 2016; Shrestha et al., 2019a; Winter et al., 2019). A comprehensive representation of floods involves detailed study and modelling of physical processes at atmospheric and catchment scale. This means that the hydrometeorological approach for flood modelling constitutes a robust framework for prediction and identification.

There are several sources of uncertainty associated with the hydrometeorological cascade. It is important to consider these sources of uncertainty and their bounds to determine and select the best techniques for cascade studies.

The first stage of the cascade is subject to the stochasticity of the atmospheric processes, as well as the uncertainties of the databases and numerical tools used for its representation. Climatological variables to drive weather modelling, as well as the model structure, parameters and the technique to project global-scale modelling to local-scale results (or downscaling, which will be elaborated on in Section 2.2.4) are the main sources of uncertainty in the first stage of the cascade. However, an analysis can be carried out to determine these uncertainty bounds and reduce them. For instance, the uncertainties that come with the choice of a numerical tool can be defined and reduced by sampling a range of models. A similar approach can be taken when selecting the downscaling technique.

On the hydrological part, common uncertainties come from the information used as climatological forcing and the model of choice, including, as stated earlier model structure and parameters. Similar to the work done in the previous stage of the cascade, sampling and testing a range of available options helps pinpoint the sources of error.

A conceptualisation of the hydrometeorological modelling cascade, including the sources of uncertainty and methods for its analysis is presented in Figure 2.1. This diagram also explains how the decisions made at each step of the cascade (regarding data and models) have different impacts on the outcomes. An important feature to note is that, like the physical processes, the uncertainty is also cascaded through the modelling framework. End-users, such as policy makers or decision makers, will only need the uncertainty bounds of the cascade at a given stage, for example, the probability of occurrence of a hydrometeorological extreme event to design defences, reservoirs, potential capacity of power-generating plants and the proposal of new infrastructure. Common questions include “how extreme are the conditions that are liable to affect the durability of a given structure, what is the magnitude of an event of a given return period?” (Smith et al., 2018).

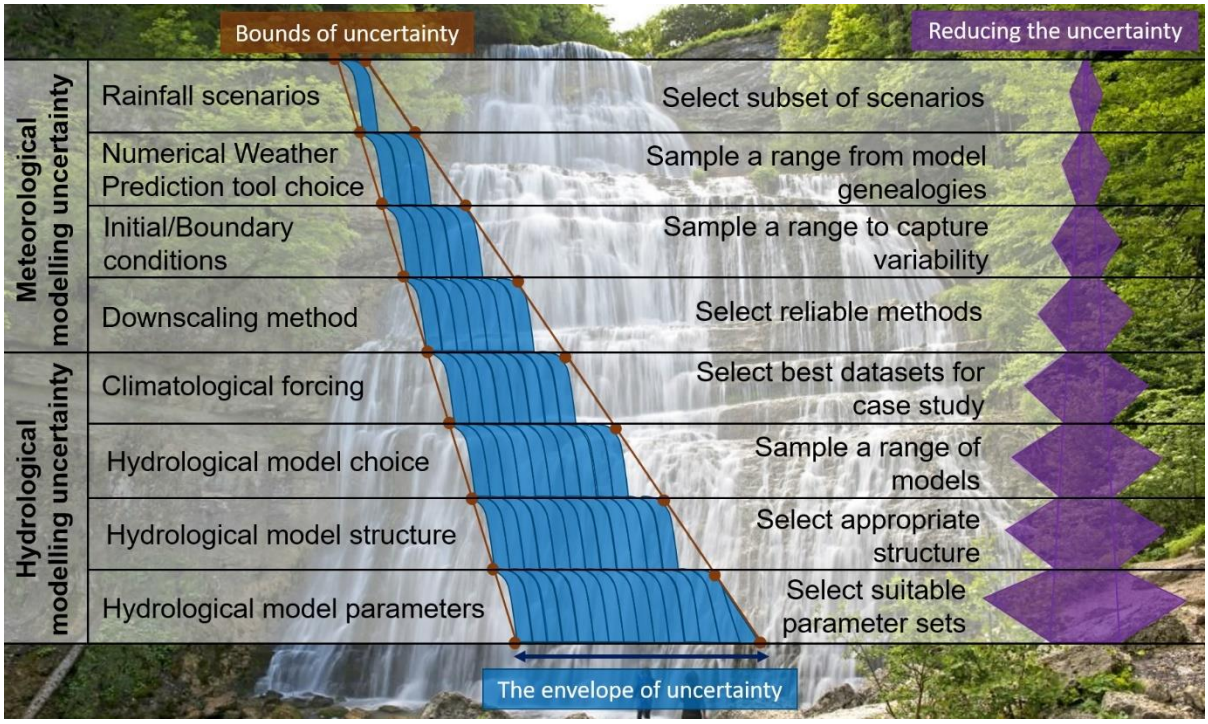

Figure 2.1. Conceptualisation of the modelling cascade given propagation, bounds and reduction of uncertainty at each step as proposed by (Smith et al., 2018). Figure adapted under the Creative Commons licence

Regarding the first stage of the cascade and as emphasized by Singh and Woolhiser (2002), rainfall remains the leading contributor of uncertainty propagation in hydrologic simulations, and Hapuarachi et al., (2001) agree on the importance of the quality of the rainfall scenarios to produce a reliable flood forecast. As the main driver for hydrological modelling, the study of many sources of rainfall should be considered when designing a modelling framework. The choice of rainfall product or model output depends on the availability and reliability of the data, its known sources of error, documented improvements as well as the required spatial and temporal accuracy (Sene, 2013; Singh et al., 2002). Flash flood characterisation and forecasting, given its rapid onset, requires the use of hourly-scale rainfall to drive the following stages of the cascade (Shrestha et al., 2019b), with some studies suggesting that the temporal resolution of the precipitation data is more relevant that its spatial variability, even in urban environments and when studying extreme rainfall scenarios (Yang, Smith, et al., 2016).

The second stage of the hydrometeorological cascade refers to the estimation of river discharge. Numerical models are widely used due to their accessible and reliable implementation at sub-daily timesteps. Simulated hydrographs are then compared to observations to determine the accuracy of the outputs, which can be timeseries of measured discharge or peak observed values from field surveys (Amponsah et al., 2016). Given that this

stage comprises numerical tools, and as seen in Figure 2.1, there needs to be an analysis of model structure and parameters to define the uncertainty. The evaluation of uncertainty with every decision taken through the cascade will help reduce it for that step, which is why uncertainty increases from one step to another. However, after it has been analysed, it is reduced, although some of it is still cascaded to the following steps.

2.1.2 Application of the cascade to urban areas: relevant physical processes

2.1.1.1 Microclimate of urban areas

The presence of urban clusters has a significant effect on the physical processes present in the atmosphere above them. As a result of the interaction of cities with the overlaying atmosphere, a microclimate is generated. Here, low albedo materials (such as asphalted surfaces and roofs) and radiation tendencies (shortwave incoming solar radiation that reaches a city is re-emitted to the atmosphere as infrared) are deeply modified. Moreover, the difference in temperature of urban clusters and the surrounding areas can be up to 3 ºC, although it can be as high as 12 ºC in clear nights (Fallmann et al., 2013).

Precipitation systems in urban areas tend to develop with greater magnitudes, and rainfall over urban areas is enhanced by the vertical heat fluxes described earlier. The effect of urban areas on thermal processes is directly reflected in the location of intense thunderstorms (Lin et al., 2011). The relationship between presence of buildings and enhanced wind circulations to produce or augment clouds has also been considered, as the converging air could be an important factor for the intensification of rainfall (NASA/Goddard Space Flight Center, 2002). There is a consistent agreement on the impacts of urbanisation on climatology. Frequency, intensity and patterns of thunderstorms are greatly influenced and become more complex given the decrease in wind speed (due to the multiple obstructions) and increase in upward motions as a result of building configuration (Patel et al., 2019). Finally, further consequences at an atmospheric level due to urbanisation include air pollution and a decrease in visibility (Wan et al., 2015).

With the changes to the land surface and subsurface, the influence of urban clusters can be seen at several scales (Burian et al., 2005; Ganeshan et al., 2013; Shepherd, 2005). The urban canopy, which comprises buildings and other human-made structures affects evaporation rates, albedo (and hence absorption and reflection capacity) and wind turbulence. The reduced vegetation also has an impact on the distribution of temperature ranges. Finally, the characteristic emission of gases and accumulation of pollutants -that act as secondary aerosols- also affect the heat and moisture land-atmosphere fluxes.

Urbanisation is responsible for the deep modification of thermodynamic, radiative and hydrometeorological process not only in the urban and peri-urban areas. It has been documented that urban areas enhance increase the severity of climate extremes. This is the case for regional-scale heatwaves, which under current climate change scenario are projected to increase in frequency and intensity as a result of urban developments (Niyogi et al., 2017; Shepherd et al., 2002). Another important effect of city-atmosphere interaction is the development of Urban Heat Islands (UHIs), in which cities act as source of thermodynamic activity. When combined with the poor capacity of soil water storage, UHIs create barriers to atmospheric fluxes, also increasing the stationary state of pollutants (Fallmann et al., 2013).

2.1.1.2 Urban riverine response to flash floods

Urbanisation deeply affects the natural drainage and recharge processes as well as the infiltration capacity of soils by introducing impervious surfaces. Moreover, some urban areas are poorly gauged, which adds complexity and difficulty when reproducing the surface flows in an urban catchment.

Impervious surfaces serve as blockages for the drainage capacity, sometimes also acting as a barrier for the natural path of the flow. Other human-made structures for transportation, such as bridges, railway networks, as well as impervious surfaces which act as embankments or ponds, which can retain rainfall for several days (National Research Council, 2012). The direct impact of impervious surfaces on surface runoff usually results in an increase of flood peaks, with minimum lag time between the start of the rainfall and the peak discharge. Moreover, asphalted surfaces and concrete walls also constitute an channel with low friction, resulting in rapid translation of flood flows (Shuster et al., 2005).

There is also a documented variability in the rainfall-runoff ratio depending on the spatial and temporal extent of the rainfall, antecedent soil storage conditions as well as the heterogeneity of surface processes. These phenomena are often accentuated by the magnitude of the storm, where small rainfall amounts produce a gradual response, in contrast to the high precipitation rates that are usually associated with a rapid response of the urban catchment. At small scales, total runoff is mainly a result of the rainfall falling on impervious surfaces, while at larger scales the dominant processes are related to pervious areas (Yang, Smith, et al., 2016). Urbanisation processes, combined with climate change, leads to an increase of two to six times the normal runoff, compared to what could be expected in a non-urbanised scenario (Hapuarachchi et al., 2011; Ramachandra et al., 2008).

The main changes that urban areas have on the hydrological cycle include (Miller et al., 2017):

- Higher proportion of rainfall transformed in overland flows, given that the infiltration and recharge rates are decreases
- A quicker response of the urban catchment to the rainfall, where the rising limb of the hydrograph is usually steep and not long after an intense rainfall pulse.
- Rise in flood peak magnitudes
- Reduced recharge to groundwater storages, so during low flows, the expected runoff is often less than that in natural catchments.
- Detriment to water quality due to the surcharges from manholes that degrade the natural flows. This is also reflected in the rise in water temperature.

At catchment and sub-catchment scales, the effects of man-made land use changes (such as deforestation and urbanisation) are crucial to the hydrology of the region (Kelsch, 2001). The spatial scale of the hydrological response of an urban catchment can be easily compared to that of storm cells that cause the intense rainfall, and it is strongly tied to soil properties such as storage and transfer capacities as these characteristics impact the infiltration rates and flows routed to the river channel (Seed et al., 1990). Other characteristics that also dictate the scale of the response of the urban catchment are the morphology and degree of urbanisation, being the most important effect of urbanisation in the hydrological response of a catchment in the increase in magnitude and frequency of peak flows, and the damaging decrease in lag time of those high values (Hofmann et al., 2019).

Finally, Christensen et al. (2007) summarised the effects of urban clusters on local weather conditions in a study that examines the role of urban features in the development of UHIs. They identified the main environmental processes affected by urbanisation as temperature, wind, clouds, precipitation land-surface hydrology and cycle of nutrients (carbon and nitrogen). When the natural features are exposed to urban features such as land cover, aerosols and anthropogenic gases emissions, there are deep changes to the environment, replacing, enhancing or modifying the natural water and nutrient cycles, such as the ones shown in Table 2.1, that depicts the main impacts of urbanisation in the relevant variables to flash floods.

Table 2.1. Impacts of urbanisation in flash flood-related environmental variables

Environmental variable	Urbanisation product		
	Urban land cover	Urban aerosols	Anthropogenic gas emissions
Clouds and precipitation	Energy budget, UHI, induced convergence zones	Aerosol effects on cloud microphysics and precipitation	Radiative and warming feedbacks
Surface hydrology	Surface runoff, decreased infiltration rates	Aerosol effects on cloud microphysics and precipitation	Radiative and warming feedbacks

The following section will describe the elements of the hydrometeorological cascade, including common sources of uncertainty in the retrieved data and advancements in the quality of the products and modelling techniques.

2.2 Stage 1: Estimation of precipitation

Given the fast response of urban catchments to rainfall and the importance of this variable in the hydrometeorological cascade, applications of precipitation estimates are required to have both a high resolution and accuracy (Ochoa-Rodriguez et al., 2019; Syed et al., 2003).

There are numerous rainfall products and estimates, and each of them were created and have been implemented in studies with a wide range of applications and spatial and temporal requirements. For example, low resolution precipitation (in terms of bot spatial and temporal aspects), are usually implemented in river basin management. With rainfall estimates of high temporal resolutions, the studies can range from extreme simulation events and insurance sector (when the spatial resolution is low) to flood warning and forecasting (when the resolution is high) (Ochoa-Rodriguez et al., 2015). This chapter describes the rainfall estimates used in flood studies and highlights the strengths and weaknesses when dealing with flash floods.

2.2.1 Point rainfall measurement

Rainfall from ground-based gauges constitutes a widely implemented database from which reliable meteorological data can be extracted. They require constant maintenance to ensure the accuracy of rainfall point estimations and the utility of the database is often related to the density of the network. However, given the type of quality checks that gauge data usually undergo (such as detection of anomalous values via neighbouring measurements), this

information can be considered as the best estimate of rainfall for hydrological applications (Patel et al., 2019; Vionnet et al., 2019; Wicht et al., 2016)

In the present work, rain gauge will refer to the ground-based instruments for point measurement of rainfall over a given period. The best example of recording gauges are the tipping bucket, weighing and level gauge designs. The rainfall rates monitored by these stations are usually implemented in catchment scale studies. Gauges provide low-cost and direct measurements, and they are often regarded as the "truth" value when calibrating and assessing the performance of other rainfall measuring devices, such as weather radars (Environment-Agency, 2013a).

Rain gauges are prone to two types of errors: the first one stems from the measuring nature of the instrument and includes systematic, spatial sampling and malfunction errors; and the second one, from the density of the network used to estimate the overall rainfall rates. Spatial sampling errors are more evident when calculating rainfall over 1-km pixels, given that the typical catching area is around 20 cm (Gires et al., 2014). Systematic errors include wrong measurements due to the effects of wind on a poorly installed gauge, loss of wetness in the internal walls of the rainfall collecting device and evaporation of the collected rainfall in warm weather. Furthermore, tipping bucket rainfall gauges are prone to underestimate rainfall intensities due to the loss of water during the operation of the device. These errors can be identified and removed or reduced through statistical analysis of the timeseries, using neighbouring gauges and, when the information has enough accuracy as has been through quality check controls, it can be compared against radar measurements (Looper et al., 2012). Accounting for the sources of error is crucial for the use of this information on its own, but also as part of a merged product (World Meteorological Organization, 2008) (see section 2.2.3).

2.2.2 Remote-sensed rainfall data

2.2.2.1 Radar

Remote-sensed rainfall information represents a high resolution estimation that is commonly used for warning systems at regional and local scale (Alfieri et al., 2011). Radar-based rainfall products allow a detailed monitoring of storm origin and track, so they facilitate the estimation of rainfall intensity and distribution (Kelsch, 2001).

Radars are used in flash flood forecasting due to their high spatial and temporal scale (usually 1 km or higher, and 15 minutes or higher, respectively) so the products can therefore be applied when using models that are built with the governing equations for rainfall-infiltration rates, and their usefulness to capture flash flood associated intense rainfall has also been

documented. However, given the fast response of an urban catchment to intense rainfall, the main source of errors in the application of weather radars in flash flood forecasting is the low lead time that they can provide (Smith et al., 2007).

To estimate precipitation, weather radars generate electromagnetic high-powered pulses transmitted through a rotating parabolic antenna which subsequently detects reflected waves or echo from a certain target towards the radar. The better the target object can rebound the waves, the stronger the echo will be. The distance of the target from the radar can be determined via the travel time of the reflected radio wave after the pulse emission. In the UK, 15 out of 18 weather radars are operated and maintained by the Met Office, each one providing data up to 255 km range distance with 1 km, 2 km and 5 km resolution coverage (Met Office, 2003).

Radars give useful information on the reflectivity of hydrometeors. However, their structure means that radars are prone to measurement errors (Hapuarachchi et al., 2011). Some of the errors include calibration and sensitivity problems (due to the hardware components that require constant maintenance), contamination in products given clutter and anaprop (ground targets in the way of the main target and “anomalous radar bean propagation”), reduction in the backscattered radiation (due to interception of ground obstacles), attenuation of the signal (sometimes so severe that the signal of the radar is completely lost), assumptions about hydrometeor size distribution (for example, a fixed ratio between reflectivity and precipitation rate that can lead to wrong readings for hail, for instance) and variations in the vertical reflectivity profile (as a consequence of evaporation, wind and melting ice rates of snowflakes that develop an outer layer of water that increases reflectivity known as bright band, orographic enhancement in the lowest 1.5 km of the atmosphere).

Techniques to correct radar rainfall data include the detection and deletion of spurious images (identified by comparing radar images to previous measurements or using statistical indexes based on neighbouring stations), detection and removal of anaprop (anomalous propagation can be reduced when radar information is combined with synoptic-scale measurements that provide a probability of precipitation give a certain threshold), diagnosing individual radar pixels to account for error in the reflectivity profile, which results in corrected precipitation that is higher than the original measurements) (Harrison et al., 2000).

A visual representation of the correction scheme is given in Figure 2.2, where rainfall was recorded in the Crug-y-Gorllwyn radar in southwest Wales. In unprocessed image, the augmented rainfall close to the radar site is visible, but after the correction the overall rainfall in the area is higher and more homogeneous.

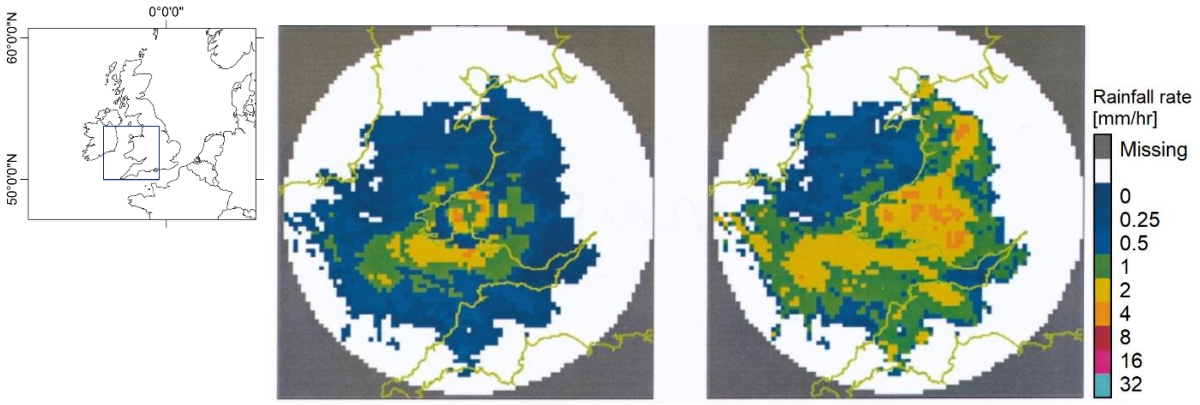

Figure 2.2. Radar snapshots before and after the vertical correction scheme for the Crug-y-Gorllwyn radar in southwest Wales, as presented by Harrison et al. (2000)

2.2.2.2 Satellite

Satellite precipitation comes from the combination of infrared and microwave sensors in geostationary satellites. This means that precipitation is not measured directly, but rather estimated from the information retrieved by the sensors (Golian et al., 2019). Satellite-derived rainfall information is used when data from rain gauges and radars is not available. Satellite databases are available over areas with inaccessible or complex terrain where gauging might be sparse and can be found in several spatial and temporal resolutions (Kuligowski et al., 2013). This information provides operational products for flood modelling once downscaling techniques are applied to make this product operational especially in poorly gauged areas (Shrestha et al., 2019a). Similar to radar rainfall estimations, satellite products can be used to produce merged precipitation data (Hapuarachchi et al., 2011).

Uncertainty in satellite data comes from the complexity of the orography of the region of interest (Gebregiorgis et al., 2013), sampling, instrumental and methodologic errors. The last three result from the satellite trajectory and orbit, including the expected sway on its movement (Nijssen et al., 2004).

Satellite estimations have been used in flash flood studies that deal with the potential impact of these events. Vergara et al. (2004) proved that the efficiency of satellite products in flash flood modelling applications depend on the resolution of the products and the spatial extent of the case study. Given that rainfall from satellites needs to be downscaled, the errors present in the final product might be a result of the downscaling technique, more than the satellite itself, so their application for flash flood studies must be done with this source of uncertainty in mind (Nikolopoulos et al., 2013).

2.2.3 Merged products

Merged products represent a combination of two sources of precipitation, considering the strengths and weaknesses of each one, and aiming at complementing their individual applications.

2.2.3.1 Satellite + gauge

Satellite and gauge rainfall data are merged using two main approaches. The first one is a simple bias correction technique, where satellite rainfall is retrieved at given gauge locations, then calculating the difference in the measurements and interpolating them to all grid points, and finally adding the result back to the satellite products. The second one is Regression Kriging, which uses deterministic (linear regression) and stochastic components to deliver a value at a given location.

The quality of this merged product depends on the quality control checks of the ground-based data, the calibration procedure of the satellite and the merging technique. The satellite-gauge products can exhibit a larger spread in the Southern Hemisphere due to a larger diversity of climates compared to the Northern Hemisphere (Golian et al., 2019). The areal mismatch of gauge and satellite data will contribute to apparent satellite underestimation of high rainfall amounts. To some extent, this deficiency is overcome by the bias removal procedure, where this correction technique sometimes shows the same trend of over and underestimation of precipitation than gauges (Manz et al., 2016). Overall, the merged product has a better accuracy in regions where gauge data is sparse (Dinku et al., 2014; Hengl et al., 2007). Some studies have also proved the applicability of these merged products to flash flood forecasting, although this is highly dependent on the quality of the gauge information (Chiang et al., 2007)

2.2.3.2 Radar + gauge

The joint use of remote sensed rainfall that is corrected with ground measurements has derived Quantitative Precipitation Estimations, QPE (Amponsah et al., 2016; Braud et al., 2014; Garambois et al., 2014; Marchi et al., 2010), provided that the reference rain gauge network has also been subjected to quality checks network (He et al., 2013). With the proper correction techniques, remote-sensed measurements can be considered as accurate as gauge-based rainfall information (Collier, 2007).

This product is very sensitive to the spatial and temporal variations of the rainfall in small urban catchments given their high responsiveness. Hence, the merged radar-gauge data must have a high accuracy and resolution to be applied in urban hydrological studies (Ochoa-Rodriguez et al., 2019). It has been proven that the final product has less negative bias in the precipitation,

and the mean square error is also reduced compared to the original hourly data (Sivasubramaniam et al., 2019).

Given that errors and uncertainty of the radar-gauge data comes from the individual weaknesses of each dataset, the correcting methods focus on their combined strengths and this is reflected in the merging techniques, for example, mean field bias correction, local bias correction (using Ordinary Kriging and Kriging with external drift), Bayesian data combination (McKee et al., 2016). However, and similar to the satellite-gauge merged products, the errors in these datasets are subject to the quality of the input data, which makes it difficult to pinpoint the source of the error: from precipitation estimation methods or from the numerical rainfall-runoff modelling, or from the numerical model itself (Qiu et al., 2020).

2.2.4 Downscaling of Global Climate Models

2.2.4.1 Definition of downscaling

Downscaling refers to the procedure of using large-scale information to make predictions at a finer spatial scale. This is done when there is available information at synoptic scale but the event of interest spans over a much smaller scale, such as flash floods. In hydrometeorology, downscaling is applied to processing Global Climate Model (GCM) outputs to studies where the fine scale and heterogeneity must be considered to make an accurate simulation, for example, relocating GCM outputs to rain gauge scale (Fowler et al., 2007). Downscaling from those two very different scales usually requires at 30 years of observations (Gadissa et al., 2019). Uncertainties in the downscaled products come from the choice on the downscaling technique (Fowler et al., 2007).

2.2.4.2 Statistical downscaling

This refers to the numerical estimators to obtain rainfall that can be used in flood modelling, such as weather generators (Khazaei et al., 2012). Accuracy of the product of weather generators depends on the method of estimation to produce weather series: rainfall, in the case of flash flood studies (Kilsby et al., 2007).

Weather generators are particularly useful in ungauged basins or when the rainfall period of record is not long enough for the required study, and they have been successfully been applied to climate change impacts when downscaling outputs from general or regional circulation models (Peleg et al., 2014). They also offer a reliable solution to the unavailability of long timeseries of rainfall at high temporal resolutions, as weather generator use low temporal resolution data (e.g. daily records) or sparse rain gauge network to derive the required information (Müller et al., 2015).

Among the disadvantage of weather generators is their inability to reproduce climate extremes, and their difficulty to reproduce also low-frequency rainfall variabilities (Fowler et al., 2007). However, weather generators can produce long timeseries of climate variables, hence reducing the uncertainty due to climate variability which can be more important than changes in average, and since the correlation between variables is kept, products from weather generators can have hydrological applications (Prudhomme et al., 2002). Weather generators are also able to capture convective events, making their application in nowcasting possible (Arnaud et al., 2002).

A common weather generation used in flash flood studies is the rainfall disaggregation methodology (Peleg et al., 2014), a that dates back to 1970 (Bürger et al., 2014).

Temporal disaggregation of rainfall are useful in urban flash flood studies or in catchments where Hortonian (saturation-excess runoff) processes are dominant (Zhang et al., 2008). An example of this application is by Müller et al. (2015), where they implemented a model based on a multiplicative micro-canonical cascade framework, a standard disaggregation variant of the cascade model for urban-hydrological investigations, for example (Licznar et al., 2011). They tested different disaggregation levels to achieve a final resolution of 5 minutes for urban hydrological applications.

2.2.4.3 Dynamical downscaling

Dynamical downscaling constitutes the other fundamental approach to downscale outputs from Circulation Models (in this case, from Regional scale) (Khazaei et al., 2012). This technique consists on the use of numerical weather tools that solve the dynamical environment and physical processes at finer scales that Global Circulation Models, so they are applied at higher spatial resolution and at a local scale. Dynamical downscaling is used whenever coarse-resolution data must be used to determine local scale impacts (Smid et al., 2018).

In a Regional Circulation Mode (or Numerical Weather Prediction tools, NWP, information from Global Circulation Models is loaded as lateral boundary conditions. This step is crucial for the downscaling process, and from here, the governing equations of the model used for the dynamical downscaling, together with locally specified data, will drive the quality of model outputs. The usual key inputs to start the downscaling are the high frequency (6-hourly) GCM climate data, and the outputs are the local-scale information on future climate (Smid et al., 2018).

There are two major procedures to process data from synoptic to local scale when using a numerical model. In the first one, the resolution of the rid over the whole domain is uniform with a high resolution (for example, Christensen et al., 2007). The second technique uses

telescopic nested domains, where a coarse grid is built over a large area and inside it, finer grids are built until the grid with the highest resolution covers the area of interest. For both cases, an increase in model resolution invariably entails a higher computational cost (Rummukainen, 2010).

From the processes within a cell, the ones than can be solved are approximated via parameterisation, and the ones than cannot be solved are directly outputted by the model. Parameterisation constitutes one f the main sources of uncertainty in dynamic downscaling modelling. This is because the choice of truncation scale is given by the computational abilities, and because the representation of the processes is done in a semi-empirical framework (Palmer, 2012). Numerical modelling of rainfall fields compensates the lack of sub-daily meteorological information than can be found in ground measurements (or when said information is not readily available), which is an important barrier to produce an operational flood modelling framework (Förster et al., 2016; Winter et al., 2019).

Numerical modelling is regarded as a powerful tool to simplify the representation of complex physical processes, and given the ongoing improvement in model efficiency and computational performance, they are becoming more widely used (Lavers et al., 2019).

Application of NWP tools is found from studies regarding global climate projection to projects that cascade the outputs for hydrological applications. The wide implementation of the models lies in the extensive consideration of atmospheric processes to determine fields of meteorological variables (Krysanova et al., 2018). The use of NWP tools to produce rainfall ensembles for flood forecasting allows the quantification of the uncertainty and ultimately the improvement in forecast lead times (Cloke et al., 2008; Smith et al., 2016; Wood et al., 2006). Moreover, the skill of the NWP tools is documented to have increased in recent years, where the lead time has increased up to two days since 2016 (Emerton et al., 2016). This has places the outputs from the numerical tools as a strong option in studies behind the proposal of hazard mitigation strategies (Alfieri et al., 2013).

Convection-permitting modelling

In meteorology, convection refers to the vertical motion of meteorological variables when the vertical profile of temperature is highly sensitive to small perturbations. This instability is usually present in the oceans and the upper atmosphere, but when water vapour rises in the atmosphere, it releases heat and condenses as releases heat as it rises in the atmosphere and condenses. One good example of convective systems are thunderstorms, where the individual convective cells that span over a few kilometres cluster together and can have an extension of tens of kilometres. These storms are usually associated to short-lived intense

rainfall (hours), which determines also the spatial resolution needed from input data to simulate them (Palmer, 2012).

An important feature related to rainfall modelling is the recent development of convection-permitting model (CPM) capabilities (Fowler et al., 2007). This refers to the parameterisation of deep convection and associated rainfall, better representation of the orography as well as variations of surface fields at high resolutions (i.e. less than 10 km). CPMs provide the starting point towards more accurate representation of hydrometeorological extremes. This framework considerably reduces the sources of error in estimations from local to global scale, therefore increasing the applicability of the models at catchment scale rainfall estimation (Patel et al., 2019). When implementing convection-permitting techniques, the numerical model no longer relies on the convection parameterisation scheme, which have been found to be a considerable source of error when implementing Land Surface Models (Prein et al., 2015). Instead, the importance in the physics parameterisations of the model are passed to the microphysics schemes, which solve the development, size, distribution and other properties of the hydrometeors (Ekström et al., 2017).

This approach has been used in numerous studies regarding intense rainfall generation with promising results as it adds value to winter simulations, in complex terrain and in monsoon thunderstorms (Pal et al., 2019; Prein et al., 2013). Applications include the simulation of 1-km rainfall fields over the United Kingdom (Remesan et al., 2015), reproducing diurnal convection cycles (Rasmussen et al., 2017), effect of terrain features in meteorological outputs (Liu et al., 2011) and determining the rainfall in climate simulations of ~3 km (Prein et al., 2013). Convection-permitting modelling is therefore considering a reliable method that provides accurate meteorological information from local to global scale, and helps solving fluxes of heat and moisture (Zhang et al., 2016)

Figure 2.3 shows a conceptual diagram on how CPMs work depending on the grid size. The CPM solves the downward fluxes of the deep convection processes that are solved on the traditional grid, and fully encapsulates and solves the shallow convective processes on the finer grid (i.e. less than 10 km) (Brisson et al., 2017).

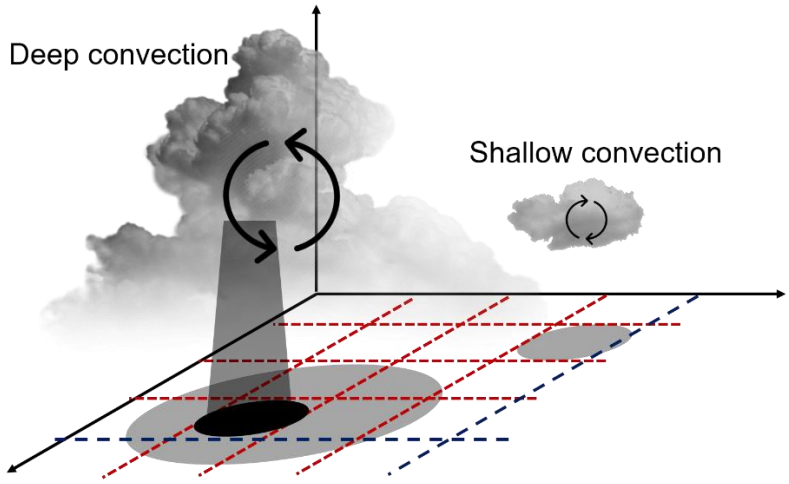

Figure 2.3. Conceptualisation of the convective processes within a cloud as solved by Convection-Permitting Models (adapted from Brisson et al., 2017)

Ensemble Prediction System

A single deterministic forecast made with NWP tools is insufficient to evaluate the uncertainty in the model outputs. To tackle this, several runs are made so than a group of simulations is obtained from varying slightly the initial conditions, the model parameterisations or the type of model used. Each simulation is called an ensemble member and the framework for their calculation is called Ensemble Prediction System (EPS). The members of an EPS are usually associated to a high computational cost, so they are normally run at double the grid size as a deterministic run of an NWP tool.

Ensembles that have been created by varying the initial conditions, the parameterisations of the model (multi-physics) and the type of model (multi-model) allow to estimate the uncertainty in a forecast as well as the most likely scenario when compared to a control forecast (without perturbations). The uncertainty varies from daily according to the synoptic conditions, so the EPS must allow the evaluation of the probability distribution function of the ensemble. This function is used, in turn, to define probabilistic forecasts (scenarios with a probability associated) (World Meteorological Organization, 2012).

When the atmosphere is in a predictable state, this will result in an ensemble with small spread. In other scenarios, the spread of the scenario will be more considerable. Given the current inherent capabilities of the NWP tools, the spread of the ensemble may be large in the model structure, model parameters or models used cannot accurately represent the rapid development of convective systems. A reliable and accurate EPS will deliver an ensemble that will contain the real weather measurements within the simulated scenarios (ECMWF, 2012)

An ensemble of forecasts is a much better tool to inform forecasters about the most likely weather scenario compares to deterministic runs. However, in practice running an EPS is computationally very expensive to extract some information from a single run, so the number of ensemble members must be reduced. Moreover, statistical analysis needs to be performed every time there is a variation in the conditions to run the ensemble, which has made difficult its implementation for forecasting purposes. However, there are currently European projects dedicates at the optimisation of these powerful numerical tools. They are outlined in section 2.4. (Bowler et al., 2008)

A variation of the EPS has been developed and implemented in flash floods and urban hydrology scenarios. When the ensemble allows the creation of forecast ensembles of meteorological variables with a lead time of several hours (Collier, 2007), called Short-Term Ensemble Prediction System (STEPS), that creates a dynamically weighted ensemble product, where the uncertainty is analysed from the meteorological analysis of the simulated variable of interest (Zanchetta et al., 2020). This ensemble has the same constraints as the EPS regarding the characterisation of convection at sub-grid scale and difficulty to gain useful data from the ensemble. However, lies in the midpoint between observed data (gauges and radar rainfall) and high-resolution NWP, the its application in flash flood forecasting is topic of active research (Cloke et al., 2009).

2.2.5 Data assimilation

Data assimilation refers to the process of combining observational data with Numerical Weather Prediction model outputs to accurately describe the stages of an evolving system. It aims at quantifying the uncertainty to initialise, for example, an ensemble forecast (ECMWF). Rainfall from data assimilation is used in operational weather applications (such as weather forecasting), in land surface processes and the evaluation of numerical tools and observations. The main benefit is, like the merged product, that data assimilation is a combination of sources that is useful to cover data gaps or unmeasured variables and accounting for errors in data and the model while maintaining consistency in the products.

There are four types of data assimilation systems which are a combination between the temporal direction of the analysis (sequential, that only considers the information from the past and up until the time of the analysis, similar to real-time assimilation systems; non-sequential, where the analysis is being done at any point in time and that can incorporate information from the future, similar to reanalysis), and the way that observations are incorporated into de model state (intermittent: batches of data are incorporated, which is computationally efficient;

continuous: data over a long period of time is smoothed and incorporated in the model) (Bouttier et al., 2002).

The main issues related to data assimilation products refer to the consideration of non-linear processes and further errors when the statistics are incorrectly specified. Moreover, if the quality in the data assimilation derived timeseries produces an ensemble with deficient spread in an ensemble, a further forecast is likely to be affected. (Whitaker et al., 2002).

2.2.6 Reanalysis

Rainfall as a product of reanalysis has the advantage of considering several numerical models that can combine their strengths to consider cloud development. The observations assimilated into the system, and the complex interaction of the model variables are preserved, so they have a direct influence in the forecasted rainfall (Golian et al., 2019)

Key limitations of reanalysis data are the natural constraints to a given variable depending on its location. Moreover, the combination of observations and models can introduce a new source of uncertainty, in addition to the ones inherent to observed data and models so diagnostic variables, such as precipitation and evaporation must undergo extra checks to ensure their applicability to flood studies (Dee et al., 2016).

Reanalyses produce gridded data with spatial consistency and can be used when analysing rainfall variability and atmospheric circulation (Lin et al., 2014). It has the major advantage con assimilating global datasets with spatial and temporal consistency and observations that span several decades. They also incorporate a vast number of variables that would not be able to be analysed individually, and the resulting datasets, although very large, do not require a large computational effort (Dee et al., 2016).

2.3 Stage 2: Estimating flash flood flows

2.3.1 Introduction

Simulating flash flood flows in urban areas represents a major challenge due to the prevailing presence of human-made structures that replace natural flow paths (Hapuarachchi et al., 2011). Rainfall-runoff modelling is a powerful tool to extrapolate current measurements to future projections and further regions, compensating the lack of measurements at a point of interest to obtain reliable hydrological estimation for climate change applications (Beven, 2012; Collier, 2007).

Given the velocity of these events, it is not unusual that flow measurements are unavailable given that river stations are sometimes destroyed during a flood event. In the United Kingdom, the period of record of some of the gauges of the network has been halted due to a hydrometeorological event, as reflected in the timeseries of the National River Flow Archive. For example, the records of gauge 72004 “Lune at Caton” were “severely damaged” in January 1995, where the peak flow during the event had to be estimated through hydrodynamic modelling Another gauge damaged during a flood event is the 45007 “Exe at Trews Weir”, which shows faulty records since an event in October 2000, and was repaired a year later. Finally, the gauge 23001 “Tyne at Bywell” (the main river station on the Tyne river) which measures flows for a 2175.6 km^2 catchment, that after an event in December 2015, there is a documented modification to the top limb during flows greater than 1130 cumecs.

Some studies have found that variations in the temporal resolution of the rainfall used to drive urban hydrological models has a huge impact in the results of the modelling and this aspect is more important than the spatial resolution of the simulations (Ochoa-Rodriguez et al., 2015). On the contrary, other studies show that there is larger sensitivity to the spatial resolution of the inputs, more that the temporal resolution of the rainfall information (Bruni et al., 2015). Furthermore, other analyses show that the drainage network in urban watersheds reduce the importance of spatial variability of the rainfall when simulating flooding (Smith et al., 2005). These contrasting results show that the result of the hydrological modelling is highly dependent on the rainfall variability and the characteristics of the watershed (Yang, Smith, et al., 2016), that also found that when simulating runoff from rainfall with different timesteps, Yang et al. (2016) found that a increment in the time interval of the rainfall timeseries results in a decrease in the simulated flood peak.

Hydrological modelling, therefore, provides a reliable tool to simulate flash flood flows in urban areas. Model outputs are used to analyse the near real-time response of urban catchments to intense rainfall, providing early warnings and other important tools for food risk reduction (McKee et al., 2016).

2.3.2 Parameterisation of urban areas in hydrological models

Parameterisation is the process of assigning the parameter values that will be used in the numerical modelling. These values are aimed at representing physical processes that are not explicitly considered in the model’s governing equations. In urban areas, the consideration of pervious and impervious surfaces accounts for the contribution of the land cover to surface runoff, so the use of satellite imagery to discretise the catchment before hydrological modelling takes place is common practice (Mason et al., 2010).

As stated in Chapter 1, the present research will deal with urban riverine response. If the surface runoff had been the variable of interest, then the overland flow components would have needed to be considered. As a brief note, the estimation of surface runoff after a rainfall event in an urban area commonly considers infiltration losses as well as evaporation and interception (Eldho et al., 2018). Other processes that are accentuated or of relevance in urban areas (apart from overland runoff), include: stream flow, tidal variations, storage properties of structures in the catchment such as ponds and retention basins (Sikorska et al., 2018).

2.3.2.1 The Hydrological Response Unit

To parameterise the response of urban catchments to intense rainfall, several approaches consider urban and non-urban land cover as separate units, where parameter regionalisation allowed areas with characteristics from each region to behave in a different way, regardless of their location (Krebs et al., 2016). These are called Hydrological Response Units (HRUs) which are defined as the smallest spatial unit in the numerical model that responds to climatological inputs. The discretization of catchments makes up for the computational high cost associated when simulating large watersheds that require modelling at fine scale (Kalcic et al., 2015)

To create HRUs, landscape layers are needed (for example, subcatchments, topography, soil type, slope, land use/land cover, see Figure 2.3). Each pixel in the basin will have its own combination of landscape classifiers where the relevance of each can be user-defined (Pina et al., 2016). This reduces the complexity of the domain and reduces the computational costs because if multiple HRUs are assigned the same properties but are not spatially contiguous, they can still be grouped and the processes are solved similarly (Chaney et al., 2016; Teshager et al., 2016). However, if none of the aforementioned landscape layers are relevant in the study area, for example a flat catchment, then other processes become more dominant (such as surface-subsurface interaction or the role of groundwater) and instead these have to be considered as landscape classifiers. For example, HRUs can be built from the thermodynamics that govern the land surface energy balance, rainfall-runoff transformation, and groundwater storage and release (Zehe et al., 2014). The configuration of the HRUs is subject to the accuracy of the representation of the physical processes in the landscape layers (Savvidou et al., 2018).

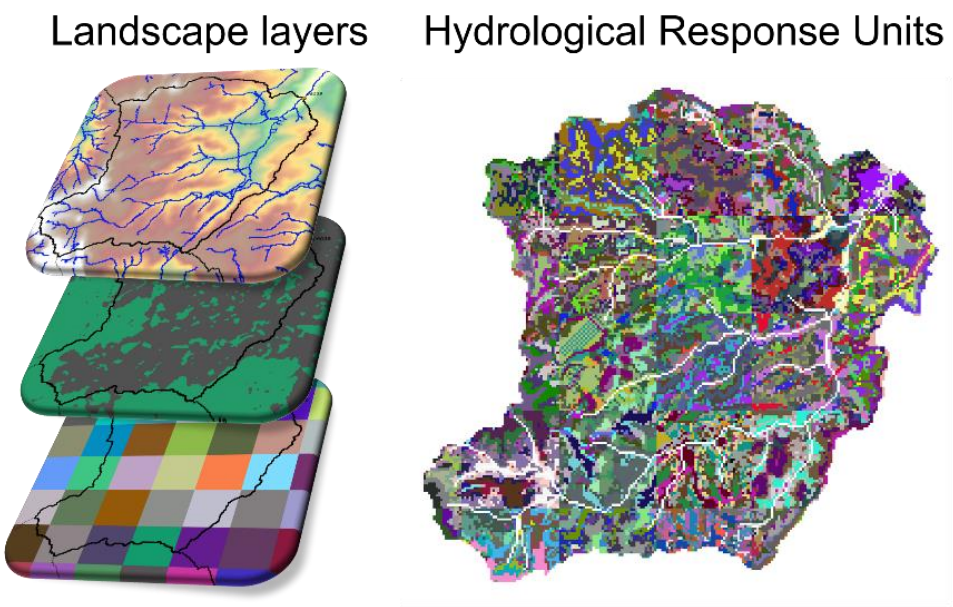

Figure 2.4. Conceptualisation of the elements and configuration of a catchment discretised in Hydrological Response Units

2.3.2.2 Diversion of flow within a cell to storage/river

Other approaches consider the runoff from building features, where the effective rainfall on roofs is calculated (green roofs are also considered), runoff from impervious surfaces is diverted to theoretical detention storages and outflow hydrographs are calculated. Flow is then routed directly to the sewage system -in the case of roofs- or to the nearest river cell -in the case of impervious surfaces- (Krebs et al., 2014). Despite the potentially necessary consideration of the sewage network and rainfall runoff modelling of the catchment, it has been documented that the critical phase of the event occurs when the sewage network capacity has been surpassed, so that the most common approach to urban flood modelling is to consider all manholes as “virtual reservoirs” where surcharged water is temporarily stored and then routed back to the drainage network if the operation capacity has not been exceeded. This method has been proven appropriate for flood damage studies where the numerical modelling focuses on the overland flows (Maksimović et al., 2009).

To parameterise the response of urban catchments to intense rainfall, several approaches consider urban and non-urban land cover as separate units, where parameter regionalisation allows areas with characteristics from each region to behave in a different way, regardless of their location (Krebs et al., 2016).

Another study that aimed at parameterising the response of an urban catchment was carried out by Cuo at al. (2008) who proposed that land cover could determine whether a surface pixel

will be treated as pervious (and solved using the infiltration parameterisation of the model) or impervious. In the latter, runoff can either (a) go to a hypothetical detention storage or (b) be immediately routed to the nearest river cell. Detention storages drain as a linear reservoir directly to the closest river cell, so the drained volume reaches the river channel at the same time-step. This detention-release scheme allows runoff generation from impervious surfaces to be emulated. A conceptualisation of the behaviour of a land cover pixel classed as urban (impervious with a fraction of pervious) is shown in Figure 2.4. Here, "detention" refers to the surface runoff that goes to flood detention ponds (that either serve as risk reduction feature or for irrigation purposes). On the other hand, "storage" refers to water that is stored near manholes as a consequence of the drainage network being saturated, and that is routed directly to the river channel in the closest pixel from which it was drained. Here, the total runoff available in a given grid cell is assigned as runoff in impervious and pervious areas (rf_i and rf_p, respectively, units m timestep^{-1}) according to the fractions (f_i and f_p, respectively). From the impervious area, a fraction goes to detention (D_i, units m timestep^{-1}) according to the detention fraction (f_d). From the detention pond, water is slowly released (D_o, units m timestep^{-1}) according to a coefficient that determines the decay in detention (C_{dd}, units timestep^{-1}) (Cuo et al., 2008).

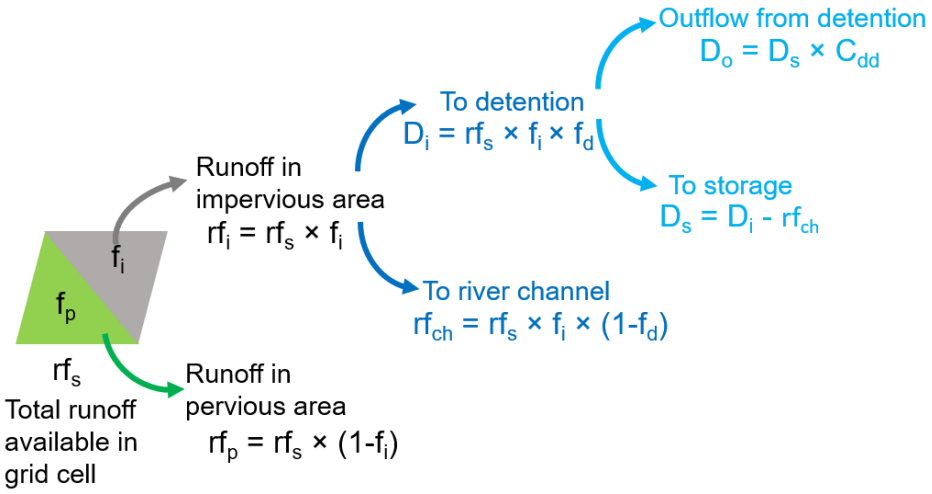

Figure 2.5. Conceptualisation of the generation of surface runoff in an urban pixel according to Cuo et al. (2008)

2.3.3 Numerical models used to characterise the hydrology of flash floods

Numerical models used to reproduce the rainfall-runoff relationship can be classifies into lumped, distributed and semi-distributed categories depending on the spatial variability of their inputs (Sitterson et al., 2018). Lumped models consider the catchment as a homogeneous

area; semi-distributed models solve the variation at a smaller scale than lumped, but some variables are not solved for each grid cell; and fully distributed models are ones where the spatial variability in the whole catchment is considered. The type of model implemented in a given study is dictated by the importance of the physical processes present in the event of interest.

The following sections describe in detail each type of model, including its structure, strengths, and weaknesses, and a summary of the main characteristics for said is given in Table 2.2.

Table 2.2. Overview of the main characteristics of the numerical models for hydrological simulations (after Sitterson et al., 2018)

Feature	Lumped	Semi-distributed	Distributed
Landscape layers	The entire catchment is simulated as one unit.	Combination of lumped and distributed parameters	Spatial variability is considered
Input data	Areal averaged data	Areal averaged and by subcatchment	Grid cells have their own data
Strengths	Computationally efficient, delivers good averaged products	Able to represent main landscape features	Hydrological processes fully accounted for
Weaknesses	Loss of spatial variability, usuitable for large catchments	Averages data into subcatchments	Data demanding, computationally expensive

2.3.3.1 Lumped models

Lumped models do not discretise the catchment, but rather use areal average-parameter, or values that are representative of the whole area. Regarding computational efficiency, lumped models have the best performance of the three types of hydrological model discussed, which is an advantage during the calibration process (Miller et al., 2017).

The consideration of urban systems involves several spatially varied parameters. This can be a challenge given the capabilities of lumped models. Nevertheless, such models have been widely used in flow forecasting studies and are currently implemented in low-impact urban planning (urban development that procures the ecological integrity of aquatic and terrestrial environments) and they still maintain their operational potential due to the simplicity and low data requirements. For example, this type of model is used for operational purposes by the

United Stated National Weather Service to produce flash flood guidance directives. More recently, its application to flash flood studies was explored, and the model type shown to deliver satisfactory results in a mountainous catchment environment (Kobold et al., 2006).

Despite the complexity of the component of surface runoff in urban areas as stated in Section 2.3.2, lumped models have also been applied in urban environments. In this case, the overland flow is calculated with the help of conceptual models such as the Soil Conservation Curve, or by solving the mathematical models such as the Saint-Venant equations (Eldho et al., 2018).

To answer the question of the need for complexity of rainfall information in urban environments, Sikorska et al. (2018) carried out a comparison study between two rainfall disaggregation methods with different levels of complexity. One of the methods is a backward approach, where the duration of wet spells is estimated based on simulated annual peaks, and the other is based on micro-canonical cascade models that do not depend on runoff to estimate the spatial distribution of the rainfall (also mentioned in section 2.2.4.2). The rainfall obtained with those two methods was applied to a lumped model in nine catchments. The found that, for both rainfall generators, the lumped model was not sensitive to the complexity of the obtained rainfall and concluded that the choice of disaggregation methods should depend on the objective of the study and the availability of the data. They also stated that for urban catchments, the behaviour of a lumped model may be much different (Müller-Thomy et al., 2019).

Finally, other limitations of the use of lumped models for flash food characterisation or forecasting are their limited capability given their coarse resolution and their unsatisfactory performance in catchments with sparse gauges (Huang et al., 2019) because of their need for calibration.

2.3.3.2 Semi-distributed models

Regardless of the catchment discretisation procedure, hydrological modelling should aim at reproducing the response of the catchment to intense, localised rainfall. When it comes to urban catchments, the delineation and implementation of contributions to the urban coverage to the runoff are of special importance. These processes might be well represented in small catchments, but for densely populated areas, there is an additional challenge when reproducing the fast response of a basin with a considerable percentage of impervious areas (Tanouchi et al., 2019).

Semi-distributed models discretise the catchment in smaller areas or subcatchments, that can be described as an array of Hydrological Response Units, which will route the flow from a grid cell to a point in the river network according to the model structure and parameters. The HRUs,

as stated in section 2.3.2.1 are obtained depending on the landscape classifiers implemented (such as slope, land cover that reflects the degree of imperviousness, infiltration properties, etc). The outlet point for any catchment is represented numerically by a computational node, and in urban areas this is usually an inlet to the sewer system.

To drive the model, rainfall is numerically assigned to the catchment and runoff volumes are calculated. In some models, runoff is calculated per pixel and then routed to the nearest river cell depending on the topography; in others, runoff is calculated per subcatchment and then directed to the river network so that hydrographs for every subcatchments can be obtained (Pina et al., 2016).

These models combine the computational efficiency of lumped models when incorporating averaged values across the catchment, but also represent a major improvement given the possibility to consider at least some spatial variability.

2.3.3.3 Distributed models

Fully distributed hydrological models are the best estimation of the catchment properties in a numerical model. They are able to integrate local geographic information and are defined by a numerical mesh, where rainfall is applied to each mesh element, for which runoff is then calculated. When coupled to hydrodynamic numerical tools to produce surface runoff they can yield an accurate estimation of overland flow (Pina et al., 2016). Given that distributed models are able to parameterise the catchment response to seasonal changes, there is no need for long timeseries of meteorological variables for parameter calibration, and they are also better suited for studies in poorly gauged or ungauged catchments. The large amount of information that distributed models require make them suitable for flash flood modelling studies. Outputs from this type of model are liable to be used as a reference for postflood indirect estimation of peak flows (Amponsah et al., 2016). Discretisation of urban catchments using distributed models are no exception to large data requirements as they built upon a vast amount of landscape information (land cover, land use, topography, etc.) (Goodrich et al., 2012).

Unsurprisingly, these models also give better results in the evaluation of the impact of meteorological extremes than the outputs from a lumped model (Huang et al., 2019). However, since they are driven with large amounts of data (to represent as many features of the landscape as possible), they tend to be more computationally expensive than lumped and semi-distributed models (Fry et al., 2017). This downside of distributed models in the computational requirements required, and given that information to run simulations in this framework is not always readily available, puts the usefulness of distributed models under question compared to simpler models (Hapuarachchi et al., 2011).

2.4 Applications of the cascade in flood characterisation and forecasting projects

2.4.1 Projects on flood characterisation

Numerical applications of the characterisation of past flood events allows verification and benchmarking of the application of numerical models to reproduce the physical processes that lead to a flash flood, identify modelling strategies to enhance model performance and factors that increase or decrease model accuracy. Event-based hindcasting analyses facilitate the determination of rainfall evolution, its relation to the start in the rise of water levels, analysis of the catchment response patterns, determine influence of seasonal phenomena and information on the interaction of the natural setting and human-made structures, if applicable.

At a wider glance, the study of historical events allows the identification of vulnerable areas that are at risk of flash flood (Coulibaly, 2008). An example of application of information on historical events is the definition of thresholds on rainfall intensity and duration that above which certain damage would be expected (EXIMAP, 2007). The preliminary detection of exposed areas facilitates the prioritisation of focused actions to assess and modify the adaptation and mitigation strategies accordingly (Arnaud et al., 2002) and allows understanding of the relationship between changes in precipitation patterns and flooding (Sharma et al., 2018).

This section lists some of the active projects that implement the hydrometeorological cascade for flood estimation and forecasting at different scales. The rationale behind these studies serves a background for the implementation of the cascade in urban areas and helped identifying the areas of opportunity.

2.4.1.1 HYdrological cycle in the Mediterranean EXperiment

HyMeX (HYdrological cycle in the Mediterranean EXperiment) is a project dedicated to the analysis and quantification of the elements of the hydrological cycle and associated processed in the Mediterranean, in specific, the impact of extreme hydrometeorological events, and seasonal and decadal variations in basin processes that are typical for the region (Drobinski et al., 2014).

This project focuses on five points, which relate to the water budget in the Mediterranean basins, coastal dynamics as well as intense rainfall in flash flooding. This European project directed a study on the impacts of rainfall produced by deterministic and probabilistic systems used for flash flood forecasts. They implemented a hydrometeorological cascade utilising

dynamically downscaled rainfall using a Numerical Weather Prediction tool and a fully distributed hydrological model to determine the rainfall-runoff relationship during a flash flood in a catchment with a sea outlet (Roux et al., 2020). Results show that an ensemble of scenarios behaves much better that a deterministic run, with a satisfactory cascade performance despite the individual low forecast skill of each ensemble member. They also showed that the uncertainty analysis of the ensemble spread can directly benefit early warning systems.

2.4.1.2 IMproving Predictions and management of hydrological Extreme

The IMPREX project is a work at European level that aims at reducing the vulnerability to hydrometeorological extremes by improving its numerical representation. One of the case studies focused on the impact of a second flash flood in a catchment that had already had one event (Silvestro et al., 2016).

The area of study is situated in the Liguria Region, in Italy, where two flash flood events (one on the 25 October 2011 and the second on 4 November 2011) occurred in two places 50 km apart (the coastal region where the towns of Monteroso and Vernazza are located, and in the city of Genoa, respectively). The premise of the work explores the impact of intense rainfall on already saturated soil during a first flash flood event, to cause a second event.

Maximum hourly rainfall values were recorded at 150 mm and 160 mm for the October and November events, respectively, which agrees with the rainfall associated with the definition of flash flood from previous studies (see section 1.2.1). They set-up a cascade modelling framework that starts with a numerical model to obtain precipitation estimates from the merged product of rain gauge data and radar rainfall at hourly, a distributed hydrological model and a 2-D hydrodynamic model to predict flood depths and extents and damages after the inundation.

The study focuses mostly on the final outputs of the cascade as it builds on previous research on the stages of the modelling cascade. This shows the usefulness of the cascade to reproduce extreme flash flood events.

2.4.1.3 Flooding From Intense Rainfall

Flooding From Intense Rainfall programme, comprised three projects that explore convective rainfall forecasting techniques, numerical modelling of catchment response to intense rainfall and a novel proposal of end-to-end forecasting system, aimed at advancing the current understanding of flash flood and surface water risk (Flack et al., 2019).

This project was based on the outcomes of the Pitt Review (2008) and the Living With Environmental Change United Kingdom Flood & Coastal Erosion Risk Management Research Strategy, which highlight the urgent need to develop a better understanding of flood risk by improving a) the representation of meteorological events affected by climate change, such as severe summer convective events, b) the understanding of catchment sensitivity to these events given changes in land use and c) the estimation of the hazard by surface water flooding and its relationship with the previous two points. The FFIR programme operates under an end-to-end framework (see section 2.1.1 for a definition of “end-to-end”) to forecast flash flooding and surface overland flows. The whole project involves the use of remote-sensed rainfall as well as outputs of a Numerical Weather Prediction model to drive runoff estimations via semi-distributed hydrological modelling, and also the retrieval of streamflow observations that serve as boundary conditions for hydrodynamic modelling. However, given the lack of data for the three stages of the modelling, the full cascade could not be validated and the propagation of uncertainty through the cascade remained an unanswered research question (Flack et al., 2019)

2.4.2 Projects on flood forecasting

Following Hapuarachi et al. (2001) and Singh et al. (2002), rainfall is the main driver for hydrological modelling for flash flood forecasting purposes. As a result, it is important to determine how rainfall accumulates and what is the response of the catchment. Under intense rainfall scenarios, the flash flood potential is driven by catchment properties (such as permeability, impervious fractions, land use and land cover and soil types). Understanding these characteristics is crucial when evaluating the uncertainties to deliver accurate flood warnings (Hapuarachchi et al., 2011).

Flood preparedness strategies refer to timely warning systems that avoid losses by informing the potential hazard and time of intense rainfall. Early warning constitutes the main strategy for flood defence (Ma et al., 2018). An accurate warning system for intense rainfall related flash flooding requires timely information on the precipitation (Collier, 2007), and as rainfall estimation improves, best practices cascade this information into rainfall-runoff models to provide forecasts of river flows.

2.4.2.1 Global Flood Awareness System and European Flood Awareness System

The Global Flood Awareness System (GloFAS) was jointly developed by the European Commission and the European Centre for Medium-Range Weather Forecasts (ECMWF). It deals with developing flood forecasting tools at continental scale to characterise hydrometeorological hazards and the development of flood events. Hydrological forecasting

at daily scale are done by using meteorological forecasts as drivers for a hydrological model. Outputs include overall river conditions at global level that serve as starting point for continental overviews and analyses.

The meteorological modelling is carried out using an ensemble approach and done by the European Centre for Medium-Range Weather Forecasts (ECMWF) Integrated Forecast System (IFS) through a data assimilation system that involves the use of a Numerical Weather Prediction tool. The relationship rainfall-runoff in computed using the Hydrology Tiled ECMWF Scheme for Surface Exchanges over Land Model (HTESSEL), which is also used in the ECMWF IFS. At European level, the hydrometeorological cascade is also implemented, with the only difference in the hydrological model. At continental scale, the LISFLOOD hydrological model is set up to compute ground water and surface processes. Groundwater is simulated using a system of two linear reservoirs, while overland flow is routed from the outlet of each cell to account for surface runoff.

Given the scope of GLoFAS and EFAS, it is not surprising that the calibration and validation processes are made over a wide area and using thousands (1287) gauge stations (Alfieri et al., 2013).

2.4.2.3 Met Office Global and Regional Ensemble Prediction System

In the United Kingdom, the Met Office (the national weather service) is the institution that produces weather forecasts. It uses an ensemble approach, and the tool to produce those forecasts is called the Met Office Global and Regional Ensemble Prediction System (MOGREPS) (Bowler et al., 2008). It has the capacity to produce global forecasts (MOGREPS-G) up to a week in advance as well as regional ensembles (MOGREPS-UK) which issues 5-day forecasts for the whole country. The meteorological model for MOGREPS-G is run at grid points every 20 km while the MOGREPS-UK simulations are run at 2.2 km spatial resolution and has 70 vertical levels (Met Office, 2019). The importance of model resolution and vertical levels is discussed in sections 2.2.4.3 and 3.3.1.1, respectively.

The Met Office also uses a Short-Term Ensemble Prediction System (STEPS) approach (see section 2.2.4.3 for details) that merged extrapolated radar rainfall with deterministic forecasts obtained with the United Kingdom Variable (UKV, part of the Met Office Unified Model, a numerical tool for weather and climate applications) to produce short-range ensemble forecasts y varying the initial conditions or the parameters of the model (Met Office, 2019).

An example of an end-to-end cascade that uses outputs from the MOGREPS-UK was implemented in Glasgow during the 2014 Commonwealth Games as a pilot project by the Scottish Flood Forecasting Service (SFFS). The system used STEPS outputs that were used

in a grid-to-grid model to transform rainfall into surface runoff. The outputs of the modelling were delivered as inundation maps that were corrected with those from the library of the Scottish Environment Protection Agency and made operational for impact assessment, which was divided in four categories (population, utilities, commercial properties and community services) to deliver effective warnings and information on likelihood of impacts that are relevant to each end user (Speight et al., 2018).

There is also an existing partnership between the Met Office and the Environment Agency under the ongoing institution of Flood Forecasting Centre. The forecast products include all forms of natural flooding, namely fluvial, surface water, coastal due to storm surge and groundwater. This information is delivered directly to Category 1 (emergency services, local authorities and NHS services) and 2 responders (co-operating bodies such as the Health and Safety Executive, transport and utility companies) as well as support for the Environment Agency (in England) and Natural Resources Wales.

2.5 Conclusion

One of the tools used to reduce flood risk is the numerical characterisation and forecasting of such events which needs to overcome the numerical and measuring difficulties that the quick onset of flash flooding entails. Another major challenge associated with the hydrometeorological characterisation of urban flash floods is the magnitude of the rainfall that precedes the event (Braud et al., 2014). This challenge is augmented by the consequent modelling of the hydrological response in an urban catchment, that may be highly responsive to climatological forcing (Collier, 2007). Given the hazard that flash floods pose, it is crucial to improve the preparedness and understanding of the hazard.

To this purpose, effective numerical and statistical tools have been developed to produce accurate and reliable products, all of which have undergone extensive study into ways to quantify the uncertainty and reduce the sources of errors. Different models can be linked via a cascade framework methodology, which allows the numerical representation of the natural processes that lead to a flash flood. The hydrometeorological modelling cascade represents an efficient framework for flood risk reduction and can be applied in urban areas under intense rainfall scenarios. It is a two-stage modelling technique that allows error propagation and sub-daily analysis of physical processes.

The cascade has been successfully implemented in a wide range of scenarios, scales and purposes. It can be applied with an end-to-end approach: starting with the rainfall, using this to drive a hydrological model, which in turn feeds into a hydrodynamic tool and finally

delivering flood risk scenarios to end users. This shows that this framework is suitable to study in detail the development of flash floods associated with intense rainfall in an integrated approach,

For research purposes, the application of the cascade to reproduce the meteorological and hydrological processes is described in the present chapter, which also presents the available sources of rainfall products and the three types of numerical hydrological models.

The choice of precipitation products to drive a rainfall-runoff model depends on the availability of the data and objective of the study (Müller-Thomy et al., 2019), and given the sources of error in the products as stated in this chapter, also on the resources available to perform the sensitivity analyses and error reduction methodologies. All the mentioned tools to produce rainfall fields are prone to measurement, statistical or calibration errors. The three types of physically based hydrological models have documented strengths and deficiencies, and the strong feature in one is often contrasted by the strength of another model in another aspect.

The application of dynamical downscaling techniques for rainfall simulations constitutes an appropriate option for the delivery of sub-daily outputs when hourly information from radar and gauges is not available. Consideration of the urban landscape in the atmospheric processes is crucial, so a parameterisation of the urban canopy must be done explicitly (Wang et al., 2019). From the thee physically based hydrological models, the semi-distributed tools lie in the midpoint between model performance but also regarding computational efficiency by incorporating the strengths of both the lumped and the distributed models. Using a semi-distributed tool, the parameterisation of an urban catchment will be possible without compromising computational efficiency.

in rainfall runoff modelling could potentially be data demanding as the sewage network is part of the city layout; however, this information is usually considerably difficult to obtain given the level of detail that it entails, so that a simple approach must be designed to overcome the lack of data and still produce reliable estimations of flood flows.

The following Chapter outlines the proposed methodology to characterise intense rainfall and the response of an urban catchment during a flash flood.

Chapter 3

Hydrometeorological modelling framework

To fulfil the aim of the study (stated in section 1.3) and following the strengths and weaknesses of the available tools to represent the stages of the cascade described in Chapter 2, this section presents the modelling framework to characterise the atmospheric processes and reproduce the hydrological response of an urban catchment under intense, localised rainfall while allowing for uncertainty estimation and propagation. The spread of the meteorological ensemble will be assessed, and model performance will be estimated at each stage.

The modelling chain starts with a Numerical Weather Prediction (NWP) model to produce rainfall fields. The meteorological output will be generated at an hourly scale to allow the influence of the urban canopy on rainfall generating mechanisms to be explored. The choice of using a numerical model to produce sub-daily precipitation outputs stems from the need to overcome the recurrent unavailability of meteorological input data for modelling purposes. (Förster et al., 2016; Kendon et al., 2018). The second part of the modelling framework comprises a rainfall-runoff, physically based hydrological model that will account for the different behaviour of urban and non-urban areas. The use of this model follows a recent study to benchmark hydrological model performance at daily scale across Great Britain (Coxon et al., 2019), where the application of different parameter bounds at sub-daily scales for a given catchment is yet to be explored. The meteorological model is described in detail in Section 3.1, and the hydrological tool is documented in Section 3.2. Justification of the use of said tools is also included in the correspondent section

The hydrometeorological modelling framework is illustrated in Figure 3.1. It starts with the retrieval of meteorological and static geographic data for meteorological modelling, where the preprocess consists of horizontally interpolating the input data to the model grid. Then, the data is dynamically downscaled (see section 2.2.4.3 for details on this concept) to the finest domains, and physics schemes are used to produce the atmospheric fields, where rainfall is the simulated output of interest. Observed rainfall information is also retrieved.

The hydrological modelling starts by determining routing information for each river and catchment masks for the gauges in the catchment. Then, the area is discretised in Hydrological Response Units (HRUs, see section 2.3.2.1 for details on this concept). Timeseries of rainfall, potential evapotranspiration and discharge processed into the HRUs,

where both simulated and observed precipitation data are used for simulation. Finally, the flow at the outlet point of interest is calculated.

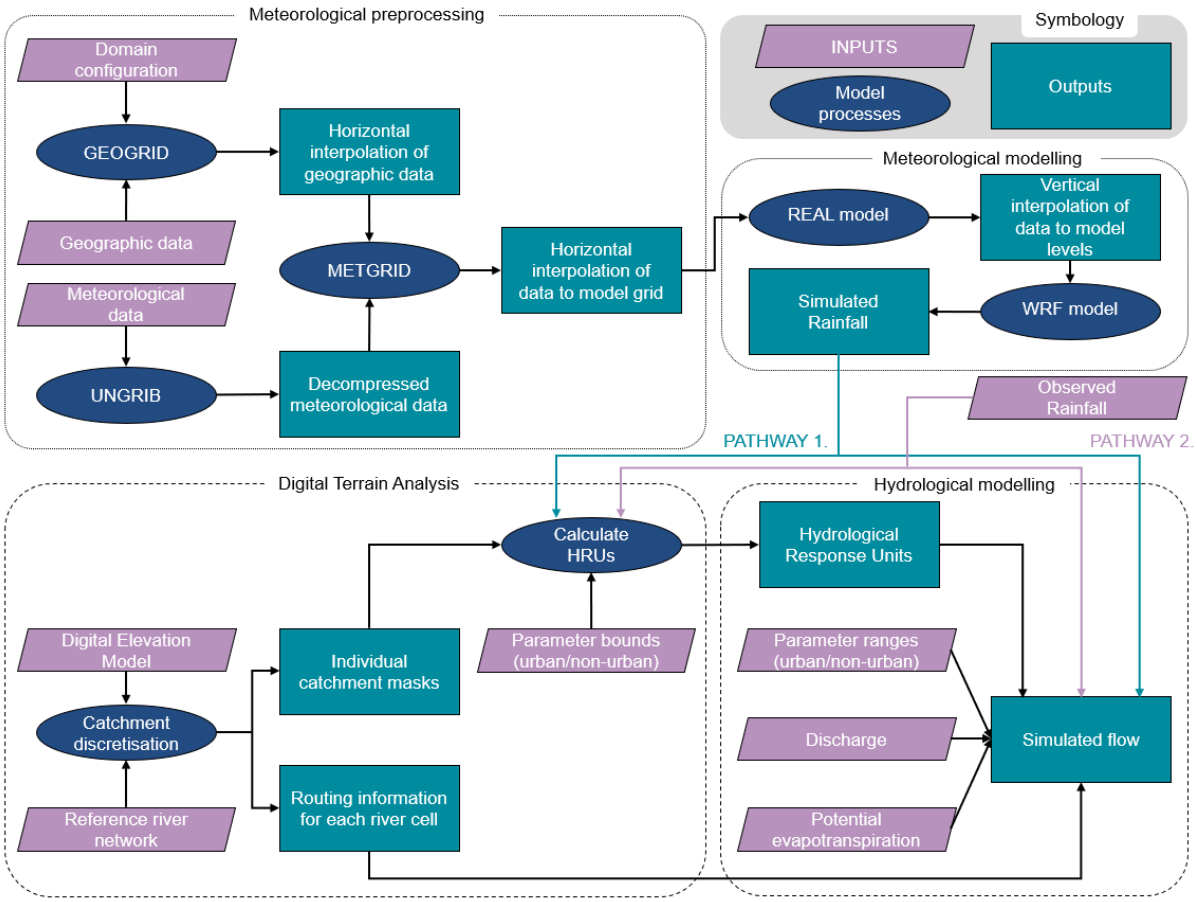

Figure 3.1. Workflow of the hydrometeorological modelling framework. For a detailed description of each stage, refer to the corresponding sections of this Chapter

3.1 Meteorological modelling

3.1.1 Model selection

The numerical tool implemented in the first stage of the hydrometeorological framework is the Weather Research and Forecasting (WRF) model, which was chosen given its documented strengths and weaknesses when reproducing the meteorological conditions that lead to flash flooding. The model has been successfully applied in a wide range of cases that are closely related to the aims of the present study, such as high-resolution simulations of convective events and precipitation that lead to exceptional flood events in the United Kingdom (Pieri et al., 2015; Remesan et al., 2015), forecasting of intense precipitation in urban areas (Patel et al., 2019), characterisation of synoptic-scale atmospheric circulation associated with this

intense rainfall events (Campos et al., 2015), warm season, mesoscale rainfall forecasts (Jankov et al., 2005) and convective storms that are significantly enhanced by the orographic component (Cassola et al., 2015) in catchments that are prone to flash floods (Kumar et al., 2014). This means that there are good grounds to determine that the WRF model is an appropriate numerical tool to simulate a) convective precipitation, b) meteorological settings of a flash flood, c) effects of urban canopy in atmospheric processes. The novelty of the present study is the integration of all the settings to explore the sub-daily impacts of the urban canopy in patterns and distribution of intense-localised rainfall. The latest version is the result of eighteen years of development which have ensure the applicability of the model in both simulations based on atmospheric observations and idealised cases, on domain extents from hundreds of meters to thousands of kilometres (Liu et al., 2012; Wee et al., 2012). The WRF model allows for the explicit treatment of cumulus convection and other sub-grid scale processes (such as turbulent vertical mixing in the planetary boundary layer and its interaction with the surface layer) that occur at smaller scales than those at which the model is able to solve for. With the inclusion of microphysics schemes that solve heat and moisture fluxes that produce precipitation (Ekström et al., 2017), the model successfully reproduces convective systems at hourly time scales and for high resolutions (less than 10 km) when switching the cumulus parameterisation off (Prein et al., 2016). The WRF model as a convection-permitting tool has been applied even at continental scales (Zhu et al., 2016), showing the value of implementing a convection-permitting scheme to reduce the temperature bias at high and low altitudes (Karki et al., 2017) and to analyse variations in the water cycle under climate change scenarios (Rasmussen et al., 2017).

Another useful feature of the numerical tool is the inclusion of urban canopy models to characterise atmospheric fluxes in cities given their distribution of sources and sinks of heat and moisture. The WRF model has documented applications in air quality studies and temperature variations at city scale due to rapid urbanisation and changes in land use (Bhati et al., 2018; Fallmann et al., 2013), even in short-lived events (Salamanca et al., 2011). Furthermore, the model has also been implemented in heatwave studies to estimate urban heat island (UHI) impacts on population health (Giannaros et al., 2018). This means that the WRF model has documented capabilities to be implemented in studies that involves, intense, localised rainfall, and in urbanised catchment where the impact of the urban land cover is of interest when resolving meteorological features.

Finally, being a highly sophisticated and accepted numerical tool for rainfall simulation, access to learning and support resources facilitates its use from the compilation to the post-processing.

3.1.2 Description of the meteorological model

The Weather Research and Forecasting (WRF version 4.0) model is a state-of-the-art, meso-scale numerical weather prediction (NWP) tool used in meteorology for research and operational purposes (Skamarock et al., 2019).

The model uses a terrain-following non-dimensional hydrostatic vertical coordinate system that takes the value of 1 at the surface and decreases to 0 at the top of the model (where pressure is considered constant) and is defined by:

$$\eta = \frac{p_h - p_{ht}}{p_{hs} - p_{ht}} \tag{3.1}$$

where p_h refers to the hydrostatic component of the pressure at a given point, p_{hs} is the value at the surface, and p_{ht} is the value at the top of the model (http://www2.mmm.ucar.edu/wrf/users/model.html, last access 15 July 2019). The independent variables can be expressed in any system of units commonly used to describe atmospheric pressure (bars, millibars, Pa, millimetres of mercury).

The horizontal grid is the Arakawa-C staggered grid, where prognostic variables (variables that are integrated in time) lie at the centre of the cell (or θ points) and velocities are at the grid cell faces (u and v), as shown in Figure 3.2.

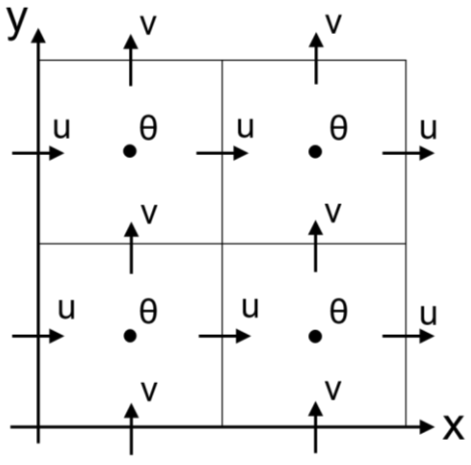

Figure 3.2. Horizontal grid structure of the Arakawa-C grid in the WRF model. Adapted from (Kang et al., 2014)

The nesting capabilities of the WRF model allow for high-resolution grids to be embedded in coarser domains. Any number of nested domains can be placed anywhere within the parent grid considering five relaxation rows and columns (where the values from the coarsest grid to the large-scale forecast are nudged or “relaxed”), and all will have the same number and spacing of vertical levels. A model configuration with multiple telescopic domains enables the downscaling of gridded lateral boundary conditions to turbulent scales while avoiding computationally expensive simulations with a uniform fine resolution over a large domain (Moeng et al., 2007).

Telescopic domains in the WRF model can feature one-way or two-way nesting. The latter, also referred to as feedback nesting, is used when the input atmospheric data have a coarser spatial and temporal resolution than the required output. When feedback is on, the lateral boundary conditions of the parent domain at the beginning and at the end of a given timestep are fed to the nest. Here, the information is time-averaged and then sent back to the parent, overwriting the value at the corresponding grid point at the end of the time step (Wang et al., 2012). See Figure 3.3 for further details on the configuration of the grid.

3.1.3 WRF preprocessing

Running the WRF requires the retrieval of certain mandatory atmospheric fields from the Research Data Archive, a repository of meteorological and oceanic observations, operational reanalyses and remote sensed dataset to run NWP models. Mandatory fields comprise 2D (sea level pressure, surface pressure and temperature) and 3D data (pressure, U and V components of wind, geopotential height, relative humidity) that is usually taken from global reanalysis datasets (Bhati et al., 2018).

The next step consists of defining simulation domains (location, extent and resolution of the nested grids). Although there are no restrictions on the grid cell ratio of the nested domains, the recommended values are always odd numbers (Skamarock et al., 2019) such as 1:3, 1:5 and 1:7 (which have been observed to perform reasonably well), being the typical value 1:3 (Liu et al., 2012) because it ensures that the values at the θpoints of the Arakawa-C grid of the child and the parent domains are aligned so the values can be directly copied from the fine to the coarse grid instead of being interpolated and then sent back, ensuring computational efficiency and accuracy, as shown in Figure 3.3.

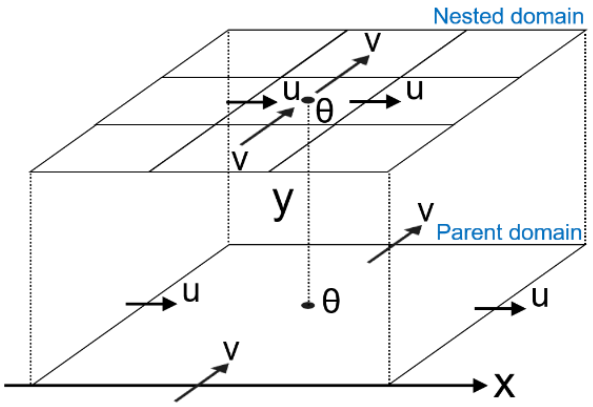

Figure 3.3. Location of the overlap of theta points of parent and nested domain with nesting ratio 1:3

After that, there are three stages of the WRF Preprocessing System (WPS) to prepare the information for meteorological modelling.

Firstly, the program GEOGRID is run to horizontally interpolate the retrieved terrestrial data and any other categorical fields to the model grids. Then, the UNGRIB program's function is to "degrib" the meteorological information (that is commonly stored in GRIB Edition 1 and 2 format) and will read the variables and levels specified in a given variable table that is usually downloaded with the atmospheric data. Finally, the METGRID function Is used to horizontally interpolate the data extracted by UNGRIB into the simulation domains configured by GEOGRID (NCAR, 2019).

3.1.4 WRF solver

3.1.3.1 Vertical interpolation of atmospheric data

Once the atmospheric and the geographic fields have been horizontally interpolated, the WRF solver starts with the vertical interpolation of the information to the predefined η levels using the REAL program. Afterwards, the meteorological modelling is done through parameterisations of surface and atmospheric processes and their interactions. A visual representation of the land-atmosphere interaction as parameterised in the WRF model is shown in Figure 3.4, where the physics schemes studied and implemented are shown and will be detailed hereafter. A more comprehensive conceptualisation of the structure of the WRF model is given in Figure 3.7 after the parameterisations have been discussed.

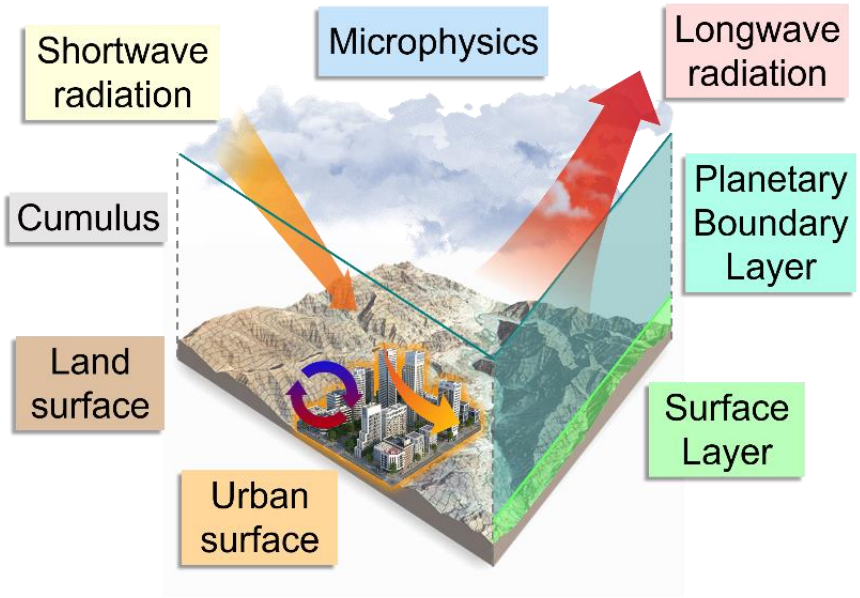

Figure 3.4. Representation of the physics schemes considered for meteorological modelling

3.1.3.2 Physics parameterisations

Microphysics

These physics schemes characterise the hydrometeor formation mechanisms from droplets which form the microstructure of warm clouds. Cloud macrophysics, on the other hand, involve processes that drive microphysics, such as probability distribution functions of humidity and cloud overlap (Morrison, 2010). Although cloud particle size can range from micrometres to centimetres, the microphysics schemes in the WRF model deal with the formation and fallout of droplets smaller than 0.5 mm. The concentration, size and shape of these cloud droplets during the development of hydrometeors defines the type of the interaction of the particles with local wind fluxes, hence determining the influence of cloud in larger physical processes such as lightning, radiation and generation of rain or snow (Lamb, 2015).

Microphysics schemes in the WRF model can be classified into two groups, depending on how they solve the particle size distribution (diameter compared to concentration number in a unit volume). Bin microphysics separate particles into boxes or "bins" depending on their diameter size. Each bin has their own set of equations to determine final particle concentration but given the continuous aggregation or size reduction of cloud particles, the actual concentration is liable to change (Plant, 2014). A large number of bins and the complexity of the numerical methods to describe cloud microphysics make bin parameterisations computationally expensive.

In contrast, bulk microphysics adopt a functional distribution to describe the concentration of particle sizes making it more computationally efficient than the bin parameterisations. The analytic form involves terms that can be easily determined with predictive equations, called free parameters. The gamma distribution, for example, is described as:

$$n(D) = N_0 D^{\mu} e^{-\lambda D} \tag{3.2}$$

where $n(D)$ is total number concentration per unit volume [m^{-3}], D is particle diameter [mm], N_0 is the intercept of the ordinate [mm^{-1} m^{-3}], μ is a shape parameter, and λ is the slope of the distribution [mm^{-1}].

The last three can be free parameters, and depending on the degree of freedom, the bulk microphysics that use the gamma distribution are single-, double- and triple-moment, which can increase the accuracy of the calculated particle size distribution (Morrison et al., 2009).

Although a finer horizontal grid resolution does not necessarily mean a better model performance when estimating precipitation, an appropriate choice of microphysics scheme ensures an adequate representation of subgrid scale processes even in complex topography (Liu et al., 2011).

Cumulus

The cumulus schemes represent the influence of cumulus clouds on the changes in vertical heat and moisture fluxes within a grid cell. These mechanisms are initialised through trigger functions, which determine the presence of cumulus clouds and define the depth and intensity of convection. Changes and intensity of the vertical motions that affect latent heat in a single column will take place until a close assumption is met, and then the cumulus parameterisation is deactivated. Each cumulus scheme features its own trigger mechanism, equations to solve updrafts and downdrafts, and closure assumptions. Since the physical processes are resolved (grid-scale), cumulus parameterisations focus on the collective effect of cumulus clouds rather than their individual behaviour within the column (Pennelly et al., 2014).

There are two types of cumulus parameterisations depending on their trigger mechanism: deep and shallow. Deep cumulus schemes which produce rainfall span across most part of the troposphere, they deal with cooling and moistening on the lower parts and warming and drying on the rest of the atmospheric layer. Shallow cumulus schemes do not usually produce significant rainfall. Spans on the lowest part of the troposphere where turbulent vertical mixing causes instabilities to the cloud layer by cooling and moistening the upper half of the cloud layer while the lower half is subject to warming and drying (Plant, 2014; Stensrud, 2012).

Land Surface

Land-surface models (LSMs) compute heat, moisture and momentum fluxes at the atmosphere-land interface, hence determining mass and energy transfer (Tomasi et al., 2017). The magnitude of these processes is determined by the roughness length (scale of surface eddies) and is heavily influenced by the type of land-use (Dudhia, 2017). In practice, LSMs differ from one another in the amount of soil and canopy layers used to compute temperature and moisture soil profiles.

The LSM provides variables such as sensible and latent fluxes at the surface, skin temperature and boundary conditions for the calculation of potential evapotranspiration. In WRF, the LSM includes a multi-layer soil model solver and a surface hydrology model, and the processes are solved sing prognostic variables such as soil temperature and moisture.

The selection of the LSM is crucial when implementing an atmospheric model to urban environments. This is because the elements of the urban canopy have different thermal properties to the vegetated areas, evoking micro-climate features such as Urban Heat Islands. To maintain numerical stability, the LSM model is coupled with the urban canopy model.

Urban Surface

The WRF model also parameterises the impact of streets and buildings on sensible and latent heat fluxes within the atmosphere at three different levels of complexity. Explicitly accounting for the urban canopy improves the characterisation of momentum and water vapour exchange, hence providing a more realistic and accurate representation of urban environment-atmosphere interactions (Sarmiento et al., 2017). The urban canopy layer parameterisations in the WRF model differ in the complexity of vertical distribution of heat and moisture, and if there is radiation exchange between indoors and outdoors.

Planetary Boundary Layer

The Planetary Boundary Layer (PBL) is the lowest layer of the troposphere where the exchanges of moisture, heat and momentum are significantly affected by the Earth's surface (Cohen et al., 2015). The height of this lower layer of the atmosphere is defined by a temperature inversion, where a warm mass of air lies on top of the coolest part of the PBL. Height of the PBL can range from tens of meters in the where the atmosphere is in hydrostatic equilibrium, up to a few kilometres in convective conditions (Holton, 2004). Visually, the PBL spans up to the base of the cloud layer.

Turbulence and mixing within the PBL in the WRF model are represented through a two-component process. The first component is the order of turbulence closure and the second is the type of approach employed to represent mixing.

- In the equations that describe the PBL, there will always be known and unknown terms, where known terms are always one order below the unknown terms, and both must be empirically related. The order of turbulence closure refers to nth moment to which the known variables belong to. For example, a 1.5-order closure PBL scheme solves first-order moments for some unknown variables, and second-order moments for others (Cohen et al., 2015).
- Vertical mixing approaches can be local or non-local. The former uses turbulent kinetic energy (TKE) to describe the processes within a single column, considering only the immediately adjacent vertical levels (Banks et al., 2016). Non-local schemes, on the other hand, use information and gradient from multiple vertical levels to determine the value of a given point in space (Bianco, 2008).

In some situations, the lower layer of clouds can be actively interacting with the PBL, so the modelling of these two layers of the atmosphere should be done in a congruent way (Arakawa, 2004). This means that the physics schemes should be compatible when doing numerical modelling.

Surface Layer

The surface layer is the lowest part of the Planetary Boundary Layer that accounts for energy exchange between the surface of the Earth and the atmosphere within 10% of the height of the PBL. The surface layer is treated separately because the variation in the vertical profile of atmospheric variables of interest (namely heat, moisture and momentum) becomes sharper with height (Jiménez et al., 2012).

Surface layer physics are closely related to the processes solved by the radiation schemes to solve emission and scattering of irradiance, and with microphysics and cumulus schemes that characterise precipitation formation mechanisms (Bianco, 2008). The choice of surface layer scheme has a significant impact in sensible and latent heat fluxes, therefore modifying the circulation patterns in the lowest part of the atmosphere. Therefore, it is mandatory that the surface layer and the Planetary Boundary Layer schemes belong to the same framework.

Radiation

Incoming and outgoing radiation are essentially differentiated in terms of wavelength. Specifically, a distinction is made between shortwave (incoming solar radiation) and longwave (outgoing terrestrial radiation) so they are solved by different physics schemes. Outputs from the radiation schemes are radiative fluxes (effects of radiation through a medium) and atmospheric temperature tendency profiles.

Shortwave radiation schemes consider solar irradiance as inputs for the system, and cloud reflection and absorption as outputs, hence accounting for cloud albedo, warming in clear sky and water vapour absorption (Zhao, 2013).

Longwave radiation deals with fluxes emitted from the surface at wavelengths from 4 to 25 μm (infrared band, IR) that are associated with cooling processes in clear air and that depend on the surface type (Dudhia, 2017).

3.2 Hydrological modelling

3.2.1 Model selection

The Dynamic Fluxes and Connectivity for Predictions in Hydrology (DECIPHeR, documented by Coxon et at., 2019) modelling tool is based the key concepts in Dynamic TOPMODEL (Beven et al., 2001a). This highly flexible framework calculates river flow timeseries at multiple spatial scales and configurations, and can be configured to run lumped, semi-distributed or fully distributed simulations by combining landscape layers (see Section 3.2.2.1 for more details). The source code is feely available at a GitHub repository (https://github.com/uob-hydrology/DECIPHeR, last access: 9 September 2019), and can be downloaded along with a user manual and sample files to test the correct compilation of the executable file.

DECIPHeR has been applied in a national-scale benchmark study on model performance, where its computationally efficient capabilities were tested at national scale using daily data. The two test cases in the present study in which the model will be applied will give valuable information on its sensitivity and skill when reproducing the flashy behaviour of a heavily urbanised catchment (Metcalfe et al., 2015). One of the main reasons behind the choice of DECIPHeR it's the current unexplored potential to be applied a) at hourly scale to analyse the discharge variations of intense, localised rainfall, and b) in a catchment with urban land cover. The advances made further from what is presented here are carried out by the Hydrology Research Group of the University of Bristol and at the moment of writing have not yet been documented.

There is currently one model structure implemented in DECIPHeR used for flow routing once the HRUs have been defined, including three soil storages and other parameters that dictate the flow transfer inside and between HRUs (See Figure 3.6 and Table 3.1 for details on the storages and flow directions implemented), and at the moment of writing, the development of further structures is ongoing. This means that the current capabilities of DECIPHeR place the tool in environments where the interaction of the upper soil storages and overland flow are

more significant, such as urban environments. This constraint was taken as opportunity to design a parameterisation of the landscape that a) would not require further model developing, that can be time consuming, b) could contribute to benchmark the capabilities of a newly released hydrological tool, and c) could test the model performance at high temporal resolution for short-lived events, where the impact of impervious surfaces in the urban riverine response is investigated for the first time.

The description of the hydrological model structure in sections 3.2.2 and 3.2.3 were taken from user manuals edited by the developers of the source code and provided to the Hydrology Research Group of the University of Bristol. These documents have been revised by the members of the group and have not been published elsewhere. This is the reason behind the lack of references in the aforementioned sections.

3.2.2 Description of the hydrological tool

DECIPHeR computes the hydrological response of a catchment as the collective behaviour of a set of individual Hydrological Response Units (HRUs), which are non-contiguous units with similar hydrological behaviour. Grouping areas with similar response into HRUs increases the computational efficiency of the model compared to a fully distributed configuration. Hydrological connectivity between the HRUs and the landscape is achieved through assigning weightings that describe the likelihood of the redistribution of fluxes from a given HRU.

Hydrological modelling using DECIPHeR is done in two stages. In the first one, the catchment is discretised into HRUs via a Digital Terrain Analysis (HRUs differ in the conceptualisation and parameterisation of the hydrological processes). In the second one, the rainfall-runoff modelling is performed to calculate river flows at the points of interest. Following the diagram of the overall hydrometeorological framework presented in Figure 3.1, Figure 3.5 summarises the Digital Terrain Analysis Procedure for catchment discretisation to determine the location and grouping of the Hydrological Response Units using simulated rainfall from the WRF model (map 1), and using observed rainfall (map 2, see Section 3.3.2.1 for details this dataset).

3.2.3 Digital Terrain Analysis

The first part of the hydrological modelling, the Digital Terrain Analysis (DTA), consists of two stages: first, the topographic index (see section 3.2.3.1) and headwater cells are derived from topographic and river network information. Then, the terrain attributes of the catchment (such as geology, land use and topography) are processed along with hourly weather inputs (such as rainfall and potential evapotranspiration, PET) to determine the location and extent of the

HRUs. This is at the beginning of the numerical modelling so that the map of the distribution of the HRUs is static during the simulation.

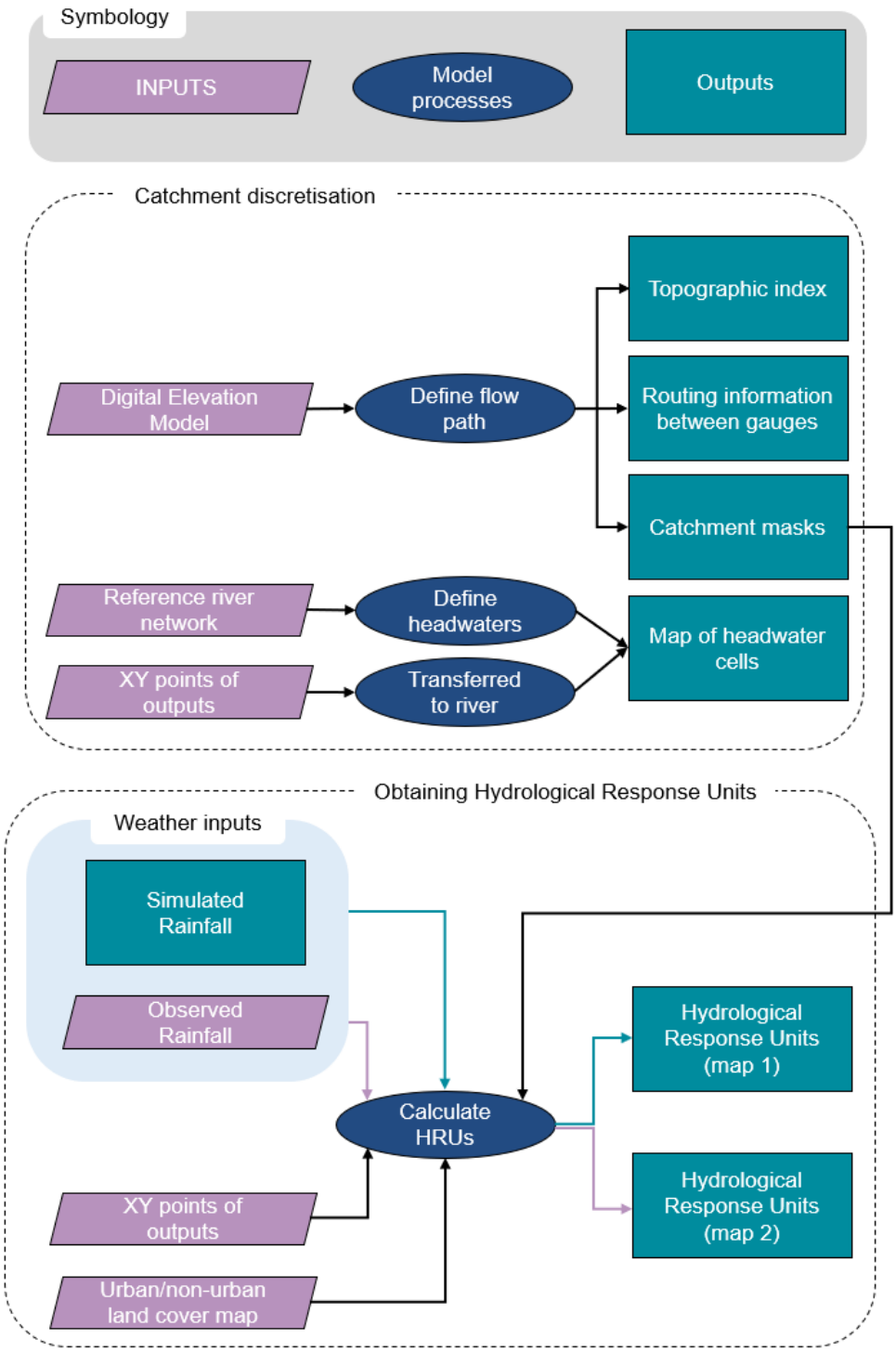

Figure 3.5. Flowchart of the Digital Terrain Analysis to determine the Hydrological Response Units using simulated rainfall (green) and observed rainfall (purple)

3.2.3.1 Catchment discretisation

Inputs

- Digital Elevation Model (DEM). A sink filled ASCII file of the topography without sinks. Having the sinks identified and filled avoids erroneous flow-direction calculations.
- XY locations of gauged or ungauged points on or as close as possible to the river network where flow timeseries are required.
- Reference river network. ASCII file with the same resolution and extent as the DEM.

Process

1. The topographic index is obtained from the slope and accumulated area to help characterise the area. It describes flow accumulation and provides the foundation to calculate saturation excess overland flow and groundwater flows, thus aiding in grouping units with similar hydrological response (Beven et al., 2001b).
2. The index is calculated using the algorithm established by (Quinn et al., 1995):

$$ln\left(\frac{a}{tan\beta}\right) \tag{3.3}$$

   Where a is the upslope contributing area (per unit contour length that contributes to a cell, in this case in m) and $tan\beta$ is the slope acting on that cell.
3. Headwaters on the river network are identified and double-checked, ruling out the ones close to a crest to avoid flow going across a nested catchment.
4. Points that require input flow data, if not located on river grid cells, are transferred to the closest point on the river network within a given radius.
5. Catchment masks for those points and nested catchment masks are produced.

Outputs

- ASCII file of the topographic index
- Refined map of headwater cells
- Tables with routing information between all gauges in the catchment.
- ASCII files of catchment and nested catchment masks.

3.2.3.1 Obtaining Hydrological Response Units

Inputs

- XY location of the points for which HRUs will be calculated.
- ASCII files of catchment and nested catchment mask obtained as result of the catchment discretisation

- ASCII files of spatially derived weather inputs. These files have the same resolution as the sink filled DEM of the catchment and each grid cell has its own ID integer value.
- ASCII files of other landscape classifiers. These files provide spatially heterogeneous information to characterise the hydrological response of the catchment. Their pattern impacts the estimation and grouping of the HRUs so that categories within the classifiers are associated to parameter ranges or model structures.

One of the advantages of DECIPHeR is the flexibility in the use of gridded layers that can be used to discretise the catchment into HRUs. Since the preprocessor in DECIPHeR is computationally inexpensive, the spatial disaggregation given a combination of gridded inputs can be fully explored without compromising simulation time.

Process

The final step of the landscape preprocessing is obtaining the HRUs for the domain. DECIPHeR calculates this for the gauge of interest and the points upstream of it. A flux-distribution matrix is created, which contains the proportion of lateral subsurface fluxes that are directed from one HRU to itself, another HRU or to a river reach hence describing the flow transfer between units. The $n \times m$ matrix, named W for weightings, describes the connectivity from unit n to unit m for a given time step as follows:

$$W = \begin{pmatrix} w_{11} & \cdots & w_{1m} \\ \vdots & \ddots & \vdots \\ w_{1n} & \dots & w_{nm} \end{pmatrix} \quad \text{where} \quad \sum_{i=1}^{n} w_{ij} = 1 \tag{3.4}$$

Outputs

- Table file of the flow distribution for all calculated HRUs in the domain that states the proportion of flux that goes to the same HRU, to other units or to the river network. Mass balance for each HRU is reflected in the sum of the routed flow to the different destinations (sum is always 1). Other useful information contained in this file includes total number of HRUs calculated, catchment area, and gauges in the catchment.
- Metadata file. For each HRU, this file contains the ID, number of cells that the HRU is comprised by, average topographic index, cell ID of the HRU classifiers that will provide the timeseries of weather data and the parameter category that will be used.
- Tables with routing information for the gauges of interest in the catchment and the ones upstream of it, including distance and slope between them.

3.2.4 Rainfall-runoff modelling

Once the HRUs have been calculated, the second part of the hydrological modelling is the obtention of flow timeseries.

Inputs

- Files derived from the calculation of the HRUs ("Outputs" from section 3.2.2.1): table listing the flow distribution for each HRU, metadata file for the array of HRUs and tables with routing data.
- Timeseries of rainfall, PET and discharge for the simulation period only. These inputs can be either lumped or gridded. In the first case, the information should be provided as areal average values. Otherwise, it is required to have the input per grid cell.
- Parameter file. Contains the parameter ranges that will be sampled through Monte Carlo. The bounds and the number of Monte Carlo runs are always user-defined. The use of this sampling technique is explained further in this section under the heading "flow routing".

Model initialisation

Initialisation in DECIPHeR is done at subsurface state, where draining and storage deficits equal the discharge at the first timestep ($Q_{t=0}$). For a given catchment, initial discharge is either: a) the corresponding value from the timeseries provided by the user; b) the average of values of all the timeseries if the initial value is missing; or c) set as 1 mm/day if there is no flow data available. The storage deficit of the catchment is calculated using the best approximation to the initial discharge (Q_{SAT}) which is found by an iteration process as follows:

1. Calculate average saturated transmissivity across the catchment, T_e [m^2 hr^{-1}]:

$$T_e = \frac{1}{A}\sum A_i T_i \tag{3.5}$$

   where A is the total area of the catchment [m^2], A_i and T_i are the area and the transmissivity value for a given HRU [in m^2 and m^2 hr^{-1}, respectively].
2. Calculate the catchment average topographic index, λ (ln(m)):

$$\lambda = \frac{1}{A}\sum A_i ln\frac{a}{tan\beta} \tag{3.6}$$

   where a and $tan\beta$ are the variables in Equation 3.3.

3. Calculate the discharge at saturation, Q_0 [m hr^{-1}]:

$$Q_0 = T_e e^{-\lambda} \tag{3.7}$$

where T_e is taken from Equation 3.5 and λ is taken from Equation 3.6.

4. Calculate the mean storage deficit across the catchment, $\overline{D}$ [m]:

$$\overline{D} = -SZM\ ln\left(\frac{Q_{t=0}}{Q_0}\right) \tag{3.8}$$

where SZM is the form of exponential decline in conductivity [m], $Q_{t=0}$ is the discharge at the first timestep [m hr^{-1}] and Q_0 is the discharge at saturation [m hr^{-1}].

5. Calculate the local storage deficit for each HRU, D_i [m]:

$$D_i = \overline{D} + SZM_i \left[\left(\lambda - ln\frac{a_i}{tan\beta_i}\right) + \left(ln(T_i) - ln(T_e)\right)\right] \tag{3.9}$$

Where SZM_i, a_i and $tan\beta_i$ refer to the form of exponential decline in conductivity [m], upslope contribution area [m^2] and local slope for an individual HRU (non-dimensional), respectively.

6. Calculate the subsurface flows for each HRU, Qs_i [m hr^{-1}]:

$$Q_{s_i} = \left(T_i\ e^{-\left(ln\frac{a_i}{tan\beta_i}\right)}\right) e^{--\frac{D_i}{SZM_i}} \tag{3.10}$$

7. Calculate the contribution to the river for each HRU (as described in Table 3.1), Q_{SZ_i} [m hr^{-1}]:

$$Q_{SZ_i} = ts \times Q_{s_i} \times w_{iriv} \times A_i \tag{3.11}$$

Where ts is the number of timestep (non-dimensional), w_{iriv} is the proportion of flux from HRU i to the river as specified in the matrix in Equation 3.4 (non-dimensional).

8. Calculate the sum of the subsurface flows from all HRUs contribution to the river for each HRU (as described in Table 3.1), Q_{SAT} [m hr^{-1}]:

$$Q_{SAT} = \sum_{i=1}^{n} Q_{SZ_i} \tag{3.12}$$

Given the assumption for the first timestep, Q_{SAT} [m hr^{-1}] must equal $Q_{t=0}$. [m hr^{-1}] If the final sum does not match this value, then a close approximation replaces $Q_{t=0}$ [m hr^{-1}] in Equation 3.8 and steps 4 to 8 are performed until the condition is satisfied.

Flow routing

After discretising the catchment in HRUs and determining the initial runoff value, flows in the HRUs are routed according to model parameters that describe soil transmissivity and storage capacity. The headwater cells obtained in the Digital Terrain Analysis (see Section 3.2.2.1) define the starting point for the flow, and its direction is given by the steepest slope until it reaches a river network cell, sea outlet of DEM boundary. Channel flow routing is computed from a set of time delay histograms based on the outputs from digital terrain analysis of the point(s) of interest, and then a uniform value of the channel wave velocity is used for the whole river network in the catchment. Model parameters within user-defined bounds are sampled through the Monte Carlo technique to assign equal likelihoods to all model runs.

Channel routing scheme

DECIPHeR uses a histogram time delay when calculating how the flow generated will be directed to the river network. In this framework, a time delay histogram (which dictates when the flow generated in each gauge will be released and for how long) is specified for each gauge, as follows:

1. The maximum cell distance [m] is calculated as the distance from the headwater of the gauge to the outlet.
2. The minimum cell distance [m] is calculated as the distance from the gauge to the outlet.
3. The reach distance [m] is the difference of the maximum cell distance [m] minus the minimum cell distance [m].
4. The reach delay [h] is calculated as the reach distance [m] divided by the channel velocity [m/h]. This is the number of timesteps during which the flow will be released.
5. Maximum reach distance [m] is calculated as the distance from the farthest headwater to the outlet.
6. The maximum delay [h] is calculated as the maximum reach distance [m] divided by the channel velocity [m/h].

7. The downstream delay for the gauge [h] (timestep when the flow from will be released) is the maximum delay [h] minus the reach delay [h].

The structure of the model is illustrated in Figure 3.6 and all variables are explained in Table 3.1 where flow units are expressed per timestep (ts; the present study implements an hourly timestep). Their interaction is detailed thereafter.

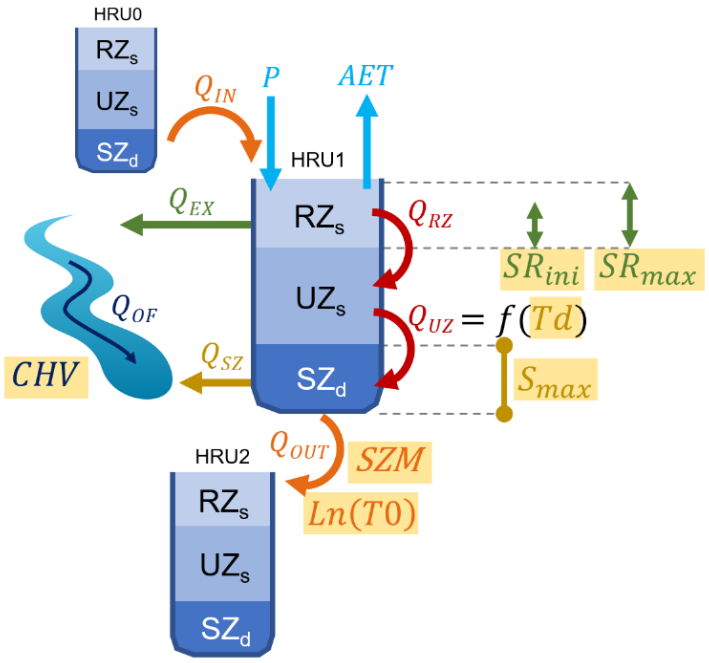

Figure 3.6. Conceptualisation of the structure of DECIPHeR. Model parameters are highlighted in yellow

Table 3.1. Model parameters and variables in DECIPHeR

Abbreviation	Model parameter	Units
RZ_s	Root zone storage	m
UZ_s	Unsaturated zone storage	m
SZ_s	Saturated zone storage	m
Inputs		
Q_{IN}	Flow from upslope HRU	m ts^{-1}
P	Precipitation	m ts^{-1}
Outputs		
AET	Actual evapotranspiration	m ts^{-1}
Q_{EX}	Precipitation excess flow from RZ	m ts^{-1}
Q_{SZ}	Saturated excess flow from SZ	m ts^{-1}
Q_{OF}	Overland flow	m ts^{-1}
Internal fluxes		
Q_{RZ}	Flow from RZ to UZ	m ts^{-1}
Q_{UZ}	Flow from UZ to SZ	m ts^{-1}
Model parameters		
SZM	Form of exponential decline in conductivity	m
$Ln(T_0)$	Lateral saturated hydraulic transmissivity	ln(m^2 ts^{-1})
SR_{max}	Maximum root zone storage	m
SR_{ini}	Root zone storage initially occupied	m
CHV	Channel routing velocity	m ts^{-1}
Td	Unsaturated zone drainage delay	ts m^{-1}
S_{max}	Maximum effective deficit of saturated zone	m

Three storages are defined within the model: root zone, unsaturated zone and saturated zone each one with an allocated storage (RZ_s, UZ_s, SZ_s, respectively).

Precipitation (P) is added directly to RZ_s and actual evapotranspiration (AET) is removed from any of the three storages once they get saturated. RZ_s is controlled by initial and maximum storage values (SR_{ini} and SR_{max}, respectively). Therefore, AET is calculated as:

$$AET = (PET)\frac{\mathrm{RZ_s}}{SR_{max}} \tag{3.13}$$

Where PET is the potential evapotranspiration.

When RZ_s has reached its saturation capacity, any excess rainfall (Q_{EX}) is treated as overland flow (Q_{OF}) where channel wave velocity (CHV) is applied uniformly along the river network.

Flow from a saturated root zone (Q_{RZ}) is then routed to the unsaturated zone and then treated as UZ_s. When the UZ_s is full, water is transferred to the SZ_s (Q_{UZ}) as:

$$Q_{UZ} = \frac{\mathrm{UZ_s}}{\mathrm{SZ_d}(Td)} \tag{3.14}$$

Where SZ_d is the deficit of the saturated zone and Td is the gravity drainage delay parameter for vertical routing.

Flow from the saturated zone into a downslope HRU (Q_{OUT}) occurs up until a maximum deficit (S_{max}) is reached. If the deficit is negative, then subsurface flow from the saturated zone (Q_{SZ}) is added to Q_{OF}.

The lateral saturated hydraulic transmissivity ($Ln(T_0)$) and the form of exponential decline in conductivity with depth (SZM) determine the transferred volume to another HRU. The former is a function of the topographic index, and the latter governs the shape of the recession curve in time.

Finally, fluctuations in time of the storage deficit in the saturated zone can be expressed as a function of inputs and outputs:

$$\frac{\mathrm{d}SZ_d}{\mathrm{d}t} = Q_{HRU} - Q_{IN} - Q_{UZ} \tag{3.15}$$

Where Q_{HRU} can be the flux that leaves the storage because the deficit is negative (Q_{SZ}) or the flux transferred to other HRUs (Q_{OUT}) while the deficit is below the maximum, and Q_{IN} is the flow from an upslope HRU.

Information on flow paths is contained in the matrix of likelihoods of distribution detailed in Section 3.2.2.1.

Outputs

- Simulated discharge. These are files with the output from the rainfall-runoff modelling at the points for which HRUs were calculated. If several points were specified, outputs for all points will be included in the same file, in different columns. Units are in meters per time step.

- Results metadata. This file includes the final parameter values used for simulation and some useful statistic information such as total precipitation and total evapotranspiration per river reach, as well as the actual evapotranspiration that was removed from the root zone during the whole simulation.

3.3 Experimental set-up

The modelling framework will be applied in two case studies. In both cases, intense localised rainfall resulted in a flash flood during summer in two major cities in the United Kingdom. The experimental set-up follows the literature review and the modelling capabilities of the numerical tools used. Boundary conditions and landscape layers as model inputs vary in the temporal and spatial extent, respectively, but not in the database or repository from which they are taken.

Although the WRF model has been proven to perform reasonably well in a wide variety of study cases (as outlined in Section 3.1.4), the sensitivity of the model to the parameterisations implemented is not well understood: a given combination of physics schemes might work well for a case study but not for another. The reason behind the inclusion of several events in a single study is to determine influence of the choice of physics schemes in the correct characterisation of the event of interest and the overall model performance (Liu et al., 2012; Madala et al., 2014), a practice that has been taking place since the early versions of the WRF model, for example, the study by (Mercader-Carbó et al., 2010) using the WRF model version 2.2.

On the other hand, the catchments of the case studies were discretised in urban and non-urban areas according to land cover information. Model calibration and validation of the hydrological model was done at hourly scale. This procedure allows to study the high responsiveness of an urban catchment under intense rainfall conditions as well as the sensitivity of model parameters given the simulated flow variations.

The aforementioned conditions require the input data to be retrieved from the same sources to make a reliable comparison of model performance. Using meteorological boundary conditions from the same dataset will allow confirmation of the strengths and weaknesses of downscaling in nested domains. Taking hydrological timeseries for modelling from a single repository means that the quality checks on the raw data are consistent throughout the analysed periods. Finally, using consistent observed rainfall data for NWP model evaluation and for hydrological validation ensures a seamless assessment of the propagation of uncertainty.

The databases that will be used for the hydrometeorological modelling will be described below, and the timeframe for which they will be retrieved for each case study will be detailed in the corresponding chapter.

3.3.1 Meteorological modelling

3.3.1.1 Model set-up and boundary conditions

Atmospheric input data

Lateral boundary conditions for meteorological modelling were taken from the Operational Global Analysis data by the National Centers for Environmental Prediction, a dataset commonly referred to as NCEP FNL. Information was prepared using the same NCEP model to run the Global Forecast System (GFS) but with an hour of delay to include more observational data.

NCEP FNL is available on 1° × 1° grids every six hours at 26 vertical levels from 1000 millibars to 10 millibars. Apart from the mandatory 2D and 3D atmospheric fields, soil values, ice cover and vertical vorticity values are also included (NCEP, 2000).

Number and ratio of nested domains

The domain configuration was set taking advantage of the nesting capabilities of the WRF model. The nesting ratio was set to 1:3 given the staggered grid architecture (as stated in Section 3.1.2) and domain arrangement commenced by defining the finest domain. The grid with the highest spatial resolution should cover the area of interest and each side should be roughly surrounded by approximately $1/r_n$ of its parent domain (r_n is the nesting ratio). The rest of the domains were then built following this practice.

The finest domain is the bottom of four telescopic nested domains (with grid cell sizes of 2 km, 6 km, 18 km and 54 km respectively). This ensures that resolution model outputs in the finest domain (2 km) is detailed enough to be compared to observed 1-km gridded rainfall (see Section 3.3.2.1 “Databases used for rainfall-runoff modelling” for more details on this dataset), while ensuring that the ratio between the coarse domain (54 km) and the input data (~111 km) is less than the nesting ratio (1:3) so that at least two cells of the parent grid will receive lateral boundary information (Wang et al., 2012).

Vertical levels

As stated previously, boundary conditions are given up to a pressure of 10 millibars (approximately 32 500 m above sea level) at 26 levels. The number of vertical levels is important to determine prognostic variables such as temperature or humidity and the #precipitation starting point.

The maximum level thickness allowed in the WRF model is 1 km so there should be a minimum of 33 vertical levels. However, this would mean a significant mismatch between the levels in the input data and in the model (26 and 33 levels, respectively). To overcome this, the model top was lowered to 60 millibars (approximately 18 500 m) and a predefined set of 28 η levels (as defined in Equation 3.1) and given by NCAR (2008):

η levels = [1.000, 0.990, 0.978, 0.964, 0.946, 0.922, 0.894, 0.860, 0.817, 0.766, 0.707, 0.644, 0.576, 0.507, 0.444, 0.380, 0.324, 0.273, 0.228, 0.188, 0.152, 0.121, 0.093, 0.069, 0.048, 0.029, 0.014, 0.000]

Length of the simulation and spin-up time

Peaks in river flow variations for both case studies were recorded within 6 hours of the highest rainfall intensities on the day during which the flash floods occurred. The total simulation time was set to 48 hours so that the rise, fall and dynamics of the hydrograph could also be explored. Other studies aimed at reproducing flash flood associated rainfall have implemented similar simulation times (Hong et al., 2009) or even shorter periods in which the WRF model is part of a larger modelling system (Varlas et al., 2018).

Although lateral boundary conditions have been corrected with the inclusion of observational data, the WRF model need a warm-up period to rectify the interpolation made by the REAL program and reach a steady state. This period is called spin-up (or lead) time and just like the physical parameterisations, it has a substantial influence on atmospheric outputs. If the period is too short, the model might not reach stability and if the spin-up time is too long, errors might accumulate and have a negative impact when capturing atmospheric features (Gong et al., 2013).

Previous studies have found appropriate lead times of 12 hours (Ulmer et al., 2016; Zhu et al., 2016), and this value frequently considered as the most suitable. Therefore, simulations for both case studies will be run for 60 hours where the first 12 hours will be regarded as spin-up time. However, this lapse had to be tested for the specific case studies. Annex A contains a brief description of the spin-up tests done to further confirm a 12-hour period as the choice for the present research.

3.3.1.2 Model parameterisations.

The choice of the physics schemes precedes the operational application of the WRF model. The parameterisations were chosen given their documented performance to simulate events with similar preceding meteorological conditions, the frequency of their use in the literature so that the results can be compared to those of existing studies, the restrictions given by the

model developers on how the parameterisations can be combined and sensitivity studies for the particular case studies.

Microphysics

Parameterisation of droplet formation processes are described using three schemes, two single-moment and one double-moment. The purpose is to benchmark simpler and more computationally efficient schemes against a more complex and realistic one that could expose model deficiencies (due to boundary conditions) but that could also have a more significant divergence of results given a larger number of degrees of freedom. Nevertheless, the three schemes used for modelling are all appropriate for high-resolution, convection-permitting simulations (Liu et al., 2011).

Thompson

The Thompson microphysics (THOM) is a bulk scheme that considers five hydrometeor species: cloud water, rain, snow, graupel and cloud ice, for which the number concentration is predicted. Given that there is only one degree of freedom, this is a single-moment scheme where particle size distributions are described using a gamma function based on measurements (Thompson et al., 2008).

This scheme mimics the calculation detail of the more sophisticated double-moment microphysics schemes by including look up tables (that have predefined values of the hydrometeor density which (combined with shape parameters, determine the mass-size relationship of hydrometeors in the cloud), increasing the accuracy of the prediction of cloud droplets. Rainfall depends directly on the rain mixing ratio and, depending on the weather conditions, melted ice can also contribute to rainfall outputs

Morrison

Morrison (MORR) is a bulk double-moment scheme that predicts the mixing ratios and number concentrations of five types of hydrometeors: cloud droplets, rain, snow, graupel and cloud ice. For simplicity, all droplets are considered as spheres, the cloud and precipitation particle size distributions are represented by gamma functions and the shape parameter μ (in Equation 3.2) is set to 0. Being a high order-moment microphysics scheme, rainfall number concentration is predicted and assumed to be the product of melting processes, and is therefore proportional to the decrease of snow and graupel concentration. (Morrison et al., 2009).

WSM6

The WRF Single-Moment 6-class (WSM6) is a bulk scheme that calculates the mixing ratio for water vapour, rain, cloud ice and snow. It a more sophisticated scheme compared to the

already existing 5-class and 3-class schemes as it considers graupel as another cloud hydrometeor. Although it has been shown that this inclusion does not have a significant impact in the evolution of simulated heavy rainfall in coarse grids, high-resolution simulations (grid cell size less than 3 km) have a better skill when predicting rainfall intensity and peaks as water volume increases with the number of hydrometeors considered

This microphysics schemes is used by the Korean Meteorological Administration (KMA) and the Korean Air Force (KAF) to provide real-time predictions in the East Asia region (Hong et al., 2010).

Cumulus

The Kain-Fritsch cumulus scheme (KF) in its latest version features deep and shallow schemes to resolve precipitating and non-precipitating convection by considering cloud radius and depth as well as cloud convection. The scheme features convective updrafts and downdrafts, where the former generate condensation into the environment that is then evaporated by downdrafts that depend on relative humidity. The remaining condensate is computed as surface precipitation. This process of deep convection occurs until only 10% of the energy available for convection (convective available potential energy, CAPE) is present (Kain, 2004).

KF has been found to overestimate the rainfall in summer events, but still outperforms other cumulus schemes (Huang et al., 2017). The model performance using this scheme in high-resolution domains (cell size of 6 km) is consistent with the skill in finer grids (3 and 4 km) where rainfall is solved explicitly (i.e. no cumulus scheme implemented) (Pennelly et al., 2014; Zhang et al., 2016; Zhu et al., 2016)

Given the capabilities of the WRF model to explicitly represent convection at sub-grid scales (as detailed in Section 3.1.4), the cumulus parameterisation is switched off for the two innermost domains.

Land surface

The Noah Land Surface Model (NoahLSM) aims to represent momentum, heat and water vapour fluxes along with surface thermodynamics as well as snow coverage, soil temperature and four layers of soil moisture, with the advantage that this scheme features an urban surface category with its own set of parameters (Chen et al., 2001). For a given grid cell, land surface parameterisation provides surface fluxes and temperature for green areas within urban environments (such as trees and parks) and the UCM scheme determines the fluxes for anthropogenic surfaces.

A major reason of choice of this Land Surface parameterisation is the instruction on the WRF user manual (NCAR, 2019) regarding the compatibility of physics schemes. One of the urban canopy layer schemes can only work with the NoahLSM, and to avoid incorporating further uncertainty to the modelling, this scheme was set fixed for all simulations.

Input land cover data is taken from the United States Geological Survey (USGS) 30-second, 24-category land use dataset that considers 4 extra categories for inland water bodies. When the resolution of this dataset is higher than the grid cell size of the domain a simple upscaling algorithm defines cell values in the coarser grid, taking the most abundant land use category that is present in that tile, and setting that as the cell value. The 24 categories used to run the WRF model are shown in Table 3.2.

Table 3.2. USGS 24-category Land Use Categories

Land Use Category	Land Use Description
1	Urban and Built-up Land
2	Dryland Cropland and Pasture
3	Irrigated Cropland and Pasture
4	Mixed Dryland/Irrigated Cropland and Pasture
5	Cropland/Grassland Mosaic
6	Cropland/Woodland Mosaic
7	Grassland
8	Shrubland
9	Mixed Shrubland/Grassland
10	Savanna
11	Deciduous Broadleaf Forest
12	Deciduous Needleleaf Forest
13	Evergreen Broadleaf
14	Evergreen Needleleaf
15	Mixed Forest
16	Water Bodies
17	Herbaceous Wetland
18	Wooden Wetland
19	Barren or Sparsely Vegetated
20	Herbaceous Tundra
21	Wooded Tundra
22	Mixed Tundra
23	Bare Ground Tundra
24	Snow or Ice

The NoahLSM is the most widely implemented land surface parameterisation, having applications in both operational and research studies for weather and climate modelling (Tomasi et al., 2017) and it has been shown to outperform more complex schemes when estimating evapotranspiration that leads to moisture fluxes (Pei et al., 2014). Since this scheme is the only one that works well with all the urban canopy models in the WRF model, it will be kept constant for all simulations.

Urban surface

The WRF model has three schemes to represent the urban canopy. The differences between them is how buildings and streets are represented and this in turn influences the calculation of latent and sensible heat fluxes. To investigate their interactions and performance when simulating rainfall, all three schemes were used.

Single Layer Urban Canopy Model

The simplest urban surface scheme, the Single Layer Urban Canopy Model (SLUCM), parameterises streets as infinitely long 3-dimensional canyons (comprised of roofs, roads and building walls). Here, energy fluxes, turbulence and radiation trapping in the surface take place, and verticostic variables are integrated to determine temperatures of those urban facets (roof, walls and streets). Finally, the wind profile in the urban canyon is assigned an exponential form because the first model level is set at a higher altitude than the building height, hence considering most processes in the urban canopy layer as homogeneous (Chen et al., 2011).

The spatial arrangement of streets and buildings also allows for the calculation of sensible heat flux transfer from the urban features to the lowest layer of the atmosphere. Anthropogenic heating is also passed to the PBL scheme (Ronda et al., 2017).

Building Effect Parameterisation

The Building Effect Parameterization (BEP) multi-layer urban canopy scheme allows for a more sophisticated interaction with the PBL. Similar to the SLUCM, the BEP also considers the three-dimensional configuration of urban facets when calculating drag forces, turbulent kinetic energy and temperature (Martilli et al., 2002). However, BEP does account for multiple vertical levels within the urban layer so processes such as absorption, reflection, emission, and radiation by streets and buildings can be parameterised and not explicitly solved. Moreover, the presence of urban surfaces is numerically solved by introducing a term in the TKE equations to correct the turbulence length. Although the temperature inside the buildings is considered constant, sinks and sources of heat, momentum and moisture from the land surface to the highest building in the domain are vertically distributed. These characteristics reduce the computational cost while increasing the complexity of the calculations, giving this scheme the capabilities of correctly reproducing urban heat island effects at night (Chen et al.,

2011). According to the WRF model User Manual, this scheme has been designed to work only with the NoahLSM.

Building Energy Model

A major improvement to the BEP scheme is the parameterisation of indoor-outdoor flux exchange and the capability to determine building energy consumption due to cooling and heating systems used in summer and winter, respectively (Salamanca et al., 2009).

Other processes considered by the Building Energy Model (BEM) scheme are: a) heat diffusion through urban facets; b) radiation between indoor surfaces and through windows; and c) radiation due to occupants and equipment. This means that a feedback process is represented in the urban canopy: the atmospheric model provides outdoor boundary conditions (air humidity and temperature) and the BEP then calculates energy consumption and heat fluxes (Salamanca et al., 2014).

Thermodynamic parameter values needed to run this urban canopy scheme with the NoahLSM (such as surface albedo and thermal conductivity of walls, roofs and roads) are contained in look up tables included in the WRF model, which correspond to standard building materials (Salamanca et al., 2014). To improve the representation of atmospheric processes, a specific building height distribution for both case studies will be implemented using information from one of the EMU Data Packs (Emu-Analytics, 2014), which is based on LiDAR data from the Environment Agency in the UK.

Planetary Boundary Layer

The Mellor-Yamada-Janjic (MYJ) PBL parameterisation is a one-and-a-half order scheme with a local vertical mixing approach, where the PBL top matches a given value of the TKE profile as is decreases with height (Janjić, 1994).

In a comparative study of all PBL parameterisations in WRF to reproduce typical atmospheric flow types over complex terrain, the MYJ scheme showed the lowest mean bias for 2-m air temperature and was found to best reproduce water vapor mixing ratio for synoptic flows that enhance local circulation systems. The largest spread of the results occurred in the lowest 500 m, where MYJ shows skill to reproduce the potential temperature. The scheme also does a good job at simulating accurately potential temperature and water vapor mixing ratio above the PBL (Banks et al., 2016).

The second reason behind the choice of Mellor-Yamada-Janjic scheme is an instruction in the WRF version 4.0 user manual (NCAR, 2019), which states that this is one of the two Planetary Boundary Layer parameterisations that can be implemented with all the urban canopy models. Finally, the Mellor-Yamada-Janjic scheme is the most widely used Planetary Boundary Layer

parameterisation (Banks et al., 2015) so implementing it would allow comparison with existing studies.

Surface Layer

To solve the processes in the lowest part the Planetary Boundary Layer (PBL), the Monin-Obukhov (MO) similarity theory framework is used (Monin et al., 1954). This scheme accounts for variable roughness height for temperature and humidity (i.e. the height at which the vertical profile of these two variables does not follow a mathematical logarithm).

Given the requirement that the Surface Layer and the Planetary Boundary Layer to belong to the same framework (Bianco, 2008), the MO parameterisation was run with the Mellor-Yamada-Janjic Planetary Boundary Layer scheme

Radiation

The following two radiation schemes have been widely implemented with the SLUCM in several studies on urban atmospheric processes. For example, (Bhati et al., 2018) and (Kusaka et al., 2012) have documented satisfactory model performance in studies on urban heat island intensity given land cover and on urban heat island effects on relative humidity, respectively. The chosen radiation schemes have also been used with the rest of the urban canopy models to analyse heat fluxes and air quality (Barlage et al., 2016).

Shortwave incoming radiation is computed using the Dudhia (DUD) scheme, which solves the radiative transfer equation to determine downward integration in columns, disregarding adjacent cells. It accounts for cloud albedo and clear air aerosol scattering to determine the downward solar flux (Dudhia, 1989).

Longwave outgoing radiation is estimated by the Rapid Radiative Transfer Model (RRTM) which solves for processes in separate columns, similar to the DUD shortwave scheme. It is an accurate scheme that used look up tables that were produced by more sophisticated schemes, increasing its complexity without compromising computational efficiency (Mlawer et al., 1997).

Physics parameterisations interaction and implementation

Figure 3.7 shows a diagram of the interaction of the physics schemes described in the previous section. It includes the processes thank link them, specifying the direction of the influence. Here, it is important to note that when an urban canopy layer model is in use, this parameterisation will replace the land surface scheme to calculate sensible and latent heat fluxes, while the Noah Land Surface Model will do so for vegetated areas (Sarmiento et al., 2017)

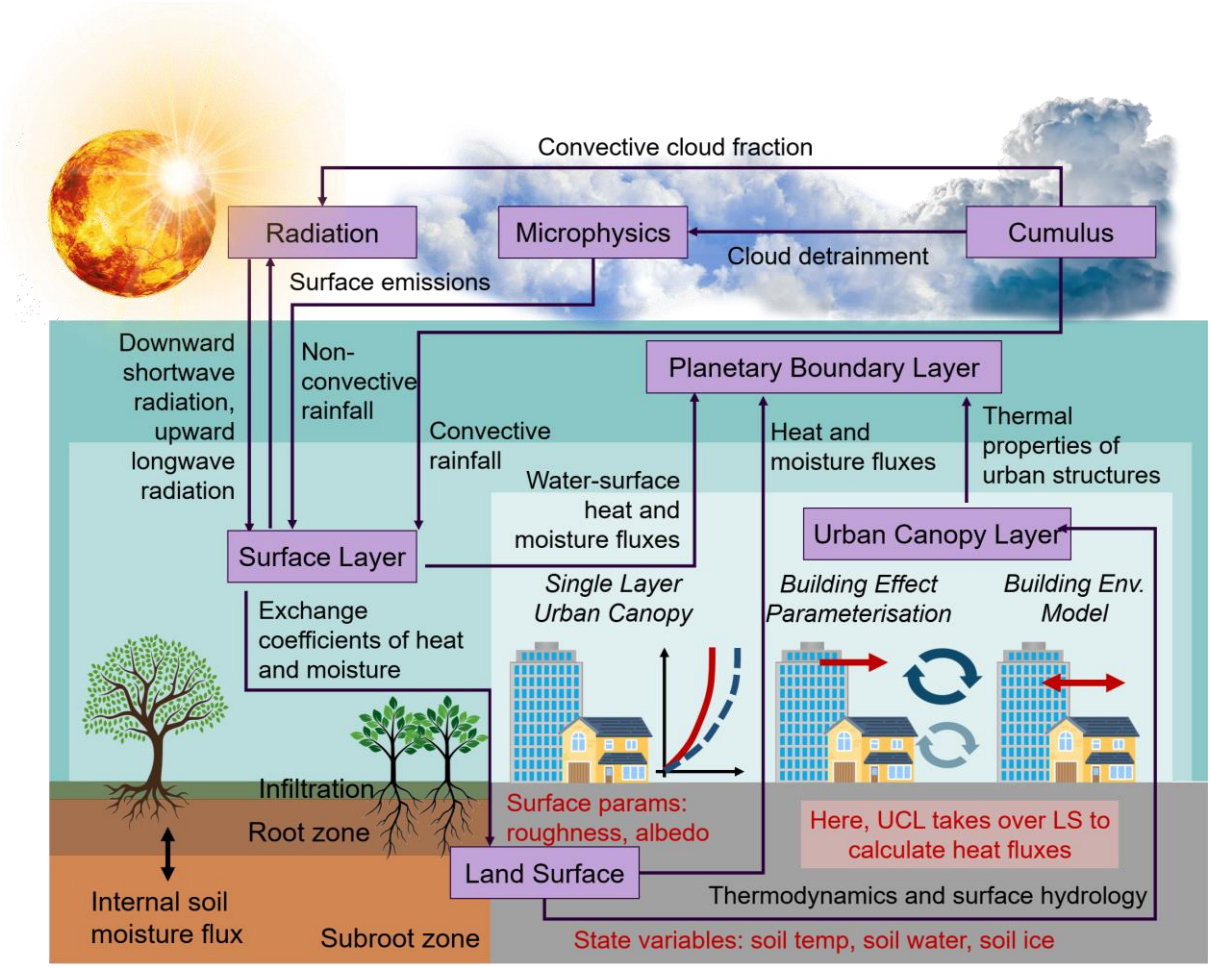

Figure 3.7. Conceptualisation of the interaction of the relevant physics schemes considered for the meteorological modelling

The combination of schemes used for simulation is shown in Table 3.3. The selected microphysics parameterisations will be combined will all urban canopy models to explore their suitability, the level of complexity needed to reproduce flash flood associated rainfall, and computational performance. A list of the acronyms used is presented at the beginning of the present document.

Table 3.3. WRF physics parameterisation for the present study

Physics scheme	Simulation number								
	1	2	3	4	5	6	7	8	9
Microphysics	THOM	WSM6	MORR	THOM	WSM6	MORR	THOM	WSM6	MORR
Cumulus	KF								
Land Surface	NoahLSM								
Urban surface	SLUCM	BEP	BEM	SLUCM	BEP	BEM	SLUCM	BEP	BEM
Planetary Boundary Layer	MYJ								
Surface Layer	MO								
Shortwave radiation	DUD								
Longwave radiation	RRTM								

3.3.2 Hydrological modelling

3.3.2.1 Information used for Digital Terrain Analysis

As stated in section 3.2.2, inputs to perform the DTA include the sink-filled topography map, reference river network, gridded climatological inputs and landscape classifiers. The information presented below corresponds to the input data used by the DECIPHeR benchmark study by (Coxon et al., 2019).

The Digital Terrain Model (DEM) was obtained from the NEXTMap British Digital Terrain Model project produced by Intermap at 50-m resolution. Data was derived from Interferometric Synthetic Aperture Radar (IFSAR) imagery, designed to quickly obtain data at high spatial resolution over large areas. The dataset has a vertical accuracy of 10 m LE95 (Intermap-Technologies, 2009). To fill the sinks in the elevation data, the topography was processed using the algorithm by (Soille, 2004), which calculates flows paths, identifies sinks and abrupt changes in the landscape to fill and cut the cell values, respectively, while ensuring any significant changes to the landscape are minimised.

The river network has the same resolution as the DEM, where headwater cells were identified based on information provided by the Ordnance Survey MasterMap Water Network Layer. Their location was validated by comparing areas and outlet points for 1366 catchments within the National River Flow Archive (NRFA) to extract the best cell candidate for a given catchment.

From the climatological information, only the rainfall is in gridded format. Since the hydrological modelling will be done using observed and simulated rainfall, there will be two maps of Hydrological Response Units for each case study, depending on the dataset used (see Section 3.3.2.2 for more information on the rainfall gridded inputs).

The crucial landscape classifier for hydrological discretisation and modelling is land cover. These 25-m maps were taken from the repository of the Centre for Ecology and Hydrology, which features information for 2007 (CEH, 2011), and 2015 (CEH, 2017). Information was resampled to match the resolution of the sink-filled DEM and the reference river network (50 m) and then transformed to a binary map of urban/non-urban surfaces, each of which will have its own parameter ranges. The way that paved roads and surfaces will be represented in DECIPHeR is through the parameter range of SR_{max}, which describes the maximum storage for the root zone. This storage will be assigned a low storage capacity so that after saturation, any excess rainfall is routed as overland flow, mimicking the role of impervious surfaces in an urban environment under intense rainfall.

3.3.2.2 Databases used for rainfall-runoff modelling

Lumped potential evapotranspiration was taken at daily scale for each catchment from the Centre for Ecology & Hydrology's Environmental Information Data Centre available at https://catalogue.ceh.ac.uk/documents/8baf805d-39ce-4dac-b224-c926ada353b7 (Robinson et al., 2016). Information has been corrected by interception of saturated grasslands on days with rainfall and is then disaggregated to hourly scale using the density of a Skew Power Exponential function.

Hourly discharge was obtained by aggregating 15-minute data provided by the Environment Agency for six regions in the United Kingdom (Anglian, Midlands, North East, North West, South East and South West). Similar to the rainfall information data, discharge data underwent quality control checks and values were assigned flags to keep, check or discard the measured discharge.

Regarding precipitation used to run the hydrological model, two datasets were used:

- Hourly observed gridded precipitation was taken from the 1-km resolution Great Britain dataset (Gridded estimates of hourly areal rainfall for Great Britain, hereafter denoted as CEH-GEAR) produced by (Lewis et al., 2018), which was created by submitting time series records from 1900 rain gauges to quality control checks (as described by (Blenkinsop et al., 2017)). In this quality checking process the most significant rules to leave out measurements were the presence of very long dry spells at any point in time

and at the beginning of the measuring period, and closeness to dry spells in summer and winter.

- Hourly simulated rainfall was taken from the WRF model outputs for the innermost domain which has a resolution of 2 km.

Given the difference in the resolution of these datasets, it is needed to ensure spatial consistency. To do so, CEH-GEAR rainfall was used to initialise the hydrological model during one year before each of the flood events. Afterwards, the simulated rainfall was used in the rainfall-runoff modelling. The 2-km rainfall data from the WRF model was resampled to 1-km using bilinear interpolation, a technique that yields better smoothing results than the nearest neighbour technique (that would also require the design of a variogram model) (Bovik, 2009) and does not entail the mathematical complexity of the bicubic interpolation (Devaraj, 2019), nor is constrained by the number of points available to execute an Inverse Distance Weighted interpolation (Kim et al., 2010). This procedure would ensure that both rainfall sources would have the same spatial resolution and that the hydrological modelling would be done implementing the same number of Hydrological Response Units, so that the outputs can be comparable.

3.4 Evaluation of model outputs

3.4.1 Meteorological modelling verification metrics

The performance of the nine WRF configurations was evaluated for the 48-hour period that spans over the start of the intense rainfall that led to the flash flood and the decrease of river levels after the event. The discussion was done at synoptic, meso- and local scale, focusing on the rainfall accumulated values obtained when combining the microphysics and Urban Canopy Model parameterisations, focusing on the correct localisation and evolution of the rainfall patterns. Observed precipitation datasets used to obtain skill score metrics include remote-sensed data and land-based rain gauges. Verification indices were implemented to evaluate the meteorological model performance, and evaluation of rainfall fields was done at synoptic (continental), meso- (national) and local (catchment) scale, as conducted by other studies that benchmark the WRF model performance (Campos et al., 2015; Cassola et al., 2015).

3.4.1.1 Evaluation of model outputs at synoptic scale using satellite-derived data

At synoptic scale, WRF model outputs for the coarsest domain were compared against rainfall data from the Global Precipitation Measurement (GPM) mission. Simulated rainfall at this scale is the sum of the outputs from the microphysics and the cumulus scheme, which produce the non-convective and the convective precipitation, respectively. The dataset that provided the observed values was derived using information from the passive-microwave instruments of the GPM constellation and processed using the Integrated Multi-satEllite Retrieval for GPM algorithm (IMERG), where precipitation rates are contained in thirty-minute files at 0.1º resolution with a full coverage 60ºN-60ºS, and partial coverage for the rest of the globe. Evaluation of WRF model outputs using GPM IMERG rainfall data was done following previous studies that used this publicly available, given its spatial resolution at global scale (Roy et al., 2018; Wehbe et al., 2019; Yi et al., 2018).

GPM information used in the present study is retrieved using passive microwave sensors which overcome the cloud-top measurement difficulties and provide data despite the cloud coverage (Li et al., 2016) which allows the inclusion of low-intensity rainfall (0.5 mm h^{-1}). The weakness in GPM data is the presence of sampling errors due to satellite orbit (Maggioni et al., 2018) which impact estimated precipitation in time over different accumulation periods producing noisy average fields, especially when estimating solid hydrometeors (Bennartz et al., 2001). However, the GPM product has a high accuracy associated when it comes to spatial distribution of the rainfall (Sun et al., 2018).

3.4.1.2 Evaluation of model outputs at meso-scale using weather radar data

Mesoscale analysis of the evolution of the rainfall was done for the innermost domain, where the rainfall is solved by the microphysics scheme only. The observed data at finer resolution is taken from the Met Office NIMROD System which processes C-band rainfall radars to deliver 5-minute, 1-km products covering the United Kingdom. Comparison of WRF model outputs with radar imagery at this scale provides crucial information on model sensitivity to physics schemes (Li et al., 2013) and the ability of the model to capture key atmospheric features involved in intense precipitation (Litta et al., 2012).

Uncertainty in NIMROD data lies in the radar beam propagation that can find obstructions on the ground, anomalous weather conditions, effects of the curvature of the Earth and variability of the vertical reflectivity profile, among other factors (Cecinati et al., 2017). Despite the large amount of sources of error, radar imagery undergoes several quality checks, such as 1) identification and removal of noisy radar images given the information previously received by the same radar and by a neighbouring radar, 2) identification and removal of anomalous

propagation by comparing NIMROD data to surface synoptic reports, 3) quantifying the vertical variations of the reflectivity profile and accounting for bright band contamination, and 4) comparing rainfall fields to gauge data. However, the contribution of the different sources of error has a considerable variation with space and time, so visual and quantitative comparison to this information must be done with care (Harrison et al., 2006).

3.4.1.2 Evaluation of model outputs at local scale using rain gauge data

At local scale, the impact of the different Urban Canopy Models on simulated rainfall was discussed. Quantitative model validation was done using a quality-controlled, hourly rainfall dataset considering all gauges in the innermost domain. This dataset was subject to previous quality-control (QC) procedures that ensure that the data do not deviate from the long-term climatological extremes. For example, records were internally checked with other gauges where records less than 25 mm must be within ± 2 mm of the check gauge, and values that exceed said threshold must lie within ± 8% of the check gauge to be flagged as “good”. Other QC checks include 1) identification of Tipping-Bucket-Rainfall (TBR) high frequency tipping which results in spurious rain intensities, 2) identification of anomalous accumulated rates, and 3) differentiation between dry spells and gauge non-operation. This dataset is currently considered as a good source of ground-measured rainfall data for analyses of extreme rainfall at hourly resolution (Blenkinsop et al., 2017).

The analysis at local scale comprises a categorical and two continuous indices, a plot of accumulated rainfall to define an over- or underestimation trend, and timeseries of the rainfall grouped by microphysics scheme to keep them constant and evaluate the impact of choice of the urban canopy schemes.

The categorical index used is the Critical Success Index (CSI), which considers binary wet/dry rainfall maps to quantify hits (observed and simulated wet cell), misses (observed wet cell, simulated dry cell) and false alarms (observed dry cell, simulated wet cell). This metric is sensitive to hits and penalises misses and false alarms, giving a balanced indicator of the model skill (Kang et al., 2005). The CSI, one of the most popular verification metrics to evaluate the correspondence between simulated values and land-based observations (Liu et al., 2012; Remesan et al., 2015), is calculated as stated in equation 3.16.

$$CSI_i = \frac{H_i}{H_i + M_i + FA_i} \tag{3.16}$$

Where H is total number of hits, M is total number of misses and FA is total number of false alarms for each simulation timestep i.

WRF outputs may contain very low rainfall values on period in which no precipitation was observed or recorded (Mendoza et al., 2015), therefore, obtaining the CSI will be done for values of 0.1 mm and above. This threshold was chosen given the current precision of the rain gauges data so anything below that value will be considered zero.

Additionally, the continuous statistical indices Root Mean Square Error (RMSE) and Mean Bias Error (MBE) were also used to describe model skill. The former penalises large errors and the latter represents the systematic error of underestimating intense precipitation events. Both were calculated using equations 3.17 and 3.18.

$$RMSE_i = \sqrt{\left(\frac{1}{n}\sum_{i=1}^{n}[S_i - O_i]^2\right)} \tag{3.17}$$

$$MBE_i = \frac{\sum_{i=1}^{n}(S_i - O_i)}{n} \tag{3.18}$$

Where O is the observed rainfall for a given rain gauge in [mm], S is the simulated rainfall in [mm] for the correspondent WRF grid cell, calculated for the n rain gauges in the innermost domain, for each simulation timestep i. Units for RMSE and MBE are the same as the observed and simulated rainfall values.

For a given simulation, these metrics were calculated per time step, where the observed time series were retrieved from all the gauges in domain 4, and simulated values were taken from the overlapping WRF grid cells. The indices were then calculated by averaging all the values per time step.

Finally, rainfall time series of observed and simulated values were plotted to determine the sensitivity of the model to the choice of urban canopy model scheme based on the choice of microphysics parameterisation. The gauges were selected based on the geographical location (to assess the spatial variability of results), magnitude of the peak values and spread of the ensemble.

3.4.2 Hydrological model calibration and validation

From the period of record, the last four years of data were considered for model calibration and validation, of the most recent date from which periods of “No Data” were shorter than two weeks. This is to ensure that records during the months considered for the simulation were at least half complete.

The Nash-Sutcliffe Efficiency (NSE) index was used to determine the behavioural modelling ensemble (Nash et al., 1970)). This metric, calculated as stated in Equation 3.19, indicates the relative magnitude of the residual variance compared to the observations and ranges (-∞ 1], where a negative NSE indicates that the mean of observed timeseries is a better descriptor than the model; a value of 0,0 is assigned to simulations that are as good as the mean observed flow; and all positive values describe model outputs that are better than the mean climatology.

$$\mathrm{NSE}=1-\frac{\sum_{i=1}^{n}(O_i - P_i)^2}{\sum_{i=1}^{n}(O_i - \bar{O})^2} \tag{3.19}$$

However, the NSE tends to overestimate of model performance during peak flow conditions and, in turn, underestimate the skill of the model during low flow values (Krause et al., 2005). In fact, this metric alone is not a robust indicator of model performance, so it is common practice to use additional statistical measures. For this study, the Root Mean Square Error (RMSE) was also implemented given that, as explained in Section 3.4.1, it assigns a high weight to large errors therefore making up for the biases when considering NSE alone. The RMSE was calculated using Equation 3.17.

Finally, the behavioural members of the hydrological ensemble were chosen as those above Q95 of the NSE index, while simultaneously belonging to the 5% of simulations with the lowest RMSE.

Another statistical tool to evaluate the skill of the simulations was the scatter plot of the parameter space compared to the NSE score. This gives useful information on the ensemble behaviour, i.e. the transition between “good” and “poor” simulations (Peters et al., 2003). The plot also allows the evaluation of parameter sensitivity related to the ability of the model to reproduce the observed flows and the hydrological response of urban and non-urban areas. Once the best performing ensemble members are identified, then the bounds for the 5th and 95th percentiles are identified using the Generalised Likelihood Uncertainty Estimation (GLUE) framework (Beven, 2006), similar to the procedure implemented by (Coxon et al., 2019) to show how well the model does at capturing the magnitude and timings of the peaks.

3.5 Conclusions

The hydrometeorological framework proposed to reproduce the intense rainfall and the rapid fluctuations in river discharge during two flash flood events was presented in this chapter. The

numerical tools, along with the justification for use, is documented given their capabilities and the novelty that their implementation for urban flash flood simulation represents.

The meteorological tool was chosen after reviewing the studies in which it has been successfully applied. These studies feature at least one characteristic that is relevant for the selected case studies: flash flood associated rainfall, urban meteorological processes, convective rainfall, high-resolution simulations and application in the United Kingdom. The present study is the first attempt at combining the different capabilities of the meteorological tool in a downscaling exercise to assess model performance at high temporal and spatial resolution for events with a rapid development. There is extensive and accessible documentation on the model structure and performance, and the numerical tool is freely available.

The hydrological model represents the latest advances in a computationally efficient framework. The numerical tool can be applied in a wide range of spatial arrangements to work as lumped, semi-distributed or fully distributed model; has the capability to feature modification to the current model structure to include more detailed representations of the landscape, such as groundwater processes, inclusion of retention structures or implementation of Natural Flood Management strategies; represents a computationally efficient tool as it discretises the landscape and groups areas of similar hydrological response; allows an easy application at different spatial extents to meet the emerging challenges at regional and continental scales; finally, it is freely available with appropriate documentation for testing.

This chapter also included the evaluation procedure of model outputs, which was done at several spatial scales (synoptic, meso-, local and catchment scale). The selected metrics allow assessment of model performance at high resolutions given the responsiveness of the urban catchments during the flash flood.

Chapter 4

Meteorological modelling case 1. Newcastle 2012 flash flood event

4.1 Introduction

In the previous chapter, the numerical tool to simulate the rainfall during the flash flood case studies was described, along with the physics parameterisations used to account for the influence of urban canopy on short-lived, intense rainfall and the datasets used to run the model.

This chapter documents the first case study, including the motivation to analyse this event, the antecedent meteorological conditions and a detailed description of the evolution of the rain on the day of the flash flood. Afterwards, the model set-up is described, including the specific lateral conditions used as inputs. Outputs from the numerical tool are analysed at synoptic, meso- and local scale. The first one compares the accumulated rainfall patterns in a spatial window that includes the United Kingdom and part of Europe. The second one was done in a specific region of the United Kingdom (an area of 96 km × 108 km). Assessment of model performance at local scale was done by making a point-to-point comparison of the simulated rainfall and data from rain gauges. The influence of the parameterisation of the urban canopy in the intensity and distribution of the rainfall is assessed. Finally, additional tests to further support the selected physics schemes and spin-up time are detailed. The chapter concludes with the main findings and outlines the next step in the hydrometeorological framework.

4.1.1 Justification of choice of the event

The first case study is the flash flood in the North-East English city of Newcastle upon Tyne, hereafter simply denoted as Newcastle. On the 28th June 2012, unusual antecedent conditions along with exceptionally severe storm cells (see Section 4.2.1 for details) caused major flooding across the city which caused significant disruption and considerable losses. Most of the public transport service came to a halt and even major highways experienced surface damage, causing delays for several hours. Road network losses were estimated to reach £8 million (Pregnolato et al., 2017). Around 500 properties were flooded, more than half of them for the first time (Archer et al., 2018). Additionally, 40% of the 54 affected businesses were forced to close temporarily (Archer et al., 2016).

The first consequences of the intense rainfall were recorded within the first hour of the start of the rainfall, at 15:00 UTC. The impacts of the event intensified due to the timing, which was close to rush hour. This event was chosen due to the considerable cost associated with the losses and damages, its key features regarding location, extent and development as a flash flood and the number of residents affected despite it not being unique as stated in historical records (See Section 4.1, on the historical aspect of floods in Tyneside, the region in which the city of Newcastle is located) (Environment-Agency, 2012).

The location of the city and some examples of the disruption during the event are shown in Figure 4.1. Water levels can be roughly defined taking vehicles and urban features as a reference.

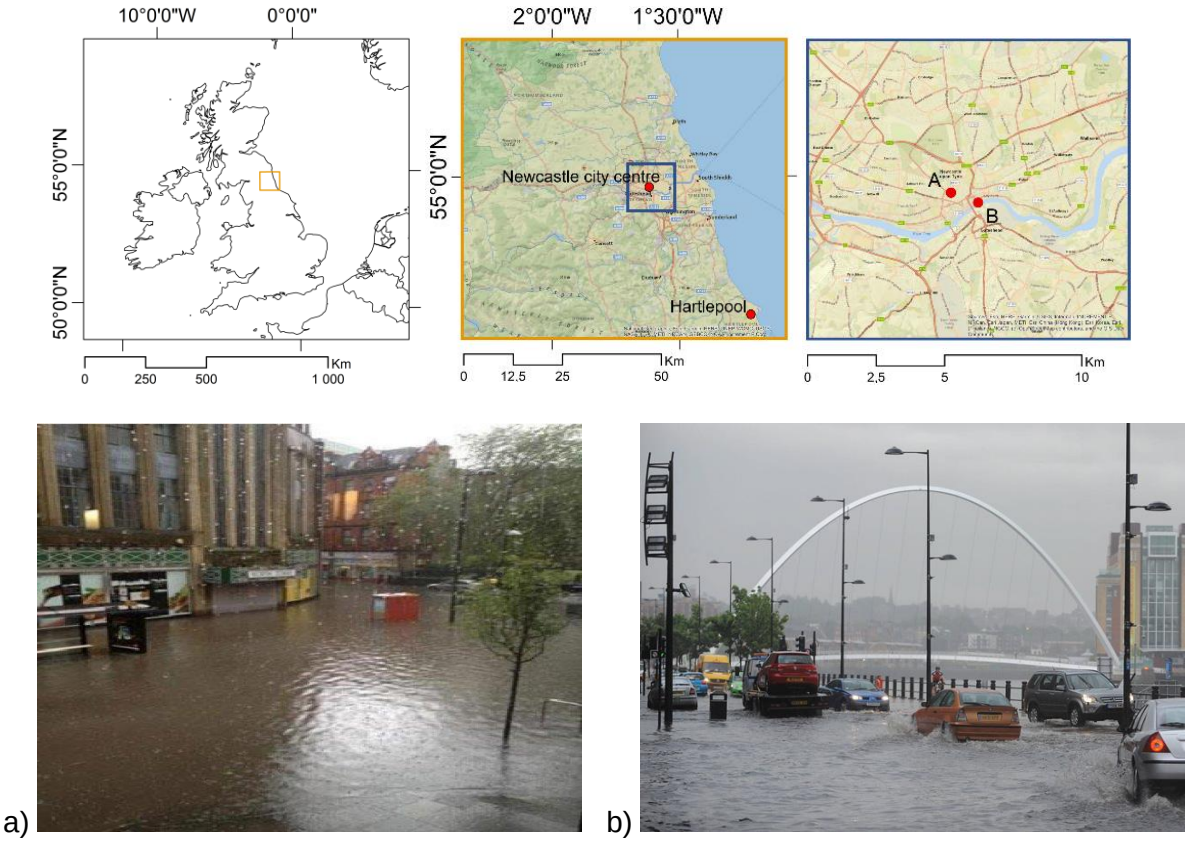

Figure 4.1. Top row: national scale map highlighting the north-east area of interest (left), location of Newcastle city centre in reference to the coast and Hartlepool (centre), places where the event photographs were taken (right). Bottom row: a) Newgate Street on 28th June 2012 (Glenis et al., 2018), b) The Quayside, north bank, viewing the Gateshead Millennium Bridge (Summers, 2012)

4.2 Meteorological setting

4.2.1 Historical context of flash floods in the Tyneside region

Tyneside is the north-east region of England on the banks of the River Tyne. It has a record of several flash flood events detailed hereafter which set the context for the 2012 event.

Records on the 16th September 1913 show a 60-cm deep flood after approximately 70 mm of rainfall were recorded in a 90-minute period. Water from roads at higher elevations accumulated near Newgate Street, a depressed area where the shopping centre is located. Virtually every shop was flooded (Kilsby et al., 2016).

Rain gauge measurements from July 1983 on the north of the Tyneside region exhibit two-hour totals of 100 mm. On the 3rd August of the following year, rainfall on Wallington Hall (nearly 30 km north-west of Newcastle) reached 30 mm in only 15 minutes causing a 1-metre river level rise in the same period. On 22nd June 1941 there was a series of intense storm cells over Newcastle. Although official records are not kept due to war restrictions, but there are ad-hoc records stating totals of 113 mm in a 140-minute period starting at 14:25 UTC, with 50 mm recorded in 35 minutes and 95 mm in only 85 minutes.

These events show that the level of accumulated rainfall during the 2012 flash flood was not without historical precedent. However, the main difference lies in the damage and disruption caused, considering total numbers of affected residents. Moreover, the fact that the road network was closed during rush hour means that the consequences of the flood went considerably beyond what would be expected given its magnitude (Environment-Agency, 2012).

4.2.2 Antecedent conditions

Precipitation values were above average during May and June 2012 and caused the soil moisture deficit values to decrease. By the first half of June, steady periods of rainfall had already been recorded due to a low-pressure, nearly stationary system which had already been observed over south-east England. Given the considerably large water vapour totals in a warm atmosphere, cloud formation and intense rainfall were not surprising (Allan, 2012). This caused the soil moisture deficit in the North East to be at its lowest value since records that date back to 1971, and the storage capacity of the soil was considerably reduced. (Environment-Agency, 2012).

During June 2012 and until the 27th of that month, the Tyneside region had already experienced nearly twice the normal rainfall expected. A numerical comparison of the rainfall

recorded during this period and the Long-Term Average (LTA, from 1971 to 2000) value for June is shown in Table 4.1 (Environment-Agency, 2012). The location of the mentioned rain gauges can be seen in Figure 4.2. The bold line in Figure 4.2 outlines the hydrometric area 23 “Tyne (Northumberland)”, one of the 107 areas into which the Centre for Ecology & Hydrology has discretised the United Kingdom to facilitate hydrometeorological data collection (National River Flow, 2014), from now on denoted as “Tyne catchment”. It contains the Ouse Burn catchment, upstream of Newcastle. The neighbouring lines represent the limits of the contiguous hydrometric areas.

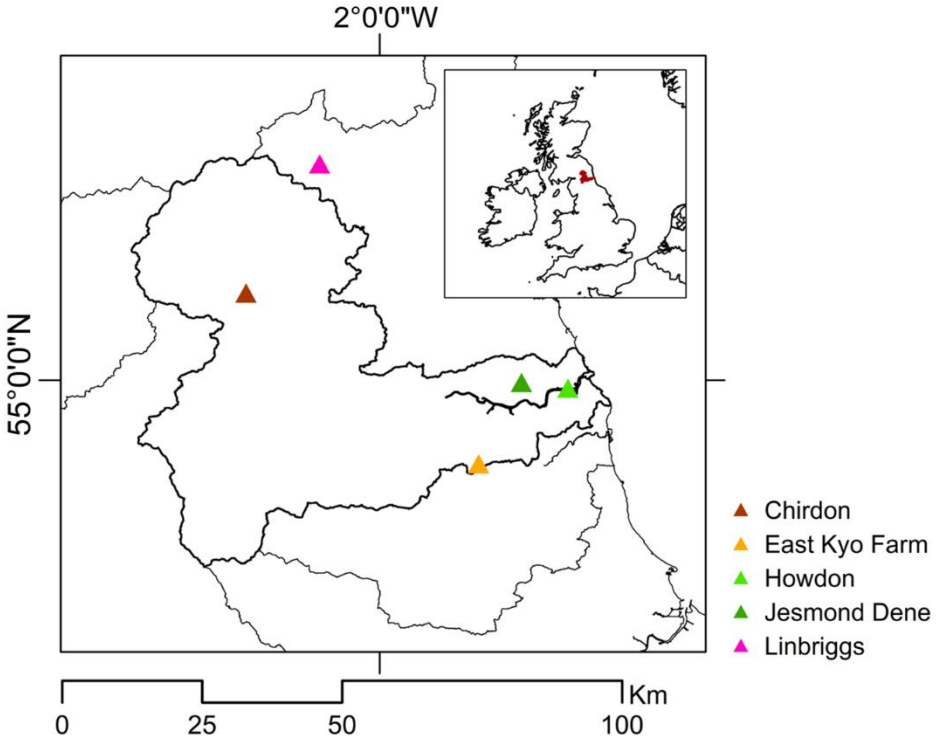

Figure 4.2. Location of the rain gauges for which the Long-Term-Average values for the Newcastle 2012 event is shown

Table 4.1. Total rainfall recorded in the Tyneside region in several stations, shown as totals and as percentage of the monthly Long-Term Average

Rain gauge	Rainfall 1st-27th June 2012 [mm]	Rainfall 1st-27th June [% of LTA]
Chirdon	121.6	173
East Kyo Farm	140.8	227
Howdon	84.6	169
Jesmond Dene	109.6	201
Linbriggs	122.2	268

4.2.3 The event

On the 28th June an atmospheric river of warm, moist air (also called the “Spanish Plume”) that extended from the tropics across England was destabilised by a cold front arriving from the West, causing intense rainfall. Troughs are formed in the area of instability between such systems, and their location is strongly associated with areas of the most intense rainfall. Figure 4.3 (Allan, 2012) shows the location of these atmospheric features at synoptic scale in the early hours of the 28th June.

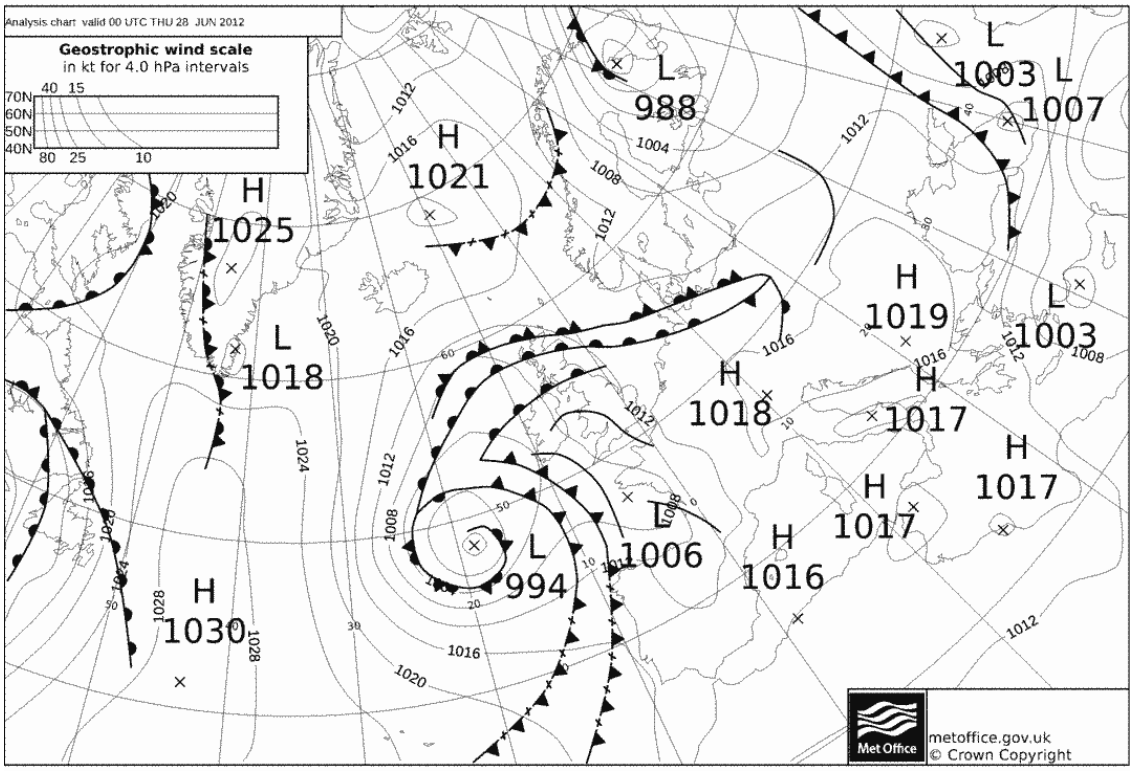

Figure 4.3. Surface pressure chart showing the location of the fronts and the troughs (thin, black lines), valid 00:00 UTC on 28th June 2012 (as shown in Allan, 2012)

Thunderstorms developed in the south-west of England in the early hours of the day, moving northwards and affecting other catchments in the Midlands and reaching Tyneside at 15:00 UTC. Upon arriving in the North-east, along with heavy downpours there was also hail and lighting. (Environment Agency, 2012)

Trough development and merging of the two fronts (which occurred around 18:00 UTC on the 28th June) is a common meteorological setting for some of the most notable flood events in England, including the summer 2007 floods, from which the second case study of this project

was chosen. It is worth noting that most of the flooding was due to the inability of the sewage system to cope with the considerable amount of rainfall, rather than from rivers overflowing (Environment Agency, 2012).

On a more local scale, radar images from the Met Office NIMROD System (Met Office, 2003) showing the 15-minute accumulated values help to visualise the north easterly track of the storm during the event. By 15:00 UTC the thunderstorm had developed into a single bulge of rainfall centred over Newcastle but with a significant spatial extent, as can be seen in Figure 4.4 (top panel). In the following hour and a half, the storm intensity decreased over the city centre and developed to the west. However, by 16:15 UTC the storm intensified again over the area and merged with a second cluster of storm cells that had formed 40 km south of the first one, forming a nearly continuous line of heavy rainfall (Figure 4.4, middle panel). By 17:15 UTC the storm intensity had decreased, the line of rainfall started moving north eastwards, delivering precipitation to other areas for another hour (Figure 4.4, bottom panel).

Return periods for different rainfall durations for the region's rain gauges are displayed in Figure 4.2 and in Table 4.2 (Environment-Agency, 2012), from which it is evident that the most extreme values were recorded for the stations in or close to the city of Newcastle.

A second pulse of intense rainfall occurred over the area on 5th August, where the 90-minute rainfall total reached 40 mm. However, since this event was over the weekend, disruption was not as significant as on the 28th June (Archer et al., 2018).

Table 4.2. Rainfall accumulations and return periods of recorded values in five stations in the Tyneside region during the 2012 flash flood event

Duration	Chirdon	East Kyo Farm	Howdon	Jesmond Dene	Linbriggs
Rainfall [mm]					
0.5 hour	12.2	18.8	15.6	26.4	16.4
1.0 hour	20.0	21.2	29.8	31.8	25.4
1.5 hour	23.8	32.8	38.2	44.0	28.8
2.0 hour	26.2	32.8	39.6	48.8	31.0
Return period [years]					
0.5 hour	5		11	68	18
1.0 hour	12	14	48	59	38
1.5 hour	14	39	77	123	30
2.0 hour	14	27	64	131	21

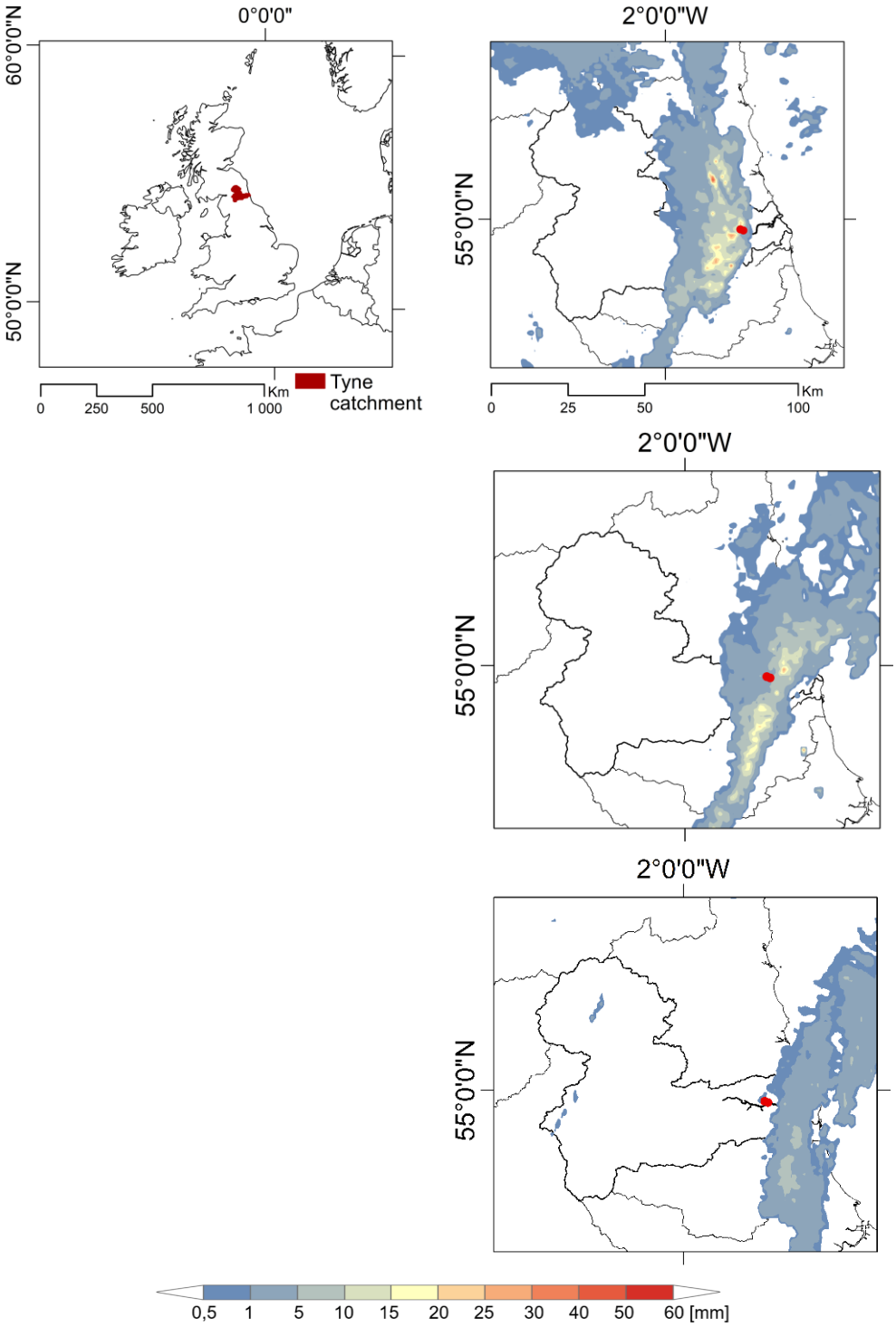

Figure 4.4. Radar imagery of the June 2012 event showing the storm track over the Tyne catchment (top left), 15-minute accumulated values for 15:00 UTC (top right), 16:15 UTC (middle), 17:15 UTC (bottom). Newcastle city centre is marked with a red dot

4.3 Meteorological model set-up

4.3.1 Domains and boundary conditions

The four telescopic nested domains (see Figure 4.5) for this case study were built following the outline of the Tyne catchment (the denomination in this study for the hydrometric area 23 “Tyne (Northumberland)”, described in Section 4.2.2). The innermost domain covers the entire Tyne catchment and the rest of the grids were built around this following the indications outlined in Section 3.3.1.1 regarding the number and ratio of nested domains. Starting from the outermost domain, the notation is assigned in increasing order, i.e., the coarsest grid is denoted as domain 1, and the finest grid is domain 4. Table 4.3 displays the extent and area of each grid.

Table 4.3. Grid cell size and area of the WRF model set-up for the Newcastle 2012 case study

Domain	Grid resolution [km]	Grid cells (rows × columns)	Domain size [km^2]
1	54	38 × 35	2 052 × 1 890
2	18	33 × 33	612 × 612
3	6	48 × 48	294 × 294
4	2	48 × 54	96 × 108

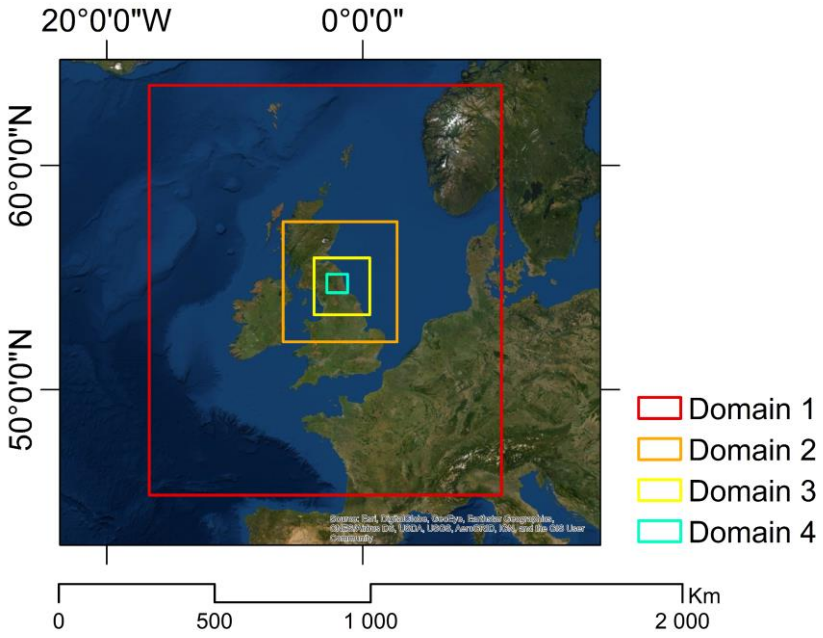

Figure 4.5. Location and extent of the nested domains for the meteorological simulation of the Newcastle 2012 case study

The simulation period started on the 28th June and continued through 29th June. This period was chosen to include the onset of the rainfall that caused the flash flooding (which occurred at 15:00 UTC 28 June 2012), as well as the falling limb of the hydrograph at the outlet of the catchment for which the hydrological modelling (i.e. the next step after the meteorological modelling) was done. Lateral boundary conditions from the Operational Global Analysis data by the National Centers for Environmental Prediction (commonly referred to as NCEP FNL) were retrieved for the 60-hour period between 12:00 UTC 27 June 2012 and 30 June 2012 00:00, the first 12 hours of which comprise the spin-up period. The reason behind the selected spin-up time is documented in Section 4.5.2.

4.3.2 Building height distribution

Properties of urban features were extracted for domain 4 only, covering an area of 96 Km × 108 Km (refer to Figure 4.5). The dataset is one of the freely available DataPacks produced by Emu Analytics Limited. The information was obtained by merging Ordnance Survey Open Map data with LiDAR information provided by the Environment Agency, and the latest update to the dataset was done in 2015. The building height map has a horizontal resolution of 1 m and a vertical accuracy of 40 cm. For this study, averaged building height values were used, which have a vertical accuracy of 15 cm (Emu-Analytics, 2014).

A visual distribution of building heights is shown in Figure 4.6, where the city centre has been enlarged and displayed in the upper left corner. The histogram with percentages per building height category is shown in Figure 4.7. It is worth noting that implementing specific building height distributions in the WRF model for a given city is only relevant for the Building Energy Parameterisation and Building Energy Model schemes, as the Single-Layer Urban Canopy Model considers the first vertical model level above the urban canopy layer.

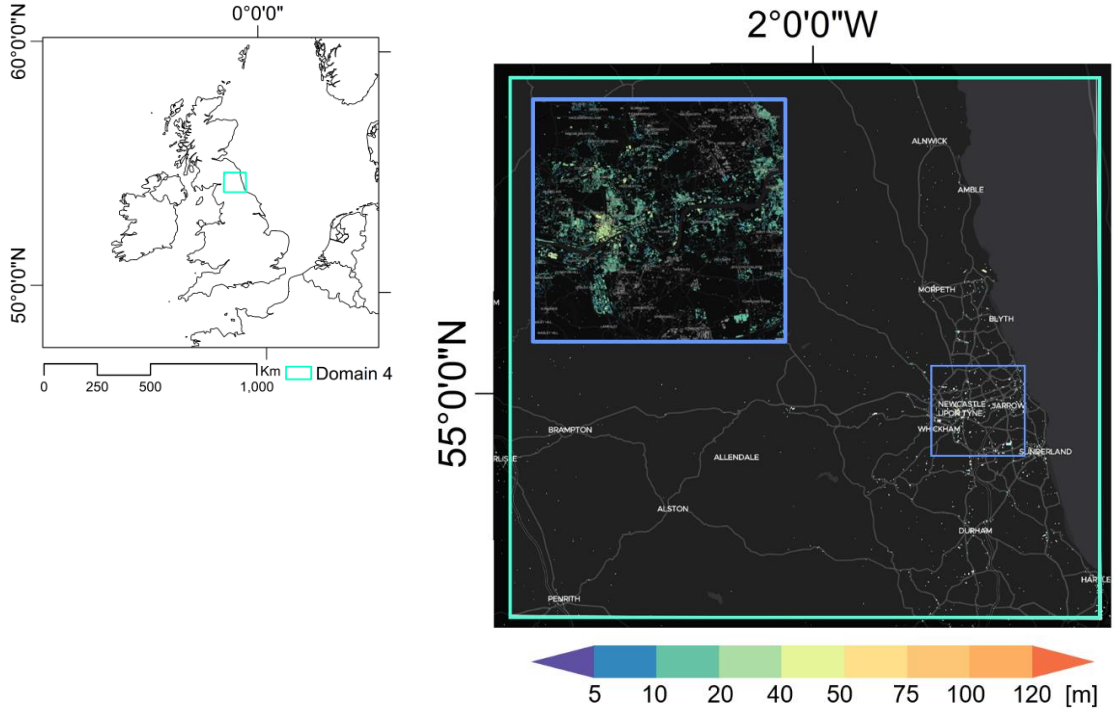

Figure 4.6. Visual distribution of building heights in the innermost domain of the Newcastle case study. Green outline corresponds to domain 4.

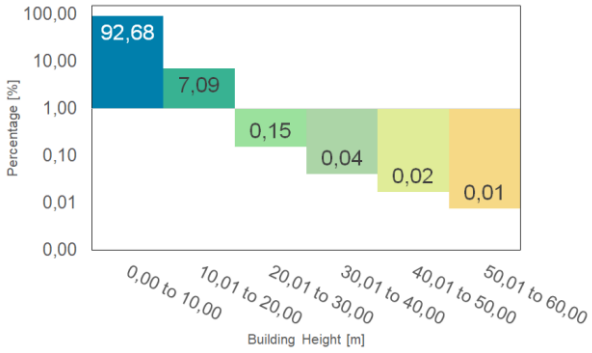

Figure 4.7. Histogram of the building height distribution for domain 4 of the Newcastle case study.

4.4 Results and discussion

4.4.1 Synoptic scale analysis

To analyse model capabilities to reproduce accumulated rainfall patterns, the first part of the analysis will be done at synoptic scale. In this section, rainfall maps for domain 1 (See Figure 4.5) will be compared against GPM data (as described in Section 3.4.1) to determine the closeness of observed vs. simulated scenarios, discussing the location and importance of several features within the rainfall pattern.

Figure 4.8 shows the observed and simulated accumulated rainfall maps for 15:00 UTC to 17:00 UTC 28 June 2012 during which the highest precipitation rates were recorded. Simulations 1-9 refer to the combination of three urban canopy models with three microphysics schemes included in the WRF model. The urban canopy parameterisations are the Single Layer Urban Canopy model (SLUCM), Building Effect Parameterisation (BEP) and Building Energy Model. The three microphysics schemes used are Thomson (THOM), WRF Single-layer 6-class (WSM6) and the Morrison (MORR) scheme. They were combined as stated in Table 4.4. For further details on each physics scheme, refer to Section 3.3.1.2).

Table 4.4. Urban canopy models and microphysics parameterisations used in the nine WRF scenarios to simulate rainfall for the Newcastle 2012 event

Physics scheme	Simulation number								
	1	2	3	4	5	6	7	8	9
Micro-physics	THOM	WSM6	MORR	THOM	WSM6	MORR	THOM	WSM6	MORR
Urban surface	SLUCM	BEP	BEM	SLUCM	BEP	BEM	SLUCM	BEP	BEM

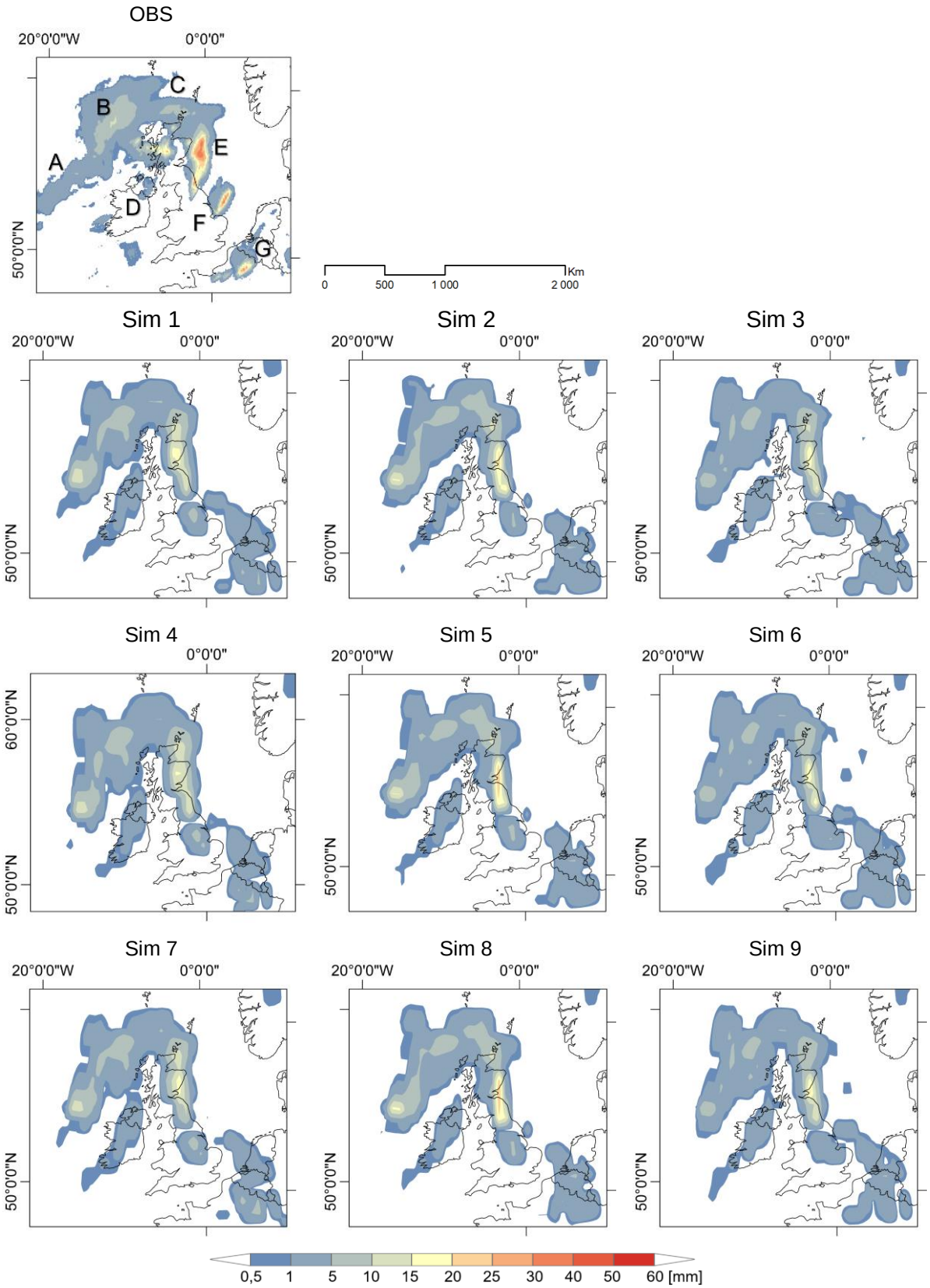

Figure 4.8. Accumulated rainfall maps from 15:00 UTC to 17:00 UTC on the 28th June 2012 using GPM IMERG data (top panel) and for simulations 1-9 (see Table 4.4 for the specific combination of the physics schemes)

For all simulations, the WRF model reproduces the extensive band of rainfall north of the United Kingdom, roughly in the form of an arc. There are some regions with larger accumulated values than in the surrounding areas, and other parts in the domain in which the model is clearly under- or overestimating the observed rainfall. A more detailed analysis is presented below.

The WRF simulations for Domain 1 (the outermost domain with 54km grid resolution) consistently underestimate the accumulated rainfall on the west part of the domain (feature A on the 'observed data' panel of Figure 4.8). While the GPM data show that there is a tongue of rainfall that indicates the storm path, the simulated scenarios fall short in this region and do not reproduce the shape of the rainfall pattern. It is important to consider that the largest uncertainties in GPM data lie in its temporal accuracy, not in the spatial patterns. This could imply that the WRF model outputs are indeed overestimating the rainfall values for some regions, but that the timing of the GPM data used as "observed" could penalise model outputs given that its temporal resolution is 30 minutes. Simulated rainfall patterns over feature A could be explained by the extent of the relaxation zone in domain 1 (four rows), as this area is merely used to match (or relax) the values from the coarsest grid to the boundary so spurious simulated values are expected.

The largest rainfall intensity in the north-west of the domain (feature B) seems to be better reproduced by the Thompson microphysics scheme (Simulations 1, 4 and 7), although still underestimated. In this case, the parameterisation that gives the best results uses look-up tables to determine hydrometeor density so the larger the extent to forecast, the more accurate the results.

Regarding feature C, GPM data show a "step" which serves as a division point between the rainfall band that extends to the east of the United Kingdom and the rainfall that is accumulated in the northernmost part of the domain. This is reproduced only by two of the scenarios using the simplest microphysics scheme (Simulations 2 and 8), meaning that the precipitable water on the north of the domain is better described by the complexity of cloud physics.

All cases deliver a band of rainfall over the Island of Ireland (feature D), where rainfall values were recorded only in the north and south of the area. The fact that all cases simulate rainfall in this region could mean that the resolution of the coarsest domain does not capture the effects of the topography. Despite this inaccuracy, results in this region (although outside the window of interest) confirm the usefulness of implementing finer (nested) grids.

Feature E is the most important to reproduce in the domain as this represents the flood-associated rainfall over Newcastle. As stated previously, at synoptic scale it is likely to find underestimated values, so it is not surprising that large accumulated rainfall values (close to

50 mm) are not well reproduced by the coarsest domain. Nevertheless, all simulations clearly show that the largest values in the whole domain are simulated over the area of interest. This is a good first indicator of model performance: quantitative metrics were applied and will be detailed in the following sections.

Another important thing to notice is the overestimation of rainfall in the Midlands region (feature F). The storm originated in the southwest and moved towards the northeast (as detailed in Section so at some point there was indeed rainfall in this region (as detailed in Section 4.2.2). Therefore, at the coarsest scale, the model is not correctly reproducing the time of arrival of storm cells. However, this consistent behaviour for all simulations means that any correcting procedure can be applied to all scenarios.

Finally, the model largely overestimated the extent of the rainfall over the north of France (feature G). This situation resembles that on feature A, where an incorrect rainfall prediction is due to the presence of the relaxation zone, which should not be considered for analysis.

Despite the apparent low skill of the WRF simulations at synoptic scale, it is important to consider the main function of the parent domain, which is to provide appropriate lateral boundary conditions for the following nested domain (Wang et al., 2012). In fact, information from this grid is not used to determine the skill of the simulation, instead serves as parting point to qualitatively assess the appropriateness of the model set-up and lateral boundary conditions used to run the simulations (Campos et al., 2015). A closer look at model results at local scale in Figure 4.9 illustrate the difference in computed rainfall by the four domains for simulation 2 and support the use of the rainfall computed in the coarse grid to drive the following nested domain.

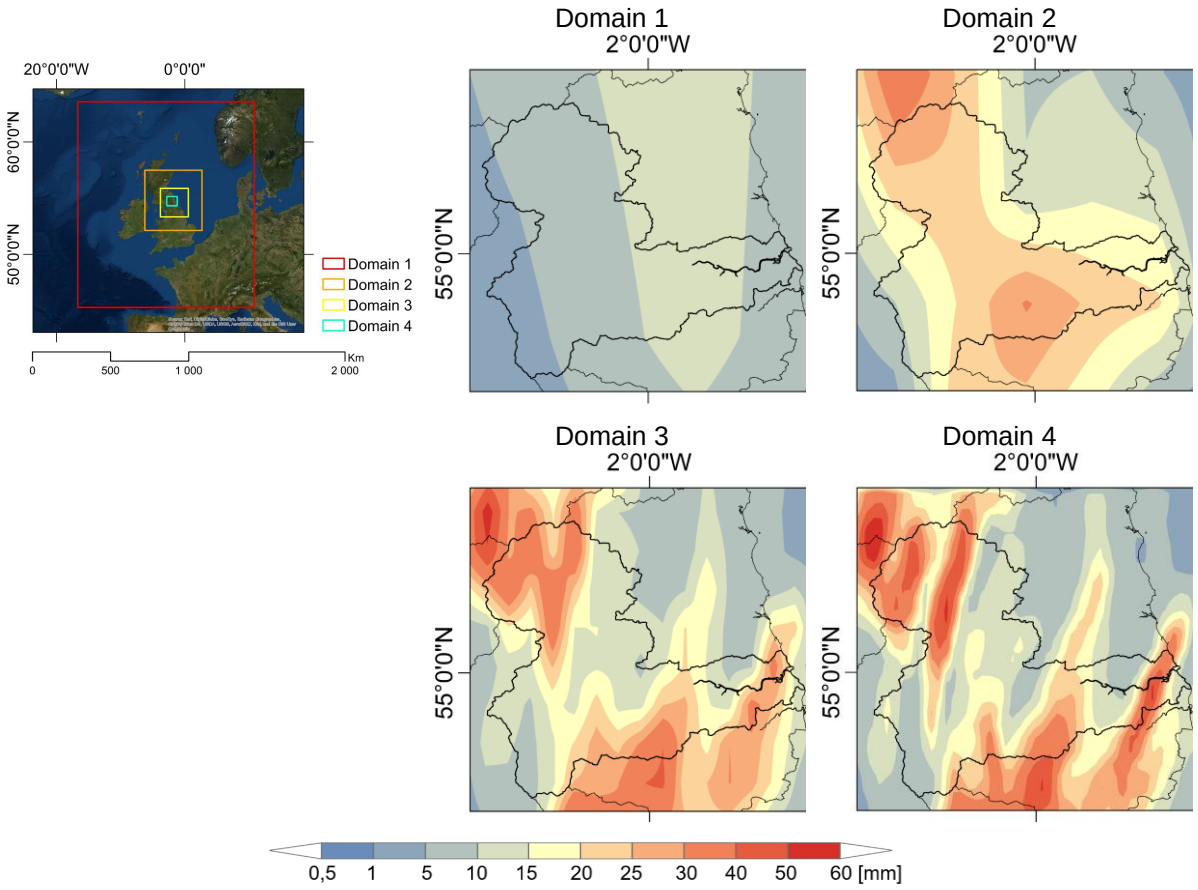

Figure 4.9. Comparison of accumulated rainfall maps from 15:00 UTC to 17:00 UTC on the 28th June 2012 using information from domains 1-4 (top to bottom, left to right) for simulation 2, across the innermost domain

At this scale, information to determine the best or worst performing simulations is insufficient. Instead, identification of the meteorological features and rainfall clusters gives a good first glimpse at the overall model performance and sets the precedent for further analysis.

4.4.2 Mesoscale analysis

The following scale for analysis spans over domain 4 only (refer to Figure 4.5 for domain configuration) which covers the entire Tyne catchment. At this scale, WRF model outputs are presented at the finest scale of the set-up (2 km) so rainfall maps are the result of the downscaling procedure thus are considered the final model outputs. Three snapshots of the NIMROD radar data (described in Section 3.4.1) were taken at 15:00 UTC, 16:00 and 17:00 UTC on the 28th June 2012 and considered as reference to compare the simulated scenarios with. Given that radar rainfall is subject to errors (as detailed in Section 3.4.1.2), some of the features in the observed data should be reproduced by the models and others are likely to be noise. The closest radar to Newcastle is located approximately 25 km south of the city, which

reduces the possibility to receive information above the cloud, a phenomenon that occurs from 100 km and beyond of the radar. NIMROD radars are also likely to overestimate rainfall from intense rainfall given the large size of hydrometeors. Moreover, weather radar data does not actually display rainfall at the surface (Met-Office, 2003). Therefore, information from NIMROD radars, similar to the rainfall from the GPM mission, will be considered for qualitative analysis as a preliminary estimation of model skill to proceed with the hydrological modelling.

Snapshots for simulations 1-3 are shown in Figure 4.10a, simulations 4-6 are shown in Figure 4.10b and simulations 4-9 are shown in Figure 4.10c. The nine WRF rainfall scenarios correspond to the parameterisations shown in Table 4.4 (for details on each scheme, refer to Section 3.3.1.2). The urban canopy schemes, in order of increasing complexity are the Single Layer Urban Canopy model (SLUCM), Building Effect Parameterisation (BEP) and Building Energy Model. The three microphysics schemes, also in order of increasing complexity, are WRF Single-layer 6-class (WSM6), Thomson (THOM), and the Morrison (MORR) scheme.

At 15:00 UTC, the storms from the south-west reached Tyneside. The radar snapshot for this time does show a small area of accumulated rainfall in the south boundary of the catchment. This is not reproduced by any rainfall simulations: all modelled rainfall occurs in the west part of the domain, with some simulations having large magnitude accumulations (such as simulations 1 and 6). This confirms what was observed at synoptic scale: the model struggles to reproduce the timing of arrival of intense storm cells, even in the finest domain. Model skill evaluation in the following hours will give more information on how the hydrometeors and precipitation forms.

At 16:00 UTC there was an intense band of precipitation over Newcastle in the observed data. By this time (and as detailed in Section 4.2.3) some of the highest values should be shown in the simulated rainfall maps. All WRF scenarios do show significant rainfall clusters, albeit in places west of domain 4. There is more agreement in the patterns produced by the same microphysics schemes than those determined by the same urban canopy layer. For example, THOM (simulations 1, 4 and 7) deliver rainfall patterns that can be more easily grouped than scenarios produced using the most complex urban canopy scheme (simulations 7, 8 and 9).

By 17:00 UTC, most simulations show good agreement in the rainfall patters. Radar shows that the rainfall band extends further south of Newcastle and this is best reproduced by WSM6 (simulations 2, 5 and 8). This corroborates the finding that at this scale, where only a small region in the entire domain is urban, results are more sensitive to the choice of microphysics scheme. In contrast, THOM (simulations 1, 4 and 7) produces a band of rainfall the one in the radar data, but in the wrong location (north of Newcastle, where one hour later the storm would dissipate) suggesting that the last stage of the storm was developed quicker in the simulations.

Similarly, MORR (simulations 3, 6 and 9) also miscalculates the amount of rainfall, largely underestimating the values.

In general, all rainfall scenarios predict the arrival of the rain cluster to Newcastle with a lag. By 16:00 the bulge of rainfall over the city is clear in the radar imagery whereas the model predicts the storm is still on its way. However, all simulations catch up with the observations by the end of the critical 2-hour period (at 17:00). This has significant repercussions in the calculation of the skill scores, as they consider the differences between measured and simulated for every time step.

The SLUCM+THOM combination (simulation 1) reproduces the storm track better than SLUCM+WSM6 or SLUCM+MORR (simulations 2 and 3). This is in line with previous studies that found THOM to outperform the complex MORR (Rajeevan et al., 2010). SLUCM+THOM (simulation 1) also show a clear path of movement of the main rain cluster, unlike SLUCM+WSM6 (simulation 2) which overestimates rainfall values for most of the period, although it provides the best representation of the pattern of storm cells over Newcastle at 17:00 UTC. Overall, SLUCM paired with THOM and MORR have accumulated values closer to the observations than simulation 2.

The Building Effect Parameterisation scheme (BEP, simulations 4-6) produces better rainfall estimates when used with the Thompson microphysics (simulation 4). Despite incorrectly reproducing the rainfall at 15:00, using BEP+THOM helps the model to catch up with the storm track two hours later The BEP urban canopy scheme tends to have a good performance over time (Fallmann et al., 2013). Using BEP+WSM6 considerably overestimate rainfall over the two hours (simulation 5), whereas BEP+MORR (simulation 6) also identifies the location of the main rainfall cluster, although underestimating it.

The most complex urban canopy model, the Building Energy Model (BEM, simulations 7-9) works best with the Thompson and Morrison schemes (simulations 7 and 9, respectively). Skill of BEM+MORR is a new finding as BEM has only been implemented other microphysics schemes on studies on the Urban Heat Island effect (Chen et al., 2011) (Sharma et al., 2017). In contrast, BEM+WSM6 (simulation 8) overestimate the values during most of the period of analysis at this scale and even produce an additional rain cluster north of Newcastle at 17:00 UTC. The low skill of WSM6 to capture spatial patterns has also been documented before (Campos et al., 2015).

These comparisons show that the WRF model correctly captures many aspects of the storm rainfall, so that errors can be propagated into discharge predictions.

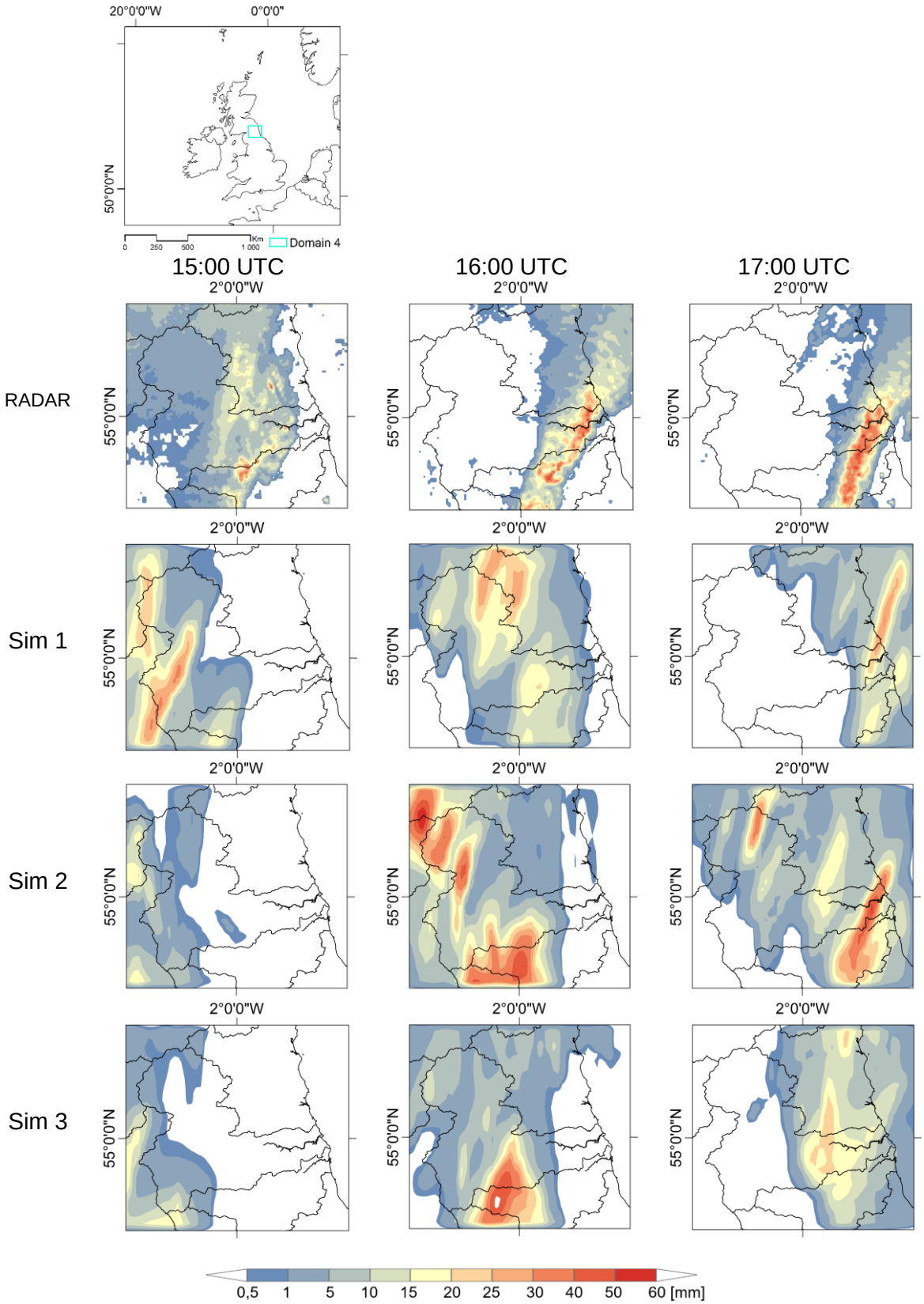

Figure 4.10a. Hourly time evolution of the rainfall on 28th June 2012 (15:00, 16:00 and 17:00 UTC). Observed radar values (top row) and rainfall patterns for WRF simulations 1, 2 and 3

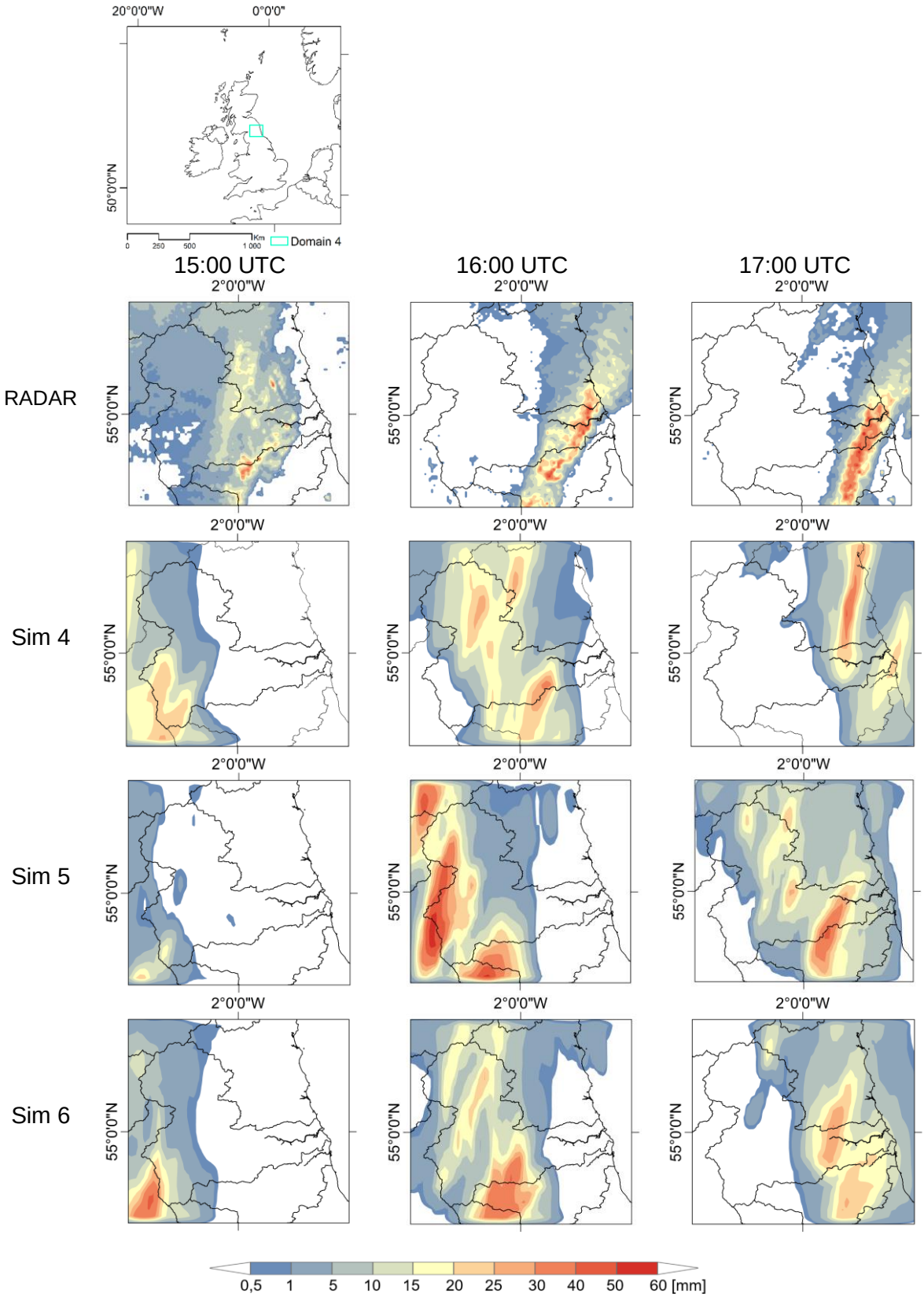

Figure 4.10b. Hourly time evolution of the rainfall on 28th June 2012 (15:00, 16:00 and 17:00 UTC). Observed radar values (top row) and rainfall patterns for WRF simulations 4, 5 and 6

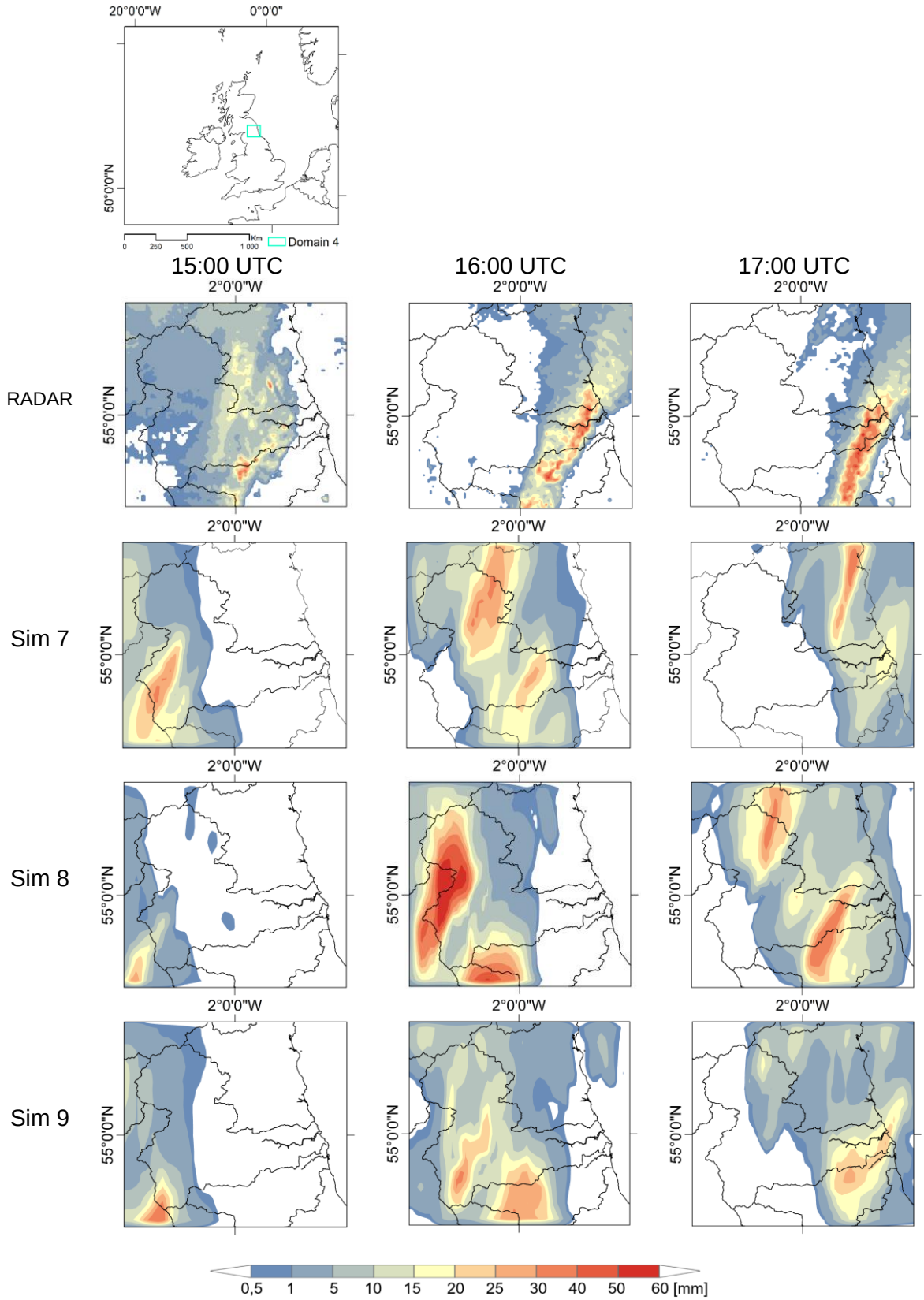

Figure 4.10c. Hourly time evolution of the rainfall on 28th June 2012 (15:00, 16:00 and 17:00 UTC). Observed radar values (top row) and rainfall patterns for WRF simulations 7, 8 and 9

4.4.3 Local scale analysis

As stated in Section 3.4.1, evaluation of model performance at local scale was done through categorical and continuous indices and plots of rainfall timeseries. Figure 4.11 shows the location of six gauges in the domain that were considered for rainfall analysis at hourly scale along with the land use coverage as processed by the WRF model. It is important to consider the accuracy of the rain gauge data in this analysis. Given that this dataset is the best estimate of the rainfall available, it is appropriate to make more detailed comparisons between the observed and the simulated data.

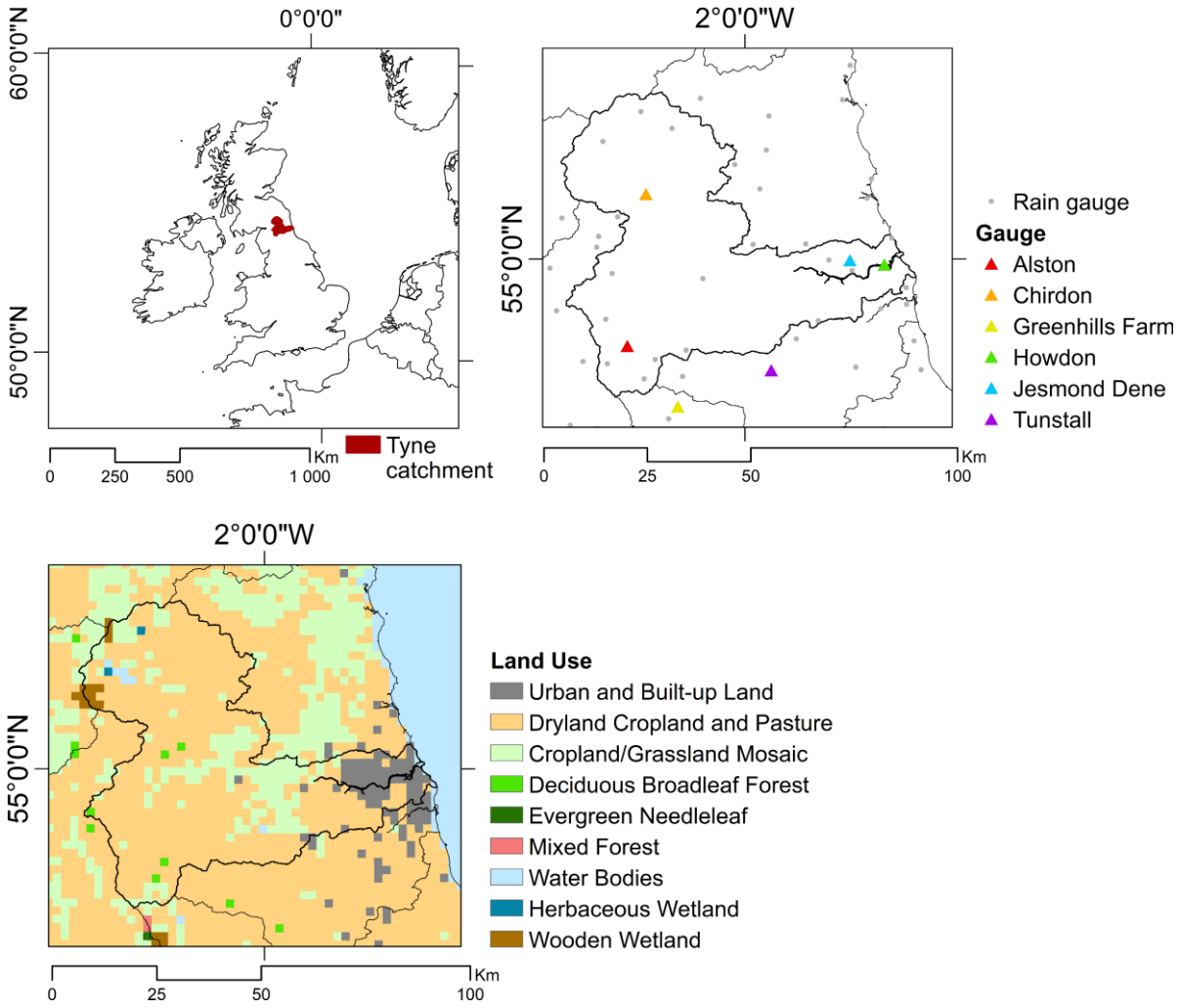

Figure 4.11. Spatial extent of the Tyne catchment (top left), location of the rain gauges used in the local scale analysis of the June 2012 event (top right) and land cover processed by the WRF model (bottom)

Figures 4.12 to 4.14 display the rainfall timeseries for said rain gauges, grouped by urban canopy model.

Rainfall recorded at the station closest to the west boundary of the domain, Alston, is better represented when using the Single-Layer Urban Canopy Model (SLUCM), where values produces by the three microphysics schemes are similar (Figure 4.12a). The Building Effect Parameterisation (BEP) and the Building Energy Model (BEM) overestimate and underestimate the rainfall (Figure 4.12b and Figure 4.12c), deviating from the peak value. Since this gauge is in a non-urban area, this result is not surprising: representation of atmospheric processes here does not involve a significant urban influence.

At Chirdon, the northernmost rain gauge, the best results are given by the BEP scheme for the three microphysics schemes (Figure 4.12e). SLUCM and BEM (Figure 4.12d and Figure 4.12f) consistently underestimate the observed rainfall except for an outstanding peak produced by combining SLUCM with the simple WRF Single Layer 6-class scheme (WSM6, Figure 4.12d).

The largest differences in recorded and simulated rainfall are at the station at the highest elevation, Greenhills Farm. All the canopy models deliver a considerable peak when paired with WSM6 (Figures 4.13g-i). On the other hand, BEP and BEM give the best results when paired with the Thompson microphysics (THOM, Figure 4.13h and Figure 4.13i). Other studies support the good performance of BEP+THOM and BEM+THOM (Barlage et al., 2016). This means that at high elevations, cloud physics need to be solved in a detailed but efficient manner- something THOM does (see Section 3.3.1.2 on details on this scheme)

At Howdon, the results using BEP and BEM are very similar (Figure 4.12k and Figure 4.13l), all underestimating the rainfall although reproducing the timing correctly. Both schemes give best results when paired with the complex Morrison microphysics scheme (MORR). The best rainfall estimate at this gauge is given by SLUCM+THOM (Figure 4.13j), which contradicts previous studies on urban meteorology (Barlage et al., 2016) but that agrees when carrying out studies over a larger areas (Yang, Wang, et al., 2016).

Rainfall at Jesmond Dene is correctly reproduced with BEP+WSM6, however, this is the only gauge where this behaviour is observed. Timing of peaks in Chirdon and Jesmond Dene exhibit the westward track of the storm described in Section 4.2.2 (passing first over Jesmond Dene at 16:00 UTC and then Howdon at 17:00 UTC). However, plots for both stations show simulated peaks at both stations by 17:00 UTC, which means that the simulated storm was generated within one hour for a larger area.

Both at Howdon, and Jesmond Dene, BEM+MORR give the best results (Figures 4.13k, 4.13l, 4.14m and 4.14o), a combination chosen in studies on Urban Heat Islands (Morini et al., 2016). The storm track over an urban area is therefore better reproduced when cloud processes and fluxes in the urban canopy are parameterised with the most detailed schemes.

Finally, an interesting development at Tunstall is shown in the panels at the bottom row of Figure 4.14. BEP and BEM show a good agreement in the simulated values for all microphysics schemes (Figure 4.14q and Figure 4.14r). In fact, BEP has been found to consistently outperform the complex BEM in urban meteorology studies (Barlage et al., 2016; Fallmann et al., 2013). From all simulations at said gauge, WSM6 performs the worst regardless of the urban canopy model used, overestimating the main rainfall peak and delivering smaller peaks before the arrival of the storm. The results at this rain gauge confirm that reproducing arrival of storm cells to an urban area is best achieved by using a complex microphysics scheme, regardless of the urban canopy model (Figure 4.14r and Figure 4.14s). Similar findings were obtained at Jesmond Dene (Figure 4.14n and Figure 4.14o).

In general, the SLUCM scheme has more variability than the other two urban canopy schemes in some stations (for example, Chirdon, Greenhills Farm and Tunstall), whereas there is more similarity in the timeseries when using either BEP or BEM (for example, Jesmond Dene and Howdon), and they work better with THOM and MORR. Given that the combination of those schemes has only been done in studies on air quality and Urban Heat Islands, these results represent a novelty in the application of the WRF model to simulate intense rainfall in urban areas. The consequent recommendation when simulating rainfall is then to use a multi-layer urban canopy scheme and a double- or a semi-double moment microphysics scheme.

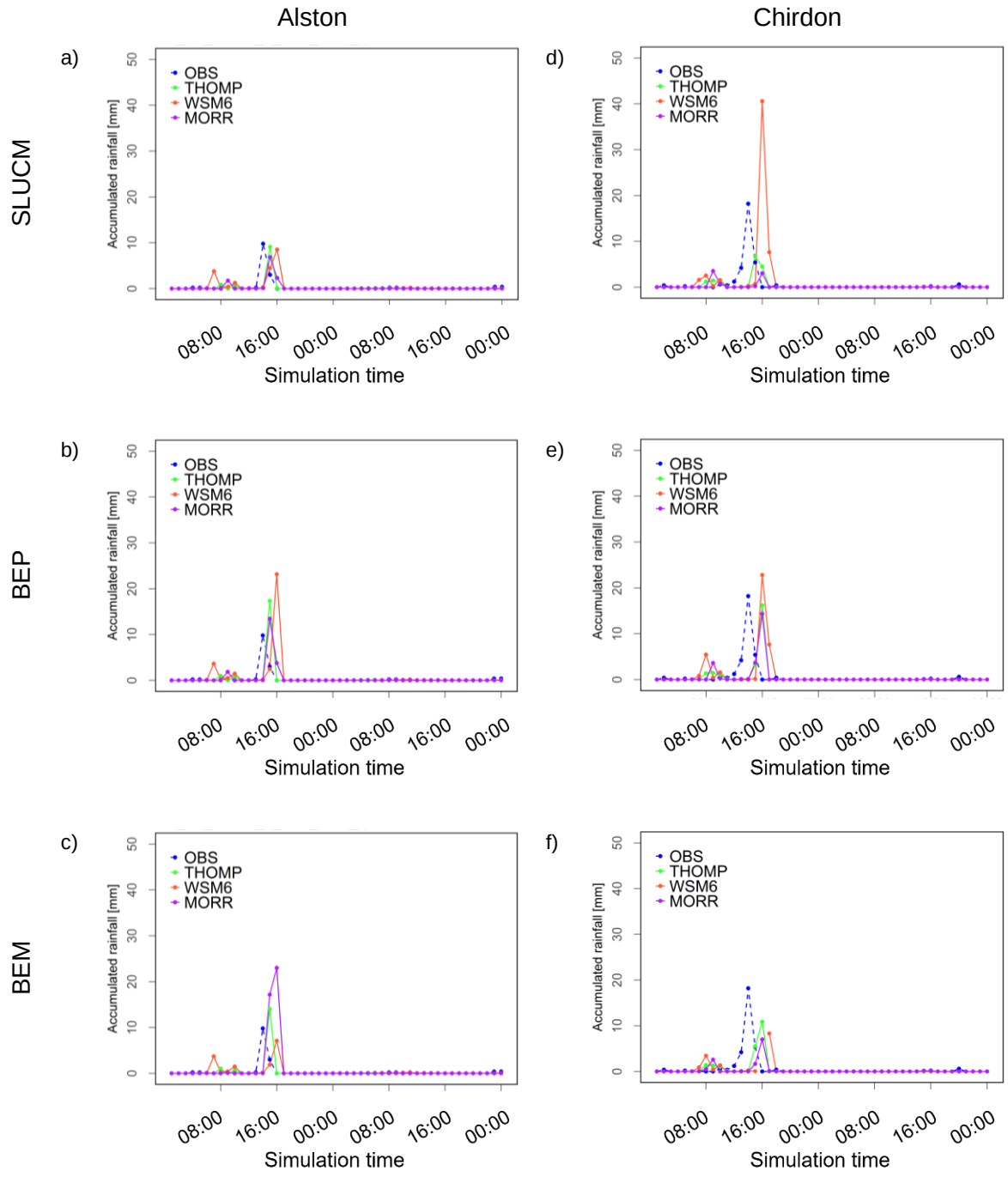

Figure 4.12. Simulated rainfall for the nine WRF scenarios (see Table 4.4), grouped by urban canopy model scheme, for two gauges in the Tyne catchment. See Figure 4.11 for location of gauges

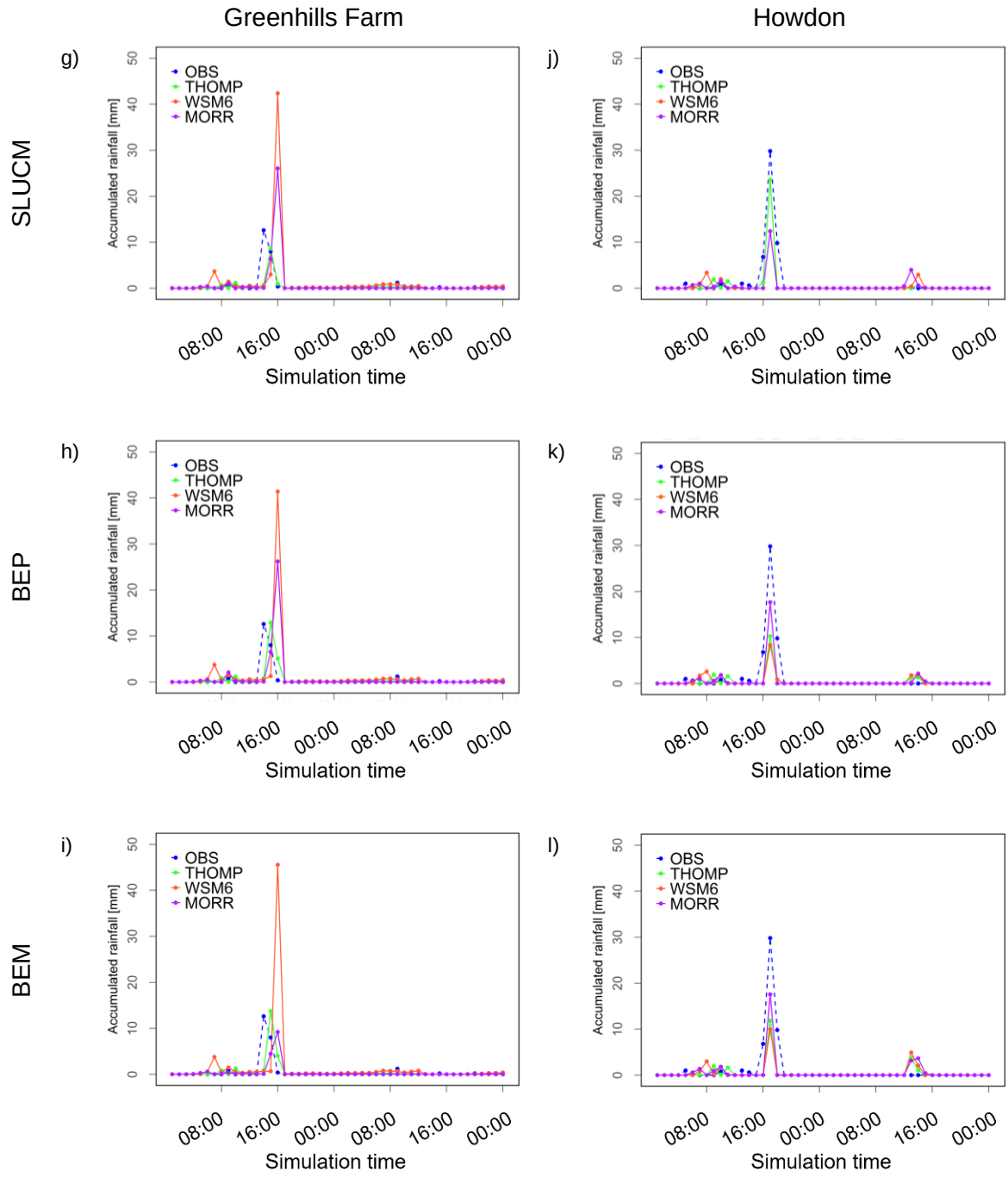

Figure 4.13. Simulated rainfall for the nine WRF scenarios (see Table 4.4), grouped by urban canopy model scheme, for two gauges in the Tyne catchment. See Figure 4.11 for location of gauges

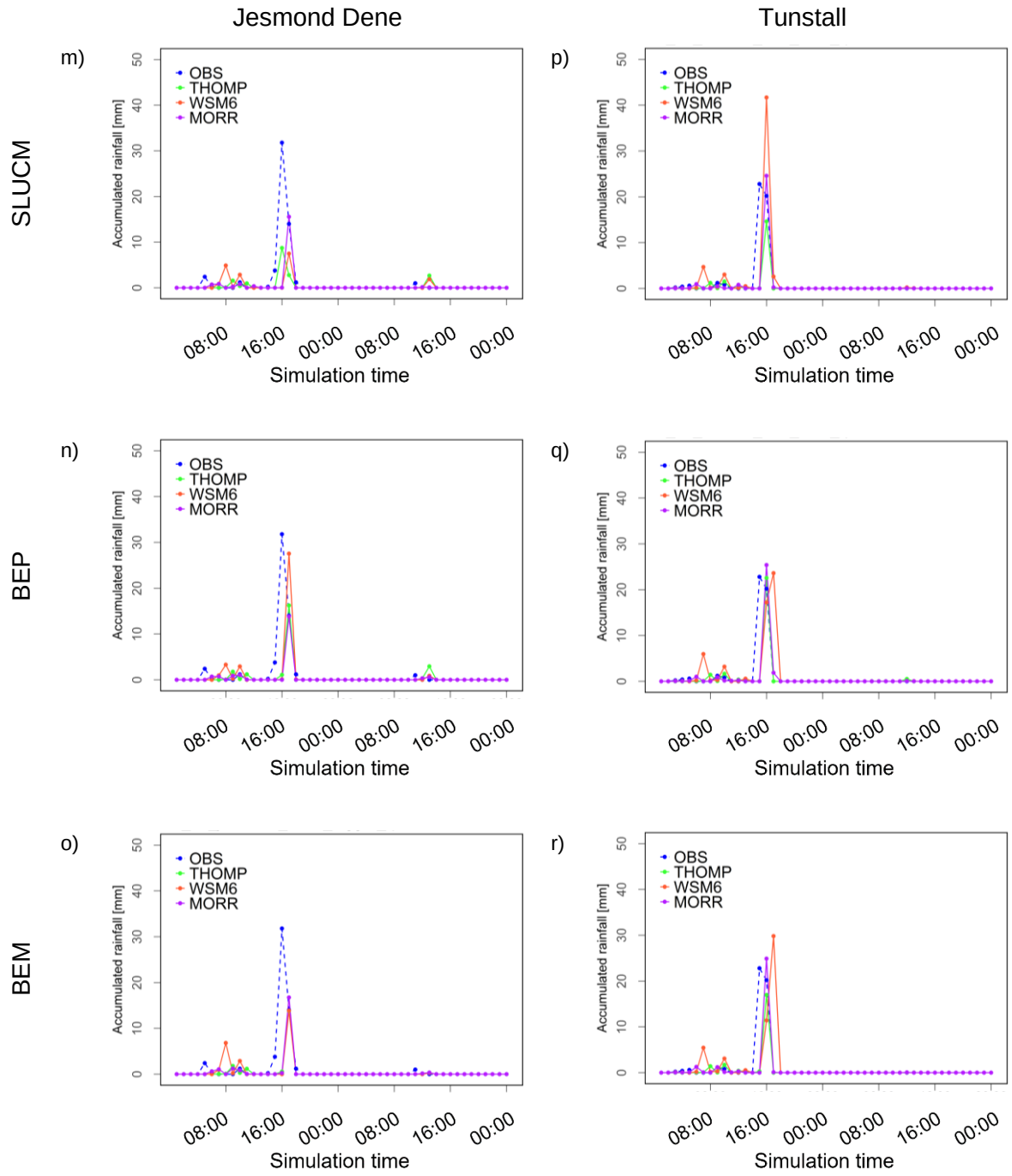

Figure 4.14. Simulated rainfall for the nine WRF scenarios (see Table 4.4), grouped by urban canopy model scheme, for two gauges in the Tyne catchment. See Figure 4.11 for location of gauges

4.4.5 Overall model performance

The following evaluation is done after the results presented at local scale.

The ensemble using the simplest urban canopy scheme (SLUCM, simulations 1-3) presents a lower ensemble spread than the rest of the scenarios but also shows the largest deviation from the observed values. Ensembles obtained using the more complex schemes (BEP and BEM, in red and lilac) are closer to the observed time series. Spread of the ensemble using BEP means that this urban canopy scheme is the most sensitive to the choice of microphysics scheme.

The performance metrics shown in Table 4.5 agree with these statements. All simulations have a negative Mean Bias Error (MBE) as all of them underestimate the rainfall when averaging values across the domain. The indices confirm that, for this case study, the model is not sensitive to the choice of urban canopy model: there is no clear trend in simulations grouped by this scheme (1-3 use SLUCM, 4-6 use BEP and 7-9 use BEM). On the other hand, the WSM6 microphysics (simulations 2, 5 and 8) presents a consistently low Critical Success Index (CSI) and the largest Root Mean Square Error (RMSE) of all simulations, whereas the Morrison scheme (simulations 3, 6 and 9) achieves the highest Critical Success Index, and two of the simulations (simulations 3 and 9) also have the lowest RMSE. However, the simulations with the lowest MBE value are those that used the WSM6 scheme (simulations 2, 5 and 8). MBE is likely to compensate large errors if in the timeseries of observed and simulated values there are considerable over- and underestimations, which then cancel each other out. Therefore, RMSE is a better indicator of the performance of the model, and MBE is taken only as an indicator of the general behaviour of the simulation.

Computation time was also considered to determine the best performing simulations. The Single Layer Urban Canopy Model (SLUCM) is the most computationally efficient urban canopy scheme, and the highest processing times are associated with BEM. Computation times for the WSM6 microphysics (simulations 2, 5 and 8) have a significant increase with the complexity of the urban canopy (a time increase of 317.22% from simulation 2 to 5, and an increase of 136.06% from simulation 5 to 8). This confirms the sensitivity of WSM6 to the choice of urban canopy model, something observed at Chirdon station (Figure 4.12d-f).

The overall model performance was obtained from the weighted sum of the ranking when considering CSI, RMSE and total computation time. For a given metric, the best performing simulation was assigned a value of 9/9, and the worst performing was assigned a value of 1/9. Figure 4.15 shows the stacked column plot for each simulation and the contribution of each metric to the final rank.

Table 4.5. Skill scores and accumulated rainfall for the nine WRF simulations of the June 2012 event

Simulation	CSI	RMSE [mm]	MBE [mm]	Computation time [hrs]
1	0.77	1.65	-0.74	16.22
2	0.68	2.13	-0.33	15.21
3	0.81	1.82	-0.74	15.65
4	0.75	1.80	-0.69	24.38
5	0.68	2.21	-0.46	48.25
6	0.82	1.89	-0.59	16.18
7	0.75	1.84	-0.69	19.46
8	0.67	2.32	-0.40	63.65
9	0.79	1.73	-0.74	19.56

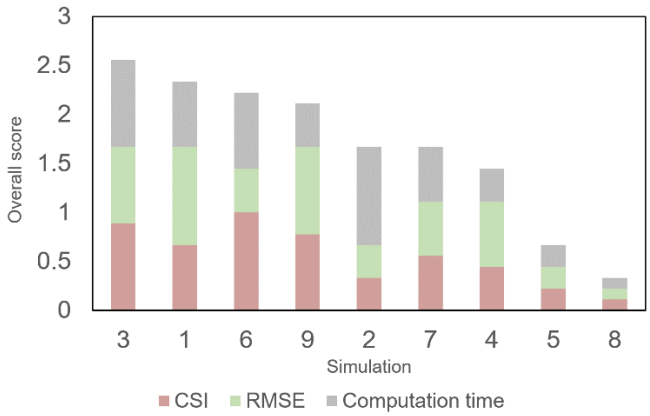

Figure 4.15. WRF simulations ranked by performance for the June 2012 case study, showing bar length as the contribution of each metric to the overall performance

Simulations 1, 3, 6 and 9 the lowest computation time. If computation times were not considered for the ranking, these simulations would still outperform the rest. This means that cloud processes are, in general, best simulated when using a complex microphysics scheme, regardless of the urban canopy model. This conclusion is perhaps not surprising given the extent of the land cover classified as urban, displayed in Figure 4.11. It is worth noticing that simulation 1 (that implements the simplest microphysics and urban canopy schemes) is the second-best combination due to its low RMSE, but the CSI is as low as simulation 7. This means that predicted wet cells have a close value to the observations, but the amount of those wet cells is lower than in other simulations.

On the other end of the ranking lie the simulations using the simplest microphysics scheme (WSM6, simulations 2, 5 and 8). This means that the skill of the numerical modelling depends on calculating the physical properties of the hydrometeors (density, mass-size relationship) rather than the number of hydrometeor classes.

4.5 Final remarks

This chapter presents the meteorology of the June 2012 case study, the model-set up and analysis of main outcomes at three spatial scales.

In this case, although the flash floods occurred in an urban area, most of the finest domain comprises natural land cover, so the model was found to be not sensitive to the choice or urban canopy parameterisation, but to the choice of microphysics. Analysis at synoptic and mesoscale does not allow determination of which simulation best reproduces the event, as all simulations present patterns than resemble the observations, some with specific deficiencies regarding the ability to reproduce the spatial evolution of the rainfall, but all of them still deliverig the expected amount of rainfall after the simulated period. Local scale analysis allowed not only the ranking of simulations by performance skill (at this scale, categorical and statistical indices are used), but also a more detailed comparison of the storm track over the area of interest, giving useful information on the strengths and weaknesses of the combination of microphysics schemes chosen.

The simplest microphysics scheme is not the most appropriate for this case, meaning that for convective events with a quick development it is more important to consider specific properties of the hydrometeors to calculate amount of precipitable water (for example, computing the mass-size relationship as a function of the diameter, which the Thompson microphysics does, leads to determining the fall velocity) is more important than considering more hydrometeor classes (which the WSM6 does).

The next step in the hydrometeorological framework is the implementation of the WRF model outputs as climatological inputs for hydrological modelling. The nine rainfall scenarios (as a result of the combination of the microphysics schemes and three urban canopy models) described in this chapter will be used for the following stage, regardless of their performance. This is done to evaluate the error propagation through the chain and to determine the importance of the accuracy of the simulated rainfall in the final outputs of the cascade.

Chapter 5

Meteorological modelling case 2. Birmingham 2007 flash flood event

5.1 Introduction

The previous chapter presented the simulation and discussion of outputs of the meteorological modelling of the first case study, including discussion of main outcomes and additional tests that support the model set-up implemented for both case studies.

This chapter introduces the numerical modelling and results of the first stage of the hydrometeorological framework, applied to the second case study. It starts with the introduction of the flash flood event and describes the motivation behind its selection as case study. Antecedent meteorological conditions that led to the setting for the flash flood precede a description of the rainfall recorded during the event as a result of the evolution of the generating weather system. Afterwards, the model set-up is documented, including the period for which the lateral boundary conditions were retrieved. Analysis of results, following the procedure for the first case study, is done at synoptic, meso- and local scale. The first scale refers to an area that covers the United Kingdom and part of Europe, which corresponds to the extent of the parent domain of the meteorological model. Mesoscale refers to the analysis over the innermost domain, which covers the hydrometric area that contains the catchment of study (details on the definition of the hydrometric area can be found in Section 5.3.1). Finally, analysis at local scale is done by making a point-to-point comparison of specific cells of the innermost domain with the correspondent rain gauges. Finally, the overall model performance is assessed and final remarks on the modelling are discussed.

5.1.1 Justification of choice of event

During June and July, severe floods affected hundreds of thousands of people in England and Wales caused by two major rainfall episodes, on 24-25 June and 19-20 July. The first one resulted from a slow-moving area of low pressure over the north of the Midlands region, and the second one was the consequence of an occluded warm front and an area of low pressure over southern England that moved northwards. The second one affected nearly 20% of England and Wales, with rainfall accumulations in excess of 50 mm over a wide area. The subsequent flooding affected at least 55 000 homes, leaving nearly 6 000 businesses flooded

and causing approximately £3 billion worth of insurance claims. In some regions, people were left without mains water supply. The damage to infrastructure, power supplies, disruption of transport links and telecommunications meant the most considerable loss of basic services since the Second World War (Marsh & Hannaford, 2007; Pitt, 2008).

Analysis of this event focuses on the unfolding of meteorological conditions that lead to a flash flood in the major city of Birmingham, located in the Midlands region of England. Among the affected places, this location was chosen as Birmingham is the second most populous city in the United Kingdom (Heaviside et al., 2015).

Figure 5.1 includes photographs in three locations of the described disruptions in the Midlands region on the day of the event, showing the severity of the flooding.

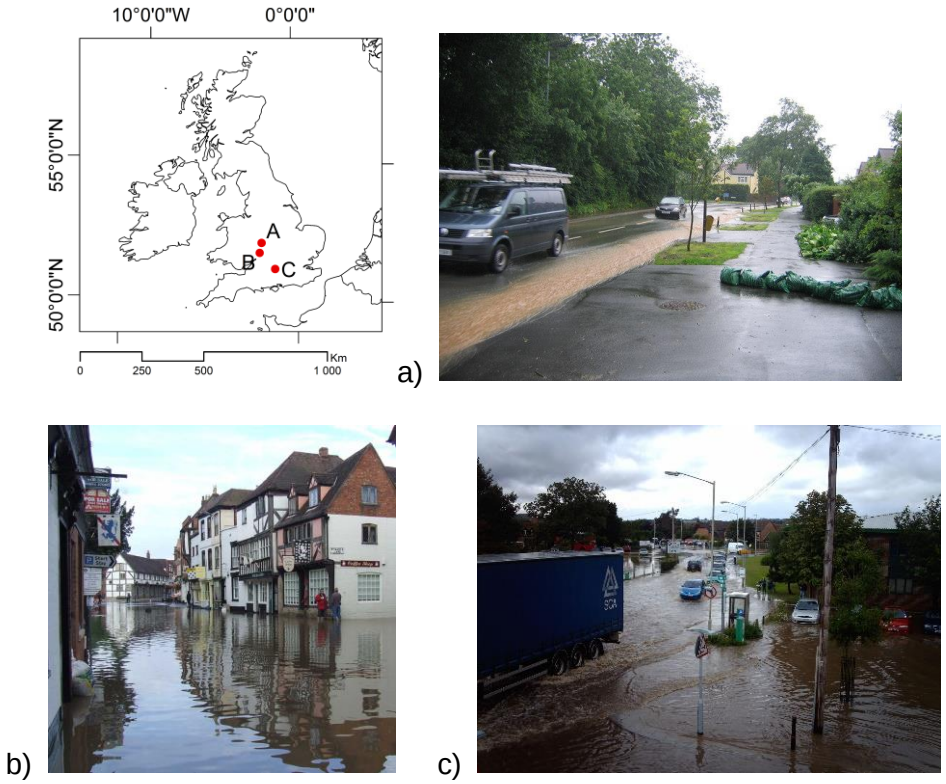

Figure 5.1. Photographs of disruption across the Midlands during 20 July 2007. Top row, left: reference map, a) Flooding in Old Birmingham Road, where sandbags could not prevent internal flooding of the houses along said road (Hughes, 2007), b) Damages on 20th July ("Church Street Tewkesbury 2007 Flood", (Tewkesbury Museum, 2007), c) Flooding outside Thatcham Railway Station (Flaschen, 2007)

5.2 Meteorological setting

5.2.1 Historical context of flash floods in the Midlands

There are many examples of intense summer flooding in this region. Even seasonally normal rainfall has resulted in areas under water, such as in 1853 and 1875. At the beginning of the 20th century, records show inundated regions as a result of steady and continuous rainfall (such as in 1903). An event with similar meteorological conditions includes the one in the East Coast in August 1912, where 228 mm of rain fell within 12 hours over the southwest of England. That year marked the wettest summer for England and Wales, until the rainfall in summer 2007. This shows that intense rainfall and consequent flooding is expected during summer months (Stuart-Menteth, 2007).

A benchmark event, named as such due to its severity and the extent of the affected area, occurred in the Midlands in March 1947. Following the coldest and driest February since 1895, snow steadily accumulated in the region, with wintry weather that lasted until mid-March. The exceptionally high and lasting snow levels were followed by usual thaw. However, this occurred along with intense rainfall, and both the combined volume of rainfall and snowmelt along with the inability of the frozen hard ground to soak up the surface flow, caused some of the worst floods in the country (Met-Office, 1948).

Another significant flood event occurred in November 2000. Groundwater levels usually decline over the May to September periods as there is a non-appearance of natural replenishment, nonetheless the groundwater levels in the Cotswolds area were above the natural winter levels by the end of July, and with rainfall records that were broken that summer, significant floods occurred in the area later in November that year. This event is largely considered as a fluvial flood, however there was significant surface runoff after unusually high precipitation rates, such as the one that preceded the 2007 event (Stuart-Menteth, 2007).

The effect that the 2007 event had on the community and urban centres led to comparisons to the benchmark 1947 event (Marsh and Hannaford 2007).

5.2.2 Antecedent conditions

As of 2018, the October 2006-February 2007 period in England and Wales was the third wettest of the record period that began in 1961, as stated by Marsh & Hannaford (2007). This has actually been surpassed by the rainfall recorded in February 2020, which is now states as the wettest February on record and 5th wettest Winter since the beginning of the period of record (Met-Office, 2020).

The unusually wet weather began in May and continued throughout the summer. This intense rainfall was the result of two major weather systems: the Polar Front Jet Stream and the front as result of high North Atlantic Sea surface temperatures. The Jet Stream manifests itself as a front that creates bands of intense rainfall and strong winds. On the other hand, increased temperatures of the North West Atlantic Ocean cause the air mass just above the ocean to retain more moisture, increasing its rainfall generating potential. In early May, the Jet Stream took an unusual southerly track that resulted in intense rainfall-producing weather systems in the central and southern parts of the United Kingdom. For most of March to June 2007 the temperatures of the North West Atlantic Ocean were higher than normal, meaning that the moisture rich air mass above the ocean contributed the delivery of large amounts of rainfall. The prolonged period of rainfall led to a decrease in soil storage capacity during May and early June, so by mid-June the ground was saturated. The combination of these two fronts lead to extreme 10-week rainfall totals which caused by serious flooding between June and July (Marsh, 2008).

For comparison purposes, Figure 5.2 (Pitt, 2008) shows the path of the Jet Stream in July in 2006 and 2007, where the unusual location of the weather system can be appreciated.

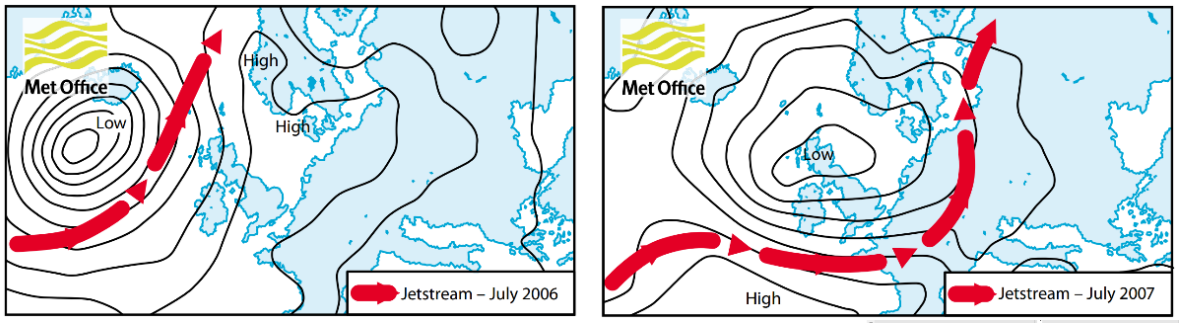

Figure 5.2. Positions of the Polar Front Jet Stream for July 2006 and 2007 (taken from Pitt, 2008)

5.2.2 The event

The combined action of the two meteorological systems mentioned above determined the development of the two major events of 24-25 June and 19-20 July. These dates correspond to standard “rainfall days”, which start at 09:00 UTC. Therefore, the July event is in fact the period from 09:00 UTC 19 July 2007 to 09:00 UTC 21 July 2007.

The slow-moving depressions that had been stationary in the south of the United Kingdom moved northwards, bringing intense rainfall across the Midlands. In the early hours of the 20th July, the low-pressure system was centred over south-east England, and moved towards the

north throughout that day. Figure 5.3 (Brown, 2016) shows the synoptic situation of the low-pressure system over the Midlands after it moved from the southwest, leaving thunderstorms behind.

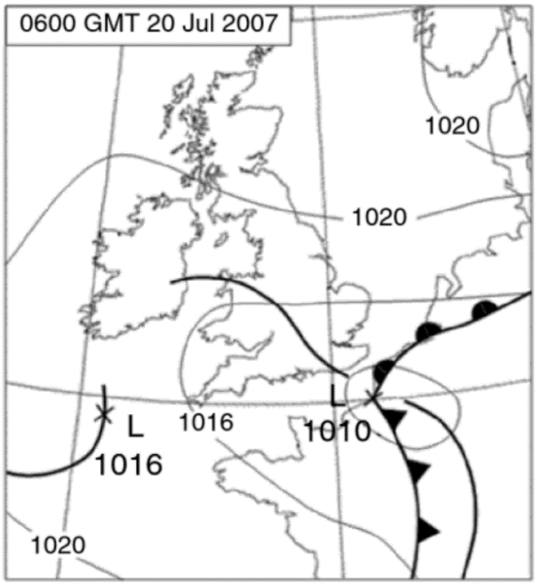

Figure 5.3. Synoptic chart for 06:00 UTC 20 July 2007 (taken from Brown, 2016)

During the afternoon, rainfall was followed by lightning, and the presence of convective storm cells which ensured that significant rainfall cores remained stationary over some regions. For example, hourly totals of 30-40 mm were recorded, and in some areas such as Gloucestershire and Worcestershire, daily totals of approximately 140 mm were not uncommon.

The saturated soil conditions and the precipitation volume in the area set the precedent for a series of severe flash floods in the south Midlands region. Rainfall recorded at Pershore College (see Figure 5.5 for the location of the gauge) reached over 10 mm for six successive hours from midday on the 20th, and the 16-hour total reached 134.8 mm at that station. 40 mm were recorded at Heathrow from late on 19 July and throughout 20 July (the usual July monthly average is 45 mm at Heathrow). In the afternoon of the 20 July, more than 10 mm of rainfall were recorded from 12:00 UTC to 18:00 in some places in the south Midlands (Marsh & Hannaford, 2007).

Recorded values show that during 19-20 July, rainfall over the area was equivalent to four times the average rainfall expected during the month (Environment Agency, 2007b). To visualise the magnitude of the intense rainfall, Figure 5.4 (Prior et al., 2008) presents the 5-km grid-point map with the accumulated rainfall for the July event.

The rainfall dissipated around midnight on 20 July, although more flood events were recorded further south of Birmingham (Gloucestershire, Buckinghamshire, Oxfordshire, Worcestershire, West Midlands and Warwickshire)

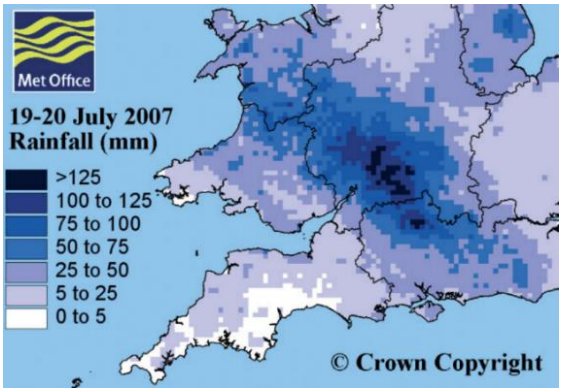

Figure 5.4. Precipitation levels for England and Wales during 19–20 July 2007 (Prior et al., 2008)

Rainfall totals for the 19-20 July period for gauges that recorded the highest values in the south Midlands region, all with a return period greater than 200 years, are presented in Table 5.1 (Prior et al., 2008). Figure 5.5 contains the location of the gauges, which are located close to and south of Birmingham. The red shading covers the hydrometric area 28 “Trent”, one of the 107 areas into which the United Kingdom has been discretised by the Centre for Ecology & Hydrology for hydrometeorological data collection purposes (National River Flow, 2014). This area will be referred to as “Trent catchment”. The black lines correspond to the limits of the adjacent hydrometric areas.

Table 5.1. Accumulated rainfall values in [mm] for the wettest rain gauges in the Midlands region on 19-20 July

Station	19 July 2007	20 July 2007	19/20 July
Pershore College (Worcestershire)	36.6	120.8	157.4
Langley (Gloucestershire)	24.4	115.4	139.6
Pershore (Worcestershire)	24.8	107.8	132.6
Brize Norton (Oxfordshire)	27.6	100.2	127.8
Sheriffs Lench (Worcestershire)	29.6	97.2	126.8
Saltley	11.8	44.6	56.4

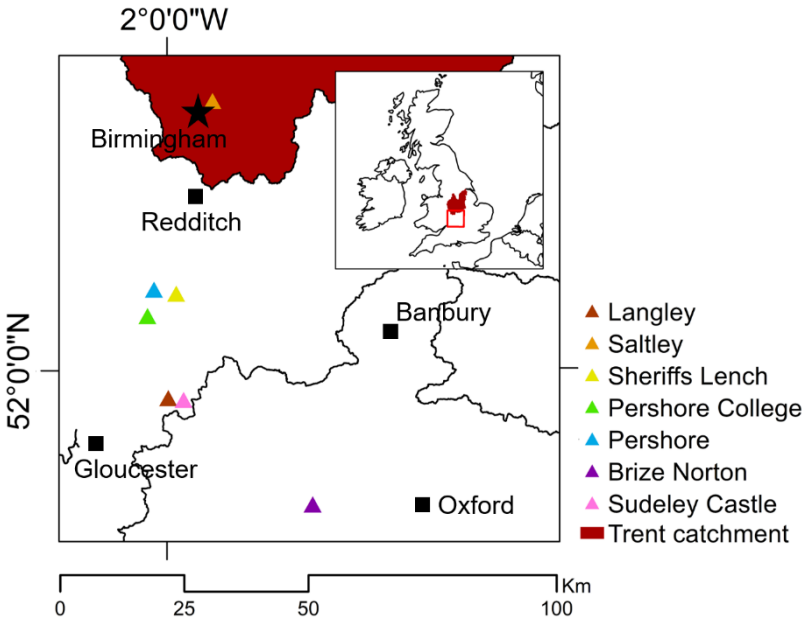

Figure 5.5. Location of the gauges with the highest recorded values on 19-20 July (see Table 5.1), located in the south Midlands region

To better visualise the storm track, 15-minute radar imagery from the Met Office NIMROD System (Met-Office, 2003) is shown in Figure 5.6. The red area corresponds to the Trent catchment and the neighbouring black lines are the limits of the adjacent hydrometric areas.

Description of the temporal evolution of the rain is presented taking the Trent river catchment as spatial reference, which is the catchment in which Birmingham is located. At 13:00 UTC (top panel) the rainfall cluster shows the storm moving from the south across the Midlands. The precipitation band covers the area over Birmingham and mostly over the south and south east of the domain. There are two bands of rainfall close to the east boundary of the domain: one well defined to the north and another that follows the major cluster of storm cells, in the lower right corner of the domain. At 14:00 UTC (middle panel) the tongue of rainfall that extended across the Trent catchment has moved northwest and weakened. The second are of high rainfall has now merged with the main cluster of storm cells and is following the northernmost bulge of rain. Given the direction of the system, Birmingham is still under significant rainfall. Finally, at 16:00 UTC (bottom panel) the main cluster of storm cells has moved outside the visible domain to the west and only the rainfall band that followed this major cluster is still in the area, in the north part of the Trent catchment.

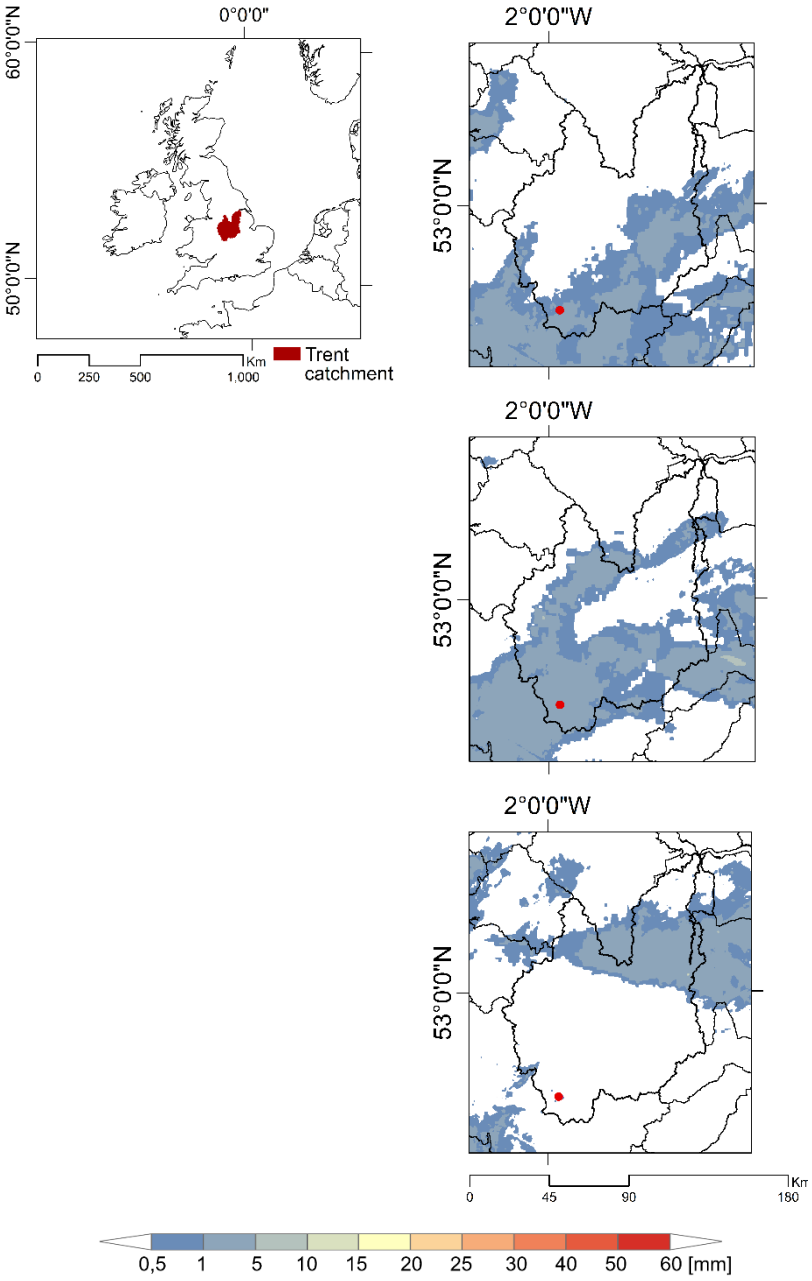

Figure 5.6. Radar imagery of the Summer 2007 event showing the storm track over the Trent catchment (top left), 15-minute accumulated values for 13:00 UTC (top right), 14:00 UTC (middle), 16:00 UTC (bottom). Birmingham city centre is marked with a red dot

5.3 Meteorological model set-up

5.3.1 Domains and boundary conditions

Similar to the set-up for the Newcastle 2012 case study, the four telescopic domains for the Birmingham 2007 event were defined starting from the innermost and highest resolution grid which covers the entire Trent catchment (as defined in Section 5.2.2), where the city of

Birmingham is located. The rest of the domains were built around it up to a mesoscale extent. The domain configuration, including extent and resolution, is stated in Table 5.2, and the spatial arrangement is shown in Figure 5.7.

Table 5.2. Grid cell size and area of the WRF model set-up for the Birmingham 2007 case study

Domain	Grid resolution [km]	Grid cells (rows × columns)	Domain size [km^2]
1	54	60 × 60	3 240 × 3 240
2	18	72 × 72	1 296 × 1 296
3	6	72 × 72	432 × 432
4	2	96 × 81	192 × 162

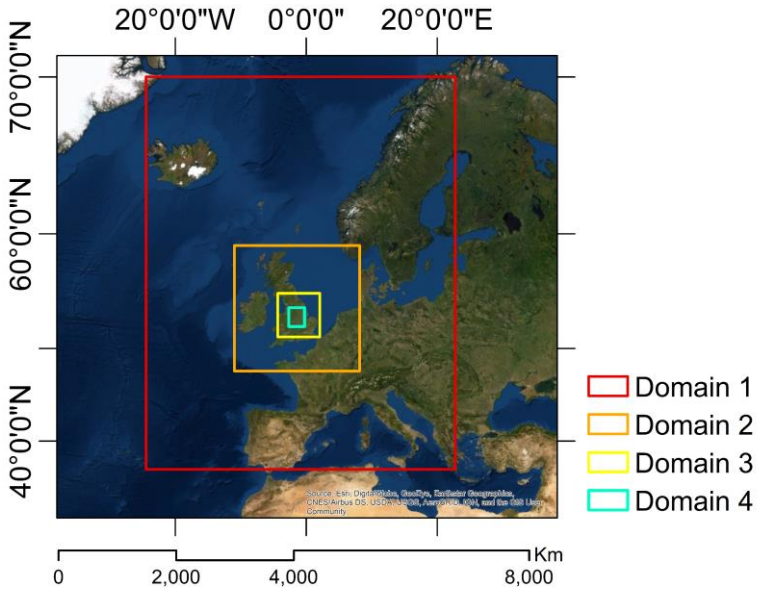

Figure 5.7. Location and extent of the nested domains for the meteorological simulation of the Birmingham 2007 case study

Numerical modelling for the flash flood event spans over a 48-hour period with 12 hours of spin-up time. Lateral boundary conditions from the Operational Global Analysis data by the National Centers for Environmental Prediction (NCEP FNL data, described in Section 3.3.1.1) were retrieved from 12:00 UTC 19 July 2007 to 00:00 UTC 22 July 2007.

5.3.2 Building height distribution

Building heights were obtained for domain 4 only from the database detailed in Section 4.3.2. The visual distribution is displayed in Figure 5.8, where the upper right corner shows the enlarged area covering Birmingham city centre. The histogram of the percentages of each building height is displayed in Figure 5.9.

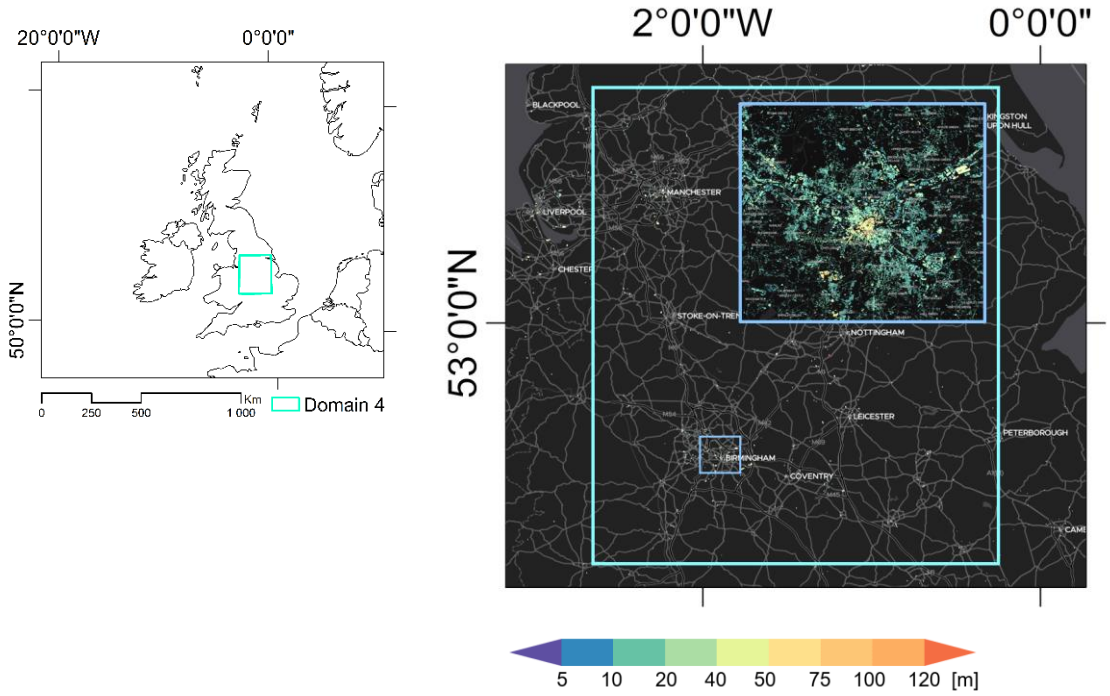

Figure 5.8. Visual distribution of building heights in the innermost domain of the Birmingham case study. Green outline corresponds to domain 4

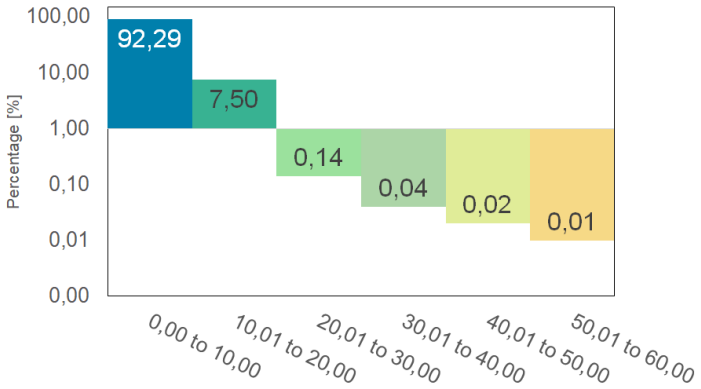

Figure 5.9. Histogram of the building height distribution [m] for domain 4 of the Birmingham case study

5.4 Results and discussion

5.4.1 Synoptic scale analysis

Analysis at the largest scale for the second case study covers the area inside the coarsest domain. Accumulated rainfall for the six-hour period 12:00 UTC to 18:00 UTC on the 20th July 2007 was extracted from the nine WRF model outputs (see Table 5.3) and compared to GPM

rainfall data. This period corresponds to when the highest rainfall rates were recorded for the south Midlands region, as pointed out in Section 5.2.2.

Similar to the analysis conducted for the Newcastle 2012 case study, comparison of WRF model outputs to GPM data is done as preliminary verification of the applicability of the current model set-up to provide lateral boundary conditions for the next nested domain. Given that rainfall in the coarsest domain tends to underestimate the rainfall, evaluation at this scale is done qualitatively.

Table 5.3. Urban canopy models and microphysics parameterisations used in the nine WRF scenarios to simulate rainfall for the Birmingham 2007 event

Physics scheme	Simulation number								
	1	2	3	4	5	6	7	8	9
Micro-physics	THOM	WSM6	MORR	THOM	WSM6	MORR	THOM	WSM6	MORR
Urban surface	SLUCM	BEP	BEM	SLUCM	BEP	BEM	SLUCM	BEP	BEM

Most of the rainfall scenarios produced by the WRF model deliver precipitation over Scotland, or at least north of the case study region (feature A). The rainfall band extends from the main cluster (over the Midlands) and to the north, something that is not observed in the GPM data. Although this area is not within the region of interest, noticing these patterns gives useful information about the overall model performance. Simulated wet cells in this area are a preliminary indicator of model overestimation.

All scenarios correctly reproduce the rainfall over the Island or Ireland (feature B), although the model is also overestimating precipitation values in this region. However, all simulations capture the location of the storm cells with the highest intensity (south of the island of Ireland) and correctly predict the extent. This last sentence does not apply to simulations 3, 6 and 9, which predict a greater rainfall extent north of the island of Ireland. Given that those scenarios have the same microphysics scheme (Morrison, MORR), it is clear that at synoptic scale, this scheme does not capture correctly the features that the other simulations do.

The greatest accumulated rainfall values are expected north of Wales and south of the Midlands as displayed in the GPM rainfall map (feature C). All simulations correctly capture the location and extent of the highest precipitation values, which means that the chosen combinations of microphysics and urban canopy models can reproduce the atmospheric

processes at large scale. Although simulations with the Morrison scheme (simulations 3, 6 and 9) underestimate the rainfall in this region as well, they still deliver the highest values of the scenario over the correct area (near Birmingham).

The north tongue of the rainfall (feature D) in the GPM data is not reproduced by the simulations: all scenarios deliver rainfall further south (around London) than observations (GPM data clearly shows significant rainfall accumulations over Cheshire and Lincolnshire). Given the extent of the finest domain (see Figure 5.7), it is possible that this miscalculation could be explained by the model set-up regarding the nested grids: a coarse grid is more likely to miscalculate the observed rainfall.

In all simulations, the bulge of rainfall that extends from the south of Ireland nearly joins the tongue that originates in France, whereas observations show negligible precipitation in that area. Similarly, all simulations predict an extensive area of rainfall over France, which does not appear in the GPM data. Features E and F corroborate the tendency of the model to overestimate rainfall values.

Despite the differences in the hourly and accumulated values, analysis at this stage is useful for preliminar verification of the model set-up. The difference found in the rainfall patterns can give information on possible bias. In this case, The consistent underestimation of rainfall in the most affected area confirms the analysis done for the Newcastle case study, where the inconsistencies are attributed to the coarse grid of the domain that begins the dynamical downscaling. Finally, although GPM rainfall fields are being considered as “true” values, these are subject to uncertainties (outlined in Chapter 2) that must be taken into consideration.

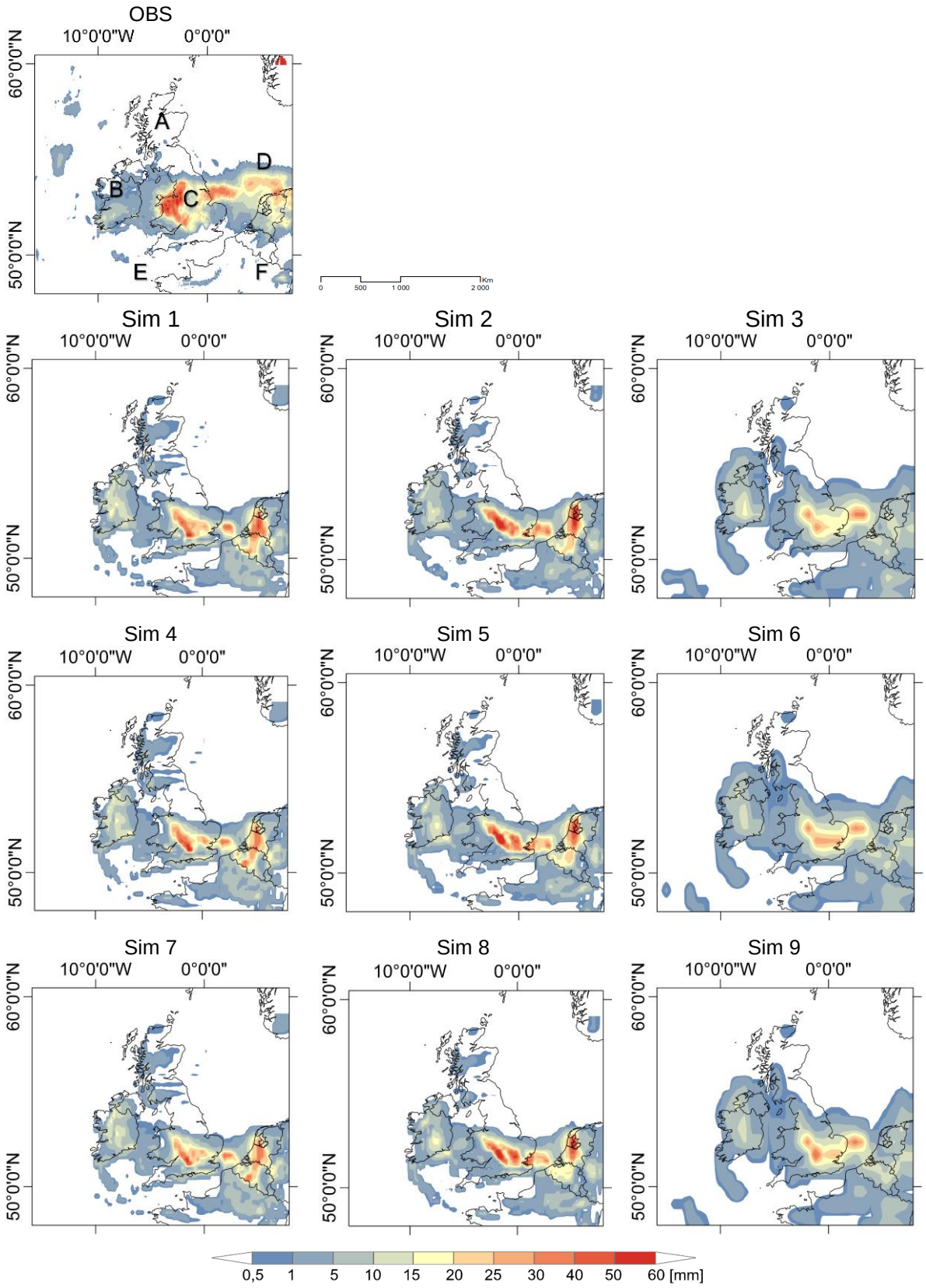

Figure 5.10. Accumulated rainfall maps from 12:00 UTC to 18:00 UTC on the 20th July 2007 using GPM IMERG data (top panel) and for simulations 1-9 (see Table 5.3 for the specific combination of the physics schemes)

5.4.2 Mesoscale analysis

Mesoscale analysis takes one-hour accumulated values from the NIMROD radar data (described in Section 3.4.1) to deliver three snapshots during the most critical rainfall period on 20 July 2007. Simulated rainfall scenarios were compared against radar data over the area within the innermost domain, which is shown in Figure 5.11 on the top left panel. These times were chosen given the storm track: these are three crucial snapshots to evaluate the model skill to reproduce the displacement of rain cells over the domain. Similar to the mesoscale analysis conducted for the Newcastle case study, inaccuracies of the radar data must be considered when using them as reference to evaluate WRF model outputs. For this case study, the closest radar to Birmingham “Clee Hill” is located 20 km west of the city, which eliminates measurement errors when the distance between the radar and the point of interest exceeds 100 km and it has proven to have considerable spurious echoes, however, the cleaned data often still includes scattered noise (Harrison et al., 2006).

Snapshots for simulations 1-3 are shown in Figure 5.11a, simulations 4-6 are shown in Figure 5.11b and simulations 4-9 are shown in Figure 5.11c. The nine WRF rainfall scenarios correspond to the parameterisations shown in Table 5.3. The three urban canopy schemes (in order of increasing complexity) are: Single Layer Urban Canopy model (SLUCM), Building Effect Parameterisation (BEP) and Building Energy Model. The three microphysics schemes (also in order of increasing complexity), are WRF Single-layer 6-class (WSM6), Thomson (THOM), and the Morrison (MORR) schemes.

At 13:00 UTC a considerable amount of rainfall has accumulated over the lowest half of the domain, with a tongue that lies on the west part of the domain and that extends north of the area. All simulations struggle to reproduce this pattern: the area with wet cells is much lower in all WRF scenarios except for simulation 7. In the rest of the cases, it seems that the model produces a thinner band of rainfall over the domain, and there is a cluster of rainfall cells south of the domain with clearly greater values. This means that the simulated storm is more intense and that is much more localised than observations suggest. Despite the possible errors in radar data, spatial extent of the rainfall differs considerably between radar and WRF model outputs.

There is a clear overestimation of rainfall values when using WSM6 (simulations 2, 5 and 8); while MORR delivers the largest underestimations of rainfall, a trend that was also found in the Newcastle case study. These results are a contribution to the existing literature since the performance of MORR and WSM6 paired with all the urban canopy models to simulate rainfall has not been documented before.

Accumulated rainfall during the following hour shows the westward evolution of the storm. At 14:00 UTC, the large area of accumulated precipitation southeast of the domain has started moving to the northwest, and rainfall intensity has slightly increased. However, this is not the case for most of the simulations. The WRF model is estimating the storm as stationary during this hour, which is reflected in the slight change in the accumulated rainfall pattern. The main cluster of the storm has indeed moved and, in some cases, changed its intensity (such as in simulations 1, 5 and 8) but the wet area remains almost without change. This behaviour is similar to that observed in the Newcastle case study (see Section 4.4.2): model predictions regarding rainfall intensity over time can be improved, but the model eventually catches up with the accumulated values at the end of the critical period during the flash flood event.

Two hours later, at 16:00 UTC, the storm has started to make its way to the north. Rainfall cells have been observed over Birmingham during the entire period, and although the storm has left the south region of the Trent catchment, most of the domain still registers wet cells. These observed values illustrate the rainfall totals described in Section 5.2.2. At this time, the simulated scenarios predict a much larger amount of rainfall over the south region of the catchment, and that the storm has remained nearly stationary, although its intensity has decreased. In some cases, like in simulations 1, 6 and 7, the extent of the rainfall matched the observed path as more wet cells are predicted close to the north boundary of the domain.

From simulations 1-3, which correspond to the simplest urban canopy parameterisation in the WRF model, the first two show more spatial similarities among them. This follows the conclusions on model performance found through the synoptic scale analysis: the Morrison microphysics scheme (simulation 3) tends to underestimate the rainfall. From this group, the simple WSM6 (simulation 2) is the one that gives the highest accumulation values and the worst performance, which, similar to the results from the Newcastle case study and (Campos et al., 2015), highlight the need of a detailed solution of physical properties of hydrometeors.

Results using BEP show a large variability among microphysics schemes (simulations 4-6). From those, BEP+THOM (simulation 4) best reproduces the changes in storm patterns over time, whereas BEP+WSM6 (simulation 5) deliver values greater than those observed, and BEP+MORR (simulation 6) fails at reproducing the main distribution of wet cells. In this case, BEP+THOM is the best combination, both schemes being the midpoint of simple and complex, a finding supported by other studies (Barlage et al., 2016).

Finally, BEM (simulations 7-9), also seems to have a much better performance when paired with THOM (simulation 7): unlike the overestimated rainfall by BEM+WSM6 (simulation 8) or the inaccuracy of BEM+MORR (simulation 9).

The nine simulations are better grouped when considering the microphysics scheme used rather than the complexity in the representation or urban atmospheric processes: in general, THOM (simulations 1, 4 and 7) delivers better results than MORR (simulations 3, 6 and 9), which agrees with (Rajeevan et al., 2010). In contrast, WSM6 (simulation 2, 5 and 8) overestimates the rainfall. This concludes, just like the Newcastle case study, that the model is more sensitive to the choice of microphysics, even for urban flash flooding events. Moreover, processes are better predicted when using MORR or THOM, implying that despite considering a larger number of hydrometeors and being computationally efficient, WSM6 is not suitable for an intense rainfall event with a rapid development over an urban area. This was also the case for the Newcastle case study, where the analysis at mesoscale also concluded that WRF simulations that implement WSM6 consistently delivers values greater than the data considered as observations.

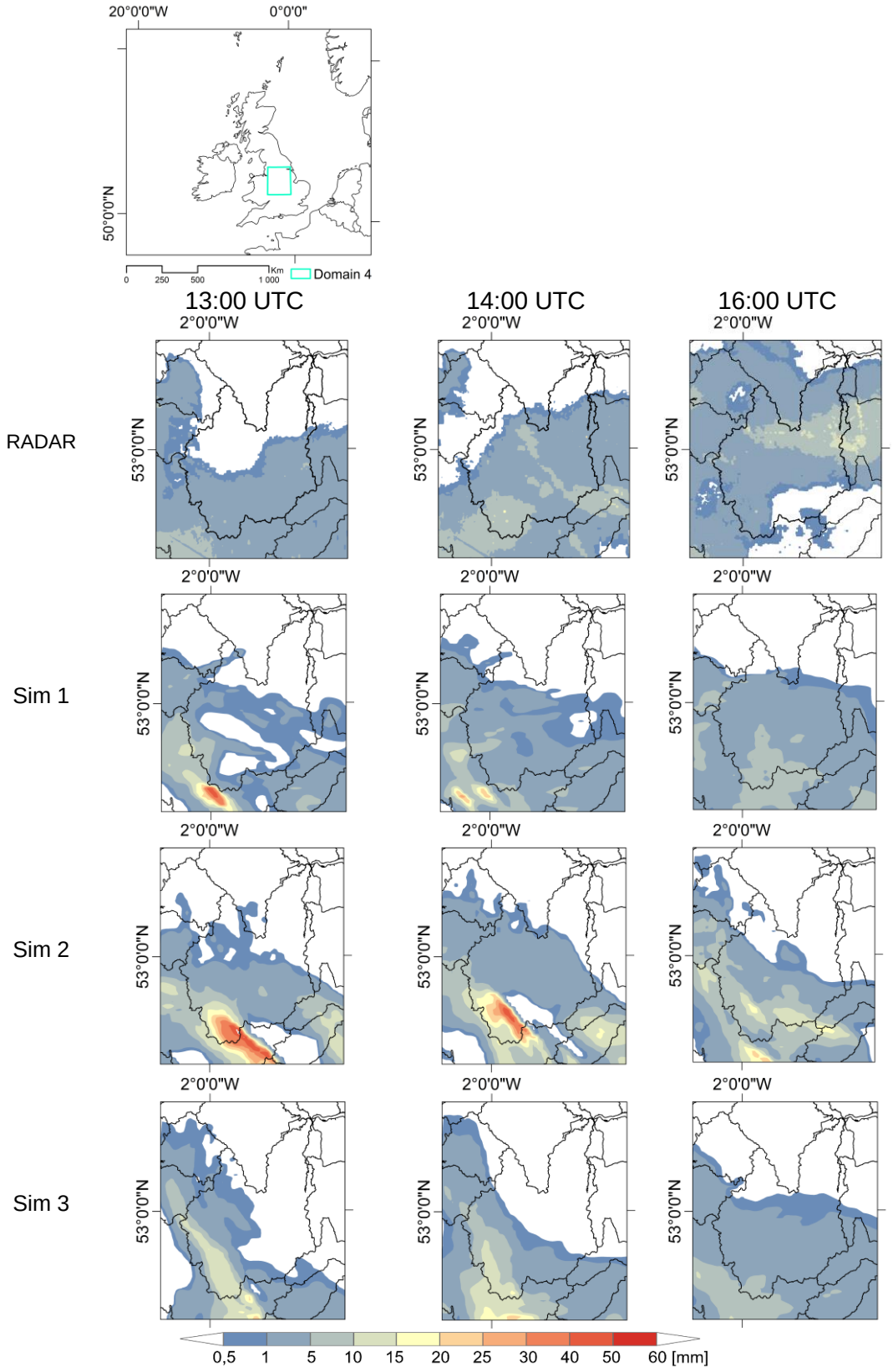

Figure 5.11a. Hourly time evolution of the rainfall on 20th July 2007 (13:00, 14:00 and 16:00 UTC). Observed radar values (top row) and rainfall patterns for WRF simulations 1, 2 and 3

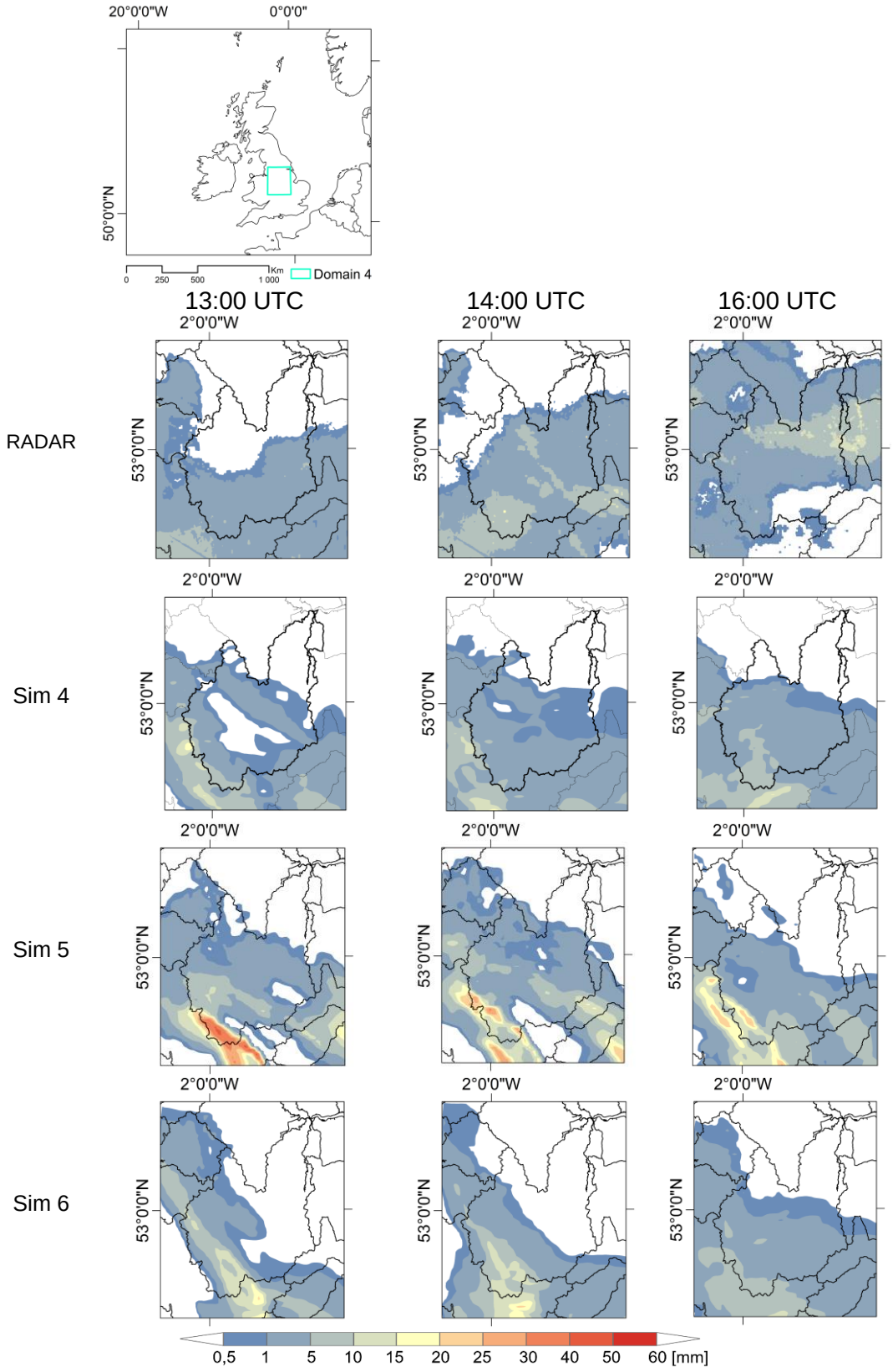

Figure 5.11b. Hourly time evolution of the rainfall on 20th July 2007 (13:00, 14:00 and 16:00 UTC). Observed radar values (top row) and rainfall patterns for WRF simulations 4, 5 and 6

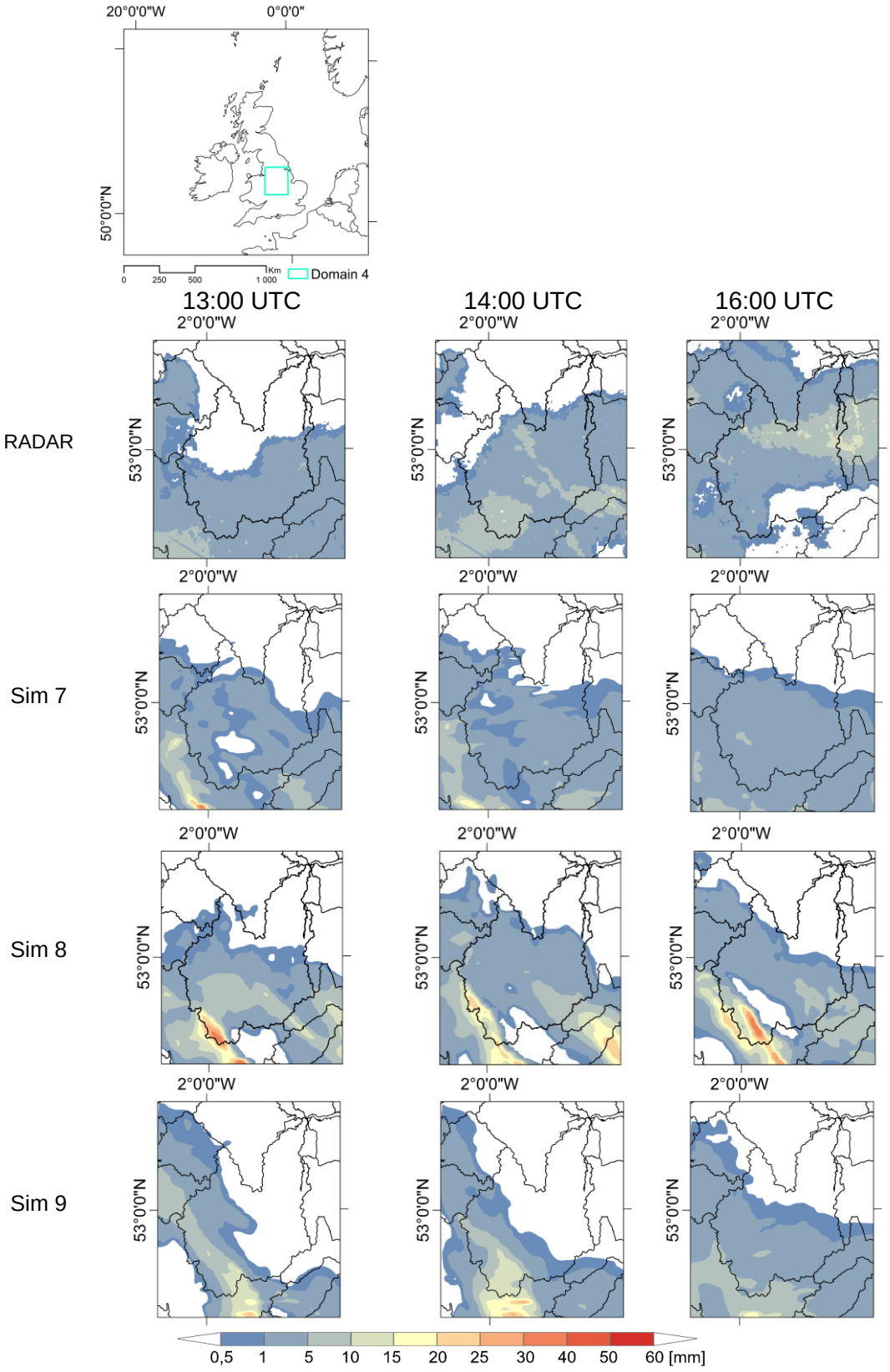

Figure 5.11c. Hourly time evolution of the rainfall on 20th July 2007 (13:00, 14:00 and 16:00 UTC). Observed radar values (top row) and rainfall patterns for WRF simulations 7, 8 y 9

5.4.3 Local scale analysis

Rainfall time series from nine gauges in the innermost domain were taken as a reference to evaluate WRF model outputs. As shown in Figure 5.12, most of them are located near Birmingham, in one of the urban cores of the domain. The rest were chosen among nearly 200 gauges with valid rainfall data to illustrate the performance of the meteorological model given the location of the gauges and their associated land cover. The following analysis refers to the panels in Figures 5.13 to 5.17. The timeseries presented correspond to the 48-hour period 00:00 UTC 20 July 2007 to 00:00 UTC 22 July 2007. Plots are grouped by urban canopy model: Single-Layer Urban Canopy Layer (SLUCM), Building Effect Parameterisation (BEP) and Building Energy Model (BEM), showing plots when using Thompson (THOM), WRF Single-Moment 6-class (WSM6) and Morrison (MORR) microphysics. The number of the simulation corresponds to the combination of the urban canopy model and microphysics scheme, as stated in Table 5.3.

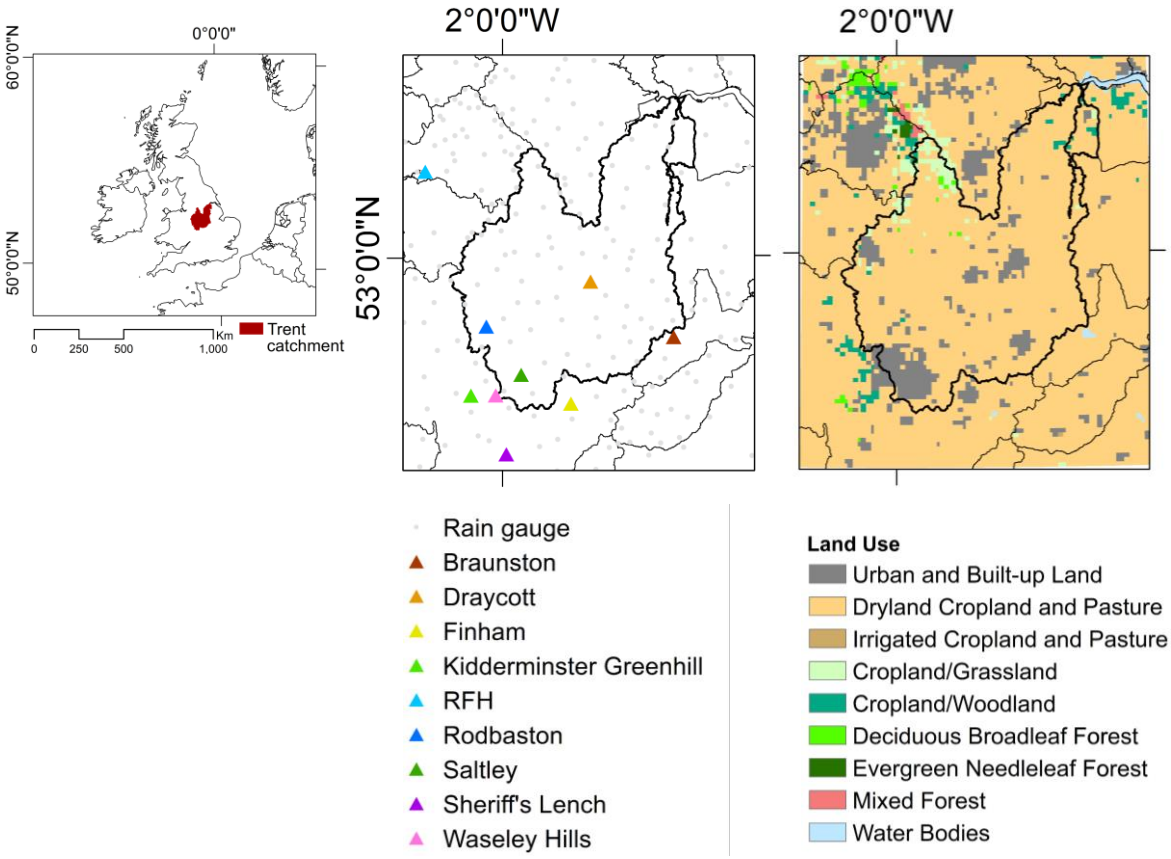

Figure 5.12. Spatial extent of the Trent catchment (left), location of the rain gauges used in the local scale analysis of the July 2007 event (middle) and land cover processed by the WRF model (right)

Braunston, the gauge farthest south, is a good indicator of the accuracy of model outputs, as this point received consistent rainfall during the event (see radar images of Figures 5.11a-c). SLUCM (Figure 5.13a) fails at reproducing the time and magnitude of the peak despite the microphysics scheme used (for example, SLUCM+WSM6 in Figure 5.13a delivers a peak nearly six hours late). On the other hand, results using BEP and BEM (Figure 5.13b and 5.13c, respectively) are more similar. For example, BEP+WSM6 and BEM+WSM6 both give a rainfall peak closer to the observations, while BEP+MORR and BEM+MORR both underestimate the rainfall during the period of analysis. The benefits of explicitly considering urban features in urban meteorology is also confirmed by (Sharma et al., 2017)

The Draycott gauge was chosen due to its central location, although both recorded and simulated values are significantly lower than the rest of the gauges in the analysis. However, it is important to note the wide spread of the ensemble for the three microphysics schemes. For all canopy models, WSM6 and THOM give similar results, although both simulating the peak rainfall with a lag, while MORR overestimates the rainfall for the period of simulation (Figure 5.13d-f). The good performance of THOM over MORR has also been documented by (Rajeevan et al., 2010)

Finham belongs to the cluster of gauges close to an urban area. However, the accuracy of results is not directly related to the complexity of the of the urban canopy model, as the best performance is given by BEP (Figure 5.14h), although all three overestimate the rainfall. From this urban scheme, the closest rainfall scenario is given by BEP+THOM (Figure 5.4h), followed by BEM+THOM (Figure 5.14i), although the timing of the rainfall is off. This means that urban areas should not be represented with a simple scheme (SLUCM), that a simplification of the microphysics is not appropriate (WSM6). This is in line with the study and findings detailed at Braunston. Also, a detailed urban scheme (BEP or BEM) requires a microphysics that solves the properties of the hydrometeors while being computationally efficient to make up for the level of detail with which a city is parameterised.

Results at Kidderminster Greenhill gauge also place SLUCM also has the lowest performance of all three urban canopy models, despite the location of this gauge in a “cropland/woodland” area (see Figure 5.12 on the location of the rain gauges and land cover processed by the WRF model). Supporting the outcomes at Finham, there is similarity in the results by BEP (Figure 5.14k) and BEM (Figure 5.14l), from which both THOM and MORR give good results, a conclusion that was also outlined in Section 4.4.3 of the Newcastle 2012 case study.

Similar to Draycott, the RFH gauge also registered low rainfall values but it was chosen for analysis to evaluate model performance in the west region of the innermost domain. In this case, the best performance is given by SLUCM, where the best estimate is obtained by

SLUCM+WSM6. Given that this gauge is in an area mostly with natural land cover (see Figure 5.12) and less low rainfall values were recorded, the simple schemes work best.

The Rodbaston gauge, north of Birmingham, shows an interesting behaviour of the simulations. Firstly, the choice of urban canopy model does not have a significant impact in the rainfall produced, except when using WSM6, which produces rainfall peaks with considerably different magnitudes in the three cases. From these, BEM produces the best results, where the most appropriate physics scheme combination is BEM+WSM6 (Figure 5.15r). Additionally, the microphysics schemes THOM and MORR have a more consistent behaviour, although both overestimate the rainfall and produce peaks before the observed ones by approximately 4 hours. As outlined in the analysis at local scale of the Newcastle 2012 case study, the documentation of performance of BEM+MORR is one of the novel results from this study, given that said combination has only been applied in Urban Heat Island studies, not considering precipitation over a city.

At Saltley (Figure 5.16 s-u), the closest rain gauge to Birmingham, there is a clear mismatch between simulations and the observed values. All WRF outputs produce an intense rainfall that largely exceeds the observed values and the duration of the storm duration at this station is estimated as longer by the model. This behaviour was also observed at Finham, another gauge close to an urban area. This shows that reproducing the effect of cities in the atmospheric fluxes with accuracy is crucial and dependant of the urban canopy model used.

At Sherrif's Lench, similar to the results at Saltley, temporal evolution of the rainfall is not well captured by the model. In this case, there are two distinctive rainfall peaks instead of a smooth rise and decrease in rainfall, as the observations suggests. However, these peaks are contained within the duration of the rainfall, which mean that although the model performance when making an hourly point-to-point comparison might not be an indicator of the overall applicability when considering the simulated rainfall during the entire simulation time.

Finally, simulated rainfall at Waseley Hills shows a similar behaviour to the timeseries produced by the WRF model at Saltley and Sherrif's Lench. Since these gauges are in the south part of the domain, is it not surprising that their performance is linked to their location, and given the model performance observed at mesoscale, the overestimation of rainfall duration and magnitude is expected, although undesired.

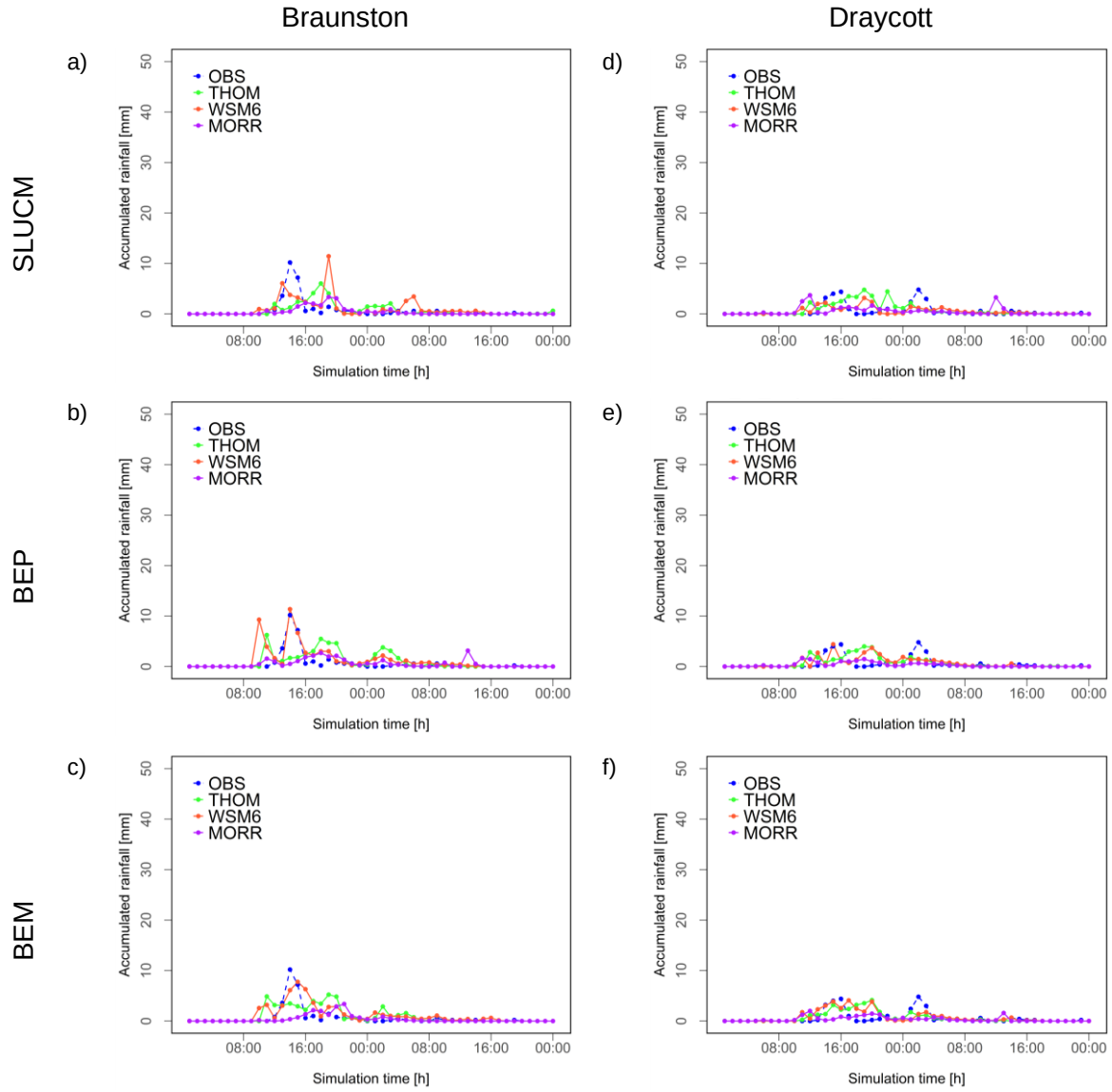

Figure 5.13. Simulated rainfall for the nine WRF scenarios, grouped by urban canopy model scheme, for two gauges in the Trent catchment

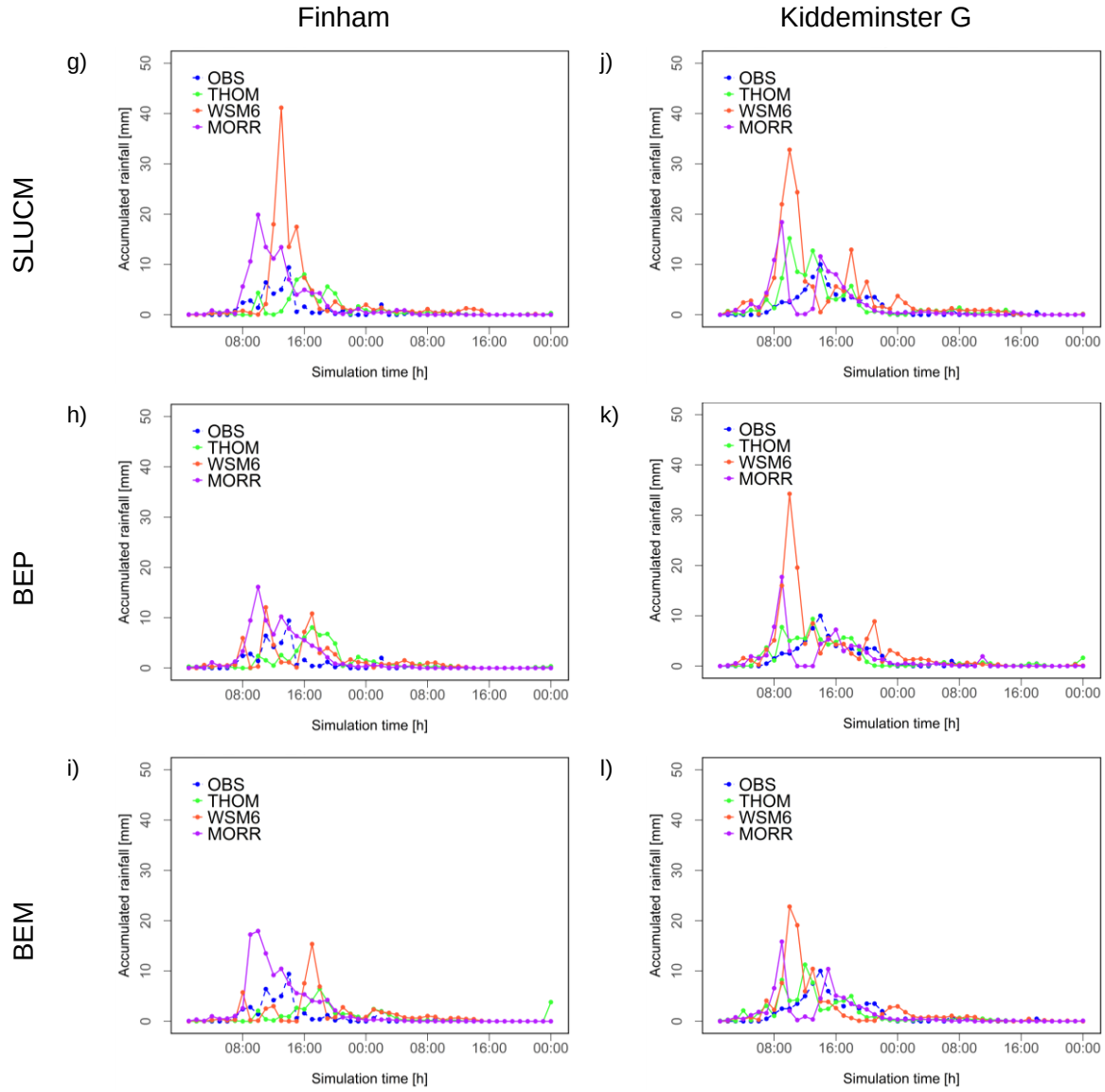

Figure 5.14. Simulated rainfall for the nine WRF scenarios, grouped by urban canopy model scheme, for two gauges in the Trent catchment. See Figure 5.12 for location of gauges

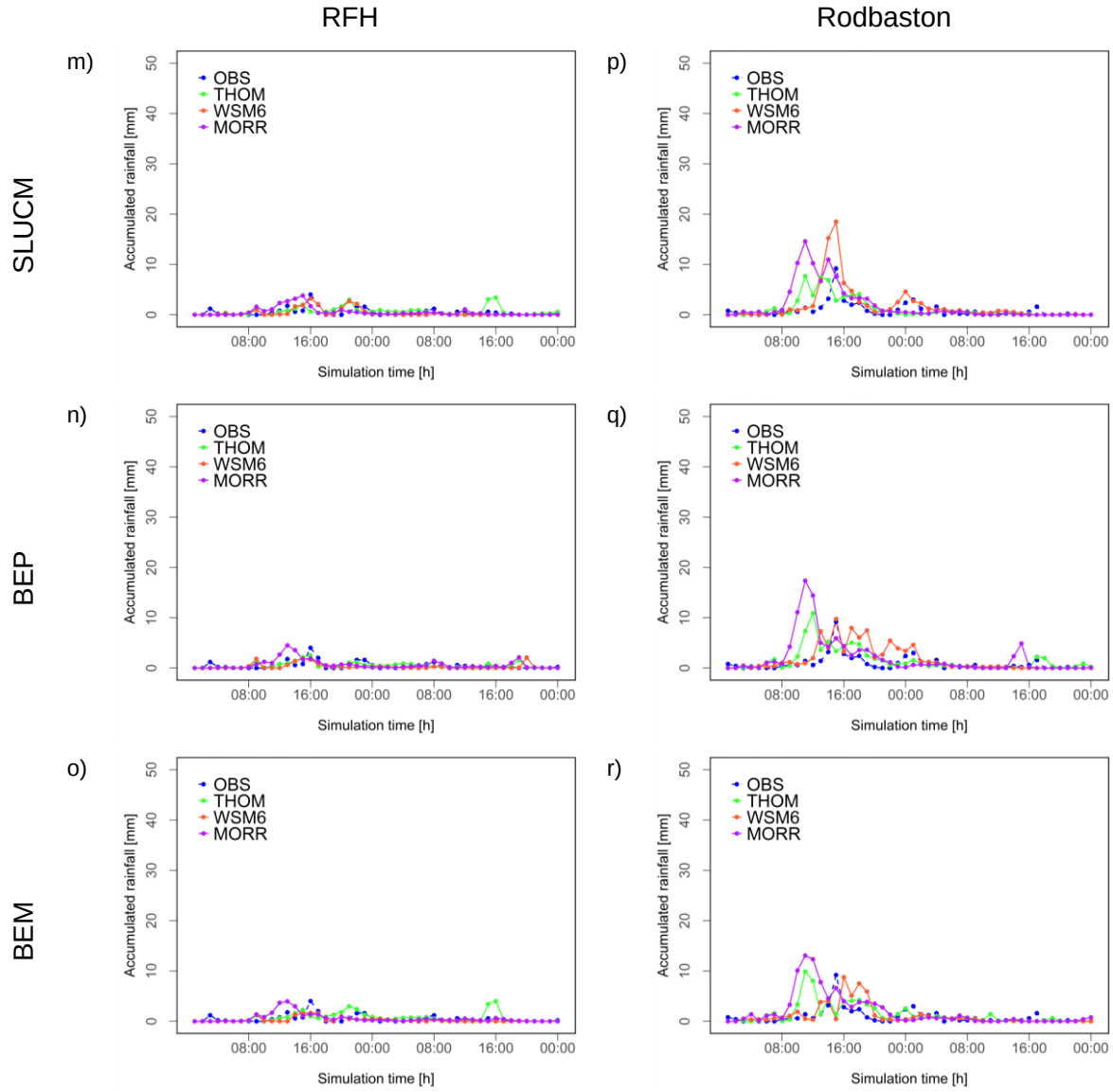

Figure 5.15. Simulated rainfall for the nine WRF scenarios, grouped by urban canopy model scheme, for two gauges in the Trent catchment. See Figure 5.12 for location of gauges

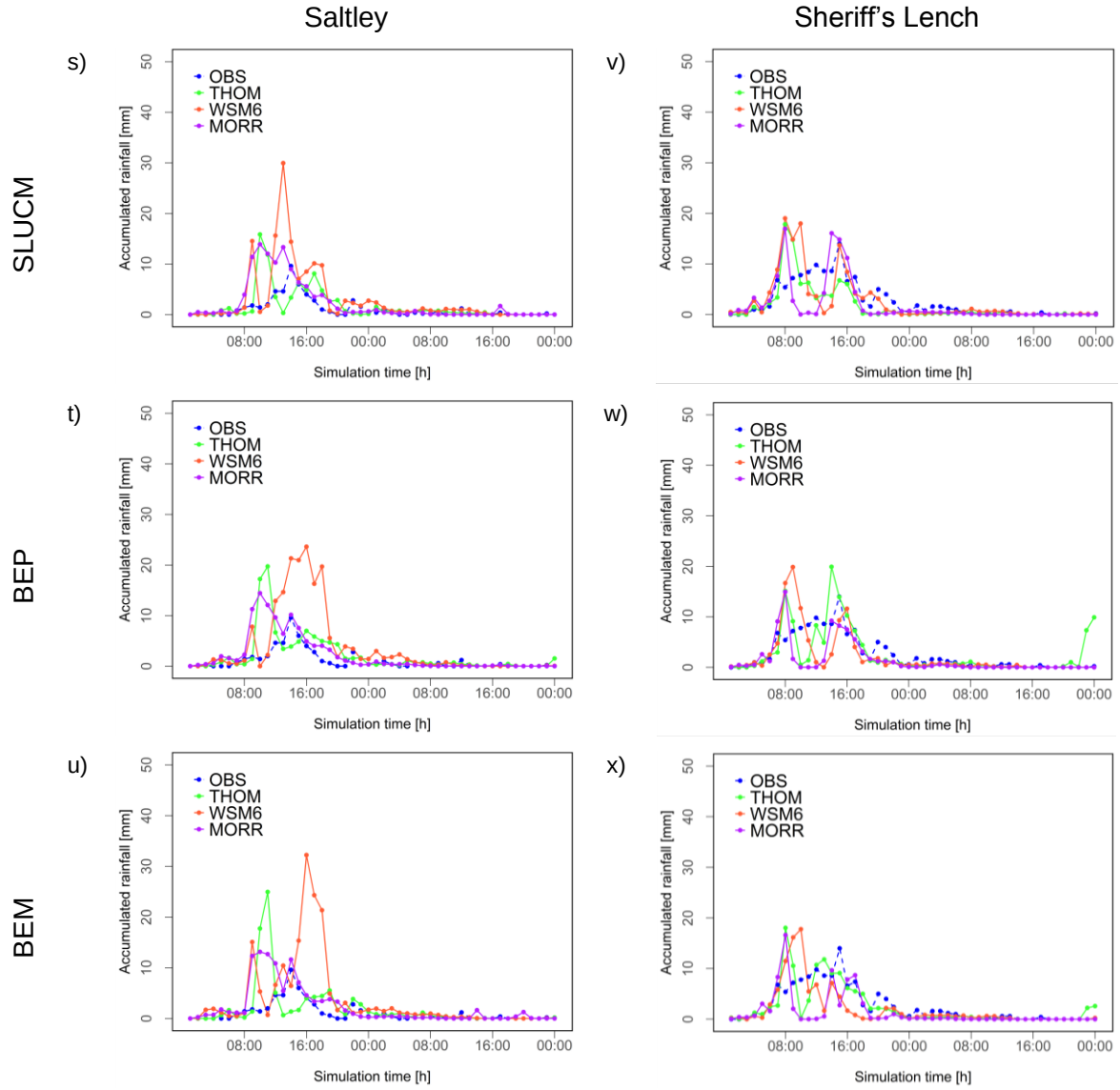

Figure 5.16. Simulated rainfall for the nine WRF scenarios, grouped by urban canopy model scheme, for two gauges in the Trent catchment. See Figure 5.12 for location of gauges

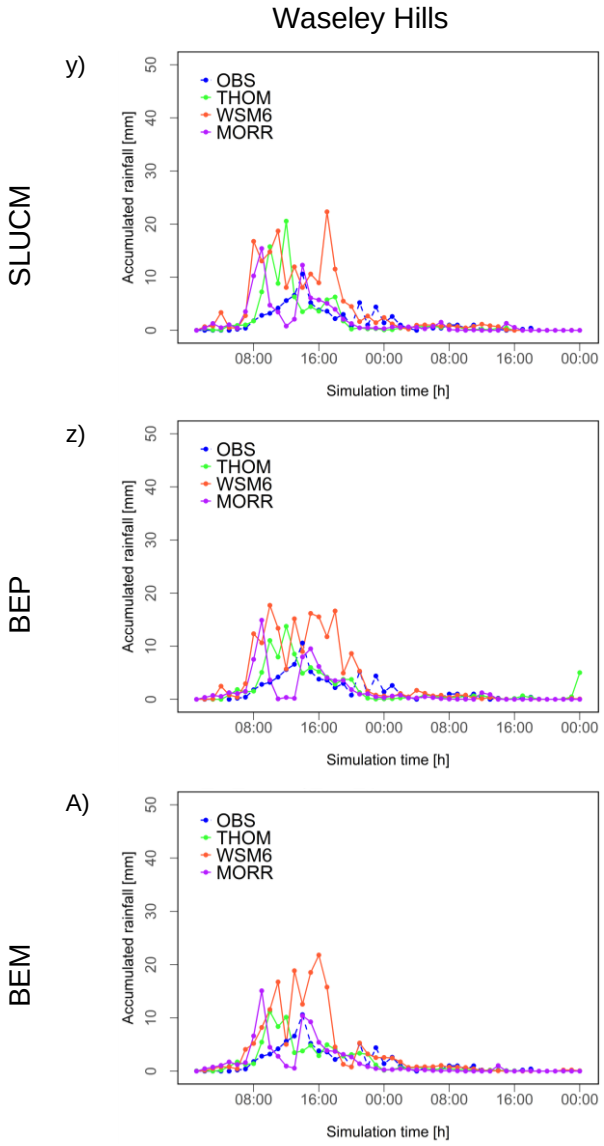

Figure 5.17. Simulated rainfall for the nine WRF scenarios, grouped by urban canopy model scheme, for a gauge in the Trent catchment. See Figure 5.12 for location of gauges

The previous analysis shows that the most appropriate urban canopy model to use in built-up land environment is either Building Effect Parameterisation or Building Energy model, i.e. complex physics schemes that explicitly account for vertical distribution of heat and momentum and indoors/outdoors heat exchange, respectively. In said environments, they work best with a the most detailed microphysics scheme in this study, Morrison. However, the second most complex microphysics parameterisation, Thompson, also works well in non-urban environments.

To rank model performance, the following section presents the quantitative metrics that evaluate prediction skill. This will confirm numerically the conclusions from the local analysis.

5.4.4 Overall model performance

The Critical Success Index (CSI), the Root Mean Square Error (RMSE) and Mean Bias Error (MBE) for the nine WRF simulations are displayed in Table 5.3. There is a correspondence between the values of the first two, where the simulations with the lowest CSI also have the highest RMSE. This means that there are large differences between observed and simulated values because of the mismatch between wet and dry cells. Since MBE represents the systematic error of under- or overestimating values compared to observations, values show that most simulations tend to predict lower values, except those with the lowest CSI and highest RMSE.

Similar to the Newcastle case study, there is no trend in simulations that are grouped by urban canopy scheme (1-3 use the Single Layer Urban Canopy Model, 4-6 use Building Effect Parameterisation, 7-9 use Building Energy Model). On the other hand, scenarios that implement the same microphysics scheme are more easily identified: Results obtained using the Thompson scheme (THOM; simulations 1, 4 and 7) clearly outperform the rest when considering the verification and the statistical indices. Model outputs that used the WRF Single-Moment 6-class (WSM6; simulations 2, 5 and 8) were placed at the bottom of the rank.

From simulations 1, 4 and 7, the best performing is the one that uses the Building Energy Model (BEM). This confirms the need to include as much detail as possible in the parameterisation of urban areas to solve the heat and moment fluxes in the lowest part of the atmosphere. Given that the largest accumulation of rainfall over the two-day period 19-20 July 2007 was over an urban area, and that the highest precipitation rates were recorded in the south Midlands (see Figure 5.4 for accumulated values and Figure 5.12 for the extent of urban land cover), this is not surprising. This is moderately in line with the results of the Newcastle 2012 flash flood event, where BEM is among the top four most skilled scenarios, but outperformed by one scenario that uses the Single Layer Urban Canopy Model and by another scenario that uses the Building Effect Parameterisation.

Finally, computation time was also evaluated. Meteorological simulation for this event, as stated in Section 5.3.1, was carried out from 00:00 20 July 2007 to 00:00 UTC 22 July 2007, plus 12 hours of spin-up time at the beginning of the period. More than half of the simulations exceed 60 hours of computation time (which corresponds to one minute of computing time per one minute of the event), two of them exceeding the 60-hour period by more than 50% (simulations 6 and 7). Since the main outcomes of the research is characterisation of the

atmospheric processes of intense rainfall associated to flash flooding and benchmarking model performance in urban areas, despite the large processing times, this will also be considered to rank the simulations.

The order of simulations from best to worst performance is shown in Figure 5.14, from where the top four simulations would keep their rank if computation time was not considered. On the other hand, the bottom four scenarios have the poorest performance as given by the indices, but they are more computationally efficient than some of the simulations at the top of the rank. Given that the model is more sensitive to the choice of microphysics than to the choice of urban canopy model, the best microphysics scheme is the Thompson, a single-moment scheme that incorporates the complexity of a double-moment regarding physical properties of hydrometeors, while maintaining is computational efficiency. This differs slightly from the results obtained in the Newcastle case study, where the microphysics scheme that was found to deliver the best results is Morrison, although Thomson, if paired with the complex Building Energy Model, is also among the best performing scenarios.

Table 5.4. Skill scores and accumulated rainfall for the nine WRF simulations of the July 2007 event

Simulation	CSI	RMSE [mm]	MBE [mm]	Computation time [hrs]
1	0.84	1.90	-0.17	57.48
2	0.79	2.33	0.12	42.58
3	0.83	1.98	-0.06	49.28
4	0.89	1.90	-0.18	64.85
5	0.77	2.28	0.04	62.05
6	0.82	1.95	-0.11	93.01
7	0.88	1.91	-0.18	97.12
8	0.78	2.21	0.01	79.37
9	0.85	1.96	-0.16	75.65

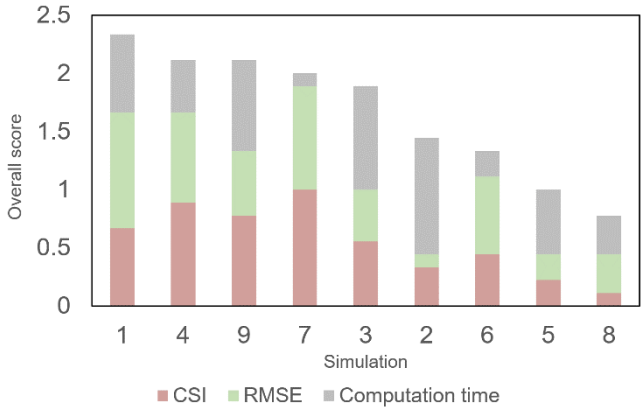

Figure 5.18. WRF simulations ranked by performance for the June 2012 case study, showing bar length as the contribution of each metric to the overall performance

5.5 Final remarks

5.5.1 On the Birmingham 2007 case study

Analysis of results at synoptic scale gives a first glimpse at overall model performance regarding its ability to reproduce the highest precipitation values. At this stage, rainfall scenarios showed similar performance regarding over- and underestimation of rainfall bands and bulges in the domain, with simulations 3, 6 and 9 (which use the Morrison microphysics scheme) clearly delivering lower rainfall values than those observed. Given that the first part of the model evaluation was done for accumulated values (in this case, 12:00 UTC to 18:00 UTC 20 July 2007), further tests at higher spatial and temporal resolution are needed.

Comparing model results to remote-sensed imagery on the innermost domain allows a more robust analysis of the correspondence between simulated and observed values during a much shorter period. In this case, model sensitivity to the physics schemes became clearer and the performance to reproduce the storm track was more evident. Mesoscale results showed that the best urban canopy model scheme was the most complex, the Building Energy Model (BEM), which not only discretises the urban canopy in several layers, hence calculating vertical profiles of heat and moisture, but also the indoors-outdoors exchange.

Point comparison of WRF model outputs with several stations within the innermost domain also gave valuable information on model skill in urban and non-urban areas. This confirmed that the most suitable urban canopy model is BEM, while corroborating that the Single-Layer Urban Canopy Model (SLUCM), the simplest scheme, works well in non-urban environments. However, since the model applies a homogeneous canopy model to the domain, BEM is preferred.

Finally, the verification and statistical indices confirmed the suitability of BEM and allowed to pinpoint the best microphysics scheme. All simulations are computationally expensive with huge differences; this was also considered for the rank of the simulations. However, a better prediction skill is preferred over processing times in this characterisation study, which in the end can be improved by simply compiling the model in a more efficient computational cluster.

5.5.2 On the comparison of simulated rainfall between the Newcastle 2012 and the Birmingham 2007 events

This section provides a discussion on the meteorological modelling of two rainfall events with similar behaviour regarding the generation of intense storm cells over two heavily urbanised catchments.

The synoptic scale comparison for both case studies was done with a qualitative approach because the results outputted by the coarsest domain are the first approximation of the model to the observations. In other words, domain 4 (the outermost grid) serves as boundary conditions for the dynamical downscaling framework. At this stage, results from the model for both cases both show mismatches in rainfall accumulated values, but the extent of the storm is well captured for both cases, confirming that the domain size and resolution is appropriate for the downscaling approach.

The meso-scale comparison of simulated rainfall with radar data yielded a good overview of the errors that this type of remote-sensed information. Given what was stated about the liability of radar rainfall to errors and the ways this has been identified and most of the times overcome (see Section 2.2.2.1 for details on the errors), it is likely that the actual weather features are reproduced by the model whereas others (such as cluster of storm cells close to an urban area, where the urban canopy affects radar measurements). For both cases, all WRF simulations tend to overestimate the precipitation during the most critical timestep of the storm (the highest hourly values). This could mean that the storm is more intense than what observations suggest, so the radar errors become more relevant for short-lived rainfall events.

Another feature observed in both case studies is the spatial evolution of the rainfall cluster. For both events, the meso-scale analysis show that the simulated storm cells have a stationary behaviour, hence giving higher precipitation values when making a timestep-by-timestep comparison. This could mean that the resolution of the grid also plays an important role in the accuracy of the results. However, more refined simulations require a larger computational capacity than the one used for the present study. Nevertheless, this identifies a limitation that can be easily overcome with different computational settings.

The nine rainfall scenarios for both case studies show a mismatch in the timing of arrival of the rainfall cells, compared to the radar information. However, all scenarios eventually reproduce the expected amount of rainfall. Nevertheless, this mismatch in timings is reflected in the final skill scores, as they are calculated on a timestep-by-timestep comparison

When simulating the most intense rainfall values, the WRF outputs for both scenarios are better grouped by microphysics scheme, meaning that the choice of this parameterisation plays an important role when simulating rainfall over urban areas.

The simulated rainfall for the Newcastle 2012 case study shows that the spread of the ensemble produced with the Thompson microphysics scheme (that lies in the midpoint between the simple WRF Single-Layer 6-class scheme and the complex Morrison scheme) is less than the ensemble produced by the complex Morrison. This is also true for the Birmingham 2007 case study, where the Thompson scheme gives the best results when implemented with the complex Building Energy Model. This gives valuable information on the sensitivity of the model to the choice of microphysics schemes, more than to the choice of urban canopy models, even when dealing with meteorological features over cities.

Comparison with radar data at meso-scale suggests that, when only a small fraction of the innermost domain is urban, the results are more sensitive to the choice of microphysics parameterisation.

The simplest urban canopy scheme (Single Layer Urban Canopy Model) gives the best results when paired with a microphysics scheme with medium to high complexity, although it gave the highest differences compared to observed value at meso-scale.

An important finding for this study is that for both cases, the urban canopy and microphysics schemes that lie in the midpoint between simplicity and complexity are the ones that gave the overall best results. Moreover, the simplest approach to solve cloud microphysics yield the results with the lowest skill, answering one of the research questions regarding the amount of complexity needed to reproduce cloud physics during a short-lived event. In the case of the Birmingham 2007 rainfall event, even pairing the simplest microphysics with the most complex urban canopy layer gives results with low skill. This result highlights the need for a microphysics scheme that is able to resolve the type and size distribution of hydrometeors when implemented to simulate flash-flood intense rainfall in urban areas, a finding that has not been documented before.

Chapter 6

Hydrological modelling

Chapter 6. Hydrological modelling

This chapter presents the second stage of the characterisation of the flash flood events: simulation of river discharge at hourly scale. It is divided in two major sections, one for each case study, with a section on final remarks at the end. For each event there is a description of the catchments, including topography, land cover, river network, meteorological characteristics as well as the gauges against which the results will be compared. This is followed by the calibration process, where scatter plots of the parameter space are presented along with two-month plots and evaluation of model performance, and any external influences on river runoff are discussed.

The core assumption to determine model parameter ranges for model calibration is that urban areas are made up of impervious surfaces with little to no storage capacity so that the urban HRUs would be "saturated" most of the time, and there would be negligible transfer to adjacent HRUs. The parameters that control these processes, as stated in Section 3.2.3 are SR_{max} (maximum root zone storage), $Ln(T_0)$ (lateral saturated hydraulic transmissivity), S_{max} (maximum effective deficit of saturated zone) and SZM (form of exponential decline in conductivity). This assumption a computationally inexpensive a novel approach to parameterise urban land cover in a hydrological model that is explored for the first time given the v1.0 release of the DECIPHeR numerical tool at the moment of modelling, and represents an advance toward benchmarking the model applicability to a wide range of scenarios and scales.

- SR_{max} in urban areas should have small values. This would mean that the storage capacity is very limited, so that any precipitation inputs are treated as excess flow and directed to the river channel. This parameter helps setting the channel velocity CHV.
- $Ln(T0)$ in the urban areas is expected to be smaller than in non-urban areas so that the storage in the former remains full most of the time, reducing the storage capacity and routing the water from the saturated zone to the river (Q_{SZ}). A similar assumption is applied to SZM, the other model parameter that controls the flow in the saturated zone. Values of SZM should not overlap so that urban and non-urban areas are separated in terms of storage.
- Parameter ranges regarding S_{max} for urban and non-urban areas should not overlap either. A near zero value for S_{max} in urban HRUs would ensure than downslope flow

does not occur, and together with $Ln(T0)$ and SZM, facilitating the transfer of any excess flow to the channel.

The validation process for each case study comprises ten discharge scenarios: one using observed rainfall and nine using outputs from the meteorological modelling. Timing and magnitude of the discharge peaks is discussed considering the hyetograph, and analysis of scatter plots of the parameter space is also included.

6.1. Case 1. Newcastle 2012 flash flood event

6.1.1 Hydrology of the event

6.1.1.1 Antecedent conditions

As stated in Section 4.2.1, the Tyneside region (north-east of England, on the banks of the River Tyne) had experienced rainfall well above average during May and June 2012, which caused river levels to be well above average in the days prior to the event. To illustrate this, river levels from four stations close to Newcastle city centre (see Figure 6.1) are displayed in Table 6.1 (Environment-Agency, 2012), which compares Long-Term Average (LTA) discharge to the mean daily flow recorded in 2012 for two separate days. Stations are 23007 “Derwent at Rowlands Hill, 23016 “Ouse Burn at Crag Hall”, 23017 “Team at Team Valley” and 23018 “Ouse Burn at Woolsington”.

The bold line in Figure 6.1 shows hydrometric area 23 “Tyne (Northumbeland)” (one of the 107 areas into which the United Kingdom is divided for collection of hydrometeorological data, (National River Flow, 2014), as defined by the Centre for Ecology and Hydrology) hereafter denoted as Tyne catchment, which contains the Ouse Burn catchment, upstream of Newcastle. The rest of the lines are the limits of the neighbouring hydrometric areas.

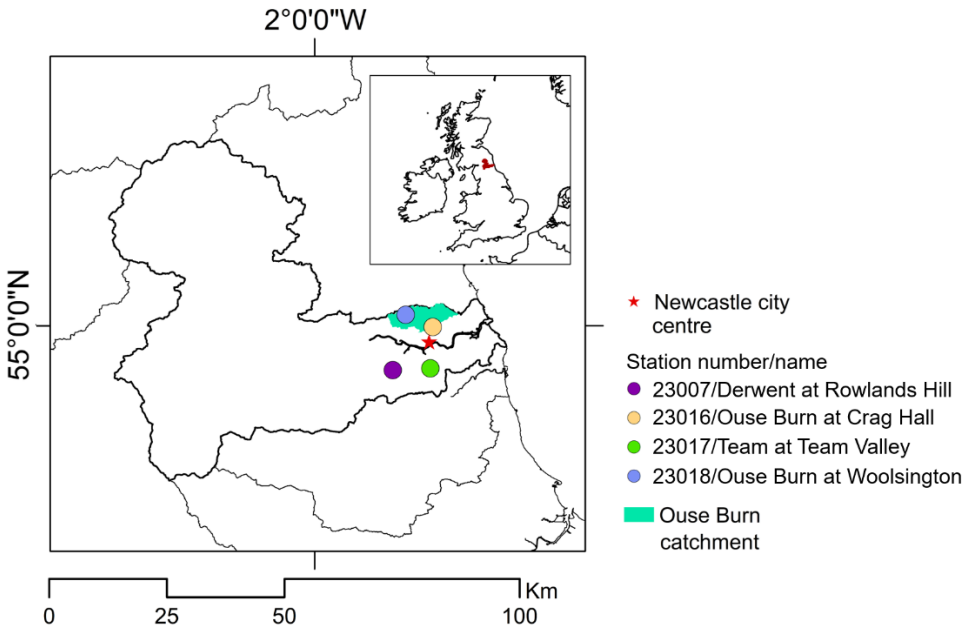

Figure 6.1. Location of the river gauges for which a flow comparison is made to highlight the severity of the June 2012 event, within the Tyne catchment

Table 6.1. Mean daily and Long-Term Average flow for three river gauges in the Tyne catchment on two dates before the June 2012 flood

Station name	Station number	May 12			June 27		
		LTA flow [$m^3 s^{-1}$]	Mean daily flow [$m^3 s^{-1}$]	% of LTA	LTA flow [$m^3 s^{-1}$]	Mean daily flow [$m^3 s^{-1}$]	% of LTA
Ouse Burn at Crag Hall	23016	0.036	0.111	308	0.041	0.128	312
Ouse Burn at Woolsington	23018	0.222	0.409	184	0.207	0.492	238
Team at Team Valley	23017	0.930	0.970	104	0.940	1.210	129
Derwent at Rowlands Hill	23007	2.030	3.87	191	1.690	3.830	227

6.1.1.2 River level and discharge during the event

On the 28th June 2012, a rapid rise in river levels was recorded for most of the reaches in the Tyne catchment. The Ouse Burn at Crag Hall and the Derwent at Rowlands Hill stations recorded an abrupt rise of river levels of 1.0 m and 1.3 m, respectively, in only 30 minutes from the start of the rainfall at 15:00 GMT. The duration of high values was enhanced by increased river levels upstream of the gauge. To illustrate the severity of the river conditions, quality controlled, 15-minute river level and flow data for the four stations shown in Figure 6.1

were retrieved from the measuring authority (the Environment Agency) and are shown in Figure 6.2.

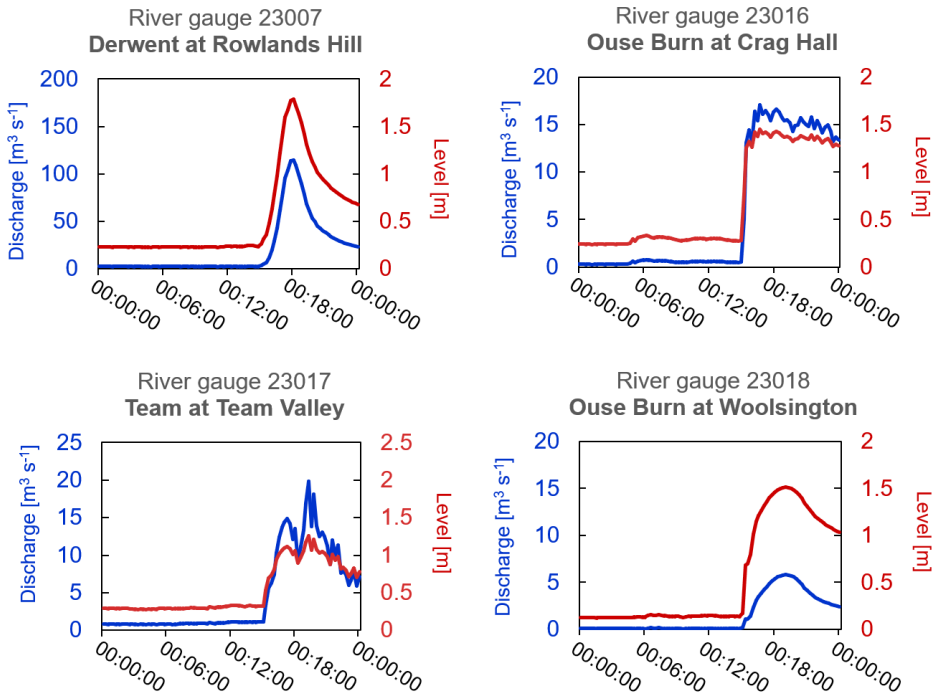

Figure 6.2. River level and discharge for gauging stations 23007, 23016, 23017 and 23018 during the 28th June 2012

To place these high values in context, Table 6.2 (Environment-Agency, 2012) contains the rank of peak stage records for the river gauges shown in Figure 6.1. Period of record for the stations Ouse Burn at Crag Hall and Ouse Burn at Woolsington is 28 years, Team at Team Valley is 30 years, and Derwent at Rowlands Hill is 50 years.

Table 6.2. Rank order of peak levels in [m] for some of the gauges in the Tyne catchment. Values from the June 2012 event are highlighted in blue

Rank	Ouse Burn at Crag Hall (23016)	Ouse Burn at Woolsington (23018)	Team at Team Valley (23017)	Derwent at Rowlands Hill (23007)
1	1.79	1.68	1.55	2.37
2	1.50	1.59	1.30	1.98
3	1.45	1.51	1.30	1.79
4	1.44	1.50	1.27	1.76
5	1.40	1.34	1.21	1.63

* For location of the gauges, refer to Figure 6.1.

6.1.2 Site description

6.1.2.1 Catchment characteristics

The area for which the hydrological modelling was done is the 55.85 Km^2 catchment of the Ouse Burn river, upstream of the city of Newcastle (see Figure 6.3).

The Ouse Burn river flows towards the south-east crossing a low-lying area until its confluence with the River Tyne. The bedrock permeability class is predominantly mixed (there is a strong presence of aquifer with local or limited potential) while superficial deposits are made up of 85.64% till and 13.17% sand. Regarding land cover, nearly half of the catchment land cover is considered urban, followed by predominantly arable agricultural land (National River Flow Archive, 2015)

The topography of the catchment, land cover distinguishing urban and non-urban areas, as well as the river network are presented in Figure 6.3, where the location of Tyne catchment (as defined in Section 6.1.1.1) is shown for reference, and the location of the Ouse Burn catchment is marked in green.

. More information about the area is contained in Table 6.3 (Marsh et al., 2008), including catchment descriptors such as the base flow index derived from the 29-class Hydrology Of Soil Types dataset (Boorman et al., 1995), denoted as BFIHOST, and the catchment wetness index (PROPWET).

BFIHOST relates soil properties with runoff response, and it is a useful index to estimate the median flow of a catchment. Low values (such as 0.2) correspond to highly impermeable soils, and values close to 1.0 denote highly permeable soils (Faulkner et al., 2012). PROPWET is a descriptor of soil moisture deficits where the higher the value, the longer period the soils are defined as wet, providing useful information on susceptibility to floods (National River Flow Archive, 2015).

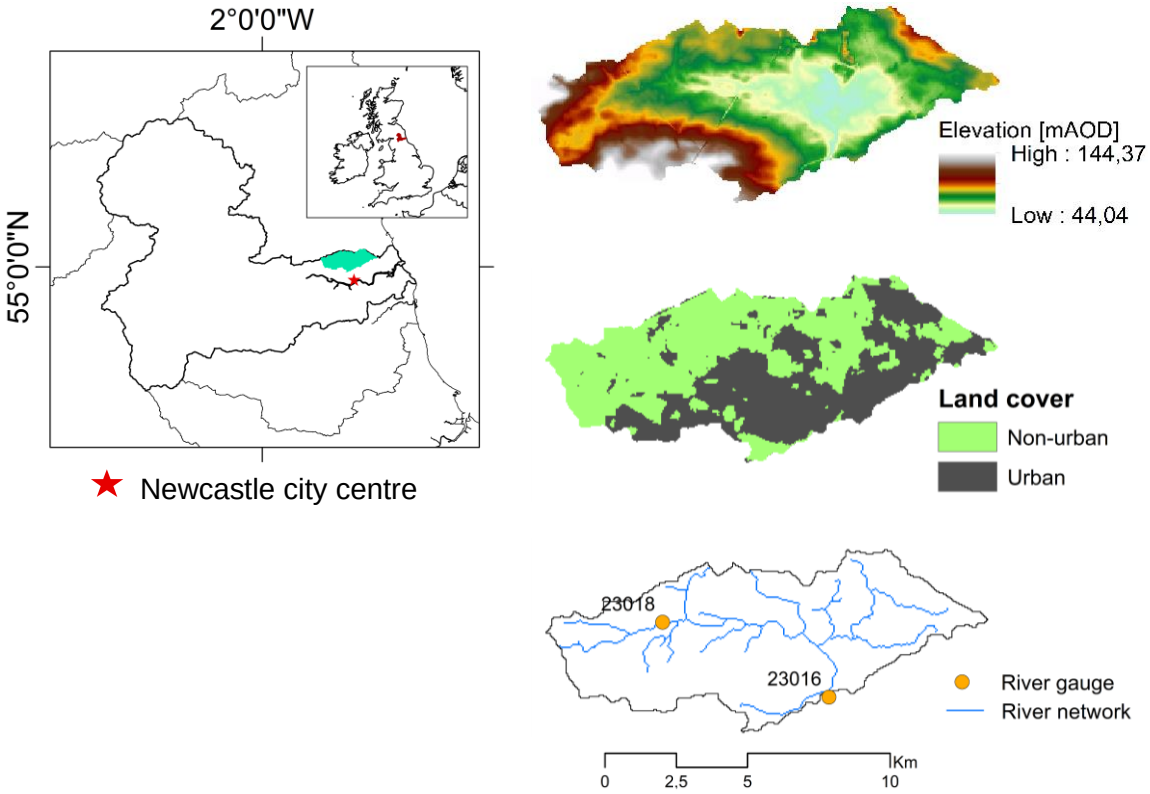

Figure 6.3. Location and physical characteristics of the Ouse Burn catchment

Table 6.3. Physical characteristics and hydrological descriptors of the Ouse Burn catchment

Catchment characteristic	Value	Units
Area	55 585 000	m^2
Mean annual rain	677	mm
Mean annual runoff	183	mm
Meann annual loss	494	mm
Descriptors		
BFIHOST	0.31	-
PROPWET	33	%
Elevation		
Station level	43	mAOD
10^{th} percentile	51	mAOD
50^{th} percentile	68	mAOD
90^{th} percentile	102	mAOD
Max level	144	mAOD
Land cover		
Woodland	5.72	%
Arable/horticultural	33.82	%
Grassland	16.34	%
Mountain/heath/bog	1.20	%
Urban	41.14	%

*mAOD = metres above ordnance datum.

6.1.2.2 River gauge

Flows are measured at the outlet, where the gauging station 23016 “Ouse Burn at Crag Hall” is located, although there is another station upstream, 23018 “Ouse Burn at Woolsington”. The 23016 station is a “rectangular, thin-plate weir with broad-crested flanks” (https://nrfa.ceh.ac.uk/data/station/info/23016, Accessed 30 August 2019), located at 36 metres above ordnance datum (see Figure 6.4).

Figure 6.4. Photographs of the station 23016 (Source: Author)

6.1.2.3 The Ouse Burn Interceptor and Trunk Sewer system

Runoff in this catchment is increased “by effluent returns”. This means, according to the National River Flow Archive, that there are inflows from sewage treatment plants from outside the catchment into the river that could have an impact on the measured and the actual river flow. However, looking at the values presented in Table 6.1, mean annual runoff compared to mean annual rainfall is unusually low for an urban catchment where nearly 40% of its surface comprises impervious areas. In fact, there is a reported bypass to the gauge due to the operation of the Ouseburn Interceptor and Trunk sewer system (Marsh et al., 2008). As part of the present research, an information request was sent to Northumbrian Water to get hold of the report that provides details of this bypass. This study, was commissioned by the Environment Agency from the consulting firm JBA as part of Flood Risk Mapping Studies for 2000-2001, and confirms the influence of the Ouseburn Interceptor combined sewer and the Trunk sewer system (OTS) on the flow measurements as it collects waters from areas beyond the Ouse Burn catchment. The maximum capacity is estimated to be 2.6 $m^3 s^{-1}$ for the Interceptor and 1.4 $m^3 s^{-1}$ for the Trunk sewer, bringing the possible total flow bypassing the gauge to 4.4 $m^3 s^{-1}$ (JBA, 2002). However, lack of information on the operation policy and on flows in the system make it difficult to reliably incorporate the bypass in the numerical

modelling. Therefore, the impact of the OTS will be qualitatively considered when evaluating model results for this site.

6.1.3 Digital Terrain Analysis

As stated in Section 3.2.2, the hydrological modelling starts with the discretisation of the catchment into Hydrological Response Units via the Digital Terrain Analysis. This procedure uses gridded inputs and landscape classifiers to define a map of HRUs, each of which has its own response to climatological inputs.

Information to discretise the catchment into Hydrological Response Units for the Ouse Burn catchment are displayed in Figure 6.5 and include:

- Topography
- Land cover as landscape classifier
- Reference river network

Since two rainfall datasets were also used as climatological information to discretise the catchment, the Digital Terrain Analysis (DTA) process delivered two maps of Hydrological Response Units. Figure 6.5a allows the comparison of both inputs, which shows that there is a clear influence of the resolution of the rainfall on the number of Hydrological Response Units obtained. The complete numerical procedure to discretise the catchment in these units is stated in Section 3.2.2.1.

In said figure, the columns show the gridded rainfall data to discretise the catchment (left column) and the product of the Digital Terrain Analysis (right column). The rows show the different sources of the gridded rainfall estimates (observed and simulated). Since the only input dataset that differs from one configuration to another is the gridded rainfall, then the discussion will focus on the impact of the resolution in the hydrological modelling.

Using observed rainfall, 81 rainfall cells overlapped the catchment which was discretised into 1087 HRUs. On the other hand, 26 rainfall cells from the gridded WRF rainfall fell within the catchment, which gave 422 HRUs. To explore the impact of the landscape classifiers in the process of obtaining the HRUs, the Digital Terrain Analysis was carried out using only the topography and the ASCII file with the two parameter sets. The result is shown in the third row/column of Figure 6.5. This analysis resulted in 36 HRUs.

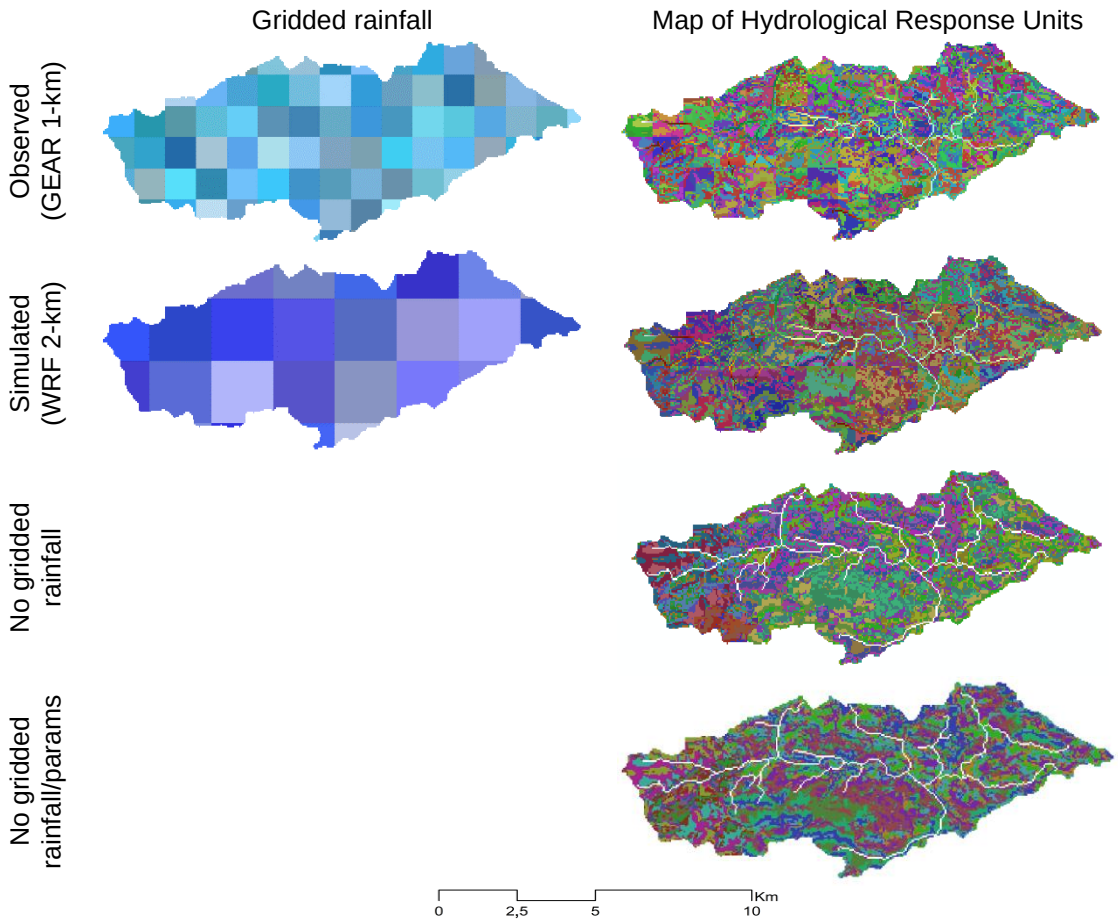

Figure 6.5. Spatial configuration of the observed and simulated gridded climatological inputs for the Ouse Burn catchment discretisation

The relationship between number of cells of the rainfall gridded data and the number of HRUs calculated clearly show that the resolution of landscape classifiers play an important role in the discretisation of the catchment. As stated in Section 3.3.2.1, the resolution of the topography (50 m) allows for the consideration in detail of the flow directions and the correct representation of the river network. This means that, in absence of gridded rainfall, the resolution of the topography is the main driver in the Digital Terran Analysis. In fact, if the parameter layer was also disregarded, the discretisation of the catchment would depend entirely on the classification fractions for slope and accumulated area. The result of this experiment is shown in the fourth row of Figure 6.5. Here, the number of HRUs calculates is half of that using a parameter layer (18 instead of 36).

It is also important to note what was stated in Section 2.3.2.1 regarding the delineation of Hydrological Response Units: in the case of the Ouse Burn catchment, the topography allows great spatial variability (see Figure 6.3 for a map of the distribution of elevations) that allow

the consideration of slope, flow direction and contributing areas in the catchment processes. But without landscape classifiers and with a flat topography, then the processes that would guide the creation of the HRUs would refer to underground storage, soil conditions and land use that will contribute to the modification of the drainage capacities in the catchment.

It is important to note that despite the difference in spatial resolution in the rainfall data used, the discretisation of the catchment using WRF 2-km rainfall was done as part of the investigation on the role of relationship between number of grid cells per landscape layer and number of HRUs. In the end and as stated in Section 3.3.2.2, the 1-km rainfall was used as the only landscape layer. This section also contains a detailed description on the use of WRF 2-km rainfall for rainfall-runoff modelling.

6.1.4. Model calibration

The calibration period for the hydrological modelling of the June 2012 event used climatological inputs (rainfall and potential evapotranspiration) from 00:00 UTC 28 February 2008 to 00:00 UTC 1 June 2012. During this period several high flow events are present, and the flashy behaviour of the catchment can be appreciated. The Monte Carlo framework was used to sample 10 000 parameter sets for which the Nash-Sutcliffe Efficiency (NSE) index and Root Mean Square Error (RMSE) were calculated.

Model parameter ranges are contained in Tables 6.4 and 6.5. At the time of the modelling, DECIPHeR implements a single channel velocity for the whole domain. In this case, the parameter ranges for the channel velocity, CHV, are 150-700 m h^{-1}.

Table 6.4. Hydrological model parameter ranges for urban areas for the June 2012 case study

Parameter	Units	Lower limit	Upper limit
SZM	m	0.0015	0.01
$Ln(T_0)$	ln(m^2 ts^{-1})	-6	0
SR_{max}	m	0.011	0.15
SR_{ini}	m	0	0.002
Td	ts m^{-1}	0.1	100
S_{max}	m	0.0012	0.02

Table 6.5. Hydrological model parameter ranges for rural areas for the June 2012 case study

Parameter	Units	Lower limit	Upper limit
SZM	m	0.02	0.08
$Ln(T_0)$	ln(m^2 ts^{-1})	0	6
SR_{max}	m	0.3	0.6
SR_{ini}	m	0	0.1
Td	ts m^{-1}	0.1	100
S_{max}	m	0.4	0.8

As stated in Section 3.4.2, the behavioural members were chosen as those scoring above the NSE 95th percentile while belonging to the 5% of the simulations with the lowest RMSE. For details on the observed discharge refer to Section 3.3.2.1 “Databases used for rainfall-runoff modelling”.

6.1.4.1 Assessment of the simulated flow

<u>During peaks in runoff</u>

Figures 6.6a-d show the model performance for three two-month plots during the calibration period. These plots were chosen because they contain at least one significant runoff peak, a key feature of the observed time series that the model should be able to reproduce (low runoff values will be analysed in the next sub-section). The graphs use the same scale in the vertical axis for comparison purposes.

The model reproduces the timing and magnitude of the significant peaks of the timeseries. Peaks in the observed hydrograph are generally contained in the envelope of the simulated discharge, meaning that the model is correctly processing the variations of soil conditions and flow routing. It seems that the model performs better during high runoff values (greater than 5 × 10^{-1} mm), such as the notably high value in Figure 6.6a, the series of discharge peaks in Figure 6.6b and both peaks in Figure 6.6c, despite the difference in the magnitude of the antecedent rainfall.

Another favourable feature to determine model performance is the good correspondence between the number of observed and simulated peaks in the period. It is worth noting that on some occasions, the model ensemble delivers a peak that is not present in the observed discharge, for example, on 19 September 2008 (Figure 6.6a), 7 December 2009 (Figure 6.6b) and 10 October 2012 (Figure 6.6d). The peak just before the 19 September 2008 occurs after a burst of rain at the end of a 12-day rainfall period. If soil storage capacity was compromised during those days, then runoff would be expected even with a smaller amount of rainfall than previous days. The second peak, just before 7 December 2009, occurs in the middle of a

period of steady rainfall, and in fact, the peak that precedes it is overestimated. The third one just after 10 October 2012 is recorded after a burst of rainfall that follows nearly two weeks of dry weather. This shows that the hydrological model tends to overestimate runoff peaks after dry or low-intensity rainfall periods. The fact that there is a trend in the overestimation of low-magnitude peaks helps pin-pointing the sources of error.

During low runoff periods

Figures 6.7a-d illustrate the model performance to reproduce periods of low flows. For both cases, runoff peaks are overestimated, sometimes by more than double the value of the observed discharge (6 November and 12 December 2008 in Fig. 6.7a and the 12-day period after 7 January 2011 in Figure 6.7b). It is worth noticing that this behaviour occurs during winter, when the rainfall is significantly less than during summer. The model also identifies the timings of the peaks, which means that the responsiveness of the catchment is well captured.

Although the present study is focused on reproducing the spatial and temporal location of runoff peaks, the combination of the Nash-Sutcliffe efficiency index and the Root Mean Square error ensure that the behavioural ensemble contains simulations that did well during both high and low flows.

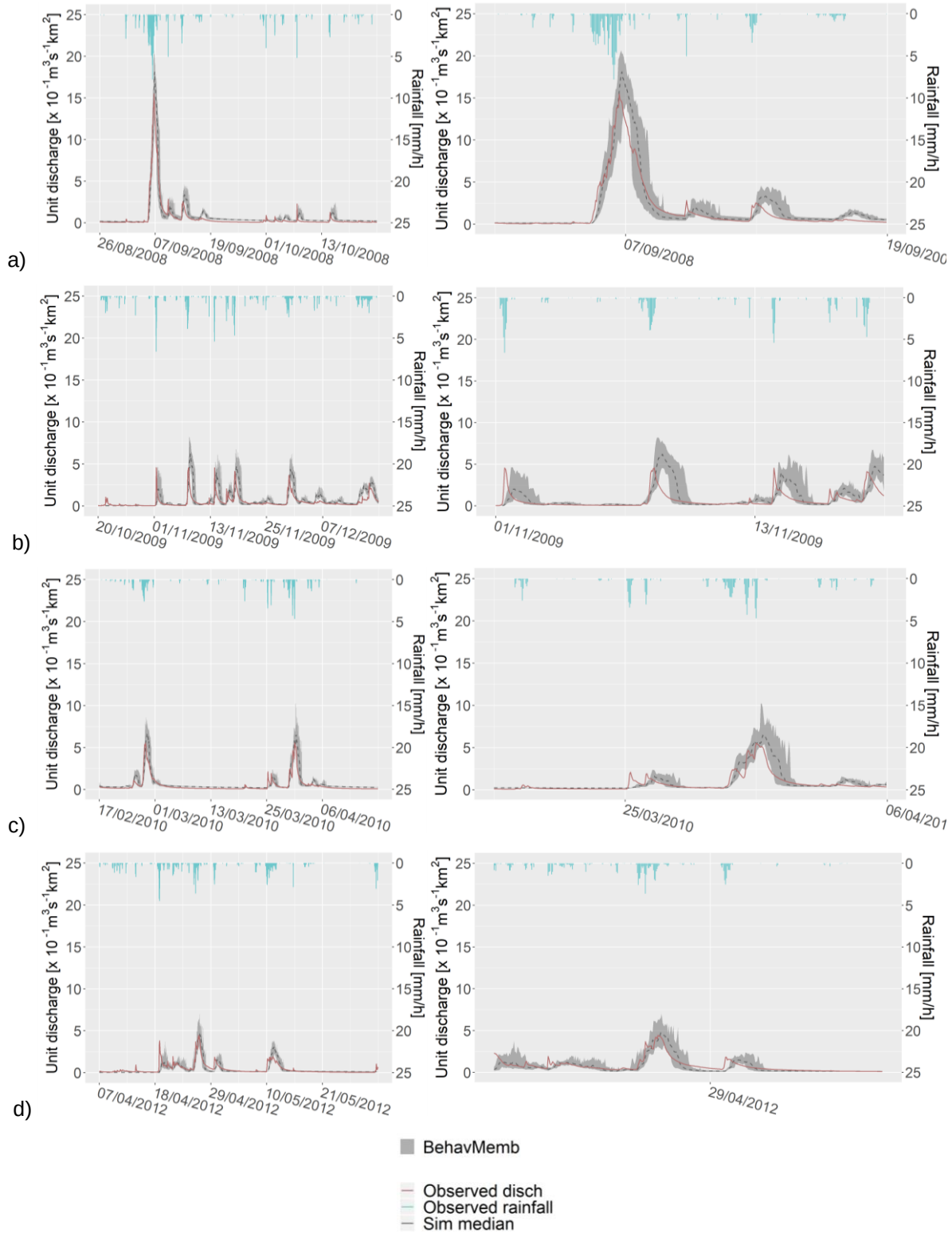

Figure 6.6. Hourly calibrated flow for the two-month period a) 26 August 2008 to 24 October 2008, b) 20 October 2009 to 19 December 2009, c) 17 February 2010 to 18 April 2010, d) 7 April 2012 to 31 May 2012. Spread of the 5th and 95th percentiles of the behavioural ensemble defined using the GLUE methodology is shown in grey, 50th percentile is shown as a dotted line, observed flow is shown as a red line. Right column= subset of left column

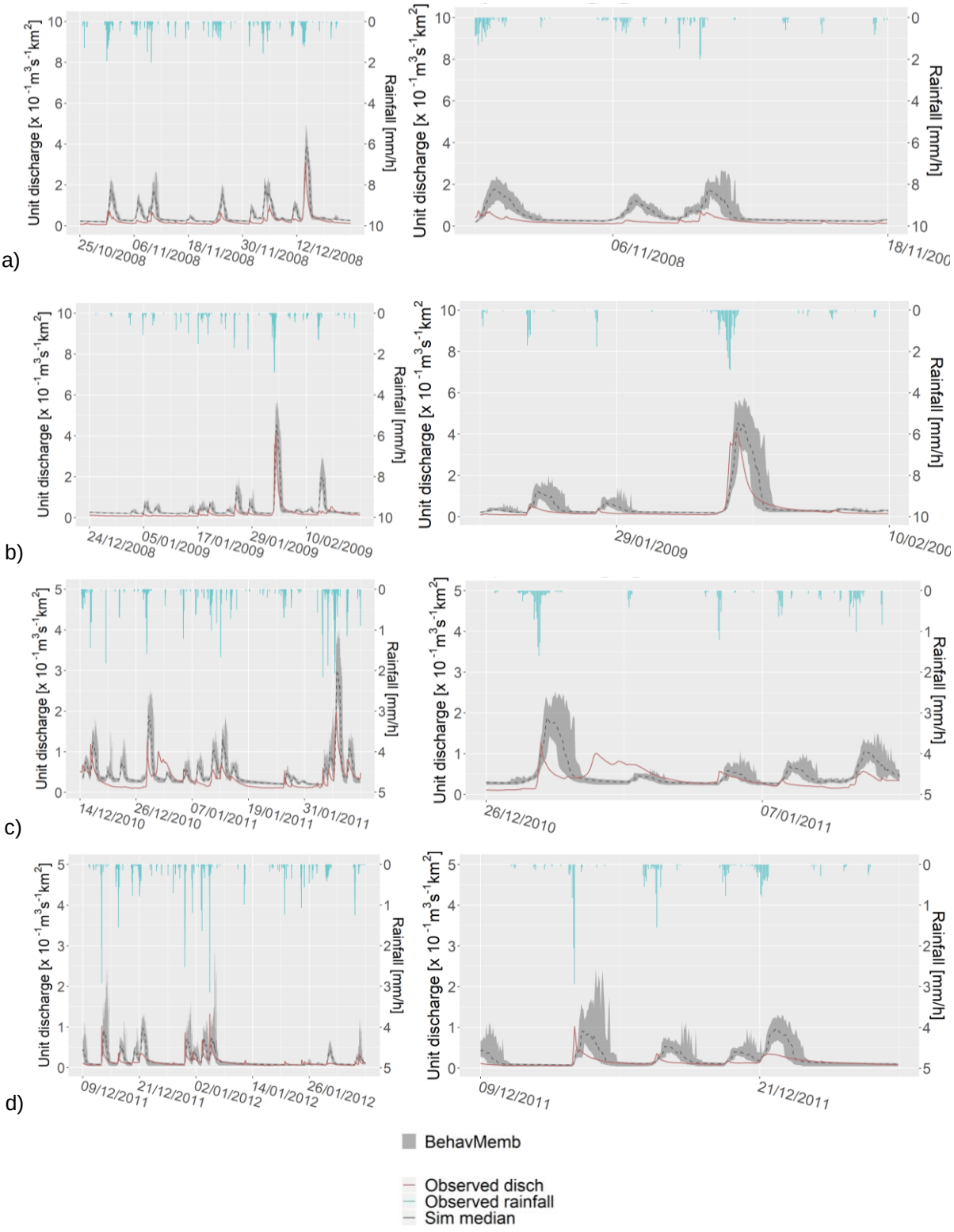

Figure 6.7. Hourly calibrated flow for the two-month period a) 25 October 2008 to 23 December 2008, b) 24 December 2008 to 21 February 2009, c) 14 December 2010 to 11 February 2011 and d) 9 December 2011 to 6 February 2012. Spread of the 5th and 95th percentiles of the behavioural ensemble defined using the GLUE methodology is shown in grey, 50th percentile is shown as a dotted line, observed flow is shown as a red line. Right column= subset of left column

Influence of the Ouse Burn Interceptor and Trunk Sewer System

There were two periods during the calibration process in which the external influence of the sewer system became evident and detrimental to evaluate model performance. During these periods, illustrated in Figure 6.8 a-b, the measured runoff deviated considerably from the behavioural ensemble, and even from the spread of the whole simulation set of 10 000 runs. Looking at the observed rainfall, the response of the river does not match the amount of rainfall received by the catchment. For example, in Figure 6.8a, up until a runoff peak at the end of 2009 (feature A) there is a reasonable correspondence between observed and simulated discharge. However, all the simulations reproduce a peak in the discharge (feature B) that comes after a period of steady rain. The ensemble also indicates that from that point, the flow increased gradually until the following important peak (D). The shape of the hydrograph on the 12 January 2010 (feature C) is not reproduced.

The second period in which the influence of the bypass can be seen is illustrated in Figure 6.8b, from 15 October to 13 February 2010. In this case, by the second half of November the observed discharge decreased considerably despite the recorded rain in the area (from point A and on). Following the magnitude of the inputs, the model ensemble reproduces high runoff values during approximately two weeks (point B). Finally, the observed data series present a peak larger than any other value in the two-month period (point C). This comes around 10 days after the rainfall, which does not correspond to the behaviour of an urban catchment, suggesting that this peak could have been caused by sudden water release.

For both cases, the periods for which observed and simulated flow values vary considerably were considered as misinformation and disregarded for model calibration. This is reflected in the plots shown in Figure 6.8a-b: when obtaining the behavioural members some period are not included in the analysis, for example, where there are significant mismatches between the observed discharge (red line) and the spread of the entire ensemble (dark grey envelope). The exact dates that were taken out of the analysis are from 13:00 UTC 3 January 2010 to 12:00 UTC 16 January 2010 (see Figure 6.8a), and from 13:00 UTC 20 November 2010 to 14:00 UTC 14 December 2010 (see Figure 6.8b).

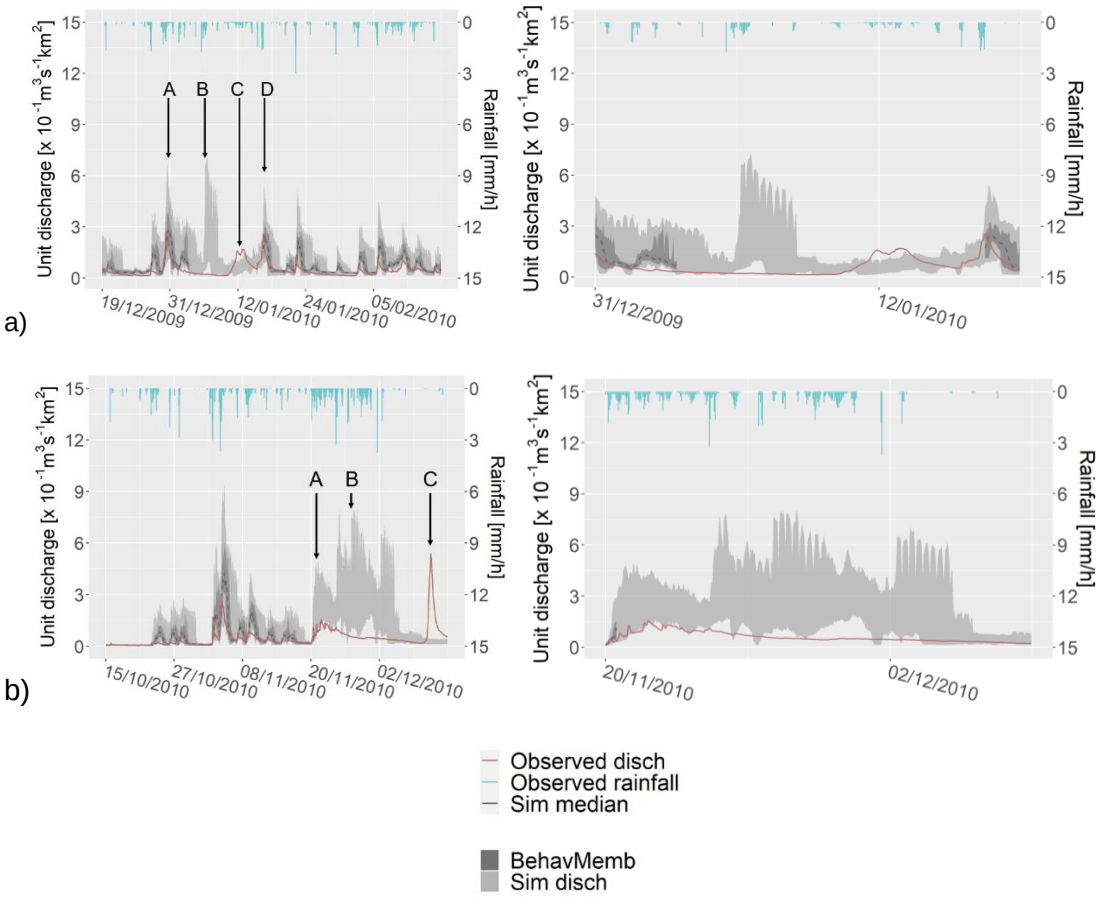

Figure 6.8. Hourly calibrated flow for the two-month period a) 19 December 2008 to 16 February 2010, b) 24 December 2008 to 21 February 2009, c) 14 December 2010 to 11 February 2011 and d) 9 December 2011 to 6 February 2012. Spread of the entire ensemble is shown as dark grey, 5th and 95th percentiles of the behavioural ensemble defined using the GLUE methodology is shown in light grey, 50th percentile is shown as a dotted line, observed flow is shown as a red line. Right column= subset of left column

6.1.4.2 Performance statistics

Figure 6.9 contains the scatter plots for the most relevant parameters to represent soils storage conditions and impervious surfaces for both urban and rural areas. The obtained parameters confirm the correctness of the assumptions detailed at the beginning of this chapter regarding soil storage and flow transfer between Hydrological Response Units (HRUs). SR_{max} (maximum storage capacity of the root zone) for urban areas is considerably lower than SR_{max} in rural regions. The low values of $Ln(T0)$ (lateral saturated hydraulic transmissivity) for urban areas describe the poor transmissivity of the urban HRUs, which together with low values of SZM (form of exponential decline in conductivity) and low values of S_{max} (maximum

effective deficit of the saturated zone), ensure that the storage is full and that the flow is routed toward the river channel.

The skill metrics for the calibration period are shown in Table 6.6. The scores indicate that although the qualitative analysis of model performance (as detailed in Section 6.1.4.1) gives a good correspondence between the timing of the observed discharge and the behavioural ensemble, the NSE index suggests that the model does struggle to simulate the measured river flow. Moreover, the maximum RMSE of the behavioural ensemble (RMSE = 0.0450 mm h^{-1}) is nearly half the value of the average observed discharge. This reflects the possibility that although the model could have performed well during high peaks, but given the constant overestimation during low flows, the overall model performance is penalised.

Table 6.6. Performance metrics for the calibration period

Metric	Value	Units
Nash-Sutcliffe efficiency index (Q95)	0.34	-
Nash-Sutcliffe efficiency index (max)	0.53	-
Root Mean Square Error (max of the 5% of simulations)	0.0450	mm h^{-1}
Root Mean Square Error (min)	0.0380	mm h^{-1}

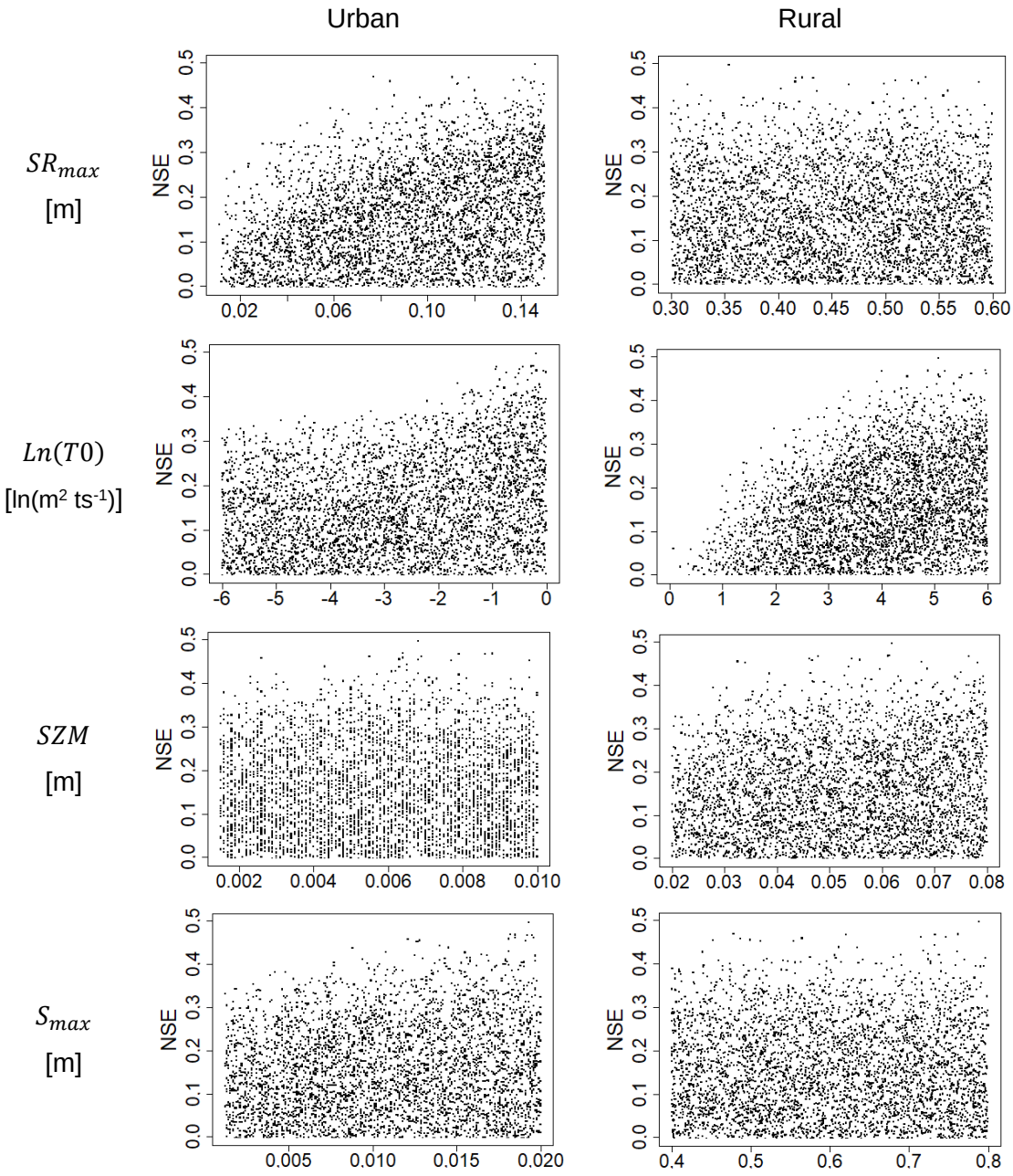

Figure 6.9. Scatter plots of the parameter space after the calibration period of the June 2012 event

The distribution of parameter values in Figure 6.9 shows that the ranges could still be changed for SR_{max} in urban areas and $Ln(T0)$ for both. However, increasing the value of SR_{max} would mean that there is storage capacity in the soil of the urban HRUs, which is not expected. Similarly, increasing the value of $Ln(T0)$ for flow routing in urban HRUs would favour downslope water transfer, contrary to the physically plausible situation of mostly saturated storages. The scatter plots for the rest of the parameters for both types of land cover do not exhibit any important role when reproducing observed flows (or increasing the NSE

value), except for the channel velocity. In this case, since a fixed CHV is used for the entire catchment, the parameter seems to reach a maximum possible NSE, before and after which lower values can be found (see Figure 6.10). The constraint that CHV imposes could be one of the reasons behind the low performance scores.

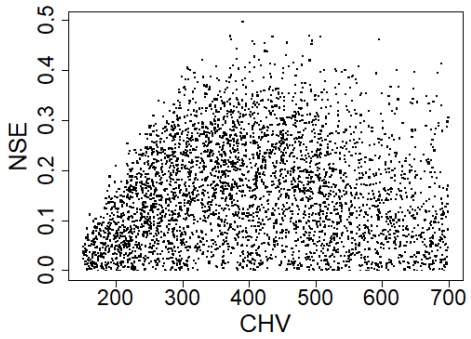

Figure 6.10. Scatter plot of the obtained values of the channel velocity during the calibration process of the June 2012 case study

6.1.5 Model validation

The validation period runs from 00:00 UTC 28th June 2012 to 00:00 30th June 2012 with one year of spin-up time. This period was chosen as it includes the two-hour period of the highest rainfall recorded in the Tyne catchment from 15:00 UTC to 17:00 UTC 28th June, and also the falling limb of the hydrograph of the gauge at the outlet of the Ouse Burn catchment.

As stated in Section 6.1.3 “Digital Terrain Analysis”, two maps of Hydrological Response Units were used for simulations forced with observed and simulated rainfall

The rainfall-runoff plots using observed gridded rainfall (Lewis et al., 2018)and simulated rainfall (WRF model outputs) are shown in Figure 6.11a-b. The notation corresponds to the nine scenarios of simulated rainfall using the WRF model, which are a combination of three microphysics schemes (Thompson, THOM; WRF Single-Moment 6-class, WSM6; Morrison, MORR) and three urban canopy models (Single Layer Urban Canopy Model, SLUCM; Building Effect Parameterisation, BEP; Building Energy Model, BEM). The spread of the 5th and 95th percentiles of the behavioural ensemble defined using the GLUE methodology is shown in grey, along with the 50th percentile (dotted line) and the observed flow (red line). Performance metrics for all simulations are contained in Table 6.7.

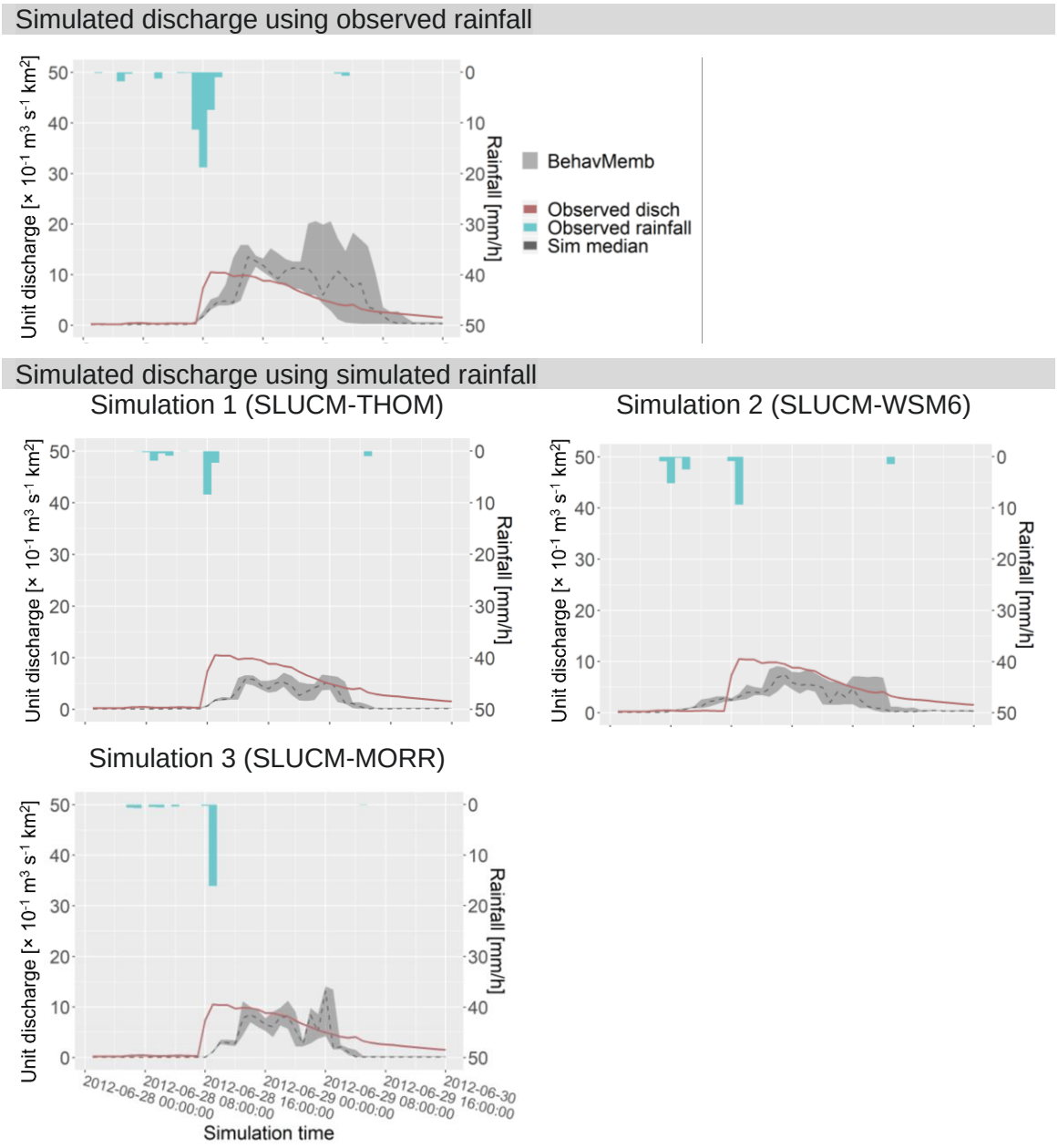

Figure 6.11a. Hourly simulated flow for the validation period of hydrological simulation of the June 2012 event using observed rainfall (top panel) and simulations 1-6 (left to right, top to bottom)

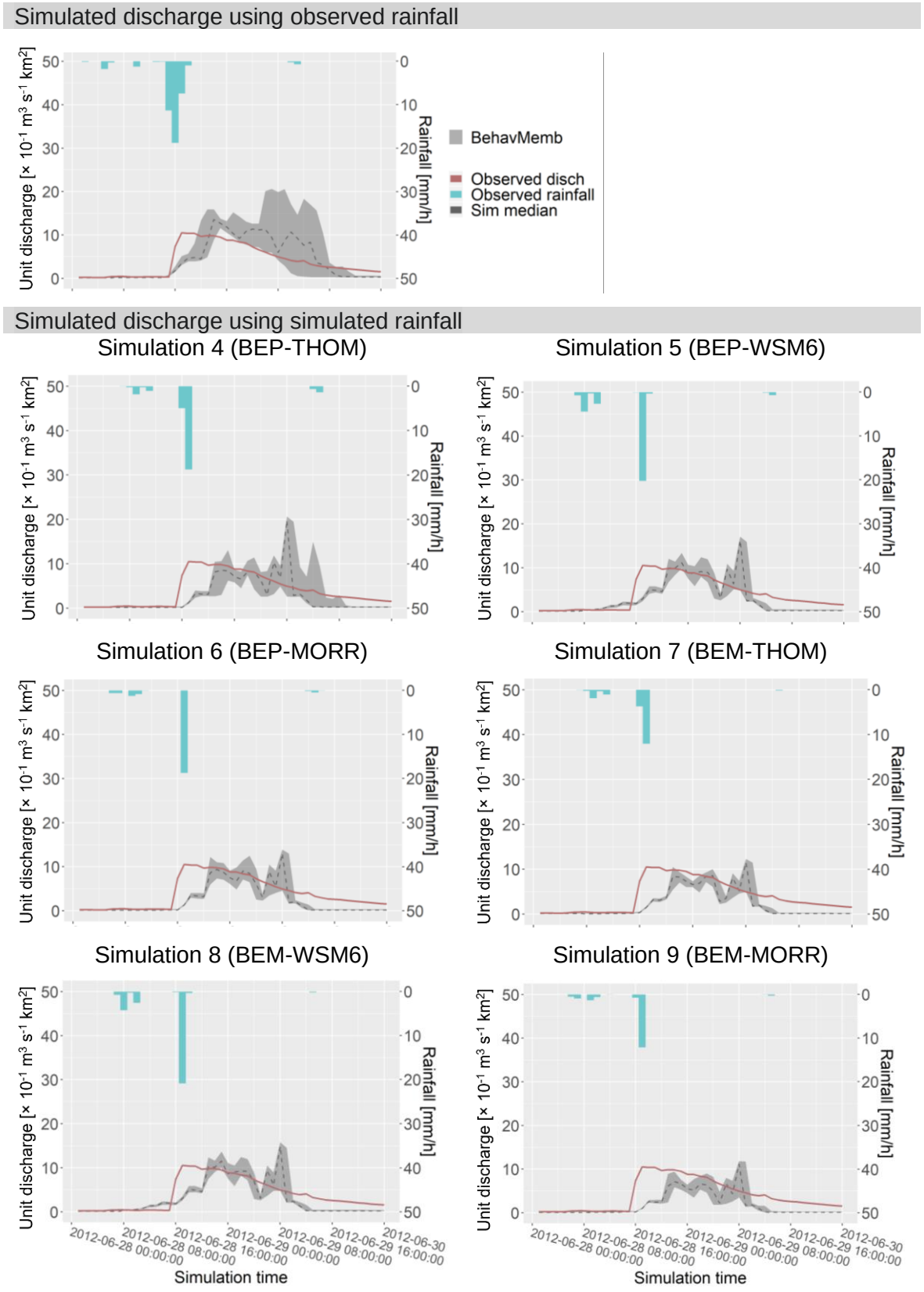

Figure 6.11b. Hourly simulated flow for the validation period of hydrological simulation of the June 2012 event using observed rainfall (top panel) and simulations 1-9 (left to right, top to bottom)

Table 6.7. Performance metrics for the calibration period of the hydrological modelling of the June 2012 event

Simulation	NSE (95th percentile)	NSE (max)	RMSE [mm h^{-1}] (max of 5% of total)	RMSE [mm h^{-1}] (min)
OBS (CEH-GEAR)	-0.13	0.15	5.87	5.10
1 (SLUCM-THOM)	0.05	0.21	5.39	4.91
2 (SLUCM-WSM6)	0.30	0.42	4.64	4.22
3 (SLUCM-MORR)	0.08	0.24	5.29	4.83
4 (BEP-THOM)	-0.10	0.02	5.79	5.48
5 (BEP-WSM6)	0.25	0.33	4.78	4.51
6 (BEP-MORR)	0.17	0.31	5.04	4.58
7 (BEM-THOM)	0.19	0.27	4.96	4.73
8 (BEM-WSM6)	0.30	0.38	4.63	4.35
9 (BEM-MORR)	0.03	0.17	5.44	5.02

For all hydrological simulations, DECIPHeR seems to produce a highly variable hydrograph, with several peaks in the 48 hours of the simulations, despite the short-lived and intense rainfall event. In general, higher rainfall values deliver a behavioural ensemble with a larger spread. See, for example, the shape of the ensemble in Simulation 4 (Figure 6.11b), with a peak rainfall of 18.77 mm h^{-1} and significant peaks in the discharge, compared to Simulation 7 with peak rainfall of 12.04 mm h^{-1} and a smoother hydrograph.

The falling limb of the behavioural ensemble from Simulations 1-9 reaches its lowest value more than 12 hours before the observed discharge. This suggests that DECIPHeR is routing water towards the outlet of the catchment quicker than what what happens in reality due to large values of the channel velocity (CHV). To correct this, lower values of CHV would be required so the flow takes longer to reach the outlet. However (and as explained in section 6.1.4.2), lowering the range of this parameter would lead to lower NSE values during the calibration.

It is worth mentioning how close the peak values of observed discharge and observed rainfall are (see top plot of Figure 6.11a). In fact, the first peak in all simulated discharge scenarios occurs nearly four hours after the peak rainfall. This shows that the model struggles to reproduce the dynamic behaviour of the catchment for this event.

Looking at the flow produced using observed rainfall (see top plot of Figure 6.11a), the median has a highly variable behaviour. At a given timestep, the median is closer to the 5th percentile of the ensemble and later on it is closer to the 95th percentile. This means that within the behavioural ensemble, some simulations correctly estimate the observed runoff at either the beginning or at the end of the validation period, but not during the entire 48 hours of the

simulation. This is reflected in the NSE scores: for all cases, NSE<0.5 suggests that model results are closer to the mean of the observed time series rather than being an actual descriptor of the measured discharge.

The skill of the simulations was ranked according to the Nash-Sutcliffe Efficiency (NSE) index and Root Mean Square Error (RMSE) values. The top ranked scenario has the highest NSE (95th percentile) and the lowest RMSE (maximum value of the best 5% of the simulations). Figure 6.12 shows the nine scenarios of simulated runoff (as stated in Table 6.7), ordered from best to worst performance.

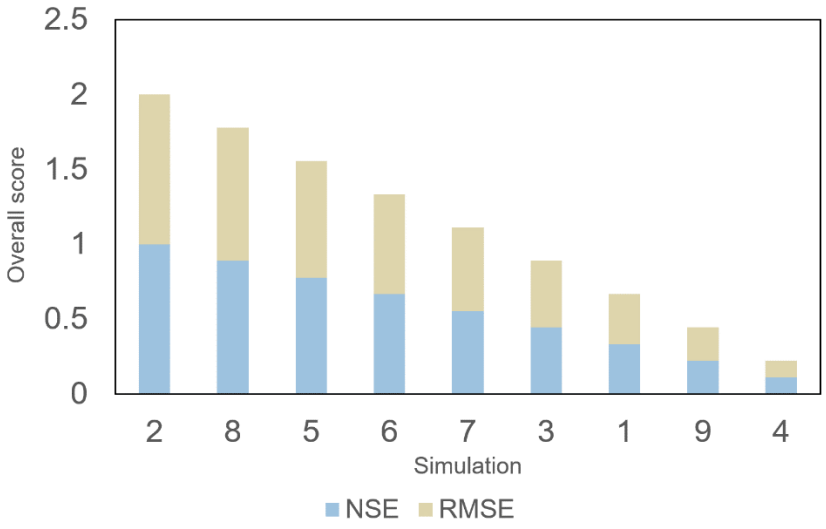

Figure 6.12. Simulated hydrological scenarios ranked by performance for the June 2012 case study, showing bar length as the contribution of each metric to the overall performance

It is worth mentioning that the simulated discharge ensemble with the highest NSE also has the lowest RMSE value, so ranking of the hydrological simulations is more straightforward than that for the meteorological model outputs. However, the top ranked hydrological simulations for the Newcastle test case are 2, 8 and 5, two of which ranked as lowest performing in the meteorological model evaluation. On the other hand, hydrological simulations 1 and 3 are among the lower half, whereas said scenarios ranked as first and second best performing meteorological scenarios.

This mismatch can be explained by looking at the shape of the hydrological ensemble. The hydrological scenarios with the highest rank in model performance either have a stable behaviour, despite the consistently low values (Simulation 2, Figure 6.11a) or feature discharge peaks large enough to match the observed runoff, but not too large so as to deviate

from the measurements (Simulations 5 and 8, Figure 6.11b). In contrast, the lowest ranked simulations present discharge peaks that are nearly four times larger than measurements (Simulation 4, Figure 6.11b) or that, despite having a more stable behaviour (no significant peaks in the timeseries), simulated values are less than those observed for nearly the whole 48-hour period.

6.1.5.1 Impact of the urban canopy layer parameterisations in runoff simulations.

There is no clear agreement on the WRF output that best produces the observed runoff: in all cases, including the hydrological simulations using observed rainfall, model outputs show that the model does not correctly reproduce the sudden increase in discharge (described in Section 6.1.1.2).

Simulation 3 (Figure 6.11a) shows that the simplest urban canopy layer (Single Layer Urban Canopy Model, SLUCM) delivers more realistic rainfall values when used with the most complex physics scheme (Morrison, MORR). The behavioural hydrological ensemble shows that it takes approximately four hours for the catchment to produce a significant response, and the hydrograph that corresponds to the median of the ensemble has a steep rising limb, despite this occurring at the wrong time. As stated previously in Section 6.1.5, the ensemble can be described as highly variable, with a significant peak at 08:00 UTC 29 June 2012. This is also the case in Simulation 8, when pairing the most complex urban parameterisation (Building Energy Model, BEM) with the single-moment microphysics scheme (WRF Single-Moment, 6-class, WSM6). This means that there is a compensation in the complexity of the physics schemes when solving for the origin and development of the hydrometeors, and the amount of rainfall produced. The ensemble of those two simulations is quite similar in terms of temporal location of the peaks as well as location of the 50^{th} percentile in relation to the minimum and maximum limits.

Simulation 2 illustrates the effect of using the simplest urban canopy model (SLUCM) with the simplest microphysics scheme (WSM6), which produces significantly low rainfall values (always below 10 m h^{-1}) which, in turn, deliver a smooth discharge ensemble and less variations of the median of the ensemble. On the other hand, Simulation 9 uses the most complex parameterisation of the urban canopy layer and microphysics (BEM and MORR, respectively), however the simulated peak rainfall falls short of the observed values, thus producing an ensemble with several peaks that still underestimates the measured flows.

The midpoint between complex and simple physics schemes, for both urban canopy layer (Building Effect Parameterisation, BEP) and microphysics (Thompson scheme, THOM) is Simulation 4 (see Figure 6.11b), in which the largest discharge values are observed despite

not having the highest rainfall values compared to the rest of the simulations. This confirms the model sensitivity to CHV, meaning that flows at the outlet of the catchment depend more on the speed with which water flows in the river than on the amount of water that is routed to the river. The current hydrological model performance could be improved if CHV is assigned different ranges depending on the land cover type that the channel is located in, instead of using a fixed value across the domain.

6.2 Case 2. Birmingham 2007 flash flood event

The second case study is one of the severe flash flooding events that occurred in summer 2007 as a result of intense, stationary rainfall as described in Section 5.2. In turn, Section 6.2.1 describes the hydrological setting during June and July 2007 in the United Kingdom, and Section 6.2.2 presents the specific catchment for which the hydrological modelling was done along with the reason behind the choice.

6.2.1 Hydrology

6.2.1.1 Antecedent conditions

An arid episode that started in January 2007 in the United Kingdom meant that soils across the country retained their storage capacity and thus their ability to moderate the impact of potential flooding. These dry conditions prevailed during March and April 2007, with the latter becoming the warmest month since records began in 1961. Soil moisture deficits were at their highest at the beginning of May, having a substantial influence in moderating flood risk (Marsh & Hannaford, 2007). However, as detailed in Section 5.1, wet conditions later in May caused soil saturation that exceeded values that are normally observable in winter. The wet conditions during the month set the precedent for the summer 2007 floods, leading to two major flooding episodes, the first one on 25th June, followed by a second one on 20th July.

By the end of May and leading to the first flooding episode, runoff values of were considerably higher than the Long-Term Average in rivers like the Great Ouse, which flows through Northamptonshire and East Anglia. Late June saw bankful flows exceeded in Oxfordshire. During this period, new river level maximum values that considerably exceeded previous levels were recorded in Yorkshire and the Midlands (some stations measured new maxima that exceeded the previous value by 1.5 m). Other cities such as Hull, despite having normal river levels, experienced saturated drainage conditions and an increase in flood risk (Marsh, 2008). Figure 6.13 shows the location of the cities and extent of the counties. During June,

several flood warnings were issued, highlighting the vulnerability of the United Kingdom to flooding if other rainfall episodes appeared.

By the end of July, soil wetness was even greater than the late-winter mean, enhancing the responsiveness of catchments. As a result of the moist mass of air moving from France and becoming stationary over central England, there was extensive flash flooding and surface runoff even in permeable catchments, and prolonged high river levels hindered the efficiency of drainage networks. The second flooding episode extended to major river catchments so inundated areas could be found along the Warwickshire Avon, Severn and the upper Thames and its tributaries, a more damaging event than the June floods. The July event was also characterised by significant infiltration that led to aquifer recharge and unusually high groundwater levels in areas such as Lincolnshire and York (Marsh & Sanderson, 2007) (Figure 6.12 shows a map of said areas).

In general, flows during the summer 2007 are well above three times the expected Long-Term Average 1961-1990, and almost doubled the previous two-month maximum value recorded in 1968. Table 6.8 (Marsh & Hannaford, 2007) contains the comparison of the historical two-month runoff values from 18 major river basins in England and Wales. The magnitude of the runoff during the Summer 2007 clearly stands out, even compared to the second highest record.

Table 6.8. Rank of the ten highest June-July recorded runoff values for England and Wales

Rank	Year	Runoff [mm]	% of Long-Term Average (1961-1990)
1	2007	121.5	332
2	1968	61.8	169
3	1985	52.0	142
4	1998	50.4	138
5	1972	49.8	136
6	1987	49.3	135
7	1988	48.1	132
8	2000	47.2	129
9	1993	46.1	126
10	2002	42.8	117

6.2.1.2 River level and discharge during the event

Some gauges in the Midlands region recorded their maximum possible discharge value on the 20th July. Other stations were overtopped, flooded or left without power, making any readings

impossible. There was a rapid rise in river levels similar to that described in Section 6.1.1.2, which created difficulties in issuing any flood warnings with at least two hours of lead time, and from the 80 warnings during the day, two of them were given once the water courses had overflowed. (Environment-Agency, 2007a; Pitt, 2008).

In the case of chalk or limestone catchments, intense rainfall meant that there was a constant flow of water percolating to the aquifers which then overflowed as springs with a time delay. At the end of the summer, the magnitude of the recorded outflows reached the expected daily maximum values (Marsh, 2008).

In the early hours of the 20th July, many small reaches overflowed due to the outstanding rainfall that the region had been experiencing in the previous months. There were scattered flash flood events across small catchments in England and Wales, including Barry in the Vale of Glamorgan, Gloucestershire, Lincolnshire, Wiltshire, Hampshire, Surrey and central London (cities and counties are shown in Figure 6.13).

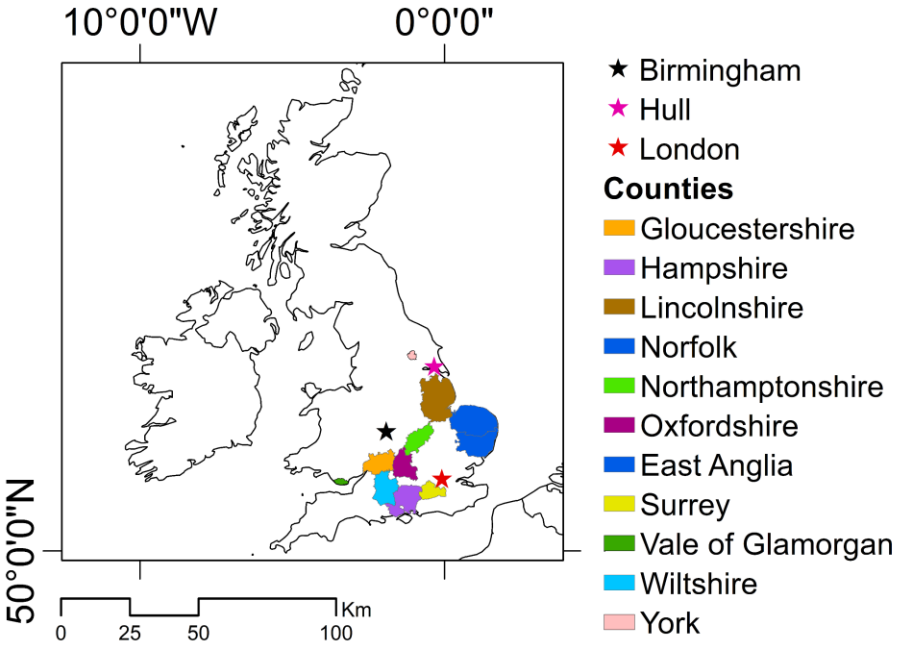

Figure 6.13. Some of the counties and cities affected during the summer 2007 floods

As runoff concentrated in larger catchments, there were major flash flood events along the Warwickshire Avon, Severn and the Thames. Flooding near the Severn mouth reached nearly two meters, and rivers levels on the Warwickshire Avon exceeded the previous maximum value, recorded in 1848 (Environment-Agency, 2007b).

In general, there was a substantial redefinition of summer maximum runoff values for England and Wales. Figure 6.14 (Marsh & Hannaford, 2007) illustrates this by showing maximum and minimum daily flows (blue and green envelopes, respectively) in a series from 1961 to 2006, and the hydrograph for the measured daily runoff during 2007.

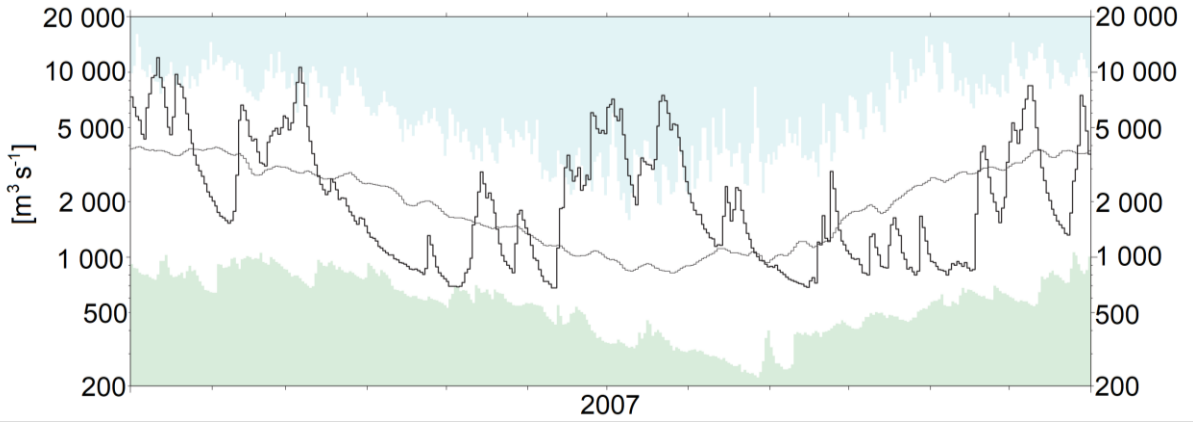

Figure 6.14. Long-term daily maxima (lower bound of blue envelope) and minima (upper bound of green envelope) during 1961-2006, estimated daily outflows (grey line) and daily hydrograph with recorded values for 2007 for England and Wales

6.2.2 Site description

6.2.2.1 Catchment characteristics

Given that the summer 2007 floods extended over most central England, the Rea catchment was chosen for modelling. This 74.08 Km^2 catchment is located south-west of Birmingham, the second most populous city in the United Kingdom (as described by (Heaviside et al., 2015) at the beginning of Chapter 5). The second reason behind the choice of this area is the highly urbanised fraction of the catchment, which emphasizes the challenge of characterising the response of an urban catchment under intense, localised rainfall.

The Rea catchment is in the the south-west of hydrometric area 28 “Trent”, one of the 107 areas in which the United Kingdom is discretised for collection of hydrometeorological data. Hydrometric area 28 is administrated by the Midlands Division of the Environment Agency (National River Flow, 2014). The catchment extent and river network for the said hydrometric area is shown in Figure 6.15, which follows the notation of Figure 6.1: river reaches display their name and some river gauging stations are included (both active and no longer in use) Birmingham city centre and the closest river gauge, station 28039 “Rea at Calthorpe Park”, are also marked.

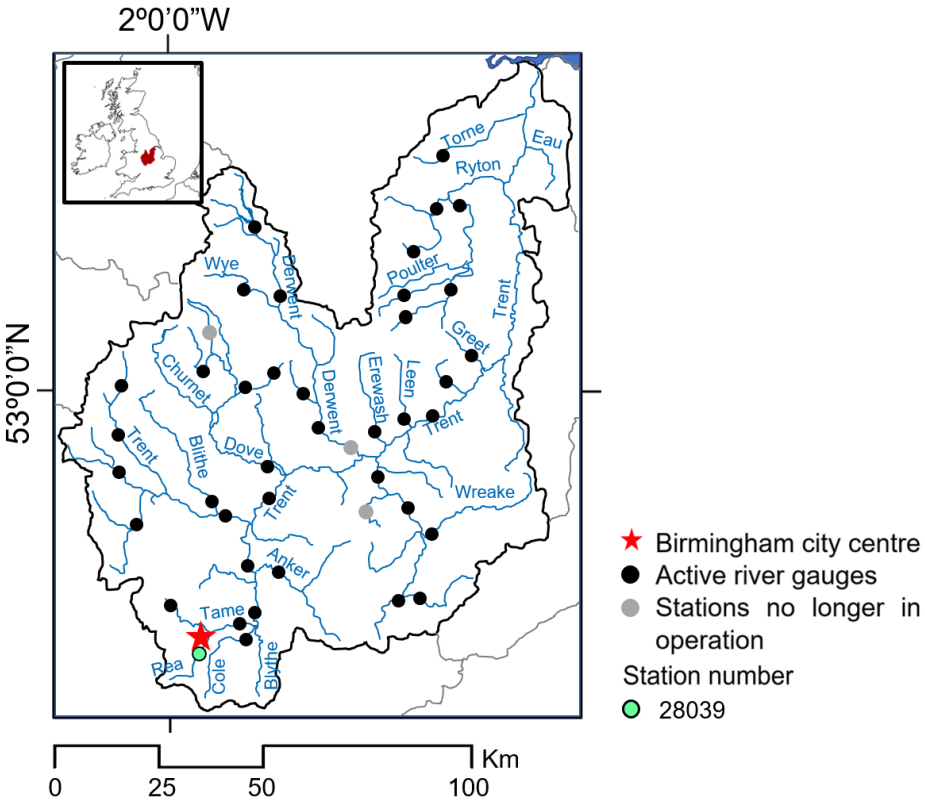

Figure 6.15. Spatial extent of the hydrometric area 28 "Trent" and river reaches within the catchment

Figure 6.16 displays some physical characteristics of the Rea catchment. The river flows from the south-west of the catchment towards the north east until it reaches the river Tame. Similar to the Ouse Burn catchment upstream of Newcastle, most of the bedrock has mixed or high permeability (68.67% is made up of concealed aquifers with limited or local potential, and 31.33% are highly productive aquifers). Nearly half of the superficial deposits are made up of clay with mixed permeability (46.76%) or with generally high permeability properties (6.29%). As mentioned before, the catchment is almost totally urbanised with 69.72% of the land cover classified as urban. The remainder is 17.95% grassland and in lesser percentages, woodland (5.96%) and arable/horticultural (3.95%). Table 6.9 contains several catchment descriptors, including the Base Flow Index derived from the 29-class Hydrology Of Soil Types map (or BFIHOST) (Boorman et al., 1995) and the catchment wetness index (or PROPortion of time soils are WET, PROPWET) (National River Flow Archive, 2015). BFIHOST expresses the relationship between soil typology and runoff response, the lower the index the lower permeability of soils. PROPWET describes the proportion of time in which soil moisture deficits are less than 6 mm, the higher the wettest catchments in the country are assigned values of 80% and over.

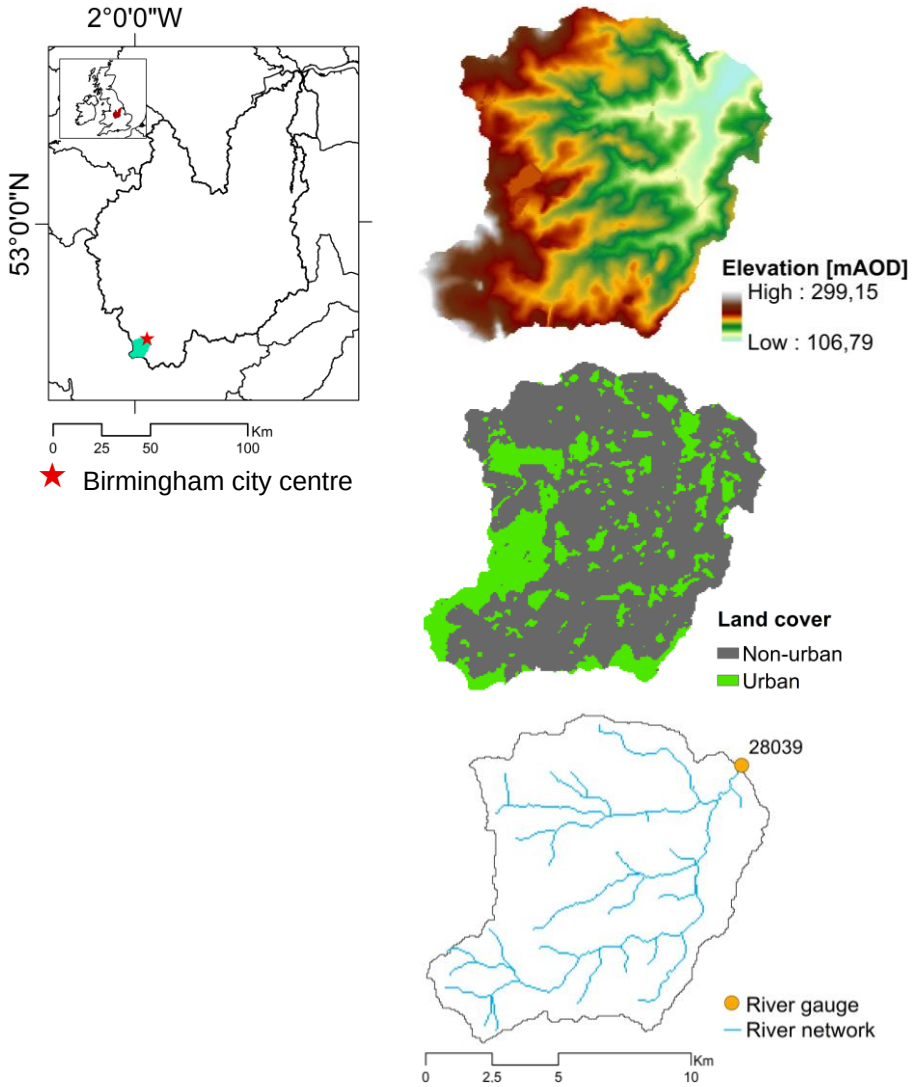

Figure 6.16. Location and physical characteristics of the Rea catchment: elevation, binary map of land cover (urban/non-urban) and river network

Table 6.9. Physical characteristics and hydrological descriptors of the Rea catchment

Catchment characteristic	Value	Units
Area	74 080 000	m^2
Mean annual rain	800	mm
Mean annual runoff	336	mm
Mean annual loss	464	mm
Descriptors		
BFIHOST	0.51	-
PROPWET	30	%
Elevation		
Station level	104	mAOD
10^{th} percentile	133	mAOD
50^{th} percentile	165	mAOD
90^{th} percentile	204	mAOD
Max level	299	mAOD
Land cover		
Woodland	5.96	%
Arable/horticultural	3.95	%
Grassland	17.95	%
Mountain/heath/bog	0.00	%
Urban	69.72	%

*mAOD = metres above ordnance datum.

6.2.2.2 River gauge

Flows in the Rea catchment are measured at the station 28039 “Rea at Calthorpe Park”, and the gauge, shown in Figure 6.17, is a “crump profile weir; 3.66m wide with flanking broad-crested weirs set in a formalised, roughly rectangular channel” (https://nrfa.ceh.ac.uk/data/station/info/28039, Accessed: 5 September 2019). Records from the gauge show a very responsive regime, with runoff increased by outflows from sewage treatment plants outside the catchment. However, no information was found on the volume or periodicity of the effluent. Runoff increase will be considered when comparing volume of observed and simulated discharge, but not the timing of the peaks.

Figure 6.17. Photographs of the station 28039 “Rea al Calthorpe Park” (Source: National River Flow Archive)

6.2.3 Digital Terrain Analysis

Three of the inputs to discretise the Rea catchment are shown in Figure 6.16, namely:

- Topography
- Land cover as landscape classifier
- Reference river network

Similar to the exercise carried out on the delineation of Hydrological Response Units (HRUs) for the Newcastle 212 case study (see Section 6.1.3), two maps of HRUs were obtained, as both observed and simulated rainfall were used as inputs for the Digital Terrain Analysis. The observed rainfall dataset is the Gridded Estimates of hourly Areal Rainfall for Great Britain (CEH-GEAR); ninety-nine cells from the 1-km input rainfall within the catchment which was discretised in 1383 HRUs. On the other hand, simulated rainfall was taken from WRF model outputs; twenty-nine cells from the 2-km WRF inputs resulted in 479 HRUs. Gridded rainfall maps and the outputs of the Digital Terrain Analysis for both datasets are shown in Figure 6.18.

Furthermore, and as specified in Section 3.3.2.2, the 2-km WRF outputs were resample using the Bilinear Interpolation technique to match the spatial resolution of the gridded observed precipitation dataset. This ensures that the number of HRUs is consistent throughout the hydrological modelling, regardless of the origin of the climatological forcing.

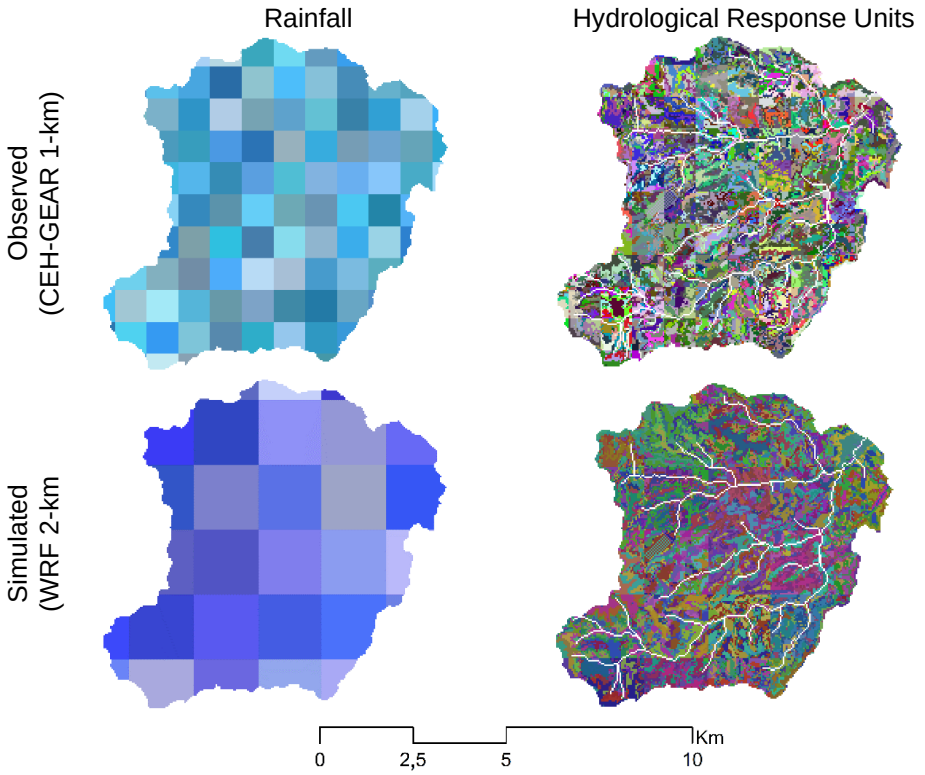

Figure 6.18. Comparison of the spatial configuration of the observed and simulated gridded rainfall inputs, and map of the Hydrological Response Units obtained for the Rea catchment

6.2.4 Model calibration

Calibration for the Birmingham 2007 event uses input data from 00:00 UTC 1 October 2003 to 00:00 UTC 1 June 2007. Following the analysis during the calibration period of the Newcastle 2012 event, evaluation of model performance was done under high and low flow conditions as well as assessment of any external influences on the measured flow (as indicated by the gauge description in Section 6.2.2.2). For details on the observed discharge refer to Section 3.3.2.1 “Databases used for rainfall-runoff modelling”.

Parameter ranges for urban and non-urban areas are displayed in Tables 6.10 and 6.11. The minimum values for the lateral saturated hydraulic transmissivity, $Ln(T0)$, and the maximum storage capacity of the root zone, SR_{max} for the urban Hydrological Response Units are lower for this case study than those implemented in the Newcastle 2012 event. Given the higher urban extent of the Rea catchment compared to the Ouse Burn (69.72% against 41.14%, respectively), the overall storage capacity of the Rea catchment is more limited as impervious surfaces are predominant. The range for the single value for the channel velocity is 800-2000 m h^{-1}, higher than that of the Newcastle 2012 event (150-700 m h^{-1}), which reflects the fact that a larger part of the river network in the Rea catchment flows through urban land cover.

Table 6.10. Hydrological model parameter ranges for the urban areas for the July 2008 case study

Parameter	Units	Lower limit	Upper limit
SZM	m	0.0015	0.01
$Ln(T_0)$	ln(m^2 ts^{-1})	-4	1
SR_{max}	m	0.005	0.15
SR_{ini}	m	0	0.015
Td	ts m^{-1}	0.1	100
S_{max}	m	0.001	0.05

Table 6.11. Hydrological model parameter ranges for the rural areas for the July 2008 case study

Parameter	Units	Lower limit	Upper limit
SZM	m	0.02	0.08
$Ln(T_0)$	ln(m^2 ts^{-1})	2	6
SR_{max}	m	0.3	0.6
SR_{ini}	m	0	0.1
Td	ts m^{-1}	0.1	100
S_{max}	m	0.3	0.8

6.2.4.1 Assessment of the simulated flow

During peaks in runoff

Four two-month plots during the calibration period are shown in Figure 6.19a-d. The episodes for analysis occur in late summer/early autumn, and one episode during winter 2006 was also selected.

The hydrological model is able to capture the observed flows when reproducing the timing and magnitude of the peaks. At this scale, there is a reasonable performance of the model when assimilating extended periods of intense rainfall to produce large runoff peaks: rise and fall of the hydrograph under wet conditions is well captured, meaning that for most of the period of significant discharge, the influence of any outflows is negligible.

The simulated runoff ensembles shown in Figures 6.19a-d follow the expected behaviour of an urban catchment (significant discharge peaks occur shortly after intense rainfall), and this is well reproduced by the model. Figure 6.19d shows a large flow peak (~12 × 10^{-1} mm) after a dry period that lasted approximately two weeks. For a heavily urbanised catchment, extended periods without rainfall should have little to no effect on soil storage conditions as the land cover is mostly impervious. The aforementioned peak is well reproduced by the model

in terms of both timing and magnitude, meaning that the parameter ranges chosen during the calibration process represent well the physical characteristics of this catchment.

There is also a good correspondence in the number of peaks in the calibration period. Subsequent peaks after an episode of high flows are also captured, meaning that the flow is correctly routed to the river in terms of time and volume; this also means that the core assumption that was implemented to define model parameters is a robust representation of the hydrological response of an urban catchment (where impervious surfaces allow for little to no infiltration).

During low runoff periods

Low runoff peaks (maximum 12×10^{-1} mm) are also found during winter in the calibration period. In these cases, the catchment received low rainfall amounts (peaks are lower than 5 mm h^{-1}). For the four two-moth plots in Figure 6.20a-d, the magnitude and number of peaks in the ensemble of simulated discharge match those of the observed runoff, meaning that the model has a good performance when reproducing rise and fall of hydrographs during dry or nearly dry conditions. It is also worth noticing that even low runoff peaks are correctly simulated: for example, the first twelve days of observed vs. simulated runoff in Figure 6.19d are characteristic of an urban catchment, having a high response rate even to the lowest rainfall rates. In this case, DECIPHeR is able to reproduce the flashy response of the catchment, maybe underestimating the recession limb of the hydrograph but still identifying the temporal and spatial location of observed flow peaks.

External influences on the river flow

A stated in Section 6.2.2., measured flows at station 28039 are subject to external inputs from wastewater treatment plants. Figure 6.21a-b illustrate a larger difference between observed and simulated runoff that that analysed previously. Both plots show that the model has a deficient performance when simulating the overall catchment response to rainfall in terms of spatial and temporal location of the runoff peaks.

The rainfall that follows the dry period from 25 January 2007 to 6 February 2007 (Figure 6.21a) produces a catchment response different to the one in the winter 2006/2007 (Figure 6.19d). In both cases, the model reproduces the flashy response of the catchment (the hydrograph follows a trend of quick rise and fall) but in the former, simulated runoff is consistently higher than the observed time series, contrary to the expected behaviour given by the description of the flows measured at the gauge (see Section 6.2.2.2). On the other hand, the magnitude of the first peak in Figure 6.20b exceeds the mean of the behavioural ensemble by more than a factor of 2 and it occurs well in advance compared to the simulated values. The second largest peak (on 28 May 2007) suggests a more sensitive response than the one produced with the

model. Despite these differences, none of these episodes compares to those considered as misinformation during the calibration period of the June 2012 event in Newcastle (see Section 6.1.4.1) so they will be kept for analysis of the July 2008 event.

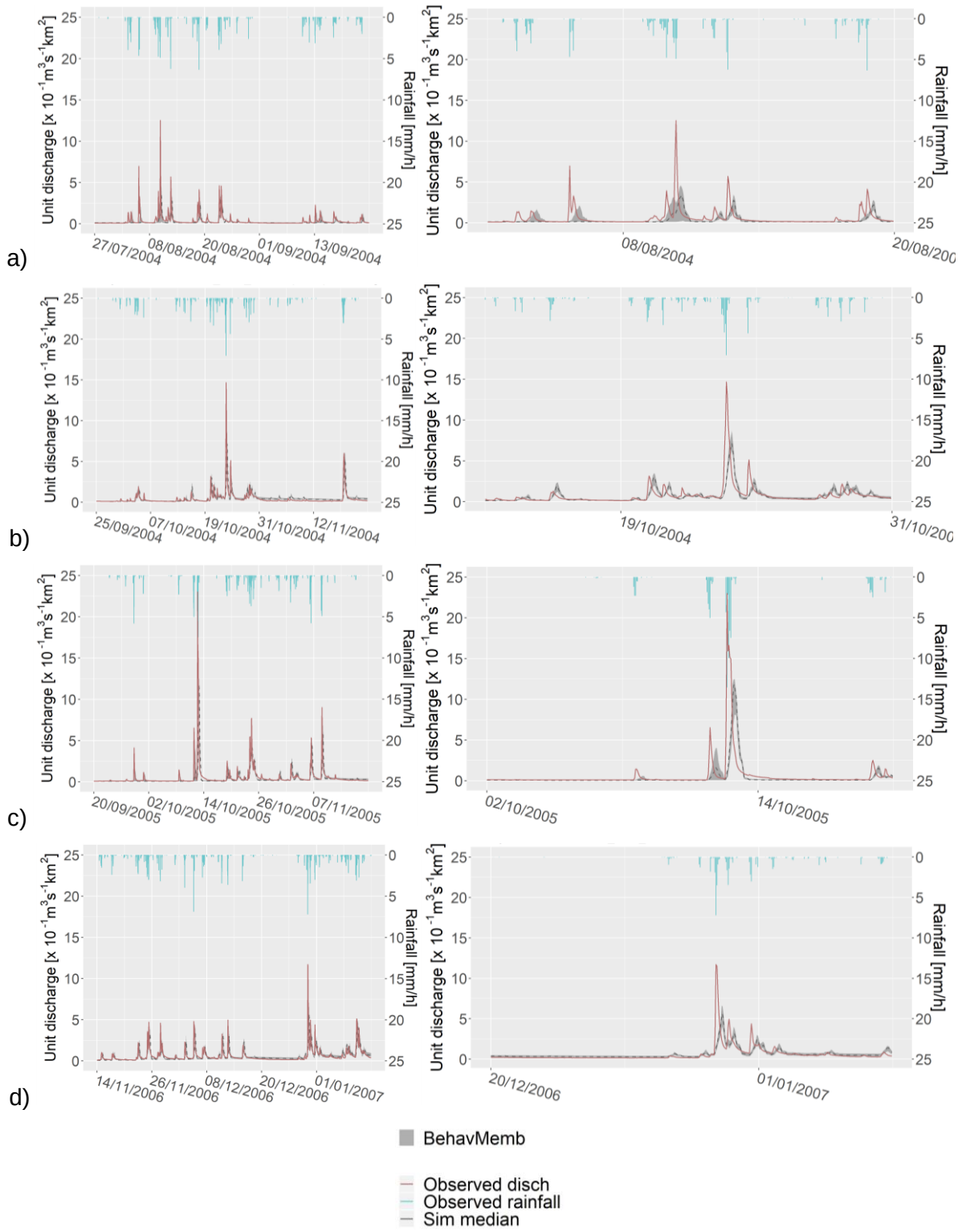

Figure 6.19. Hourly calibrated flow for the two-month period a) 27 July 2004 to 24 September 2004, b) 25 September 2004 to 23 November 2004, c) 20 September 2005 to 18 November 2005, d) 14 November 2006 to 12 January 2007. Spread of the 5th and 95th percentiles of the behavioural ensemble defined using the GLUE methodology is shown in grey, 50th percentile is shown as a dotted line, observed flow is shown as a red line. Right column= subset of left column

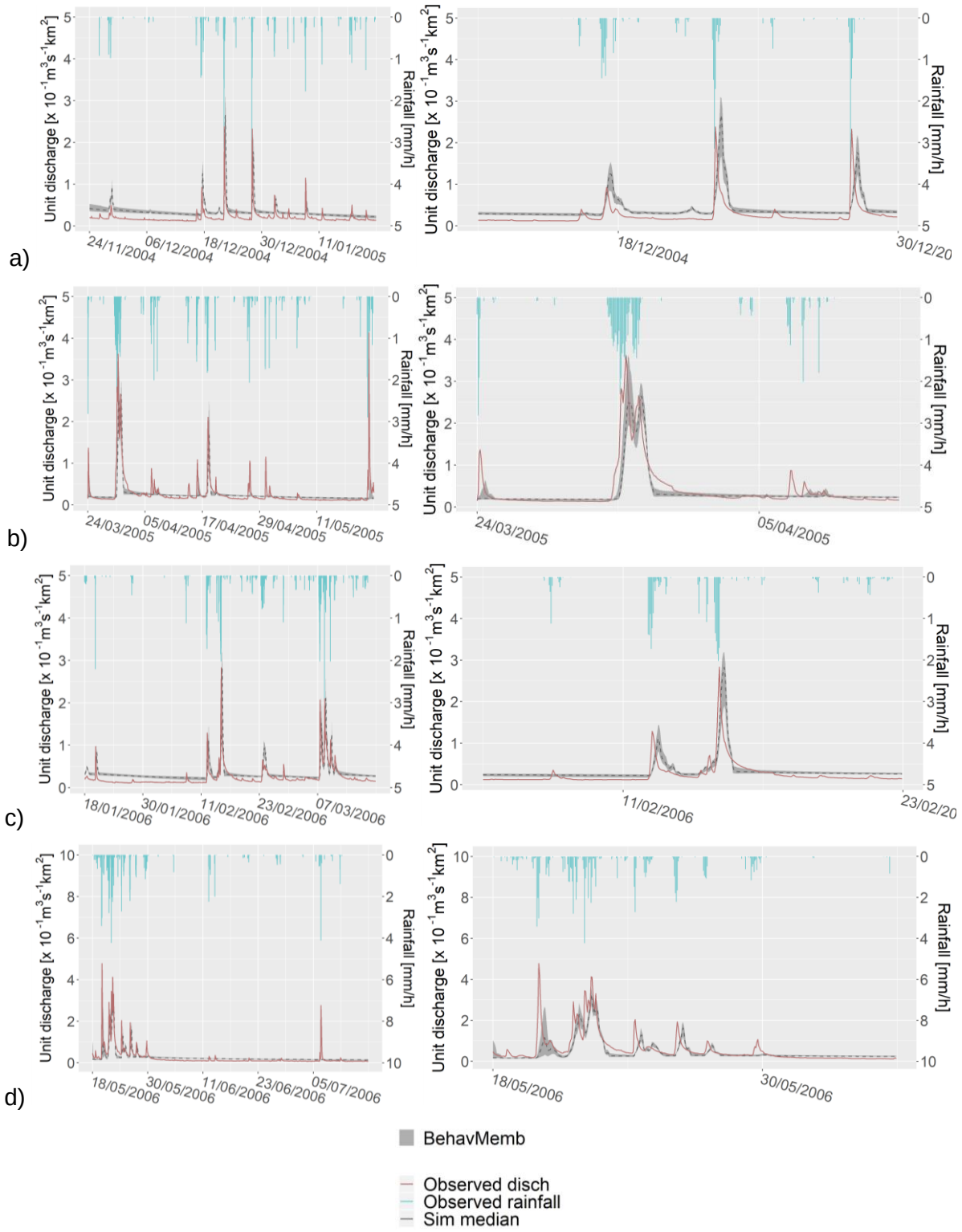

Figure 6.20. Hourly calibrated flow for the two-month period a) 24 November 2009 to 22 January 2005, b) 24 March 2005 to 22 May 2005, c) 18 January 2006 to 18 March 2006, d) 18 May 2006 to 16 July 2006. Spread of the 5th and 95th percentiles of the behavioural ensemble defined using the GLUE methodology is shown in grey, 50th percentile is shown as a dotted line, observed flow is shown as a red line. Right column= subset of left column

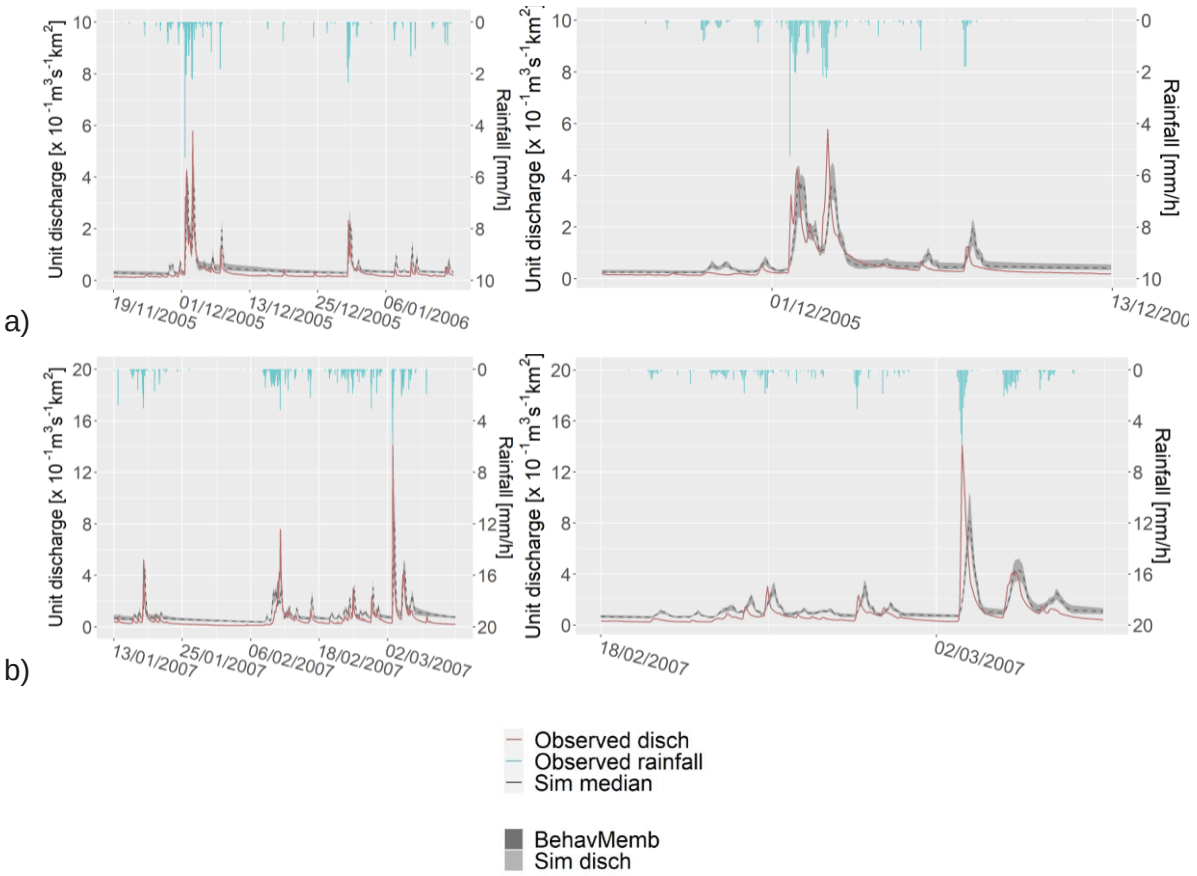

Figure 6.21. Hourly calibrated flow for the two-month period a) 19 November 2011 to 27 January 2006, b) 13 January 2007 to 13 March 2007. Right column= subset of left column

6.2.4.2 Performance statistics

Figure 6.22 contains the scatter plots for the parameters that control the storage capacities and water transfer from the Hydrological Response Units (HRUs), namely SR_{max} (maximum storage capacity of the root zone), $Ln(T0)$ (lateral saturated hydraulic transmissivity), S_{max} (maximum effective deficit of the saturated zone) and SZM (form of exponential decline in conductivity).

As stated at the beginning of the chapter, the low values assigned to these parameters for the urban HRUs describe the reduced storage capacity of the unit and its poor transmissivity properties to ensure that the compartment is always full and that all excess rainfall will be routed as overland flow, simulating the behaviour of impervious surfaces. From said Figure, it can be seen that the most relevant NSE distribution compared to parameter range is found for SR_{max} in urban areas. This means that the storage capacity of the most superficial soil layer should be extremely low to properly parameterise impervious surfaces.

On the other hand, the highest values of the Nash-Sutcliffe efficiency score for SZM in rural areas are obtained as the value of this parameter increases, reaching a plateau around SZM = 0.06 m, which means that the chosen range is enough to determine the sensitivity of this parameter and the most likely values it should have for a skillful simulation; the same occurs for $Ln(T0)$ in rural areas for values greater than 4 ln(m^2 ts^{-1}). This behaviour reflects a top limit in the transmissivity capacities to adjacent units. The rest of the parameters show a homogeneous behaviour for the selected lower and upper bounds so the parameter range is suitable for the Birmingham 2007 case study. Performance metrics are shown in Table 6.12.

Table 6.12. Performance metrics for the calibration period

Metric	Value	Units
Nash-Sutcliffe efficiency index (Q95)	0.53	-
Nash-Sutcliffe efficiency index (max)	0.65	-
Root Mean Square Error (max of 5%)	0.920	mm h^{-1}
Root Mean Square Error (min)	0.799	mm h^{-1}

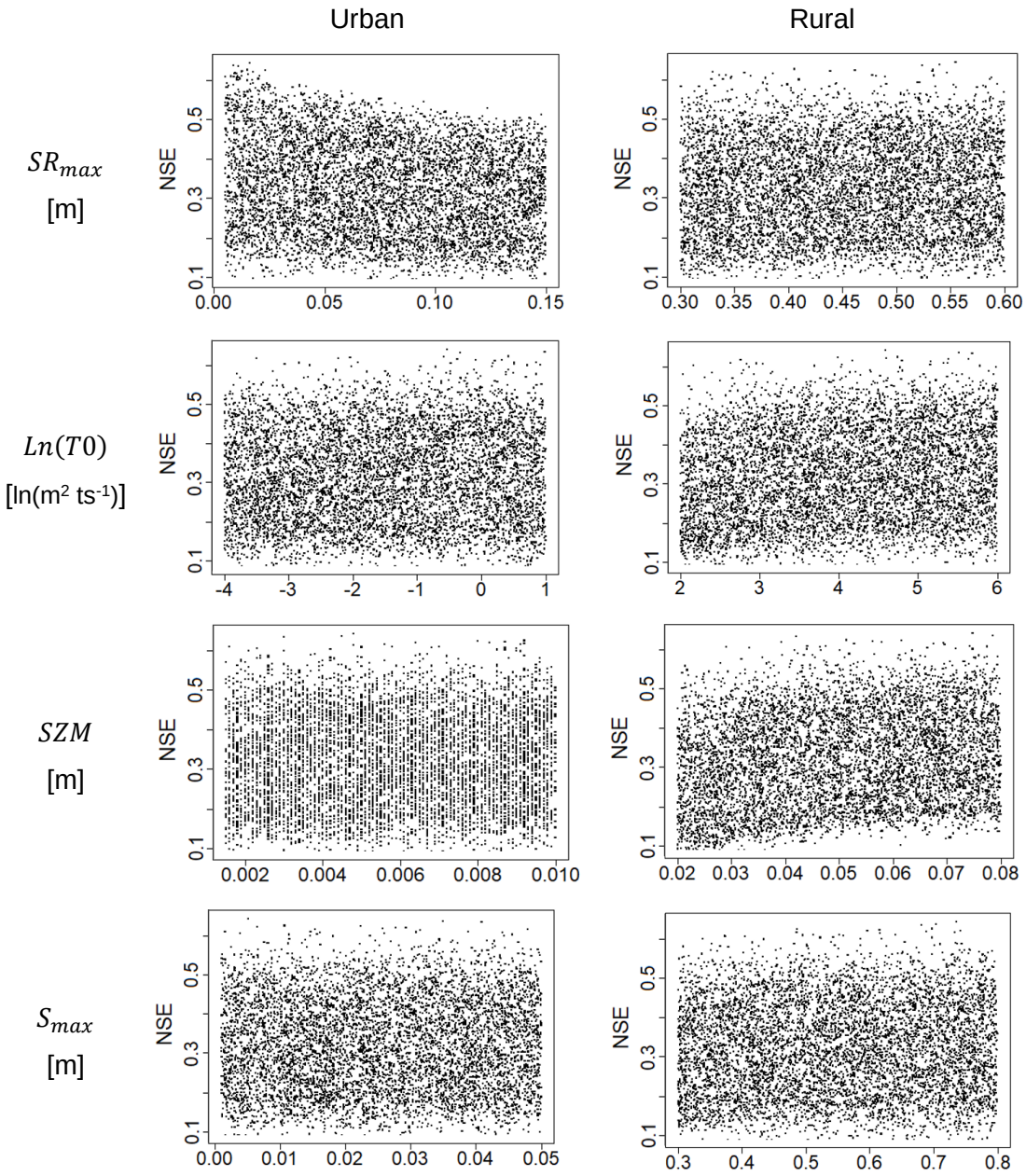

Figure 6.22. Scatter plots of the parameter space after the calibration period of the July 2008 event

6.2.5. Model validation

The 48-hour discharge period that includes the flash flood event and the falling limb of the hydrograph goes from 00:00 UTC 20 July 2007 to 00:00 UTC 22 July 2007, with one year of spin-up time. Results of the hydrological modelling using both observed and simulated rainfall from the nine WRF scenarios which combine three urban canopy models and three microphysics schemes is displayed in Figure 6.23a-b. Hourly observed discharge is plotted in red, the shaded grey area is limited by the 5th and the 95th percentile of the behavioural

members, and the 50th percentile is also included (dotted line). The performance metrics for all simulations are contained in Table 6.13.

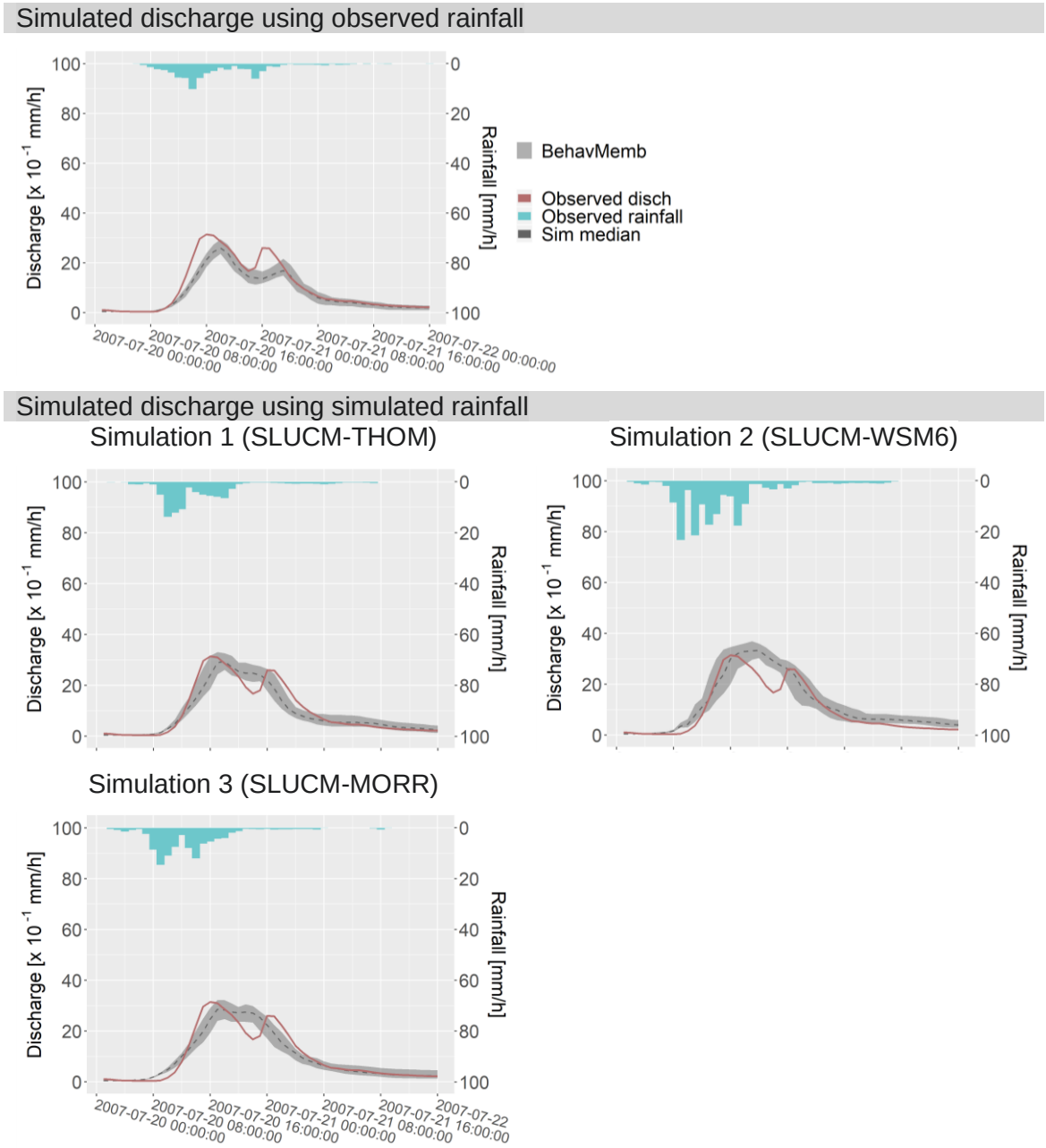

Figure 6.23a. Hourly simulated flow for the validation period of hydrological simulation of the July 2007 event using observed rainfall (top panel) and simulations 1-3 (left to right, top to bottom)

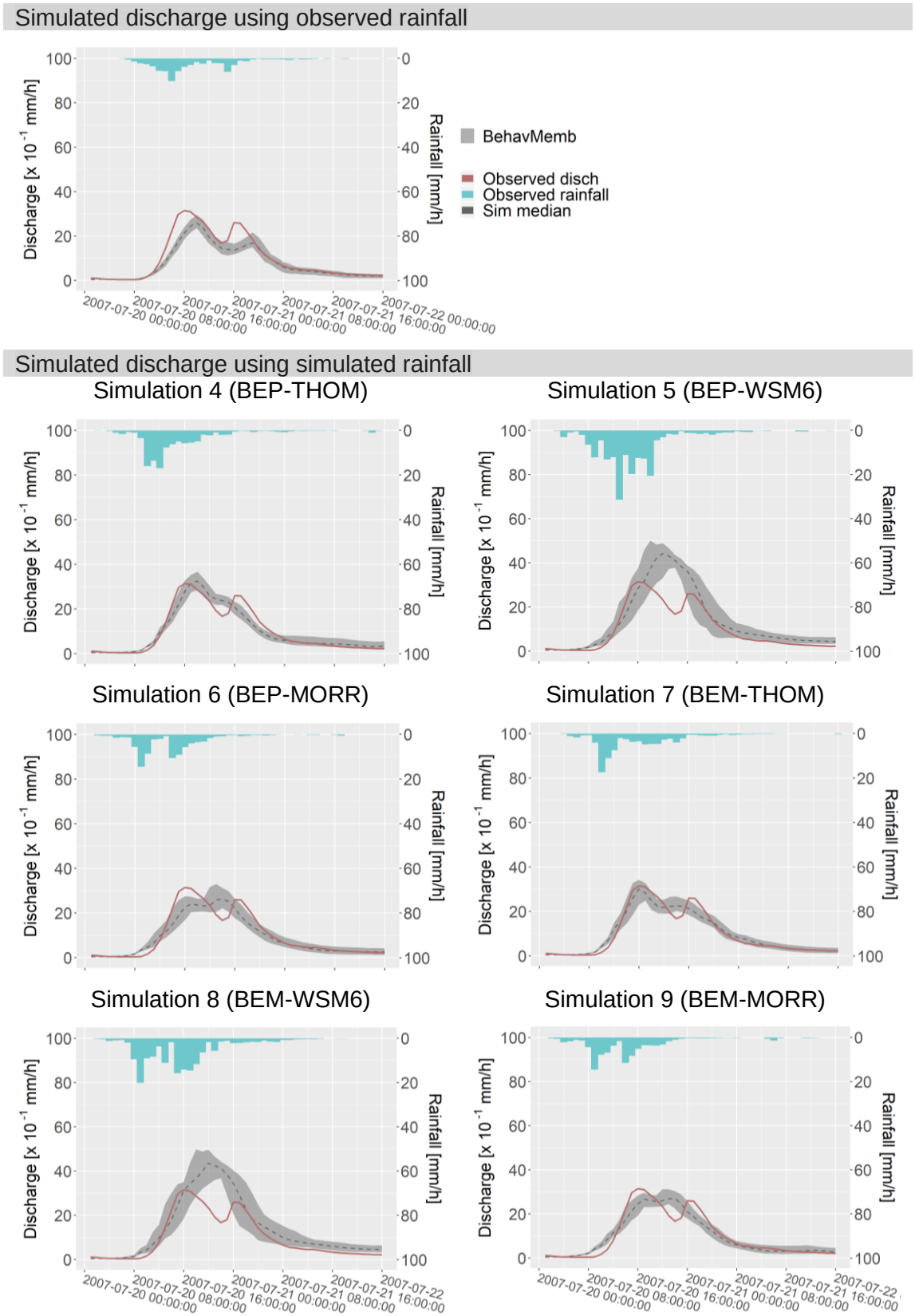

Figure 6.23b. Hourly simulated flow for the validation period of hydrological simulation of the July 2007 event using observed rainfall (top panel) and simulations 4-9 (left to right, top to bottom)

Table 6.13. Performance metrics for the calibration period of the hydrological modelling of the July 2008 event

Simulation	NSE (95^{th} percentile)	NSE (max)	RMSE [mm h^{-1}] (max of 5% of total)	RMSE [mm h^{-1}] (min)
OBS (CEH-GEAR)	0.76	0.91	9.87	6.10
1 (SLUCM-THOM)	0.83	0.88	8.37	7.22
2 (SLUCM-WSM6)	0.71	0.87	10.95	7.32
3 (SLUCM-MORR)	0.84	0.87	8.25	7.32
4 (BEP-THOM)	0.88	0.90	7.17	6.47
5 (BEP-WSM6)	0.20	0.55	18.43	13.85
6 (BEP-MORR)	0.81	0.86	8.98	7.82
7 (BEM-THOM)	0.90	0.94	6.42	5.07
8 (BEM-WSM6)	0.18	0.58	18.60	13.41
9 (BEM-MORR)	0.84	0.87	7.40	8.11

Reproducing the discharge for this event represents another type of challenge for the hydrological model: while the Newcastle case study has a particularly sudden rise in the hydrograph, flows in the Rea catchment during this event present two peaks that correspond to the two bursts of rainfall recorded. The response of the catchment, given the extent of the urban coverage, can be seen shortly after the peak rainfall.

Simulated runoff produced with the observed rainfall (top panel of Figure 6.23a) features two peaks which match the observed flows, albeit with a lag in time. This reflects the ability of the model to reproduce the high responsiveness of the catchment.

Discharge produced using outputs from the meteorological modelling shows that the model does substantially better in this case study than for the Newcastle 2012 event, with the drawback that the hydrological outputs lack the two distinct flow peaks due to the magnitude and temporal distribution of the rainfall: in all cases, precipitation is either overestimated or produced ahead of time. However, in most cases, the peak discharge values are well captured and the rising and falling limbs of the observed hydrograph have a good correspondence with the spread and median of the behavioural ensemble. The Nash-Sutcliffe efficiency score for simulations 1, 3, 4, 6, 7 and 9 suggests that simulated discharge in said scenarios is close to the observed values. Despite the lack of two distinct flow peaks, the first peak is correctly captured in simulations 1, 4 and 7, something that was not achieved using the CEH-GEAR (observed gridded) rainfall.

From the nine simulated rainfall scenarios, only simulations 1, 3, 6 and 9 produce two distinctive rainfall events, very close in time from each other, and this is reflected in the behavioural ensemble obtained for those scenarios. Since the time between rainfall peaks is short, the water is not drained from the catchment for long enough before the second rainfall peak, so discharge levels do not vary enough and the two peaks in discharge are not reproduced.

Rainfall produced in simulations 4 and 7 (Figure 6.23b) features only one significant peak. This peak is enough to produce the expected rising limb in the hydrograph regarding timing and magnitude. The second discharge peak is not reproduced by the model, but the median of the behavioural ensemble does not deviate significantly from the observed values. This is supported by the values of the Root Mean Square Error (RMSE), which has the lowest values for these two simulations.

The hydrological model outputs for the scenarios with the largest amount of rainfall for this case study (simulations 5 and 8 shown in Figure 6.23b) have the lowest performance skill of all the scenarios. This is due to the significant overestimation of rainfall over the 48-hour period. The median of the hydrological ensemble presents only one peak which occurs four hours after the first peak in the observed discharge and exceeds the magnitude of the measured flow by approximately 15 mm h^{-1}. The same response is observed for simulation 2, where rainfall is also overestimated although in smaller amounts so the single peak in the simulated ensemble is closer in magnitude to the observed flow.

Finally, as stated in section 6.2.2.2, discharge measured at station 28039 “Rea at Calthorpe Park” is affected by outflows from sewage treatment plants outside the catchment, so river discharge is augmented by external inputs. This means that the actual river discharge is lower than the values currently considered as “observed”, and that the model is in fact overestimating river flows. If timing and magnitude of external flows into the catchment were known, they could be subtracted from the current observed values and hydrological model calibration would have to be redone. A preliminary numerical approach to decrease the magnitude of the simulated flows is to lower the value of the channel velocity (CHV). Since the urban soil storages should remain saturated, the parameters that control this state (maximum storage capacity of the root zone, SR_{max}; lateral saturated hydraulic transmissivity, $Ln(T0)$; maximum effective deficit of the saturated zone, S_{max}; form of exponential decline in conductivity, SZM) should keep their low values. Instead, since all the excess rainfall is routed directly to the river channel, flow velocity within the channel would have a larger impact on the discharge.

The performance of the nine simulated discharge scenarios were ranked according to the values of the NSE score and the RMSE. The final rank is the weighted sum of the individual rank considering the NSE score or the RMSE. In other words, the simulation with the highest NSE score was given a weighted value of 9/9, the simulation with the second highest NSE score has a weighted value of 8/9, the simulation with the lowest NSE score has a weighted value of 1/9. The same procedure was applied to the RMSE values: the simulation with the lowest RMSE is given a weighted value of 9/9, the simulation with the second lowest RMSE has a weighted value of 8/9, the simulation with the highest RMSE has a weighted value of 1/9. The length of the stacked bars corresponds to said weighted values (performance metrics are given in Table 6.13. Figure 6.24 shows the nine scenarios of simulated runoff, ordered from best to worst performance.

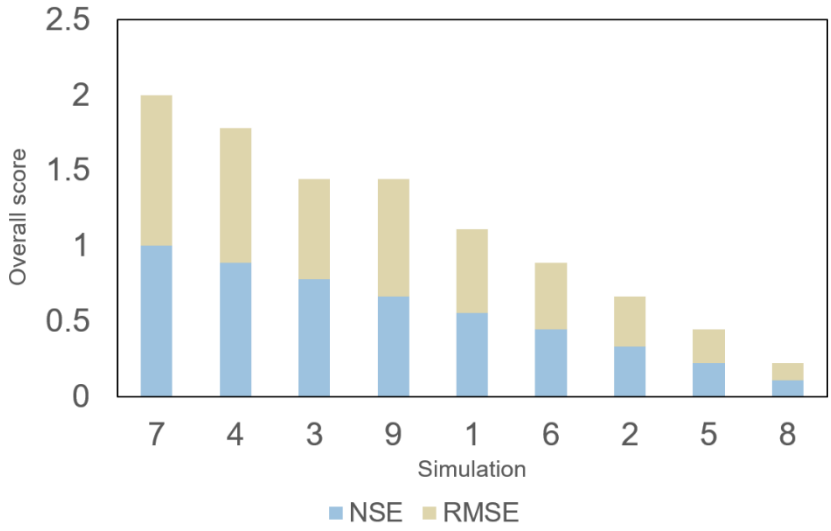

Figure 6.24. Simulated hydrological scenarios ranked by performance for the July 2007 case study, showing bar length as the contribution of each metric to the overall performance

Similar to the Newcastle case study, the simulation with the highest NSE score also has the lowest RMSE. The top two ranked simulations (4 and 7) do not have an associated rainfall with a pattern with some similarities to the observed values (see Figure 6.23b), however, the behavioural ensemble brackets the measured flow. Simulation 3 presents two significant rainfall peaks (see Figure 6.23a) although the hydrological model outputs differ more from the observations than simulations 4 and 7. On the other extreme of the performance rank are, unsurprisingly, the hydrological scenarios that resulted from the largest simulated rainfall amounts. These simulations (2, 5 and 8) have a better skill than the best performing scenario of the Newcastle case study for two reasons: the first one is that the behavioural ensemble

presents maximum two peaks instead of having high variations; the second reason is that the rising and falling limbs of the simulated ensemble match much better (in terms of timing and magnitude) the observations than the ensembles produced for the Newcastle case study.

In this case study, there is a better correspondence between the best ranked meteorological model outputs and the results from the hydrological modelling. Using the most complex urban canopy model (BEP) is likely to deliver better results at the meteorological and hydrological stages of the modelling framework: the WRF model and the DECIPHeR model parameters of simulations 7 and 9 feature among the top 4 best performing scenarios. Similarly, simulation 4 also gives remarkable results in the meteorological and hydrological modelling (second best in both). However, this must be taken with caution as the rainfall patterns are not well reproduced (although the accumulated rainfall over the 48-hour validation period is) but the hydrological model does a good job when routing flows to the river channel. This means that in a heavily urbanised catchment, reproducing intense, short-lived precipitation with errors in pattern and magnitude can still lead to a good agreement between observed and simulated discharge as long as accumulated observed and simulated rainfall values match before there is a significant increase in river discharge. See, for example, simulation 9 in Figure 6.23b, where the two simulated rainfall peaks occur hours before the observed precipitation, but the accumulated values are similar, so the behavioural ensemble has a good correspondence with the observed discharge.

6.2.5.1 Impact of the urban canopy layer parameterisations in runoff simulations.

When implementing the simplest urban canopy representation (Single Layer Urban Canopy Model) with the simplest microphysics scheme (WRF Single-Moment 6-class, WSM6), is one of the scenarios with the worst performance (simulation 2, Figure 6.23a). In fact, regardless of the urban canopy model, this WSM6 scheme delivers a much larger amount of rainfall and therefore, discharge ensembles that significantly overestimate the observed flow. This means that for a heavily urbanised catchment, a simple parameterisation of cloud processes is inadequate to represent the formation of hydrometeors. In turn, the SLUCM model works well with the other two microphysics (Thompson, THOM and Morrison, MORR), which translates to the need of a detailed solution of cloud processes when using an urban canopy model than simplifies the vertical fluxes of heat, moisture and momentum in a city.

Using rainfall produced when implementing the Building Effect Parameterisation (BEP, the midpoint between a simple and a complex representation of the urban processes) produces better results when paired with THOM and MORR (simulations 4 and 6, respectively, Figure 6.23b) although ensemble spread is larger for simulation 6 and the largest peak is actually the second. On the other hand, simulation 4 produces an ensemble that adheres more to the

observations and this is reflected in the performance metrics. However, it is worth noticing that the simulated rainfall pattern is this case differs from the observed precipitation.

The most complex urban canopy scheme (Building Energy Model, BEM) also works really when paired with the THOM parameterisation (simulation 7, Figure 6.23b). In fact, this is the best performing simulation. Two peaks in the simulated discharge can be appreciated (although not as clearly as in the observed hydrograph). Even when using MORR, the behavioural ensemble has a good correspondence with the measured flows. This confirms the need for microphysics and urban canopy models that do not simplify the parameterisation of the physical processes that they should describe (i.e., the Single Layer Urban Canopy Model and the WRF Single-Moment 6-class are not suitable to produce intense rainfall that leads to a rapid increase in river discharge).

The urban canopy model is highly sensitive to the choice of microphysics scheme. BEP and BEM seem to work better with THOM, which means that urban atmospheric processes must be described with multi-layer parameterisations (instead of the Single Layer Urban Canopy Model). Using the most complex microphysics scheme (MORR) with any of the aforementioned urban canopy schemes (simulations 6 and 9, Figure 6.23b) delivers rainfall with a similar pattern than the observed precipitation, and the hydrological model performance is among the upper half.

6.3 Final remarks

This Chapter presented the results of the hydrological modelling for the June 2012 and the July 2007 severe hydrometeorological events in Newcastle and Birmingham, respectively. Model performance varied significantly. In the Newcastle case study, the behavioural ensemble features a high variability, and, in all cases, discharge is significantly underestimated. Performance metrics for the June 2012 event reflect the difficulty in reproducing the observed discharge. In the Birmingham case study, results are much reassuring regarding the hydrological model capabilities to predict the measured flows. The assumptions described at the beginning of this Chapter regarding the representation of the urban land cover are successfully implemented as defined by the performance metrics.

An explanation to this difference in model performance is given by the extent of the catchments (Pappenberger et al., 2008) and the degree of urbanisation in each one. In smaller catchments such as the Ouse Burn, the resolution of the input data is relevant when defining the sensitivity of model parameters. In larger catchments, the dominant factor in model performance becomes clearer during the calibration process. In the case of the Rea catchment, results show that the most sensitive parameter is the channel routing, which highlights the need to develop a more refined formulation for this parameter.

In the Newcastle event, there is a single rainfall peak in a 48-hour period that the meteorological model reproduces with errors in timing. This is reflected in the simulated runoff, where discharge hardly matches the observations in terms of timing and magnitude. However, since this is the case also when using observed rainfall, it could mean that the model has a numerical limitation when routing flows through and out of the hydrological response units, namely the way the channel velocity is implemented (a single value over the entire domain, despite the discretisation of the catchment into urban and non-urban areas). In the Birmingham case study, the hydrological model reproduces accurately the observed flows. Given that the catchment is almost entirely urban, the need for two values of the channel velocity is much less significant that for the Ouse Burn catchment.

Model performance can be further improved when considering the effluents and inflows from external sources that could have a significant impact in the observed hydrograph. Given the lack of information of operation policies and magnitude of these flows for both the Ouse Burn and the Rea catchments, the current observed discharge is considered as the best estimate of the actual river flow. The influence of external factors can have a larger influence in small catchments such as the Ouse Burn, and in larger areas such as the Rea catchment the impact of urban infrastructure in model skill might be less significant.

Finally, the error propagation from the meteorological model to the hydrological model was also discussed considering the ranking of model performance at both stages. A more comprehensive discussion on the overall best hydrometeorological configuration is given in the next and final chapter on conclusion and main outcomes of the present research.

Chapter 7

Conclusions

7.1 Summary

The economical and societal cost of floods place them amongst the most dangerous natural hazards. From these events, flash floods are associated with a greater severity given the short response time of the catchment and, in the case of urban flash floods, an inefficient response of the population to organise their defences in addition to damage to transport network and services, spreading the impact of the event beyond the actual extent of the flood (Coles et al., 2017). This demonstrates the need for methods that recognise the combined effects of physical processes at different scales and settings, i.e. numerical modelling of meteorological and hydrological circumstances.

Chapter 3 “Hydrometeorological modelling framework” documents the proposed methodology to simulate flash flood-associated rainfall and flows in cities. It comprises a Numerical Weather Prediction model to produce dynamically downscaled rainfall fields that serve as the main forcing for a hydrological tool.

The hydrometeorological cascade is the framework of choice in projects at national, continental and global level that aim to simulate the intense, localised rainfall and the consequent flows as a result of the high responsiveness of an urban catchment. The successful application supports the choice of methods to address the characterisation of the most dangerous non-geophysical, climate-related hydrometeorological hazard.

Among the different methods to obtain rainfall fields (see section 2.2 for a review on this techniques) , rainfall products were produced via dynamical downscaling using a Numerical Weather Prediction Tool. This procedure was chosen due to a) the widely documented performance and applicability of the numerical tool to case studies that share similarities with the events studies in this study, b) the availability of the numerical tool, which has no requirements to be downloaded from a publicly available repository, c) the availability and documented extensive testing of the products of a Global Circulation System that serve as boundary conditions for the downscaling which have minimum requirements for access (online registration as new user) and d) the identified opportunity areas regarding the implementation of the tool in urban areas to reproduce the rainfall that drives a flash flood (see section 7.2, which elaborates on the novelty of the modelling at the meteorological stage).

Outputs from the meteorological modelling were evaluated via qualitative comparison of rainfall fields at synoptic and meso-scale, and the products of the finest domain (over the area of interest) were evaluated using performance skill scores and statistical indexes. These metrics allow an appropriate evaluation of the model outputs and the identification of the model parameterisations that produce the most accurate representation of the spatial and temporal evolution of the rain, while identifying possible sources of error.

The hydrological modelling framework implemented in the present research was chosen due to a) the advantages that semi-distributed hydrological models offer over lumped and fully distributed tools, b) the availability of the datasets to be used in the modelling, c) the possibility to explore disaggregation techniques to derive hourly products from datasets of climatological variables at daily scale, d) the potential to collaborate closely with the model developers to test the numerical tool and e) the identified opportunity areas regarding the implementation of a recently released numerical tool in urban environments (see section 7.2, which gives further details on the novelty of the modelling at hydrological stage).

Outputs from the hydrological stage were assessed by determining the behavioural members and uncertainty bounds of the ensemble using an estimation framework based on a likelihood function combined with a statistical metric that assigns a high weight to large errors. Using these parameters to evaluate model outputs gave useful information on the influence of the model structure in the final outputs, assuming that the spread of the ensemble directly reflects the deficiencies in a newly developed numerical tool when implemented at high temporal resolution.

The final outputs of the hydrometeorological cascade were evaluated considering model performance metrics at meteorological and hydrological stages so the optimal scenarios were those that share high performance metric values at both stages. This provided useful insight into the propagation of the uncertainty and how this was bounded at each stage (similar to the procedure shown in Figure 1.1). The choice of best model set-up and best parameterisation is discussed in detail in section 6.1.5 and 6.2.5 for both case studies of the present research.

Both case studies delivered different results in terms of the best meteorological model set-up to reproduce intense, localised rainfall over an urban area. A complete analysis on the rationale behind this behaviour is presented in section 7.3.

7.2 Novelty of the research

The Weather Research and Forecasting (WRF) model, the Numerical Weather Prediction (NWP) tool of choice was applied, for the first time, to simulate intense rainfall at fine scales (2 km) over a domain that contains an urban area, considering the capabilities of the tool in representing the physical processes of urban meteorology (described in section 2.1.1.1). Previous studies have successfully applied this tool to reproduce the rainfall over urban areas but without using the three urban canopy models included in the NWP tool (Barlage et al., 2016; Haberlie et al., 2015; Niyogi et al., 2017; Sarmiento et al., 2017). Studies that have implemented the full capabilities of the model to represent urban meteorological processes have done so focussing on other environmental problems derived from the city-atmosphere interaction, such as urban heat islands in cities in America, Europe and Asia (Bhati et al., 2018; Fallmann et al., 2013; Li et al., 2013; Salamanca et al., 2011) as well as over one of the cities included in the present research (Heaviside et al., 2015). The use of the three urban canopy model in the Numerical Weather Prediction tool of choice to represent intense rainfall over urban environments also reflects the originality of the research.

The second novelty in the research is the implementation of three microphysics schemes that vary in the degree of complexity to represent the particle size distribution and type of hydrometeors. Although these schemes have also been used to reproduce intense rainfall (Hong et al., 2010; Morrison et al., 2009; Pieri et al., 2015; Rajeevan et al., 2010), the combination of the microphysics schemes with the urban canopy layer parameterisations has never been implemented before in studies that explore the potential of the numerical tool for urban flash flood applications. The nine resulting rainfall fields therefore facilitate the analysis of the uncertainty in model parameterisations. Given that the schemes have low, medium and high complexity, one of the research questions answered was: how much complexity is needed to simulate intense, localised rainfall over urban areas when considering the dominant processes to be the cloud microphysics and the urban meteorological processes? The results gave information on the optimal model set-up regarding physics parameterisations, model set-up, lateral boundary conditions and spin-up time (see Appendix A on the modelling work undertaken to support the choice of optimal model configuration).

The second stage of the cascade framework was done using the Dynamic fluxEs and ConnectIvity for Predictions of HydRology (DECIPHeR) model. This numerical tool is built based on the core equations and assumptions of a pre-existing hydrological model that has been applied to a wide range of scenarios including small catchments (Metcalfe et al., 2015), catchments with significant seasonal variations in the response to rainfall (Beven et al., 2001a), forested catchments (Peters et al., 2003), and catchments with poor drainage properties

(Rathjens et al., 2016). This shows the remarkable flexibility as well as the documented satisfactory performance of the hydrological model of choice.

Given the recent development of DECIPHeR, its implementation in urban environments to reproduce short-lived events that require high spatial resolution is explored for the first time. The present research takes advantage of the flexibility of the model to discretise the catchment in urban and non-urban areas with clearly differentiated soil properties that effectively emulate the behaviour of impervious surfaces during an intense rainfall event. Using said binary map of land cover as a landscape classifier for catchment discretisation is a computationally inexpensive procedure given the extent of the catchments of study. This model set-up gave useful information on the uncertainty in model structure when simulating the urban riverine response during a flash flood. Here, the research questions answered refer to the built-in capabilities of the numerical tool. For example, given that at the moment of writing, the model performance has only been tested at daily scale (Coxon et al., 2019), is the current model structure (catchment discretisation technique and channel routing methods) appropriate also for urban catchments that involve the simulation of flows at hourly scale? Results regarding the first case study suggest that the routing process seems to play a major role in the accuracy of the results (see hydrographs from section 6.1.5 and section 7.4 3 for further discussion). Results regarding the second case study suggest that the size of the catchment is also an important driver to produce more accurate flow estimations due to its larger extent compared to the catchment of the first case study.

Finally, the implementation of the chosen numerical tools for the hydrometeorological cascade constitutes a major novelty in the research given the specific combination WRF-DECIPheR is tested for the first time. Using dynamically downscaled rainfall to drive the hydrological model allows evaluating how the uncertainty (from meteorological model parameterisation) propagates through the cascade. A method for the reduction of uncertainty is not applied (there is no selection of best models at meteorological stage to drive the hydrological modelling), instead, all scenarios are evaluated to assess the correspondence between best performing rainfall scenarios against best performing hydrological simulations. The research questions answered at the end of the cascade refer to the level of detail that is needed at atmospheric stage to deliver accurate flow simulations, and the impact of rainfall behaviour on rainfall runoff modelling, namely, what is more important: that the hourly simulated rainfall matches the observations timestep by timestep, or is the similarity in the accumulated rainfall values (simulated vs observed) more important? Answers to this question are discussed in section (6.1.5 and 6.2.5).

7.3 On the error propagation through the hydrometeorological modelling framework

7.3.1 Considering the Newcastle 2012 flash flood event

The simulation of the rainfall of the Newcastle 2012 event shows a disparity in the skill of top ranked meteorological outputs and the performance of the simulated flows. The best performing rainfall scenarios produce discharge with the lowest efficiency score and vice versa. This is explained in Section 6.1.5 “[Hydrological] Model validation”, which states that the temporal variability of simulated discharge is directly associated with the rates of rainfall. Therefore, simulated rainfall must be either a) exceptionally high to produce enough high and low simulated values that match the accumulated observed discharge, or b) significantly low to produce more stable runoff simulations despite the underestimation of observed discharge. Because of this, the two worst performing rainfall scenarios are associated to two of the best performing hydrological simulations, namely simulation 5 (that uses the Building Effect Parameterisation and the WRF Single-Moment 6-class scheme) and simulation 8 (that uses the Building Energy Model and the WRF Single-Moment 6-class scheme). This shows that, for this case study, the choice of a meteorological configuration for hydrological applications depends on how the hydrological model computes the flows, not on the accuracy of the simulated rainfall fields.

The computation time of the meteorological modelling is also considered to rank the cascade outputs by performance (simulation time of the hydrological modelling varied less than half an hour among scenarios, which represents 0.5% of the total simulation time). Simulations 1, 2 and 3 use the Single Layer Urban Canopy Model, the simplest urban physics scheme, which could explain the highest computational efficiency (see Table 4.5 for the duration of the meteorological modelling). This finding sets the precedent for further meteorological model runs with a similar domain configuration (see Table 4.3 and Figure 4.5) and physics parameterisations (see Table 3.3) given the computational resources used (see Appendix A.3). However, had the computational power not been considered for the ranking, the top four performing simulations (1, 3, 6 and 9) would have remained the same and the WRF Single-Moment 6-class would still be classed as the least recommended, albeit its simplicity.

For the Newcastle 2012 event, the final outcomes of the cascade are more easily grouped by microphysics scheme that by urban canopy model. This means that the cascade is more sensitive to the scheme that represents the formation of hydrometeors than to the effects of urban microclimate, which can be explained by looking at the extent of the urban and built-up land for innermost domain of the meteorological model (shown in Figure 4.10) which is clearly

not predominant, albeit accounting for more than 40% of the of the land cover the Ouse Burn catchment.

The modelling framework produced one outcome whose efficiency and accuracy are consistent throughout the cascade: simulation 6 (that uses the Building Effect Parameterisation and the Morrison microphysics scheme). This finding could be transferred to case studies with similar precedent meteorological conditions (intense rainfall associated to two fronts merging). Given that the largest sources of error come from the hydrological model structure, it is difficult to select another scenario whose skill is placed among the top four in both stages of the cascade. In other words, the optimal meteorological model configuration is the one that sits in the mid-point between simplicity and complexity regarding urban canopy models but that solves the microphysics of the cloud with enough detail. River flows obtained in this scenario are among the four hydrological simulations with the highest skill metrics.

7.3.2 Considering the Birmingham 2007 flash flood event

Analysis of the meteorological model outputs of the Birmingham 2007 case study show that the WRF tool is also more sensitive to the choice of microphysics than to the urban canopy model scheme used, similar to the outcomes of the meteorological modelling of the Newcastle 2012.

Addressing the microphysics scheme used, 3 out of the 4 top performing simulations use the Thompson microphysics parameterisation (simulations 1, 4 and 7; see Table 3.3 for more details on the physics schemes used), an efficient five-hydrometeor scheme that provides mass-size relationship based on look-up tables instead of using a numerical solution. This confirms that the optimal microphysics scheme lies in the mid-point between simplicity (Single Layer Urban Canopy Model) and complexity (Morrison microphysics scheme), a conclusion that was also drawn from the Newcastle case study.

Regarding the urban canopy model, model results place the most complex scheme, the Building Energy Model (which considers vertical distribution of sinks, sources and indoor-outdoor exchange of heat as a result of building height, material and occupants), as a consistent option to obtain reliable hydrological simulation. As stated before, this case study allowed a more evident the relationship between the meteorological model outputs with the highest skill and the best performing simulated flow.

Another finding that agrees with the findings from the Newcastle 2012 case study was the role of the computational efficiency of the meteorological modelling to define the best model configuration. The innermost domain for this case covers the Trent catchment (192 × 162 km^2, see Section 5.3.1 “Domains and boundary conditions”), a larger area than the Tyne catchment

(96 × 108 km^2, see Section 4.3.1 “Domains and boundary conditions”). However, this does not affect the final ranking: simulations 1, 4, 7 and 9 would still outperform the rest. This shows that if the computational power available had been larger than the one currently implemented (as stated in Appendix A.3), the size of the modelling domain does not affect the choice of best performing scenarios.

For the Birmingham 2007 case study, there is more consistency between meteorological model outputs with the highest skill and the top performing simulated flow scenarios. In this case, rainfall is overestimated by the Numerical Weather Prediction tool, as shown in the comparison of the simulated fields with the observed data (see Section 5.4.2 “[Meteorological] Mesoscale analysis”).

Interesting results were found for this case study regarding the hydrological simulation. Gridded rainfall produces discharge underestimate the observed values, and six out of the nine simulated rainfall scenarios overestimate the observed rainfall fields, so they give a better estimate of the observed discharge. The three WRF model outputs that do not follow this trend (simulations 2, 5 and 8) use the simplest microphysics scheme (WRF Single-Layer 6-class). Another feature to notice is that although the two peaks in the discharge are not clearly reproduced when using WRF model outputs, the metrics still support the conclusion that the simulated rainfall has an overall better performance over the observed data. This stems from the fact that, in the 48-hour period, simulated discharge using rainfall produced with the WRF model is, on average, closer to the observed discharge, and although all behavioural ensembles produced with WRF rainfall overestimate the discharge, timing and magnitude of the peaks is well captured.

Analysis of the final outputs of the cascade show that from the three rainfall scenarios produced using the Building Energy Model, two of them rank among the top four best performing simulations at both stages (simulations 7 and 9). Similar results were obtained using the Thompson microphysics scheme, where two of the three rainfall scenarios that used this parameterisation are among the four simulations with the highest skill considering the final outputs of the cascade (simulations 4 and 7). This means that for catchments with larger and scattered urban coverage (see Figure 5.12), it is crucial to explicitly consider the presence of cities in the atmospheric processes in a comprehensive way (done by the Building Energy Model) and that the microphysics of the cloud do not necessarily have to be solved by the most complex equations or considering the largest amount of hydrometeors as long as the mass-size distribution is defined (as solved by the Thompson microphysics). Therefore, the scenarios that consistently outperformed the rest are simulations 4, 7 and 9. More details on the physics schemes used in the meteorological modelling are stated in Table 3.3.

7.3.3 Final remarks

There is no agreement in which specific WRF scenario gives the best results at the end of the modelling framework: rainfall and runoff of the Newcastle 2012 case study are best represented with simulation 6, whereas rainfall and flows during the Birmingham 2007 case study are best simulated in scenarios 4, 7 and 9 (see Table 3.3 for more details on the physics schemes used). Although one of the nine meteorological scenarios was expected to give consistent good results at hydrological level, the outcomes of the modelling have pinpointed the physics schemes that should be explored to reproduce flash flood associated rainfall and the consequent river flows. The four rainfall scenarios involve the use of the Building Effect Parameterisation, the Building Energy Model, the Thompson scheme and the Morrison scheme. This reflects the need to parameterise an urban area with its building height distribution to accurately reproduce the rainfall that preceded a flash flood event. Furthermore, hydrological modelling showed that the approach used to emulate the flashy response of an urban catchment proved to be useful to reproduce the observed flows during the flood event, which effectively answers the research questions with some caveats, as stated in the following sections.

7.4 Critique of the modelling framework

7.4.1 On the choice of microphysics schemes

The motivation behind the choice of the physics schemes used for the meteorological modelling are outlined in Section 3.3.1.2 “Model parameterisations”. However, the present research could be expanded by implementing a different set-up (Liu et al., 2012) to compensate the underestimation of the rainfall produced by the merging of two frontal systems (during the Newcastle 2012 event) and the overestimation of rainfall as a result of the weather systems developed due to the unusual position of the jet stream further south during summer (during the Birmingham 2007 event).

The largest differences between observed and simulated precipitation occurred at the stations on the highest elevations in the catchment (which are also the ones with more natural land cover), which opens the door for further testing on the microphysics parameterisations of the WRF model. This scheme cascades the physical processes into the surface layer parameterisation, which contains the urban canopy layer. Section 7.5 outlines the possible microphysics schemes that could be used in further testing

7.4.2 On the calibration and validation of the hydrological model

7.4.2.1 Use of rainfall datasets with different spatial resolution

The resolution of the meteorological model is constrained by the efficiency of the computational tools available to perform the simulations. Tests on model cell size configuration were carried out following the guidelines in section 3.1.2, and results indicate that doubling the cell size would result in simulation times four times greater than the current set-up (see section A.3 for more details). Despite the fact that forecasting capabilities are not in the scope of the present research (thus the modelling time is not an issue in the design of the cascade), one of the strengths of the proposed framework is its applicability to other case studies, where minimising computational time without compromising the accuracy of the results is crucial. However, given the available computational power the innermost domain of the meteorological modelling was set to 2 km, a configuration that largely outperformed a resolution of 1 km in terms of simulation time (see Appendix A.3 for details on the processors used and the tests carried out to draw this conclusion). This mismatch in spatial resolution of the observed and the simulated rainfall was afterwards overcome by a resampling procedure, which had a good match regarding areal averaged precipitation (see section 6.1.3 for more details on the resampling procedure).

7.4.2.2 Split time for calibration and validation

The length of record used for calibration in watershed-scale studies usually ranges from one to four years (Douglas-Mankin et al., 2010). This length of time tends to be shorter to initialise model variables that solve groundwater processes, and longer when the study addresses microscale processes such as nutrient circulation (Daggupati et al., 2015). Ideally, a model should be able to reproduce the hydrological variability so that the model can reproduce, for example, high flows, low flows, and seasonal changes in soil water content. The chosen calibration period depends on the purpose of the modelling (i.e. which of the previous physical processes are going to be considered) and the response time of the system (the documented sensitivity of the study area to climatological forcing). If the modelling exercise focuses on extremes, as in the present study, then the calibration period should capture other extreme events. For this purpose, the rainfall-runoff plots with observed daily data for each hydrological year for the outlet gauges of each catchment contained in the United Kingdom National River Flow Archive repository were revised. Some considerations were made when choosing the calibration period for both case studies: 1) that the length of the record should span approximately four years, 2) that the record would contain rainfall of similar magnitude to that observed during the flash flood event, 3) that the records of rainfall, discharge and potential

evapotranspiration would have no gaps in the record greater than two weeks, 4) that the period of record would be close to, but not overlap with, the occurrence of the event. The closeness of the calibration period ensures that the dominant processes that lead to intense rainfall in the validation are also considered during the calibration. Additionally, the closeness of the calibration period to the event of study follows the current extensive literature on the intensification of climatological extremes, so the potential evapotranspiration rates (one of the inputs for the hydrological modelling) and the magnitude of the rainfall rates included in the calibration period would be as similar as possible to the conditions that lead to the event.

Two major drawbacks are identified with this rationale: the first one is that the chosen calibration period does not ensure that there will be a discharge of magnitude close to that of the event, so a similar rainfall-runoff response may not be observed for the calibration process. The second is that the impact of the hydrological model complexity (hence its capacity to reproduce the event of study) was not considered in determining the length of the calibration period. This is due to the recent development of the model structure, thus testing has barely commenced. The length of the calibration period is therefore based on recommendations from the literature.

The period chosen for the calibration process of the hydrological modelling for both case studies contains either no blanks in the records, or missing values that span over no longer of two weeks, a threshold that was assigned empirically. In order to fulfil this constraint, the calibration period of the Birmingham 2007 case study was reduced from four years (June 2003 – June 2007) to three years and 9 months (October 2003 – June 2007).”. However, despite having a shorter calibration period than the Newcastle 2012 case study (February 2008 to June 2012), the Birmingham model outputs have a better prediction skill.

The validation period spans one year before the event for both case studies as this is enough length to serve as spin-up time for the model (Gemma Coxon, University of Bristol; Jim Freer, University of Bristol; Iskra Mejía-Estrada, University of Bristol, personnel communication April 2018). There were no further tests on the impact of the length of the validation period on the outputs of the simulation.

7.4.3 On the hydrological uncertainty evaluation

The analysis of uncertainty plays an important role in hydrological modelling. In the GLUE approach, model outputs are evaluated against a likelihood function (e.g. The Nash-Sutcliffe efficiency index) and accepted according to a likelihood threshold. Simulations with likelihood above this value are considered behavioural. Members of the behavioural ensemble are assigned likelihood weights at each time step to produce a cumulative distribution of model

outputs per time step. From here, uncertainty quantiles can be calculated (Freer et al., 1996). However, one of the main disadvantages is that the decisions to drive it are prone to subjectivity instead of error models, therefore results depend on threshold values (Blasone et al., 2008).

The Nash-Sutcliffe Efficiency (NSE) index for the Newcastle 2012 case study does not go beyond NSE= 0.42 (see Table 6.7). This means that model outputs are almost as accurate as the mean of the observed values. In this case the "behavioural" ensemble members were taken using the Q5 and Q95 percentiles from the whole ensemble rather than assigning a fixed threshold (for example, rejecting simulations with NSE below 0.8), meaning that the chosen ensemble members a) are not actually behavioural and b) put into evidence that the GLUE framework can be useful if an appropriate likelihood function for the distribution error is found, instead of assigning an arbitrary behavioural threshold (Beven et al., 2007).

7.4.4 On the hydrological model structure

Modifications to the structure of the Dynamic fluxEs and ConnectIvity for Predictions of HydRology (DECIPHeR) model are being developed further, presenting some areas of opportunity regarding the current and modified model structure.

At the time of writing, a homogeneous value of the channel velocity (CHV) is implemented in the whole catchment. This means that the river response is under-represented, given the inherent difficulties of fully specifying the differences in urban and non-urban channel velocities. The results of the Birmingham 2007 case study (74.08 km^2) compared to the Newcastle 2012 case study (55.85 km^2) suggest that at larger scales, this homogeneous model parameter becomes more dominant when reproducing flood flows.

Another reason for the attenuate forecasting skill of the hydrological model in the first case study could be attributed to the channel routing scheme that depends on a time delay histogram (detailed in section 3.2.4). This attribution describes a linear relationship between the distance of a given river cell and the channel velocity, which does enable simple computation and thus, model efficiency. However, the channel routing scheme depends heavily on the river network configuration to calculate the distance from a gauge to the outlet. The river network is derived from the sink-filled Digital Elevation Model where pits have been removed or filled. The pre-processing of the topographic data is therefore a source of uncertainty in the parameterisation of the landscape also.

7.4.5 On the number of case studies.

The present research analyses the results of the proposed hydrometeorological cascade's implementation and reproduction of two major flash flood events in the United Kingdom. There are significant differences in model performance (both meteorological and hydrological) for both case studies so the experiments to put forward the hypothesis are proved only under the United Kingdom's climatological settings and under recent (2007 and 2012) meteorological extreme scenarios.

The number of case studies presented is bounded by the time constraints inherent in the production of a doctoral thesis. Moreover, the model structure used in the second stage of the meteorological cascade necessitated several major enhancements as the research was carried out, allowing a shorter duration for implementing the proposed methodology in further test cases. The preparation of climatological input variables (e.g. the disaggregation of potential evapotranspiration timeseries from daily to hourly scale, and the retrieval hourly rainfall data for several years) proved to be a necessary but particularly time consuming and computationally demanding enhancement.

7.5 Future lines of research

- Given that the methodology proposed represents a novel approach to characterise flash floods, necessary future directions of study have been identified towards strengthening the practise informed by this methodology. Of primary significance is the inclusion of two additional modelling parameterisations, applied to a lesser extent in flash flood studies, yet which evidence further good performance: The Revised MM5 Surface Layer scheme (Jiménez et al., 2012), which a difference of the Monin-Obhukov scheme, does not include a parameterisation of the roughness length. Instead, it calculates heat, moisture and momentum profiles using stability functions that allow a sharper transition to the upper region of the atmosphere. This scheme has shown good performance when paired with the Single Layer Urban Canopy model when exploring the hourly variations of vertical turbulent mixing and urban temperature due to the Urban Heat Island effect (Giannaros et al., 2018).
- The Yonsei University (YSU) Planetary Boundary Layer scheme (Hong et al., 2006), that vertically diffuses heat faster via turbulent eddies, depends on the Prandtl number (ratio of momentum diffusivity to thermal diffusivity) to determine momentum fluxes. A difference of the implemented Mellor-Yamada-Janjic scheme, the YSU parameterisation of the Planetary boundary Layer is a first-order, non-local scheme that enhances vertical mixing. This scheme has proved to accurately reproduce near-

surface variables (such as temperature and relative humidity when reproducing synoptic flows and in studies on air quality (Banks et al., 2016; Banks et al., 2015), showing its potential to be used to simulate local variations due to mesoscale systems.

Another enhancement relevant to the current methodology is the creation of a time-lagged ensemble for each of the nine WRF model scenarios (three urban canopy models and three microphysics schemes). It has been documented that for a fixed lead time, the skill of the ensemble increases with its size (Chen et al., 2013). A reason to use time-lagged ensembles is because they act as source of perturbed initial conditions which reflect the evolution in time of the atmospheric conditions, where each of the short-range predictions of the ensemble can be assigned a weight depending on the least square error compared to the "true" value (Lu et al., 2007). The advantage of using time-lagged ensembles is that it improves the skill of the forecast at high spatial and temporal resolutions by reducing type-I errors (missed forecast events) (Mittermaier, 2007). Since this procedure emulates the averaging of an ensemble produced by varying initial conditions, the same can be applied to the average of the ensemble, serving as the climatological forcing for the hydrological stage of the cascade. This would effectively reduce the cascaded uncertainty from the meteorological to the hydrological stage serving climatological forcing by only considering the rainfall scenarios with a good correspondence between observations and simulations

The final step of the three-stage cascade implemented in flood forecasting systems could therefore be integrated in the proposed modelling framework. Using the hydrological model outputs as boundary conditions for a hydrodynamic model could enhance the significance of the work, as water depths and inundation extent of a flash flood could be evaluated within a probabilistic framework, offering information on the spatial distribution of the societal exposure and the at-risk areas. Once the enhanced hydrodynamic modelling is completed, enhanced flood risk reduction strategies can be developed and evaluated.

Finally, there is also room for improvement regarding the number and location of case studies analysed. As stated in Section 1.1.2, the flash flood events in the present study were selected given a) their hydrometeorological importance in the historical record, b) the availability of information of building height distribution as well as climatological data (hourly rainfall and evapotranspiration) to run the hydrological model, c) the high degree of urbanisation (at least 40% of the land cover is urban), d) a maximum extent of 100 km^2 to comply with the definition of flash flood for the present study given in Chapter 2, and e) their closeness to a major city that experienced significant losses during the event. As long as these requirements are fulfilled, current results can benefit from the addition of events for analysis.

These outlined measures show the potential of the implementation of the proposed hydrometeorological modelling framework to other flash flood events. It signifies a relevant contribution to the understanding of these hazards by quantifying the innate errors and uncertainties, specifying necessary data requirements and qualifying the requirement for enhanced numerical modelling. The findings also highlight the significance of the methodology as a hindcasting tool, an elementary resource in providing reliable assessment of, and guidance for, the effective reduction of future flash flood risk.

Appendix A. Tests that helped shaping the meteorological modelling set-up implemented

Additional tests were carried out to test the appropriateness of the model set-up, including another microphysics scheme, model requirements regarding spin-up time given the very short length of the simulation (48 hours) compared to other studies and the resolution of the innermost domain. All the tests were carried out for the Newcastle 2012 case study only considering the constraint in computational power available.

A.1 Testing an additional microphysics scheme

As stated in Section 3.3.1.2, three microphysics parameterisations from the Weather Research and Forecasting (WRF) model were used in the present study. They were chosen given their documented efficiency in simulating convective events and slow-moving storm cells. Another frequently applied scheme is the ETA microphysics, which is the operational parameterisation in models developed by the National Centers for Environmental Prediction (NCEP), such as the WRF and used in other studies that use a high-resolution (< 5 km) innermost grid to reproduce intense rainfall (Efstathiou et al., 2013; Skamarock et al., 2019). This scheme considers four condensates of water vapour (cloud water, rain, cloud ice and precipitation ice) which are each advected in the model, which makes the Eta parameterisation highly efficient. To test its efficiency, this scheme was implemented with the Single-Layer Urban Canopy Model (and the same model set-up detailed in Section 4.3) for the Newcastle 2012 case study, and denominated Simulation 10. It was not paired with the other two urban canopy schemes because the purpose of this test was to complement the results presented here, which show that SLUCM gives the top two best performing rainfall scenarios (see Table 4.4 and Figure 4.15).

The accumulated precipitation for the two-hour period where the highest rainfall rates were recorded during the flash flood event (as mentioned in section 4.2.3) is shown in Figure A.1, where outputs from the meteorological modelling are compared to rainfall data from the Global Precipitation Measurement (GPM) mission, following the analysis displayed in Figure 4.8.

Similar to the findings in section 4.4.1, the WRF model outputs reproduce the high-intensity rainfall area north-west of the United Kingdom (feature B), and the distribution of wet cells over Ireland which is not present in the observed data (feature D). The latter is also the case for considering the rainfall extent over and west of the Netherlands and north of France (feature

G), a behaviour that could be nonetheless explained by the closeness to the relaxation zone at the edge of the domain (feature G). Rainfall on the East coast of the United Kingdom is misplaced: the WRF produces rainfall over the Midlands (feature F). However, a band of intense rainfall over Newcastle (feature E) is also present, although the values are underestimated.

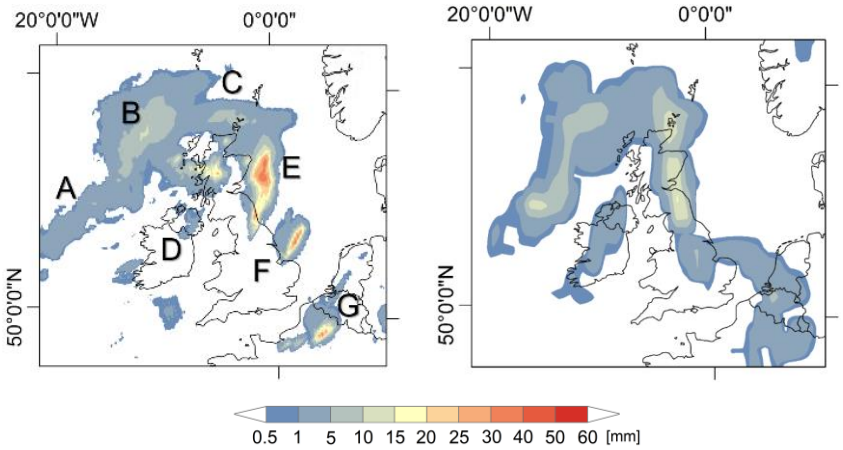

Figure A.1. Accumulated rainfall map from 15:00 UTC to 17:00 UTC on the 28th June 2012 from GPM data (left) and for the WRF simulation using the Eta microphysics (right)

The Eta parameterisation, although explicitly designed for model grids less than 5 km in size and to be used with NCEP boundary conditions (Efstathiou et al., 2013), is unable to reproduce the rainfall intensity during the most critical period as well as the spatial patters observed in the rest of the simulations (see section 4.4.1), something also observed in studies that first tested the efficiency of this scheme (Jankov et al., 2005) although more recent work suggests that the Eta parameterisation tends to overestimate rainfall totals and is overperformed by the WRF Single-Moment 6-class (Maw et al., 2017).

Plots of the hourly rainfall for six stations and the simulated rainfall of the correspondent grid cell is displayed in Figure A.2. Compared to the rest of the simulations (see top row of Figures 4.12, 4.13 and 4.14), Only Greenhills Farm show a good correspondence in the time and magnitude of the rainfall peak, performance of at Jesmond Dene of Simulation 10 agrees with the results of the other rainfall scenarios, and the underestimated values at Chirdon still outperform the rest of the model outputs. However, it is the only scenario that performs poorly at Alston (overestimating the peak values) and largely underestimates rainfall Howdon and Tunstall.

The low efficiency of the Eta microphysics is also reflected in the skill metrics in Table A.1, where although the Root Mean Square error and the Mean Bias Error are similar to those of the nine WRF rainfall scenarios (see Table 4.5), the Critical Success Index suggests that the

model overestimates the amount of wet cells in the innermost domain, and the accumulated rainfall value is largely underestimated. Therefore, this microphysics scheme was not used for the second case study of the present research.

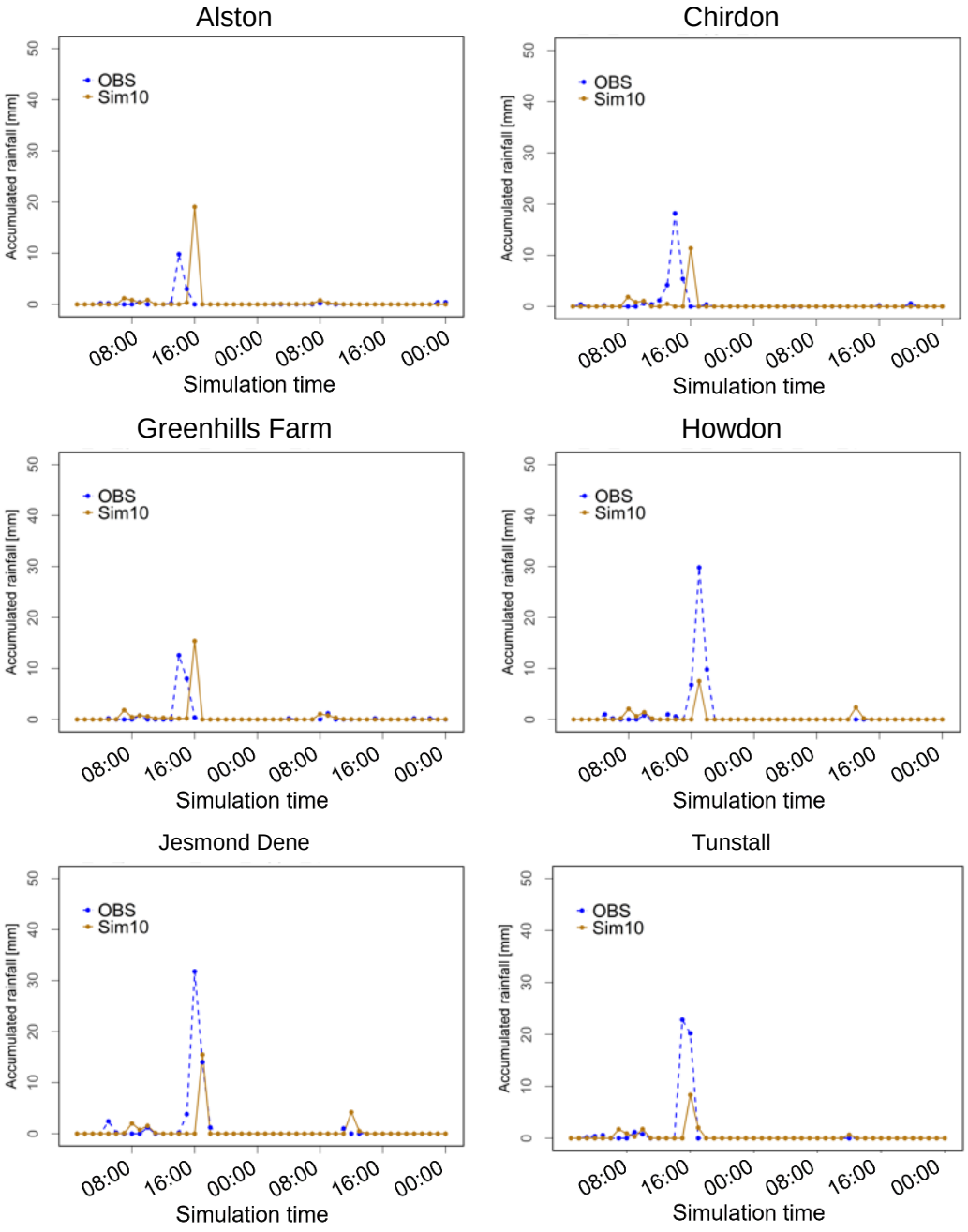

Figure A.2. Simulated rainfall using the Eta microphysics scheme for six gauges in the Tyne catchment. See Figure 4.11 for location of gauges

Table A.1. Skill scores for the WRF simulation using the Eta microphysics

Simulation	CSI	RMSE [mm]	MBE [mm]	Accumulated rainfall [mm]
10	0.49	1.83	-0.77	18.18

A.2 Testing model spin-up time

An important aspect of numerical weather modelling is the length of the period needed for the model to stabilise, capture large-scale circulations and capture precipitation from an early stage, called spin-up time. When simulating rainfall, this period has a substantial influence on the amount and timing of the precipitation (Bonekamp et al., 2018) so the time to allow for model stability is crucial for its performance.

The WRF user manual states that the ideal spin-up time is 6 to 12 hours, a recommendation that has been followed when forecasting convective rainfall in the warm season (Jankov et al., 2007). Another study on flash flood associated rainfall concluded that the optimal spin-up time is determined by the temporal resolution of the lateral boundary conditions (Bonekamp et al., 2018). It has also been suggested to use only one timestep of the lateral boundary conditions, the one that immediately precedes the start of the simulation, as these conditions are regarded as the most accurate to produce a flash flood (Vincendon et al., 2017). Other studies on summer precipitation have also tested 24 and 48 hours as warm-up periods to simulate events that last 10 days without finding a clear trend between an increase of spin-up time and model performance (Bonekamp et al., 2018), while others have experimented with lead times of 72, 90 and 120 hours to simulate the development of quasi-stationary weather fronts during 60 hours (Yáñez-Morroni et al., 2018).

Given the length of the simulation for the present study, spin-up times of 6 and 24 hours were chosen for testing. These values follow the ones described in the literature and ensure that at least one analysis of boundary conditions is assimilated. The test was performed on simulation 1 only for the reasons outlined in Section 4.5.1.

Figure A.3 shows the accumulated rainfall maps during the two critical hours on 28 June 2012 for both selected warm-up periods. When using 6 hours of spin-up time (left panel), the atmospheric conditions assimilated into the model are not enough to simulate the intense rainfall associated with the June 2012 flash flood. This contradicts the conclusion by (Vincendon et al., 2017) despite them also performing a 48-hour analysis. However, their study uses a different source of boundary conditions at a higher spatial resolution, which means that the meteorological setting is better represented. Although underestimated, the model still reproduces the band of rainfall to the north of the United Kingdom and over the north-east region. This means that the system had started developing but that only one analysis of

boundary conditions is not enough for the model to reproduce the intense rainfall over the region. On the other hand, the right panel of Figure 4.18 shows the accumulated rainfall when using 24 hours as spin-up time. In this case, rainfall is clearly underestimated, and the precipitation patterns are not observed at all. This confirms the results from (Bonekamp et al., 2018), where model runs with the longest spin-up time produce the lowest intensities for the period of study.

Both simulations, correctly deliver rainfall over the Newcastle area, which is reflected in the high Critical Success Index although with values much different to those observed as can be inferred by the high Root Mean Square Error (see Table A.2). However, both cases considerably underestimate the rainfall across the domain. Given these results, a spin-up time of 12 hours was used for the second case study.

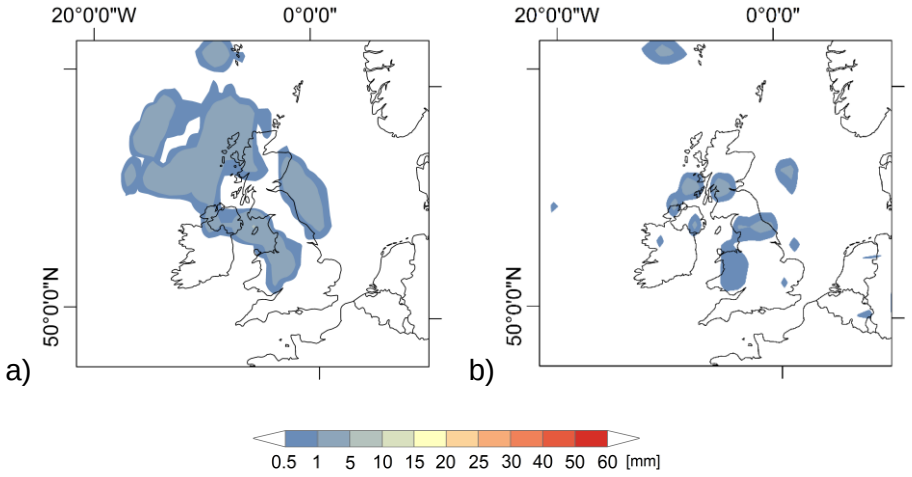

Figure A.3. Accumulated rainfall map from 15:00 UTC to 17:00 UTC on the 28th June 2012 for the WRF simulations a) with 6 hours of spin-up time, b) with 24-hours of spin-up time

Table A.2. Skill scores for the WRF simulations using 6 and 24 hours of spin-up time

Spin-up time [h]	CSI	RMSE [mm]	MBE [mm]
6	0.84	3.14	-1.78
24	0.64	3.36	-2.44

A.3 Testing resolution of the innermost domain

All modelling was performed using the University of Bristol's high-performance computing facility, BlueCrystal Phase 3 (BCp3). It comprises 223 standard computer nodes, each one with 2 x 2.6GHz 8-core Intel E5-2670 (SandyBridge) chips and a total of 64 GB of Ram distributed in 16 processors per node. Additional to this, BCp3 also has 18 large memory nodes, each one with 16 processors with 256 GB of memory. Users can access BCp3 via a

bash shell interpreter as BCp3 uses the Linux OS, and it is equipped with a default GNU compiler (ACRC, 2014).

The meteorological model simulations with the chosen domain resolution (54 km, 18 km, 6 km and 2 km) were run requesting all 16 processors of a node (total 64 GB).

A single model run using the parameterisation given in Table 3.3 for simulation number 1 but with an innermost domain resolution that matches that of the observed gridded data (using domains with resolution 27 km, 9 km, 3 km and 1 km) took nearly four times as much processing time given the increased number of grid cells (from 48 × 54 cells in a 96 × 108 km^2 domain to 96 × 104 in the same area). Moreover, even requesting 8 processors of a large memory node (total 128 GB) the job had to be submitted to a queueing system to be run, and the time spent in the queue exceeded the computation time given the request for large memory.

References

[Church Street Tewkesbury 2007 Flood] [image]. (n.d.). (2007). Church Street Tewkesbury 2007 Flood. tewkesbury-2007-flood-03.jpg, Tewkesbury Museum.

Acosta-Coll, M., Ballester-Merelo, F., Martinez-Peiró, M., & De la Hoz-Franco, E. (2018). Real-Time Early Warning System Design for Pluvial Flash Floods-A Review. *Sensors (Basel, Switzerland), 18*(7), 2255. doi:10.3390/s18072255

ACRC. (2014). "BlueCrystal phase 3." Retrieved 24 July 2019, from https://www.acrc.bris.ac.uk/acrc/phase3.htm.

Ahmadalipour, A., & Moradkhani, H. (2019). A data-driven analysis of flash flood hazard, fatalities, and damages over the CONUS during 1996–2017. *Journal of Hydrology*, 578, 124106. doi:10.1016/j.jhydrol.2019.124106

Alfieri, L., Burek, P., Dutra, E., Krzeminski, B., Muraro, D., Thielen, J., & Pappenberger, F. (2013). GloFAS - global ensemble streamflow forecasting and flood early warning. *Hydrol. Earth Syst. Sci., 17*(3), 1161-1175. doi:10.5194/hess-17-1161-2013

Alfieri, L., Velasco, D., & Thielen, J. (2011). Flash flood detection through a multi-stage probabilistic warning system for heavy precipitation events. *Adv. Geosci., 29*, 69-75. doi:10.5194/adgeo-29-69-2011

Ali, K., Bajracharyar, R., & Raut, N. (2017). Advances and Challenges in Flash Flood Risk Assessment: A Review. *Journal of Geography & Natural Disasters, 7*(2), 6. doi:10.4172/2167-0587.1000195

Allan, R. P. (2012). Flooding in Newcastle, June 28 2012. Retrieved from http://www.met.reading.ac.uk/~sgs02rpa/latest/FLOODING1206.html

Amengual, A., Romero, R., Gómez, M., Martín, A., & Alonso, S. (2007). A Hydrometeorological Modeling Study of a Flash-Flood Event over Catalonia, Spain. *J. Hydrometeor. 8*(3), 282-303. doi:10.1175/jhm577.1

Amponsah, W., Marchi, L., Zoccatelli, D., Boni, G., Cavalli, M., Comiti, F., . . . Borga, M. (2016). Hydrometeorological Characterization of a Flash Flood Associated with Major Geomorphic Effects: Assessment of Peak Discharge Uncertainties and Analysis of the Runoff Response. *J. Hydrometeor., 17*(12), 3063-3077. doi:10.1175/jhm-d-16-0081.1

Anagnostou, E. N., Grecu, M., & Anagnostou, M. N. (2006). X-band polarimetric radar rainfall measurements in keys area microphysics project. *Journal of the atmospheric sciences*, 63(1), 187-203. doi:10.1175/JAS3592.1

Arakawa, A. (2004). The Cumulus Parameterization Problem: Past, Present, and Future. *J. Climate, 17*(13), 2493-2525. doi:10.1175/1520-0442(2004)017<2493:Ratcpp>2.0.Co;2

Archer, D. R., & Fowler, H. J. (2018). Characterising flash flood response to intense rainfall and impacts using historical information and gauged data in Britain. *J. Flood Risk Management, 11*(S1), S121-S133. doi:10.1111/jfr3.12187

Archer, D. R., Parkin, G., & Fowler, H. J. (2016). Assessing long term flash flooding frequency using historical information. *Hydrology Research*. doi:10.2166/nh.2016.031

Arnaud, P., & Lavabre, J. (2002). Coupled rainfall model and discharge model for flood frequency estimation. *Water Resour. Res., 38*(6), 11-11-11-11. doi:10.1029/2001wr000474

Banks, R. F., Tiana-Alsina, J., Baldasano, J. M., Rocadenbosch, F., Papayannis, A., Solomos, S., & Tzanis, C. G. (2016). Sensitivity of boundary-layer variables to PBL schemes in the WRF model based on surface meteorological observations, lidar, and radiosondes during the HygrA-CD campaign. *Atmospheric Research*, 176-177, 185-201. doi:10.1016/j.atmosres.2016.02.024

Banks, R. F., Tiana-Alsina, J., Rocadenbosch, F., & Baldasano, J. M. J. B.-L. M. (2015). Performance Evaluation of the Boundary-Layer Height from Lidar and the Weather Research and Forecasting Model at an Urban Coastal Site in the North-East Iberian Peninsula. *Boundary-Layer Meteorology, 157*(2), 265-292. doi:10.1007/s10546-015-0056-2

Barlage, M., Miao, S., & Chen, F. (2016). Impact of physics parameterizations on high-resolution weather prediction over two Chinese megacities. *J. Geophys. Res. Atmos., 121*(9), 4487-4498. doi:10.1002/2015jd024450

Bennartz, R., & Petty, G. W. (2001). The Sensitivity of Microwave Remote Sensing Observations of Precipitation to Ice Particle Size Distributions. *J. Appl. Meteor., 40*(3), 345-364. doi:10.1175/1520-0450(2001)040<0345:Tsomrs>2.0.Co;2

Beven, K. (2006). A manifesto for the equifinality thesis. *Journal of Hydrology, 320*(1), 18-36. doi:10.1016/j.jhydrol.2005.07.007

Beven, K. (2012). Down to Basics: Runoff Processes and the Modelling Process. In *Rainfall‐Runoff Modelling* (pp. 1-23)

Beven, K., & Freer, J. (2001a). A dynamic TOPMODEL. *Hydrological Processes, 15*(10), 1993-2011. doi:10.1002/hyp.252

Beven, K., & Freer, J. (2001b). Equifinality, data assimilation, and uncertainty estimation in mechanistic modelling of complex environmental systems using the GLUE methodology. *Journal of Hydrology, 249*(1), 11-29. doi:10.1016/S0022-1694(01)00421-8

Bhati, S., & Mohan, M. (2018). WRF-urban canopy model evaluation for the assessment of heat island and thermal comfort over an urban airshed in India under varying land use/land cover conditions. *Geoscience Letters, 5*(1), 27. doi:10.1186/s40562-018-0126-7

Bianco, L. (2008). "Surface layer parameterization in WRF." Retrieved 23 July 2019, from http://cires1.colorado.edu/science/groups/pielke/classes/at7500/Bianco_SFC.pdf.

Blasone, R.-S., Madsen, H., & Rosbjerg, D. J. J. o. H. (2008). Uncertainty assessment of integrated distributed hydrological models using GLUE with Markov chain Monte Carlo sampling. *Journal of Hydrology, 353*(1-2), 18-32. doi:10.1016/j.jhydrol.2007.12.026

Blenkinsop, S., Lewis, E., Chan, S. C., & Fowler, H. J. (2017). Quality-control of an hourly rainfall dataset and climatology of extremes for the UK. *J. Climatol., 37*(2), 722-740. doi:10.1002/joc.4735

Bonekamp, P. N. J., Collier, E., & Immerzeel, W. W. (2018). The Impact of Spatial Resolution, Land Use, and Spinup Time on Resolving Spatial Precipitation Patterns in the Himalayas. *Journal of Hydrometeorology, 19*(10), 1565-1581. doi:10.1175/JHM-D-17-0212.1

Boorman, D. B., Hollis, J. M., & Lilly, A. (1995). *Hydrology of soil types: a hydrologically based classification of the soils of the United Kingdom*.

Borga, M., Anagnostou, E. N., Blöschl, G., & Creutin, J. D. (2011). Flash flood forecasting, warning and risk management: the HYDRATE project. *Environmental Science & Policy, 14*(7), 834-844. doi:10.1016/j.envsci.2011.05.017

Bouttier, F., & Courtier, P. (2002). *Data assimilation concepts and methods*. Retrieved from https://www.ecmwf.int/sites/default/files/elibrary/2002/16928-data-assimilation-concepts-and-methods.pdf

Bovik, A. C. (2009). Chapter 3 - Basic Gray Level Image Processing. In A. Bovik (Ed.), *The Essential Guide to Image Processing* (pp. 43-68). Boston: Academic Press.

Bowler, N. E., Arribas, A., Mylne, K. R., Robertson, K. B., & Beare, S. E. (2008). The MOGREPS short-range ensemble prediction system. *Q.J.R. Meteorol. Soc., 134*(632), 703-722. doi:10.1002/qj.234

Braud, I., Ayral, P. A., Bouvier, C., Branger, F., Delrieu, G., Le Coz, J., . . . Wijbrans, A. (2014). Multi-scale hydrometeorological observation and modelling for flash flood understanding. *Hydrol. Earth Syst. Sci., 18*(9), 3733-3761. doi:10.5194/hess-18-3733-2014

Brisson, E., Leps, N., & Ahrens, B. (2017). Konvektionserlaubende Klimamodellierung (Convection Permitting Climate Modeling). In D. Wetterdienst (Ed.), Regionale Klimamodellierung I - Grundlagen. Germany. Retrieved from https://www.dwd.de/DE/leistungen/pbfb_verlag_promet/pdf_promethefte/99_pdf.pdf;jsessionid=A77208EDDC4F9D2737BB719F7865A812.live21074?__blob=publicationFile&v=2.

Brown, P. (2016). Synoptic charts for 0600 GMT 20 and 21 July 2007. In: John Wiley & Sons.

Bruni, G., Reinoso, R., Van De Giesen, N., Clemens, F., & Ten Veldhuis, J. (2015). On the sensitivity of urban hydrodynamic modelling to rainfall spatial and temporal resolution. *Hydrol. Earth Syst. Sci., 19*(2), 691. doi:10.5194/hess-19-691-2015

Bürger, G., Heistermann, M., & Bronstert, A. (2014). Towards Subdaily Rainfall Disaggregation via Clausius–Clapeyron. *J. Hydrometeor., 15*(3), 1303-1311. doi:10.1175/jhm-d-13-0161.1

Burian, S. J., & Shepherd, J. M. (2005). Effect of urbanization on the diurnal rainfall pattern in Houston. *Hydrological Processes: An International Journal, 19*(5), 1089-1103. doi:10.1002/hyp.5647

Caldwell, R. J., Gangopadhyay, S., Bountry, J., Lai, Y., & Elsner, M. M. (2013). Statistical modeling of daily and subdaily stream temperatures: Application to the Methow River Basin, Washington. *Water Resour. Res., 49*(7), 4346-4361. doi:10.1002/wrcr.20353

Campos, E., & Wang, J. (2015). Numerical simulation and analysis of the April 2013 Chicago Floods. *Journal of Hydrology*, 531, Part 2, 454-474. doi:10.1016/j.jhydrol.2015.09.004

Cassola, F., Ferrari, F., & Mazzino, A. (2015). Numerical simulations of Mediterranean heavy precipitation events with the WRF model: A verification exercise using different approaches. *Atmospheric Research, 164-165*, 210-225. doi:10.1016/j.atmosres.2015.05.010

Cave, B., Cragg, L., Gray, J., Parker, D., Pygott, K., & Tapsell, S. (2008). *Understanding of and response to severe flash flooding: literature review*. Retrieved from https://assets.publishing.service.gov.uk/government/uploads/system/uploads/attachment_data/file/291139/scho0509bqar-e-e.pdf

Cecinati, F., Rico-Ramirez, M. A., Heuvelink, G. B. M., & Han, D. (2017). Representing radar rainfall uncertainty with ensembles based on a time-variant geostatistical error modelling approach. *Journal of Hydrology, 548*, 391-405. doi:10.1016/j.jhydrol.2017.02.053

CEH. (2002). Land Cover Map 2000. Retrieved 5 February 2019, from Centre for Ecology and Hydrology https://www.ceh.ac.uk/services/land-cover-map-2000

CEH. (2011). Land Cover Map 2007. Retrieved 5 Februay 2019, from Centre for Ecology and Hydrology https://www.ceh.ac.uk/services/land-cover-map-2007

CEH. (2017). Land Cover Map 2015. Retrieved 5 Februay 2019, from Centre for Ecology and Hydrology https://www.ceh.ac.uk/services/land-cover-map-2007

Chaney, N. W., Metcalfe, P., & Wood, E. F. (2016). HydroBlocks: a field-scale resolving land surface model for application over continental extents. *Hydrol. Process., 30*(20), 3543-3559. doi:10.1002/hyp.10891

Chen, F., & Dudhia, J. (2001). Coupling an Advanced Land Surface–Hydrology Model with the Penn State–NCAR MM5 Modeling System. Part I: Model Implementation and Sensitivity. *Monthly Weather Review, 129*(4), 569-585. doi:10.1175/1520-0493(2001)129<0569:CAALSH>2.0.CO;2

Chen, F., Kusaka, H., Bornstein, R., Ching, J., Grimmond, C. S. B., Grossman-Clarke, S., . . . Zhang, C. (2011). The integrated WRF/urban modelling system: development, evaluation, and applications to urban environmental problems. *Int. J. Climatol., 31*(2), 273-288. doi:10.1002/joc.2158

Chen, M., Wang, W., & Kumar, A. (2013). Lagged Ensembles, Forecast Configuration, and Seasonal Predictions. *Mon. Wea. Rev., 141*(10), 3477-3497. doi:10.1175/mwr-d-12-00184.1

Chiang, Y.-M., Hsu, K.-L., Chang, F.-J., Hong, Y., & Sorooshian, S. (2007). Merging multiple precipitation sources for flash flood forecasting. Journal of Hydrology, 340(3), 183-196. doi:10.1016/j.jhydrol.2007.04.007

Christensen, J. H., Carter, T. R., Rummukainen, M., & Amanatidis, G. (2007). Evaluating the performance and utility of regional climate models: the PRUDENCE project. In: Springer.

Cloke, H. L., & Pappenberger, F. (2009). Ensemble flood forecasting: A review. *Journal of Hydrology*, 375(3), 613-626. doi:10.1016/j.jhydrol.2009.06.005

Cloke, H. L., & Pappenberger, F. (2008). Evaluating forecasts of extreme events for hydrological applications: an approach for screening unfamiliar performance measures. *Met. Apps, 15*(1), 181-197. doi:10.1002/met.58

Cohen, A. E., Cavallo, S. M., Coniglio, M. C., & Brooks, H. E. (2015). A Review of Planetary Boundary Layer Parameterization Schemes and Their Sensitivity in Simulating Southeastern U.S. Cold Season Severe Weather Environments. *Wea. Forecasting, 30*(3), 591-612. doi:10.1175/waf-d-14-00105.1

Coles, D., Yu, D., Wilby, R. L., Green, D., & Herring, Z. (2017). Beyond 'flood hotspots': Modelling emergency service accessibility during flooding in York, UK. Journal of Hydrology, 546, 419-436. doi:10.1016/j.jhydrol.2016.12.013

Collier, C. G. (2007). Flash flood forecasting: What are the limits of predictability? *Quarterly Journal of the Royal Meteorological Society, 133*(622), 3-23. doi:10.1002/qj.29

Coulibaly, M. (2008). Spatial analysis of an urban flash flood survey results. *Geocarto International, 23*(3), 217-234. doi:10.1080/10106040701207258

Coxon, G., Freer, J., Lane, R., Dunne, T., Knoben, W. J. M., Howden, N. J. K., . . . Woods, R. (2019). DECIPHeR v1: Dynamic fluxEs and ConnectIvity for Predictions of HydRology. *Geosci. Model Dev., 12*(6), 2285-2306. doi:10.5194/gmd-12-2285-2019

CRED. (2015). What is the human cost of natural disasters? (1994-2013) [Press release]. Retrieved from http://cred.be/sites/default/files/CredCrunch38.pdf

Cuo, L., Lettenmaier, D. P., Mattheussen, B. V., Storck, P., & Wiley, M. (2008). Hydrologic prediction for urban watersheds with the Distributed Hydrology–Soil–Vegetation Model. *Hydrol. Process., 22*(21), 4205-4213. doi:10.1002/hyp.7023

Cutter, S. L., Emrich, C. T., Gall, M., & Reeves, R. (2018). Flash Flood Risk and the Paradox of Urban Development. Natural Hazards Review, 19(1), 05017005. doi:10.1061/(ASCE)NH.1527-6996.0000268

Daggupati, P., Pai, N., Ale, S., R. Douglas-Mankin, K., W. Zeckoski, R., Jeong, J., . . . A. Youssef, M. (2015). A Recommended Calibration and Validation Strategy for Hydrologic and Water Quality Models. *Transactions of the ASABE, 58*(6), 1705-1719. doi:10.13031/trans.58.10712

Dee, D., Fasullo, J., Shea, D., Walsh, J., & NCAR, S. (2016). The climate data guide: atmospheric reanalysis: overview & comparison tables. National Center for Atmospheric Research, Boulder, CO). Available at https://climatedataguide. ucar. edu/climatedata/atmospheric-reanalysis-overview-comparison-tables. Accessed June, 1, 2019.

Devaraj, S. J. (2019). *Chapter 2 - Emerging Paradigms in Transform-Based Medical Image Compression for Telemedicine Environment*. In H. D. Jude & V. E. Balas (Eds.), Telemedicine Technologies (pp. 15-29): Academic Press.

Dinku, T., Hailemariam, K., Maidment, R., Tarnavsky, E., & Connor, S. (2013). Combined use of satellite estimates and rain gauge observations to generate high-quality historical rainfall time series over Ethiopia. *International Journal of Climatology, 34*(7), 2489-2504. doi:10.1002/joc.3855

Doswell, C. A. (2015). *Hydrology, Floods and Droughts | Flooding*. In G. R. North, J. Pyle, & F. Zhang (Eds.), Encyclopedia of Atmospheric Sciences (Second Edition) (pp. 201-208). Oxford: Academic Press.

Drobinski, P., Ducrocq, V., Alpert, P., Anagnostou, E., Béranger, K., & Borga, M. et al. (2014). HyMeX: A 10-Year Multidisciplinary Program on the Mediterranean Water Cycle. *Bulletin of The American Meteorological Society, 95*(7), 1063-1082. doi:10.1175/bams-d-12-00242.1

Dudhia, J. (1989). Numerical Study of Convection Observed during the Winter Monsoon Experiment Using a Mesoscale Two-Dimensional Model. *Journal of The Atmospheric Sciences, 46*(20), 3077-3107. doi: 10.1175/1520-0469(1989)046<3077:nsocod>2.0.co;2

Dudhia, J. (2014). Overview of WRF physics. University Corporation for Atmospheric Research, Boulder, CO, Available at http://www2.mmm.ucar.edu/wrf/users/tutorial/201401/Physics_full. pdf. Accessed June 2019.

ECMWF. (2012). The ECMWF Ensemble Prediction System. The rationale behind probabilistic weather forecasts. Available at https://www.ecmwf.int/sites/default/files/the_ECMWF_Ensemble_prediction_system.pdf. Accessed July 2019

Efstathiou, G. A., Zoumakis, N. M., Melas, D., Lolis, C. J., & Kassomenos, P. (2013). Sensitivity of WRF to boundary layer parameterizations in simulating a heavy rainfall event using different microphysical schemes. Effect on large-scale processes. *Atmospheric Research*, 132–133, 125-143. doi:10.1016/j.atmosres.2013.05.004

Ekström, M., & Gilleland, E. (2017). Assessing convection permitting resolutions of WRF for the purpose of water resource impact assessment and vulnerability work: A southeast Australian case study. *Water Resources Research*, 53(1), 726-743. doi:10.1002/2016WR019545

Eldho, T. I., Zope, P. E., & Kulkarni, A. T. (2018). *Chapter 12 - Urban Flood Management in Coastal Regions Using Numerical Simulation and Geographic Information System*. In P. Samui, D. Kim, & C. Ghosh (Eds.), Integrating Disaster Science and Management (pp. 205-219): Elsevier.

Emerton, R., Stephens, E., Pappenberger, F., Pagano, T., Weerts, A., Wood, A., Salamon, P., Brown, J., Hjerdt, N., Donnelly, C., Baugh, C. and Cloke, H., 2016. Continental and global scale flood forecasting systems. Wiley Interdisciplinary Reviews: *Water, 3*(3), pp.391-418.

Emu-Analytics. (2020). Building Heights in England. Available at https://buildingheights.emu-analytics.net/. Accessed May 2019

Environment-Agency (2012). *The Tyneside Flood 20th June 2012: Hydrological Report*, Environment Agency - Yorkshire & North East Region Hydrology.

Environment-Agency. (2007a). *2007 summer floods - Environment Agency* - A table showing the number of properties that received flood warnings in the affected areas. Environment Agency.

Environment-Agency. (2007b). *Review of 2007 summer floods*. Retrieved from https://assets.publishing.service.gov.uk/government/uploads/system/uploads/attachment_data/file/292924/geho1107bnmi-e-e.pdf

Environment-Agency. (2013a). Quality Controlled Daily and Monthly Raingauge Data from Environment Agency Gauges (AfA148). Available at: https://data.gov.uk/dataset/2089f922-8b12-4f67-b042-10091dbc71ae/quality-controlled-daily-and-monthly-raingauge-data-from-environment-agency-gauges-afa148. Accessed April 2019

Environment-Agency. (2013b). Your community is at risk of Flash Flooding. Available at: https://www.oldham.gov.uk/downloads/file/2339/your_community_is_at_risk_of_flash_flooding

European-Commission. (2013). Flash floods in Europe characterised. Science for Environmental Policy, (40). Available at https://ec.europa.eu/environment/integration/research/newsalert/pdf/40si4_en.pdf. Accessed March 2019

EXIMAP. (2007). Handbook on good practices for flood mapping in Europe. Available at https://ec.europa.eu/environment/water/flood_risk/flood_atlas/pdf/handbook_goodpractice.pdf. Accessed June 2019

Fallmann, J., Suppan, P., & Emeis, S. (2013, April). *Modeling of the Urban Heat Island (UHI) using WRF-Assessment of adaptation and mitigation strategies for the city of Stuttgart*. In EGU General Assembly Conference Abstracts (Vol. 15).

Faulkner, D., Kjeldsen, T., Packman, J., & Stewart, L. (2012). *Estimating flood peaks and hydrographs for small catchments: Phase 1*. Flood and Coastal Erosion Risk Management Research and Development Programme.

Flack, D. L., Skinner, C. J., Hawkness-Smith, L., O'Donnell, G., Thompson, R. J., Waller, J. A., ... & Blenkinsop, S. (2019). Recommendations for improving integration in national end-to-end flood forecasting systems: An overview of the FFIR (Flooding From Intense Rainfall) programme. Water, 11(4), 725. doi:10.3390/w11040725

Flaschen, M. (2007). Flooding outside Thatcham railway station on 20 July. Available at: https://commons.wikimedia.org/wiki/File:ThatchamFloods2007.JPG.

FloodRe. (2019). Investing in flood risk management and defences. Available at https://www.floodre.co.uk/wp-content/uploads/Flood-Re-RMS-Results-Summary-ABI-version.a.pdf. Accessed March 2019

Förster, K., Hanzer, F., Winter, B., Marke, T., & Strasser, U. (2016). An open-source MEteoroLOgical observation time series DISaggregation Tool (MELODIST v0.1.1). *Geosci. Model Dev., 9*(7), 2315-2333. doi:10.5194/gmd-9-2315-2016

Fowler, H., Blenkinsop, S. and Tebaldi, C., 2007. Linking climate change modelling to impacts studies: recent advances in downscaling techniques for hydrological modelling. *International Journal of Climatology, 27*(12), pp.1547-1578.

Freer, J., Beven, K., & Ambroise, B. (1996). Bayesian Estimation of Uncertainty in Runoff Prediction and the Value of Data: An Application of the GLUE Approach. Water Resources Research, 32(7), 2147.

Fry, T. J., & Maxwell, R. M. (2017). Evaluation of distributed BMP s in an urban watershed—High resolution modelling for stormwater management. *J Hydrological Processes, 31*(15), 2700-2712.

Gadissa, T., Nyadawa, M., Behulu, F., & Mutua, B. (2019). *Chapter 13 - Assessment of catchment water resources availability under projected climate change scenarios and increased demand in Central Rift Valley Basin*. In A. M. Melesse, W. Abtew, & G. Senay (Eds.), Extreme Hydrology and Climate Variability (pp. 151-163): Elsevier.

Ganeshan, M., Murtugudde, R., & Imhoff, M. (2013). A multi-city analysis of the UHI-influence on warm season rainfall. *Urban Climate, 6*, 1-23. doi: 10.1016/j.uclim.2013.09.004

Garambois, P. A., Larnier, K., Roux, H., Labat, D., & Dartus, D. (2014). Analysis of flash flood-triggering rainfall for a process-oriented hydrological model. *Atmospheric Research*, 137, 14-24. doi:doi.org/10.1016/j.atmosres.2013.09.016

Gaume, E. and Borga, M., 2008. Post-flood field investigations in upland catchments after major flash floods: proposal of a methodology and illustrations. *Journal of Flood Risk Management, 1*(4), pp.175-189.

Gaume, E., Bain, V., Bernardara, P., Newinger, O., Barbuc, M., Bateman, A., . . . Viglione, A. (2009). A compilation of data on European flash floods. *Journal of Hydrology, 367*(1), 70-78. doi:10.1016/j.jhydrol.2008.12.028

Gebregiorgis, A. S., & Hossain, F. (2013). Understanding the Dependence of Satellite Rainfall Uncertainty on Topography and Climate for Hydrologic Model Simulation. IEEE *Transactions on Geoscience and Remote Sensing, 51*(1), 704-718. doi:10.1109/TGRS.2012.2196282

Giannaros, C., Nenes, A., Giannaros, T. M., Kourtidis, K., & Melas, D. (2018). A comprehensive approach for the simulation of the Urban Heat Island effect with the WRF/SLUCM modelling system: The case of Athens (Greece). *Atmospheric Research*, 201, 86-101. doi:10.1016/j.atmosres.2017.10.015

Gires, A., Tchiguirinskaia, I., Schertzer, D., Schellart, A., Berne, A., & Lovejoy, S. (2014). Influence of small scale rainfall variability on standard comparison tools between radar and rain gauge data. Atmospheric Research, 138, 125-138. doi: 10.1016/j.atmosres.2013.11.008.

Glenis, V., Kutija, V., & Kilsby, C. (2018). A fully hydrodynamic urban flood modelling system representing buildings, green space and interventions. *Environmental Modelling & Software, 109*. doi:10.1016/j.envsoft.2018.07.018

Golian, S., Javadian, M., & Behrangi, A. (2019). On the use of satellite, gauge, and reanalysis precipitation products for drought studies. *Environmental Research Letters, 14*(7), 075005. doi:10.1088/1748-9326/ab2203

Gong, W., Meyer, F., Webley, P. and Morton, D., 2013. Performance of the high-resolution atmospheric model HRRR-AK for correcting geodetic observations from spaceborne radars. *Journal of Geophysical Research: Atmospheres, 118*(20), pp.11,611-11,624.

D. C. Goodrich, I. S. Burns, C. L. Unkrich, D. J. Semmens, D. P. Guertin, & M. Hernandez et al. (2012). KINEROS2/AGWA: Model Use, Calibration, and Validation. *Transactions of the ASABE, 55*(4), 1561-1574. doi: 10.13031/2013.42264

Haberlie, A., Ashley, W. and Pingel, T., 2015. The effect of urbanisation on the climatology of thunderstorm initiation. *Quarterly Journal of the Royal Meteorological Society, 141*(688), pp.663-675. doi:10.1002/qj.2499

Hall, A. J. (1981). *Flash Flood Forecasting. Operational Hydrology*, Report No.18. Available at from: https://library.wmo.int/doc_num.php?explnum_id=8391. Accessed March 2019

Handmer, J., Henson, R., Sneeringer, P., Konieczny, R., & Madej, P. (2001). *Warning systems for flash floods: research needs, opportunities and trends*. In Coping With Flash Floods (pp. 77-89). Springer, Dordrecht.

Hapuarachchi, H., Wang, Q., & Pagano, T. (2011). A review of advances in flash flood forecasting. *Hydrological Processes, 25*(18), 2771-2784. doi: 10.1002/hyp.8040

Harrison, D., Driscoll, S., & Kitchen, M. (2006). Improving Precipitation Estimates from Weather Radar Using Quality Control and Correlation Techniques. Meteorological Applications, 7, 135-144. doi:10.1017/S1350482700001468

He, X., Sonnenborg, T., Refsgaard, J., Vejen, F. and Jensen, K., 2013. Evaluation of the value of radar QPE data and rain gauge data for hydrological modeling. Water Resources Research, 49(9), pp.5989-6005.

Heaviside, C., Cai, X. and Vardoulakis, S., 2014. The effects of horizontal advection on the urban heat island in Birmingham and the West Midlands, United Kingdom during a heatwave. Quarterly Journal of the Royal Meteorological Society, 141(689), pp.1429-1441.

Hengl, T., Heuvelink, G., & Rossiter, D. (2007). About regression-kriging: From equations to case studies. Computers & Geosciences, 33(10), 1301-1315. doi: 10.1016/j.cageo.2007.05.001

Hofmann, J., & Schüttrumpf, H. (2019). Risk-Based Early Warning System for Pluvial Flash Floods: Approaches and Foundations. Geosciences, 9(3), 127. doi: 10.3390/geosciences9030127

Holton, J. R. (2004). Chapter 5 The planetary boundary layer. In J. R. Holton (Ed.), International Geophysics (Vol. 88, pp. 115-138): Academic Press.

Hong, S. and Lee, J., 2009. Assessment of the WRF model in reproducing a flash-flood heavy rainfall event over Korea. Atmospheric Research, 93(4), pp.818-831.

Hong, S.-Y., Lim, K.-S., Yong-Hee, L., Jong-Chul, H., Hyung-Woo, K., Sook-Jeong, H., & Dudhia, J. (2010). Evaluation of the WRF Double-Moment 6-Class Microphysics Scheme for Precipitating Convection. Advances in Meteorology, 2010. doi:10.1155/2010/707253

Hong, S., Noh, Y. and Dudhia, J., 2006. A New Vertical Diffusion Package with an Explicit Treatment of Entrainment Processes. Monthly Weather Review, 134(9), pp.2318-2341.

Huang, D., & Gao, S. (2017). Impact of different cumulus convective parameterization schemes on the simulation of precipitation over China. Tellus A: Dynamic Meteorology and Oceanography, 69(1), 1406264. doi:10.1080/16000870.2017.1406264

Huang, W., Cao, Z., Huang, M., Duan, W., Ni, Y., & Yang, W. (2019). A New Flash Flood Warning Scheme Based on Hydrodynamic Modelling. Water, 11(6), 1221. doi: 10.3390/w11061221

Hughes, R. (2007). Old Birmingham Road - Flooding 20 July 2007. Available at: https://www.geograph.org.uk/photo/1095408.

IAHS, U. WMO.(1974). Flash floods, proceedings of the Paris symposium. Ed. IAHS-UNESCO-WMO, vol. publication 112.

Intermap-Technologies. (2009). NEXTMap British Digital Terrain 50m resolution (DTM10) Model Data by Intermap. Available at http://catalogue.ceda.ac.uk/, Accessed May 2019.

IPCC. (2014). Climate Change 2014: Synthesis Report. Contribution of Working Groups I, II and III to the Fifth Assessment Report of the Intergovernmental Panel on Climate Change.

Janjić, Z., 1994. The Step-Mountain Eta Coordinate Model: Further Developments of the Convection, Viscous Sublayer, and Turbulence Closure Schemes. Monthly Weather Review, 122(5), pp.927-945.

Jankov, I., Gallus, W., Segal, M. and Koch, S., 2007. Influence of Initial Conditions on the WRF–ARW Model QPF Response to Physical Parameterization Changes. Weather and Forecasting, 22(3), pp.501-519.

Jankov, I., Jr., W. A. G., Segal, M., Shaw, B., & Koch, S. E. (2005). The Impact of Different WRF Model Physical Parameterizations and Their Interactions on Warm Season MCS Rainfall. Weather and Forecasting, 20(6), 1048-1060. doi:10.1175/WAF888.1

JBA. (2002). Ouseburn Flood Study. Appendix C: Flood Hydrology. Flood Risk Mapping Studies.

Jiménez, P., Dudhia, J., González-Rouco, J., Navarro, J., Montávez, J. and García-Bustamante, E., 2012. A Revised Scheme for the WRF Surface Layer Formulation. Monthly Weather Review, 140(3), pp.898-918.

Kain, J. (2004). The Kain–Fritsch Convective Parameterization: An Update. Journal Of Applied Meteorology, 43(1), 170-181. doi: 10.1175/1520-0450(2004)043<0170:tkcpau>2.0.co;2

Kalcic, M. M., Chaubey, I., & Frankenberger, J. (2015). Defining Soil and Water Assessment Tool (SWAT) hydrologic response units (HRUs) by field boundaries. International Journal of Agricultural and Biological Engineering, 8(3), 69-80.

Kang, D., Eder, B. K., Stein, A. F., Grell, G. A., Peckham, S. E., & McHenry, J. (2005). The New England Air Quality Forecasting Pilot Program: Development of an Evaluation Protocol and Performance Benchmark. Journal of the Air & Waste Management Association, 55(12), 1782-1796. doi:10.1080/10473289.2005.10464775

Kang, Y.-H., Kwak, d., & Park, K. (2014). Multigrid methods for improving the variational data assimilation in numerical weather prediction. Tellus A, 66. doi:10.3402/tellusa.v66.20217

Karbasi, M., Shokoohi, A., & Saghafian, B. (2018). Loss of Life Estimation Due to Flash Floods in Residential Areas using a Regional Model. Water Resources Management, 32(14), 4575-4589. doi: 10.1007/s11269-018-2071-9

Karki, R., ul Hasson, S., Gerlitz, L., Schickhoff, U., Scholten, T., & Böhner, J. (2017). Quantifying the added value of convection-permitting climate simulations in complex

terrain: a systematic evaluation of WRF over the Himalayas. Earth Syst. Dynam., 8(3), 507-528. doi:10.5194/esd-8-507-2017

Kelsch, M. (2001). Hydrometeorological characteristics of flash floods. In Coping with flash floods (pp. 181-193). Springer, Dordrecht.

Kelsch, M., Caporali, E., & Lanza, L. G. (2001). Hydrometeorology of flash floods. In Coping with Flash Floods (pp. 19-35). Springer, Dordrecht.

Kendon, E., Blenkinsop, S., & Fowler, H. (2018). When Will We Detect Changes in Short-Duration Precipitation Extremes?. Journal Of Climate, 31(7), 2945-2964. doi: 10.1175/jcli-d-17-0435.1

Khazaei, M., Zahabiyoun, B., & Saghafian, B. (2011). Assessment of climate change impact on floods using weather generator and continuous rainfall-runoff model. International Journal Of Climatology, 32(13), 1997-2006. doi: 10.1002/joc.2416

Kilsby, C., Jones, P., Burton, A., Ford, A., Fowler, H., & Harpham, C. et al. (2007). A daily weather generator for use in climate change studies. Environmental Modelling & Software, 22(12), 1705-1719. doi: 10.1016/j.envsoft.2007.02.005

Kilsby, C., V. Glenis and V. Kutija (2016). Mapping and managing flood risk in Newcastle with CityCAT. Available at http://www.bluegreencities.ac.uk/documents/bgc-newcastle-cgk.pdf

Kim, S. N., Lee, W. K., Shin, K. I., Kafatos, M., Seo, D. J., & Kwak, H. B. (2010). Comparison of spatial interpolation techniques for predicting climate factors in Korea. Forest Science and Technology, 6(2), 97-109. doi:10.1080/21580103.2010.9671977

Kobold, M., & Brilly, M. (2006). The use of HBV model for flash flood forecasting.

Konrad, C. (2016). Effects of Urban Development on Floods. Available at https://pubs.usgs.gov/fs/fs07603/. Accessed August 2019

Krause, P., Boyle, D., & Bäse, F. (2005). Comparison of Different Efficiency Criteria for Hydrologic Models. Advances in Geosciences, 5. doi:10.5194/adgeo-5-89-2005

Krebs, G., Kokkonen, T., Setälä, H., & Koivusalo, H. (2016). Parameterization of a Hydrological Model for a Large, Ungauged Urban Catchment. Water, 8(10), 443. doi: 10.3390/w8100443

Krebs, G., Kokkonen, T., Valtanen, M., Setälä, H., & Koivusalo, H. (2014). Spatial resolution considerations for urban hydrological modelling. Journal Of Hydrology, 512, 482-497. doi: 10.1016/j.jhydrol.2014.03.013

Krysanova, V., Donnelly, C., Gelfan, A., Gerten, D., Arheimer, B., Hattermann, F., & Kundzewicz, Z. W. (2018). How the performance of hydrological models relates to credibility of projections under climate change. Hydrological Sciences Journal, 63(5), 696-720. doi:10.1080/02626667.2018.1446214

Kuligowski, R. J., Li, Y., & Zhang, Y. (2013). Impact of TRMM Data on a Low-Latency, High-Resolution Precipitation Algorithm for Flash-Flood Forecasting. Journal of Applied Meteorology and Climatology, 52(6), 1379-1393. doi:10.1175/JAMC-D-12-0107.1

Kumar, A., Houze Jr., R. A., Rasmussen, K. L., & Peters-Lidard, C. (2014). Simulation of a Flash Flooding Storm at the Steep Edge of the Himalayas. Journal of Hydrometeorology, 15(1), 212-228. doi:doi:10.1175/JHM-D-12-0155.1

Kusaka, H., Chen, F., Tewari, M., Dudhia, J., Gill, D. O., Duda, M. G., . . . Miya, Y. (2012). Numerical Simulation of Urban Heat Island Effect by the WRF Model with 4-km Grid Increment: An Inter-Comparison Study between the Urban Canopy Model and Slab Model. Journal of the Meteorological Society of Japan. Ser. II, 90B, 33-45. doi:10.2151/jmsj.2012-B03

Lamb, D. (2015). CLOUDS AND FOG | Cloud Microphysics. In G. R. North, J. Pyle, & F. Zhang (Eds.), Encyclopedia of Atmospheric Sciences (Second Edition) (pp. 133-140). Oxford: Academic Press.

Lavers, D. A., Harrigan, S., Andersson, E., Richardson, D. S., Prudhomme, C., & Pappenberger, F. (2019). A vision for improving global flood forecasting. Environmental Research Letters, 14(12), 121002. doi:10.1088/1748-9326/ab52b2

Lewis, E., Quinn, N., Blenkinsop, S., Fowler, H., Freer, J., & Tanguy, M. et al. (2018). A rule based quality control method for hourly rainfall data and a 1 km resolution gridded hourly rainfall dataset for Great Britain: CEH-GEAR1hr. Journal Of Hydrology, 564, 930-943. doi: 10.1016/j.jhydrol.2018.07.034

Li, D., Bou-Zeid, E., Baeck, M., Jessup, S., & Smith, J. (2013). Modeling Land Surface Processes and Heavy Rainfall in Urban Environments: Sensitivity to Urban Surface Representations. Journal Of Hydrometeorology, 14(4), 1098-1118. doi: 10.1175/jhm-d-12-0154.1

Li, Y., Grimaldi, S., Walker, J., & Pauwels, V. (2016). Application of Remote Sensing Data to Constrain Operational Rainfall-Driven Flood Forecasting: A Review. Remote Sensing, 8(6), 456. doi: 10.3390/rs8060456

Licznar, P., Łomotowski, J., & Rupp, D. E. (2011). Random cascade driven rainfall disaggregation for urban hydrology: An evaluation of six models and a new generator. Atmospheric Research, 99(3), 563-578. doi:doi.org/10.1016/j.atmosres.2010.12.014

Lin, C., Chen, W., Chang, P., & Sheng, Y. (2011). Impact of the Urban Heat Island Effect on Precipitation over a Complex Geographic Environment in Northern Taiwan. Journal Of Applied Meteorology And Climatology, 50(2), 339-353. doi: 10.1175/2010jamc2504.1

Lin, R., Zhou, T., & Qian, Y. (2014). Evaluation of global monsoon precipitation changes based on five reanalysis datasets. J Journal of Climate, 27(3), 1271-1289.

Litta, A. J., Mary Ididcula, S., Mohanty, U. C., & Kiran Prasad, S. (2012). Comparison of Thunderstorm Simulations from WRF-NMM and WRF-ARW Models over East Indian Region. The Scientific World Journal. 2012, 20. doi:10.1100/2012/951870

Liu, C., Ikeda, K., Thompson, G., Rasmussen, R., & Dudhia, J. (2011). High-Resolution Simulations of Wintertime Precipitation in the Colorado Headwaters Region: Sensitivity to Physics Parameterizations. Monthly Weather Review, 139(11), 3533-3553. doi: 10.1175/mwr-d-11-00009.1

Liu, J., & Niyogi, D. (2019). Meta-analysis of urbanization impact on rainfall modification. Scientific reports, 9(1), 7301-7301. doi:10.1038/s41598-019-42494-2

Liu, J., Bray, M., & Han, D. (2012). Sensitivity of the Weather Research and Forecasting (WRF) model to downscaling ratios and storm types in rainfall simulation. Hydrological Processes, 26(20), 3012-3031. doi:10.1002/hyp.8247

Looper, J. and Vieux, B., 2012. An assessment of distributed flash flood forecasting accuracy using radar and rain gauge input for a physics-based distributed hydrologic model. Journal of Hydrology, 412-413, pp.114-132.

Lu, C., Yuan, H., Schwartz, B. and Benjamin, S., 2007. Short-Range Numerical Weather Prediction Using Time-Lagged Ensembles. Weather and Forecasting, 22(3), pp.580-595.

Lutoff, C., Creutin, J.-D., Ruin, I., & Duvillard, S. (2018). 1 - Mobility Exposure Scales of Analysis in the Face of Flash Floods. In C. Lutoff & S. Durand (Eds.), Mobilities Facing Hydrometeorological Extreme Events 1 (pp. 1-22): Elsevier.

Ma, M., He, B., Wan, J., Jia, P., Guo, X., Gao, L., Maguire, L. and Hong, Y., 2018. Characterizing the Flash Flooding Risks from 2011 to 2016 over China. Water, 10(6), p.704.

Madala, S., Satyanarayana, A. N. V., & Rao, T. N. (2014). Performance evaluation of PBL and cumulus parameterization schemes of WRF ARW model in simulating severe thunderstorm events over Gadanki MST radar facility — Case study. Atmospheric Research, 139, 1-17. doi:10.1016/j.atmosres.2013.12.017

Maggioni, V., & Massari, C. (2018). On the performance of satellite precipitation products in riverine flood modeling: A review. Journal of Hydrology, 558, 214-224. doi:10.1016/j.jhydrol.2018.01.039

Maksimović, Č., Prodanović, D., Boonya-Aroonnet, S., Leitão, J. P., Djordjević, S., & Allitt, R. (2009). Overland flow and pathway analysis for modelling of urban pluvial flooding. Journal of Hydraulic Research, 47(4), 512-523. doi:10.1080/00221686.2009.9522027

Manz, B., Buytaert, W., Zulkafli, Z., Lavado, W., Willems, B., Robles, L. and Rodríguez-Sánchez, J., 2016. High-resolution satellite-gauge merged precipitation climatologies of the Tropical Andes. Journal of Geophysical Research: Atmospheres, 121(3), pp.1190-1207.

Marchi, L., Borga, M., Preciso, E., & Gaume, E. (2010). Characterisation of selected extreme flash floods in Europe and implications for flood risk management. Journal of Hydrology, 394(1), 118-133. doi:10.1016/j.jhydrol.2010.07.017

Marsh, T., 2008. A hydrological overview of the summer 2007 floods in England and Wales. Weather, 63(9), pp.274-279.

Marsh, T. J., & Hannaford, J. (2007). The summer 2007 floods in England and Wales–a hydrological appraisal. NERC/Centre for Ecology & Hydrology.

Marsh, T. J., & Hannaford, J. (2008). Hydrometric Register. Hydrological Data UK Series.

Core.ac.uk. 2020. Hydrological Summary For The UK: July 2007. Available at: https://core.ac.uk/reader/59098. Accessed August 2019

Martilli, A., Clappier, A. and Rotach, M., 2002. An Urban Surface Exchange Parameterisation for Mesoscale Models. Boundary-Layer Meteorology, 104(2), pp.261-304.

Mason, D. C., Schumann, G. J. P., & Bates, P. D. (2010). Data Utilization in Flood Inundation Modelling. Flood Risk Science and Management (pp. 209-233). Wiley-Blackwell.

Maw, K. and Min, J., 2017. Impacts of Microphysics Schemes and Topography on the Prediction of the Heavy Rainfall in Western Myanmar Associated with Tropical Cyclone ROANU (2016). Advances in Meteorology, 2017, pp.1-22.

McKee, J. L., & Binns, A. D. (2016). A review of gauge–radar merging methods for quantitative precipitation estimation in hydrology. Canadian Water Resources Journal / Revue canadienne des ressources hydriques, 41(1-2), 186-203. doi:10.1080/07011784.2015.1064786

Mendoza, P., Rajagopalan, B., Clark, M., Ikeda, K., & Rasmussen, R. (2015). Statistical Postprocessing of High-Resolution Regional Climate Model Output. Monthly Weather Review, 143, 1533-1553. doi:10.1175/MWR-D-14-00159.1

Mercader-Carbó, J., Codina, B., Sairouni, A., & Cunillera, J. (2010). Results of the meteorological model WRF-ARW over Catalonia using different parametrizations of convection and cloud microphysics. Tethys Journal of Weather and Climate of the Western Mediterranean, 7, 75-86. doi:10.3369/tethys.2010.7.07

Merz, R. and Blöschl, G., 2008. Flood frequency hydrology: 1. Temporal, spatial, and causal expansion of information. Water Resources Research, 44(8).

Metcalfe, P., Beven, K., & Freer, J. (2015). Dynamic TOPMODEL: A new implementation in R and its sensitivity to time and space steps. Environmental Modelling & Software, 72, 155-172. doi:10.1016/j.envsoft.2015.06.010

Met Office (2003). Met Office Rain Radar Data from the NIMROD System. NCAR British Atmospheric Data Centre.

Met Office (Producer). (2003). Met Office Rain Radar Data from the NIMROD System. Available at http://catalogue.ceda.ac.uk/uuid/82adec1f896af6169112d09cc1174499. Accessed July 2019

Met-Office (1948). The weather of 1947 in Great Britain. Weather 3(1), 27-30. doi:10.1002/j.1477-8696.1948.tb00856.x

Met Office. (2019). The Met Office ensemble system. Weather Science. Available at https://www.metoffice.gov.uk/research/weather/ensemble-forecasting/mogreps. Accessed April 2019

Met Office (2020). Record breaking rainfall. Available at https://www.metoffice.gov.uk/about-us/press-office/news/weather-and-climate/2020/2020-winter-february-stats. Accessed March 2019

Miller, J. D., & Hutchins, M. (2017). The impacts of urbanisation and climate change on urban flooding and urban water quality: A review of the evidence concerning the United Kingdom. Journal of Hydrology: Regional Studies, 12, 345-362. doi:10.1016/j.ejrh.2017.06.006

Mittermaier, M. P. (2007). Improving short-range high-resolution model precipitation forecast skill using time-lagged ensembles. *Q.J.R. Meteorol. Soc., 133*(627), 1487-1500. doi:10.1002/qj.135

Mlawer, E. J., Taubman, S. J., Brown, P. D., Iacono, M. J., & Clough, S. A. (1997). Radiative transfer for inhomogeneous atmospheres: RRTM, a validated correlated-k model for the longwave. *J. Geophys. Res., 102*(D14), 16663-16682. doi:10.1029/97jd00237

Moeng, C.-H., Dudhia, J., Klemp, J., & Sullivan, P. (2007). Examining Two-Way Grid Nesting for Large Eddy Simulation of the PBL Using the WRF Model. *Monthly Weather Review, 135*, 2295-2311. doi:10.1175/MWR3406.1

Monin, A. S., & Obukhov, A. M. (1954). Basic laws of turbulent mixing in the surface layer of the atmosphere. *Contributions of the Geophysical Institute of the Slovak Academy of Sciences, 24*(151), 163–187. doi:10.1155/2014/451578

Morini, E., Touchaei, A., Castellani, B., Rossi, F., & Cotana, F. (2016). The Impact of Albedo Increase to Mitigate the Urban Heat Island in Terni (Italy) Using the WRF Model. *Sustainability, 8*, 999. doi:10.3390/su8100999

Morrison, H. (2010). *An overview of cloud and precipitation microphysics and its parameterization in models*. Retrieved 12 July 2019, from http://www2.mmm.ucar.edu/wrf/users/workshops/WS2010/presentations/Lectures/morrison_wrf_workshop_2010_v2.pdf.

Morrison, H., Thompson, G., & Tatarskii, V. (2009). Impact of Cloud Microphysics on the Development of Trailing Stratiform Precipitation in a Simulated Squall Line: Comparison of One- and Two-Moment Schemes. *Mon. Wea. Rev., 137*(3), 991-1007. doi:10.1175/2008mwr2556.1

Müller, H., & Haberlandt, U. (2015). Temporal Rainfall Disaggregation with a Cascade Model: From Single-Station Disaggregation to Spatial Rainfall. *Journal of Hydrologic Engineering, 20*(11), 04015026. doi:10.1061/(ASCE)HE.1943-5584.0001195

Müller-Thomy, H., & Sikorska-Senoner, A. E. (2019). Does the complexity in temporal precipitation disaggregation matter for a lumped hydrological model? *Hydrological Sciences Journal, 64*(12), 1453-1471. doi:10.1080/02626667.2019.1638926

NASA/Goddard Space Flight Center (2002). *NASA Satellite Confirms Urban Heat Islands Increase Rainfall Around Cities*. Retrieved from https://www.sciencedaily.com/releases/2002/06/020619074019.htm

Nash, J. E., & Sutcliffe, J. V. (1970). River flow forecasting through conceptual models part I—A discussion of principles. *Journal of Hydrology, 10*(3), 282-290.

National River Flow, A. (2014). *Integrated Hydrological Units of the United Kingdom: Hydrometric Areas with Coastline*, NERC Environmental Information Data Centre. Retrieved from: https://doi.org/10.5285/1957166d-7523-44f4-b279-aa5314163237

National Research Council. (2012). *Urban Meteorology: Forecasting, Monitoring, and Meeting Users' Needs*. Washington, DC: The National Academies Press.

National River Flow Archive. (2015). *Flood Estimation Handbook Catchment Descriptors*. Retrieved 28 September 2018, from https://nrfa.ceh.ac.uk/feh-catchment-descriptors

NCAR. (2008). *WRF-NMM Online Tutorial*. Retrieved 25 May 2016, from https://dtcenter.org/wrf-nmm/users/OnLineTutorial/NMM/WRF-NMM/nmm_real_1dom.php.

NCAR. (2019). *User's Guide for the Advanced Research WRF (ARW) Modeling System Version 4.0*. National Center for Atmospheric Research. Mesoscale & Microscale Meteorology Division. Retrieved 11 July 2019 from https://www2.mmm.ucar.edu/wrf/users/docs/user_guide_V4/WRFUsersGuide.pdf

NCEP (2000). *NCEP FNL Operational Model Global Tropospheric Analyses, continuing from July 1999*. Boulder, CO, Research Data Archive at the National Center for Atmospheric Research, Computational and Information Systems Laboratory. Retrieved from: https://doi.org/10.5065/D6M043C6

Nijssen, B., & Lettenmaier, D. P. (2004). Effect of precipitation sampling error on simulated hydrological fluxes and states: Anticipating the Global Precipitation Measurement satellites. *J. Geophys., 109*(D2). doi:10.1029/2003jd003497

Nikolopoulos, E. I., Anagnostou, E. N., & Borga, M. (2013). Using High-Resolution Satellite Rainfall Products to Simulate a Major Flash Flood Event in Northern Italy. *J. Hydrometeor., 14*(1), 171-185. doi:10.1175/jhm-d-12-09.1

Niyogi, D., Lei, M., Kishtawal, C., Schmid, P., & Shepherd, M. (2017). Urbanization Impacts on the Summer Heavy Rainfall Climatology over the Eastern United States. *Earth Interact., 21*(5), 1-17. doi:10.1175/ei-d-15-0045.1

NOAA. (2019). *Severe Weather 101 - Floods*. Retrieved from https://www.nssl.noaa.gov/education/svrwx101/floods/types/

Ochoa-Rodriguez, S., Wang, L.-P., Gires, A., Pina, R. D., Reinoso-Rondinel, R., Bruni, G., . . . van Assel, J. (2015). Impact of spatial and temporal resolution of rainfall inputs on urban hydrodynamic modelling outputs: A multi-catchment investigation. *Journal of Hydrology, 531*, 389-407. doi:10.1016/j.jhydrol.2015.05.035

Ochoa-Rodriguez, S., Wang, L.-P., Willems, P., & Onof, C. (2019). A Review of Radar-Rain Gauge Data Merging Methods and Their Potential for Urban Hydrological Applications. *Water Resour. Res., 55*(8), 6356-6391. doi:10.1029/2018wr023332

Pal, S., Chang, H.-I., Castro, C. L., & Dominguez, F. (2019). Credibility of Convection-Permitting Modeling to Improve Seasonal Precipitation Forecasting in the Southwestern United States. *Frontiers in Earth Science, 7*(11). doi:10.3389/feart.2019.00011

Palmer, T. (2012). Prediction of hydro-meteorological, meteorological and climatological hazards. Retrieved from https://assets.publishing.service.gov.uk/government/uploads/system/uploads/attachment_data/file/286649/12-1302-prediction-hydro-meteorological-climatological-hazards.pdf

Pappenberger, F., Scipal, K., & Buizza, R. (2008). Hydrological aspects of meteorological verification. *Atmosph. Sci. Lett., 9*(2), 43-52. doi:10.1002/asl.171

Paprotny, D., Sebastian, A., Morales-Nápoles, O., & Jonkman, S. N. (2018). Trends in flood losses in Europe over the past 150 years. *Nature Communications, 9*(1), 1985. doi:10.1038/s41467-018-04253-1

Patel, P., Ghosh, S., Kaginalkar, A., Islam, S., & Karmakar, S. (2019). Performance evaluation of WRF for extreme flood forecasts in a coastal urban environment. *Atmospheric Research, 223*, 39-48. doi:10.1016/j.atmosres.2019.03.005

Pei, L., Moore, N., Zhong, S., Luo, L., Hyndman, D. W., Heilman, W. E., & Gao, Z. (2014). WRF Model Sensitivity to Land Surface Model and Cumulus Parameterization under Short-Term Climate Extremes over the Southern Great Plains of the United States. *J. Climate, 27*(20), 7703-7724. doi:10.1175/jcli-d-14-00015.1

Peleg, N., & Morin, E. (2014). Stochastic convective rain-field simulation using a high-resolution synoptically conditioned weather generator (HiReS-WG). *Water Resour. Res., 50*(3), 2124-2139. doi:10.1002/2013wr014836

Pennelly, C., Reuter, G., & Flesch, T. (2014). Verification of the WRF model for simulating heavy precipitation in Alberta. *Atmospheric Research, 135-136*, 172-192. doi:10.1016/j.atmosres.2013.09.004

Peters, N. E., Freer, J., & Beven, K. (2003). Modelling hydrologic responses in a small forested catchment (Panola Mountain, Georgia, USA): a comparison of the original and a new dynamic TOPMODEL. *Hydrological Processes, 17*(2), 345-362.

Pidcock, R. (2014). How much flooding is in the UK's future? a Look at the IPCC report. https://www.carbonbrief.org/how-much-flooding-is-in-the-uks-future-a-look-at-the-ipcc-report

Pieri, A. B., Hardenberg, J. v., Parodi, A., & Provenzale, A. (2015). Sensitivity of Precipitation Statistics to Resolution, Microphysics, and Convective Parameterization: A Case Study with the High-Resolution WRF Climate Model over Europe. *J. Hydrometeor., 16*(4), 1857-1872. doi:10.1175/jhm-d-14-0221.1

Pina, R. D., Ochoa-Rodriguez, S., Simoes, N. E., Mijic, A., Marques, A. S., & Maksimovic, C. (2016). Semi- vs. Fully-Distributed Urban Stormwater Models: Model Set Up and Comparison with Two Real Case Studies. *Water, 8*(2), 20. doi:10.3390/w8020058

Pitt, M. (2008). *The Pitt Review: Learning lessons from the 2007 floods*: Pitt Review.

Plant, R. (2014). "Microphysics Parameterization." Retrieved 17 June 2019, from http://www.met.reading.ac.uk/~sws00rsp/teaching/nanjing/microphysics.pdf.

Pregnolato, M., Ford, A., Wilkinson, S. M., & Dawson, R. J. (2017). The impact of flooding on road transport: A depth-disruption function. *Transportation Research Part D: Transport and Environment, 55*, 67-81. doi:10.1016/j.trd.2017.06.020

Prein, A. F., Gobiet, A., Suklitsch, M., Truhetz, H., Awan, N. K., Keuler, K., & Georgievski, G. (2013). Added value of convection permitting seasonal simulations. *Climate Dynamics, 41*(9), 2655-2677. doi:10.1007/s00382-013-1744-6

Prein, A. F., Langhans, W., Fosser, G., Ferrone, A., Ban, N., Goergen, K., . . . Leung, R. (2015). A review on regional convection-permitting climate modeling: Demonstrations, prospects, and challenges. *Reviews of geophysics (Washington, D.C. : 1985), 53*(2), 323-361. doi:10.1002/2014RG000475

Prein, A. F., Rasmussen, R. M., Ikeda, K., Liu, C., Clark, M. P., & Holland, G. J. (2016). The future intensification of hourly precipitation extremes. *Nature Climate Change, 7*, 48. doi:10.1038/nclimate3168

Prior, J., & Beswick, M. (2008). The exceptional rainfall of 20 July 2007. 63, 7. https://www.metlink.org/wp-content/uploads/2013/11/articles/rainfall_20july07.pdf

Prudhomme, C., Reynard, N., & Crooks, S. J. H. p. (2002). Downscaling of global climate models for flood frequency analysis: where are we now?*, Hydrol. Process., 16*(6), 1137-1150.

Qiu, Q., Liu, J., Tian, J., Jiao, Y., Li, C., Wang, W., & Yu, F. (2020). Evaluation of the Radar QPE and Rain Gauge Data Merging Methods in Northern China. *Remote Sensing , 12*(3), 363. doi: 10.3390/rs12030363

Quinn, P. F., Beven, K. J., & Lamb, R. (1995). The in(a/tan/β) index: How to calculate it and how to use it within the topmodel framework. *Hydrol. Process., 9*(2), 161-182. doi:10.1002/hyp.3360090204

R. Douglas-Mankin, K., Maski, D., A. Janssen, K., Tuppad, P., & M. Pierzynski, G. (2010). Modeling Nutrient Runoff Yields from Combined In-Field Crop Management Practices Using SWAT. *Transactions of the ASABE, 53*(5), 1557-1568. doi:10.13031/2013.34914

Rajeevan, M., Kesarkar, A., Thampi, S. B., Rao, T. N., Radhakrishna, B., & Rajasekhar, M. (2010). Sensitivity of WRF cloud microphysics to simulations of a severe thunderstorm event over Southeast India. *Ann. Geophys., 28*(2), 603-619. doi:10.5194/angeo-28-603-2010

Ramachandra, T., & Kumar, U. (2008). Wetlands of greater Bangalore, India: automatic delineation through pattern classifiers. *J Electronic Green Journal, 1*(26). doi:10.5070/G312610729

Ramsbottom, D., Sayers, P., & Panzeri, M. (2012). Climate Change Risk Assessment for the Floods and Coastal Erosion Sector. Retrieved from http://randd.defra.gov.uk/Document.aspx?Document=10075_CCRAfortheFloodsandCoastalErosionSector16July2012.pdf

Rasmussen, K. L., Prein, A. F., Rasmussen, R. M., Ikeda, K., & Liu, C. (2017). Changes in the convective population and thermodynamic environments in convection-permitting regional climate simulations over the United States. *Climate Dynamics*, doi:10.1007/s00382-017-4000-7

Rathjens, H., Bieger, K., Chaubey, I., Arnold, J. G., Allen, P. M., Srinivasan, R., . . . Volk, M. (2016). Delineating floodplain and upland areas for hydrologic models: a comparison of methods. *Hydrol. Process., 30*(23), 4367-4383. doi:10.1002/hyp.10918

Remesan, R., Bellerby, T., Holman, I., & Frostick, L. (2015). WRF model sensitivity to choice of parameterization: a study of the 'York Flood 1999'. *Theoretical and Applied Climatology, Theoretical and applied climatology, 122*(1), 229-247. doi:10.1007/s00704-014-1282-0

Robinson, E. L., Blyth, E., Clark, D. B., Comyn-Platt, E., Finch, J., & Rudd, A. C. (2016). *Climate hydrology and ecology research support system potential evapotranspiration dataset for Great Britain (1961-2015) [CHESS-PE]*. Retrieved from: https://doi.org/10.5285/8baf805d-39ce-4dac-b224-c926ada353b7

Rodríguez-Rincón, J. P., Pedrozo-Acuña, A., & Breña-Naranjo, J. A. (2015). Propagation of hydro-meteorological uncertainty in a model cascade framework to inundation prediction. *Hydrol. Earth Syst. Sci., 19*(7), 2981-2998. doi:10.5194/hess-19-2981-2015

Ronda, R. J., Steeneveld, G. J., Heusinkveld, B. G., Attema, J. J., & Holtslag, A. A. M. (2017). Urban Finescale Forecasting Reveals Weather Conditions with Unprecedented Detail. *Bull. Amer. Meteor. Soc., 98*(12), 2675-2688. doi:10.1175/bams-d-16-0297.1

Roux, H., Amengual, A., Romero, R., Bladé, E., & Sanz-Ramos, M. (2020). Evaluation of two hydrometeorological ensemble strategies for flash-flood forecasting over a catchment of the eastern Pyrenees. *Nat. Hazards Earth Syst. Sci., 20*(2), 425-450. doi:10.5194/nhess-20-425-2020

Roy, A., Thakur, P. K., Pokhriyal, N., Aggarwal, S. P., Nikam, B. R., Garg, V., . . . Choksey, A. (2018). *Intercomparison of different rainfall products and validation of WRF modelled rainfall estimation in N-W Himalaya during monsoon period.* Paper presented at the ISPRS TC V Mid-term Symposium “Geospatial Technology – Pixel to People, India.

Rummukainen, M. (2010). State-of-the-art with regional climate models. *Wiley Interdisciplinary Reviews: Climate Change, 1*(1), 82-96. doi:10.1002/wcc.8

Salamanca, F., Georgescu, M., Mahalov, A., Moustaoui, M., & Wang, M. (2014). Anthropogenic heating of the urban environment due to air conditioning. *J. Geophys. Res. Atmos., 119*(10), 5949-5965. doi:10.1002/2013jd021225

Salamanca, F., Martilli, A. J. T., & Climatology, A. (2009). A new Building Energy Model coupled with an Urban Canopy Parameterization for urban climate simulations—part II. Validation with one dimension off-line simulations. *Theor. Appl. Climatol., 99*(3), 345. doi:10.1007/s00704-009-0143-8

Salamanca, F., Martilli, A., Tewari, M., & Chen, F. (2011). A Study of the Urban Boundary Layer Using Different Urban Parameterizations and High-Resolution Urban Canopy Parameters with WRF. *J. Appl. Meteor. Climatol., 50*(5), 1107-1128. doi:10.1175/2010jamc2538.1

Salvadore, E., Bronders, J., & Batelaan, O. (2015). Hydrological modelling of urbanized catchments: A review and future directions. *Journal of Hydrology, 529*, 62-81. doi:10.1016/j.jhydrol.2015.06.028

Sarmiento, D. P., Davis, K. J., Deng, A. J., Lauvaux, T., Brewer, A., & Hardesty, M. (2017). A comprehensive assessment of land surface-atmosphere interactions in a WRF/Urban modeling system for Indianapolis, IN. *Elementa-Science of the Anthropocene, 5*, 22. doi:10.1525/elementa.132

Savvidou, E., Efstratiadis, A., Koussis, A. D., Koukouvinos, A., & Skarlatos, D. (2018). The Curve Number Concept as a Driver for Delineating Hydrological Response Units. *Water, 10*(2), 194. doi:10.3390/w10020194

Seed, A., & Austin, G. L. (1990). Variability of summer Florida rainfall and its significance for the estimation of rainfall by gages, radar, and satellite. *J. Geophys. Res., 95*(D3), 2207-2215. doi:10.1029/JD095iD03p02207

Şen, Z. (2018). Climate Change Impact on Floods. In *Flood Modeling, Prediction and Mitigation* (pp. 337-379). Cham: Springer International Publishing.

Sene, K. (2013). Precipitation Measurement. In *Flash Floods: Forecasting and Warning* (pp. 33-70). Dordrecht: Springer Netherlands.

Sharif, H. O., Yates, D., Roberts, R., & Mueller, C. (2006). The Use of an Automated Nowcasting System to Forecast Flash Floods in an Urban Watershed. *J. Hydrometeor., 7*(1), 190-202. doi:10.1175/jhm482.1

Sharma, A., Fernando, H. J. S., Hamlet, A. F., Hellmann, J. J., Barlage, M., & Chen, F. (2017). Urban meteorological modeling using WRF: a sensitivity study. *Int. J. Climatol., 37*(4), 1885-1900. doi:10.1002/joc.4819

Sharma, A., Wasko, C., & Lettenmaier, D. P. (2018). If Precipitation Extremes Are Increasing, Why Aren't Floods?*, Water Resour. Res, 54*(11), 8545-8551. doi:10.1029/2018wr023749

Sheng, J., & Wilson, J. P. (2009). Watershed urbanization and changing flood behavior across the Los Angeles metropolitan region. *Natural Hazards, 48*(1), 41-57. doi:10.1007/s11069-008-9241-7

Shepherd, J. M. (2005). A review of current investigations of urban-induced rainfall and recommendations for the future. *J Earth Interactions, 9*(12), 1-27. doi:10.1175/EI156.1

Shepherd, J. M., Pierce, H., & Negri, A. J. (2002). Rainfall modification by major urban areas: Observations from spaceborne rain radar on the TRMM satellite. *Journal of Applied Meteorology, 41*(7), 689-701. doi:10.1175/1520-0450(2002)041<0689:RMBMUA>2.0.CO;2

Shrestha, P. K., Shrestha, S., & Ninsawat, S. (2019b). How significant is sub-daily variability of rainfall for hydrological modelling of floods? A satellite based approach to sub-daily downscaling of gauged rainfall. *Meteorological Applications, 26*(2), 288-299. doi:10.1002/met.1762

Shuster, W. D., Bonta, J., Thurston, H., Warnemuende, E., & Smith, D. (2005). Impacts of impervious surface on watershed hydrology: A review. *Urban Water Journal , 2*(4), 263-275. doi:10.1080/15730620500386529

Sikorska, A. E., Viviroli, D., & Seibert, J. (2018). Effective precipitation duration for runoff peaks based on catchment modelling. *Journal of Hydrology, 556*, 510-522. doi:10.1016/j.jhydrol.2017.11.028

Silvestro, F., Rebora, N., Rossi, L., Dolia, D., Gabellani, S., Pignone, F., . . . Masciulli, C. (2016). What if the 25 October 2011 event that struck Cinque Terre (Liguria) had happened in Genoa, Italy? Flooding scenarios, hazard mapping and damage estimation. *Nat. Hazards Earth Syst. Sci., 16*(8), 1737-1753. doi:10.5194/nhess-16-1737-2016

Singh, V. P., & Frevert, D. K. (2002). *Mathematical models of large watershed hydrology*: Water Resources Publication.

Sitterson, J., Knightes, C., Parmar, R., Wolfe, K., Muche, M., & Avant, B. (2018). An Overview of Rainfall-Runoff Model Types. Retrieved from U.S.A.: https://cfpub.epa.gov/si/si_public_record_report.cfm?dirEntryId=339328&Lab=NERL

Sivasubramaniam, K., Sharma, A., & Alfredsen, K. (2019). Merging radar and gauge information within a dynamical model combination framework for precipitation estimation in cold climates. *Environmental Modelling & Software, 119*, 99-110. doi:10.1016/j.envsoft.2019.05.013

Skamarock, W. C., Klemp, J. B., Dudhia, J., Gill, D. O., Liu, Z., Berner, J., . . . Huang, X.-Y. (2019). A Description of the Advanced Research WRF Version 4. *NCAR Technical Notes*(NCAR/TN-556+STR), 145.

Smid, M., & Costa, A. C. (2018). Climate projections and downscaling techniques: a discussion for impact studies in urban systems. *International Journal of Urban Sciences, 22*(3), 277-307. doi:10.1080/12265934.2017.1409132

Smith, J. A., Baeck, M. L., Meierdiercks, K. L., Miller, A. J., & Krajewski, W. F. (2007). Radar rainfall estimation for flash flood forecasting in small urban watersheds. *Advances in Water Resources, 30*(10), 2087-2097. doi:10.1016/j.advwatres.2006.09.007

Smith, J. A., Baeck, M. L., Meierdiercks, K. L., Nelson, P. A., Miller, A. J., & Holland, E. J. (2005). Field studies of the storm event hydrologic response in an urbanizing watershed. *Water Resour. Res., 41*(10). doi:10.1029/2004WR003712.

Smith, K. A., Wilby, R. L., Broderick, C., Prudhomme, C., Matthews, T., Harrigan, S., & Murphy, C. (2018). Navigating Cascades of Uncertainty — As Easy as ABC? Not Quite…. *Journal of Extreme Events, 05*(01), 1850007. doi:10.1142/S2345737618500070

Smith, P., Pappenberger, F., Wetterhall, F., del Pozo, J. T., Krzeminski, B., Salamon, P., . . . Baugh, C. (2016). On the operational implementation of the European Flood Awareness System (EFAS). In *Flood Forecasting* (pp. 313-348): Elsevier.

Soille, P. (2004). Optimal removal of spurious pits in grid digital elevation models. *Water Resour. Res., 40*(12). doi:10.1029/2004wr003060

Speight, L., Cole, S. J., Moore, R. J., Pierce, C., Wright, B., Golding, B., . . . Ghimire, S. (2018). Developing surface water flood forecasting capabilities in Scotland: an operational pilot for the 2014 Commonwealth Games in Glasgow. *Journal of Flood Risk Management, 11*, S884-S901. doi:10.1111/jfr3.12281

Stallins, J. A., Carpenter, J., Bentley, M. L., Ashley, W. S., & Mulholland, J. A. (2013). Weekend–weekday aerosols and geographic variability in cloud-to-ground lightning for the urban region of Atlanta, Georgia, USA. *Regional Environmental Change, 13*(1), 137-151. doi:10.1007/s10113-012-0327-0

Stensrud, D. J. (2012). *An Overview of Convection Parameterization*. Retrieved 2 July 2019, from http://www2.mmm.ucar.edu/wrf/users/workshops/WS2012/ppts/lecture1.pdf.

Stuart-Menteth, A. (2007). *U.K. Summer 2007 Floods*. I. Risk Management Solutions. Retrieved from https://forms2.rms.com/rs/729-DJX-565/images/fl_2007_uk_summer_floods.pdf

Summers, M. (2012, 28 June 2012). *Roads turn to rivers in a flash as thunderstorms hit region*. The Northern Echo. Retrieved from https://www.thenorthernecho.co.uk/sport/horseracing/9788748.roads-turn-to-rivers-in-a-flash-as-thunderstorms-hit-region/

Sun, W., Sun, Y., Li, X., Wang, T., Wang, Y., Qiu, Q., & Deng, Z. (2018). Evaluation and Correction of GPM IMERG Precipitation Products over the Capital Circle in Northeast China at Multiple Spatiotemporal Scales. *Advances in Meteorology*. *2018*, 14. doi:10.1155/2018/4714173

Surminski, S., & Eldridge, J. (2014). Flood insurance in England – an assessment of the current and newly proposed insurance scheme in the context of rising flood risk. Retrieved from http://www.lse.ac.uk/GranthamInstitute/wp-content/uploads/2014/02/WP144-Flood-insurance-in-England.pdf

Svetlana, D., Radovan, D., & Ján, D. (2015). The Economic Impact of Floods and their Importance in Different Regions of the World with Emphasis on Europe. *Procedia Economics and Finance, 34*, 649-655. doi:10.1016/S2212-5671(15)01681-0

Syed, K. H., Goodrich, D. C., Myers, D. E., & Sorooshian, S. (2003). Spatial characteristics of thunderstorm rainfall fields and their relation to runoff. *Journal of Hydrology, 271*(1-4), 1-21.

Tanouchi, H., Olsson, J., Lindström, G., Kawamura, A., & Amaguchi, H. (2019). Improving Urban Runoff in Multi-Basin Hydrological Simulation by the HYPE Model Using EEA Urban Atlas: A Case Study in the Sege River Basin, Sweden. *Hydrology, 6*(1), 28. doi:10.3390/hydrology6010028

Teshager, A. D., Gassman, P. W., Secchi, S., Schoof, J. T., & Misgna, G. (2016). Modeling Agricultural Watersheds with the Soil and Water Assessment Tool (SWAT):

Calibration and Validation with a Novel Procedure for Spatially Explicit HRUs. *Environmental management, 57*(4), 894-911. doi:10.1007/s00267-015-0636-4

Tewkesbury Museum. (2007). *Church Street Tewkesbury 2007 Flood*. Retrieved from: https://www.tewkesburymuseum.org/the-collection/the-image-collection/2007-flood/

Thompson, G., Field, P. R., Rasmussen, R. M., & Hall, W. D. (2008). Explicit Forecasts of Winter Precipitation Using an Improved Bulk Microphysics Scheme. Part II: Implementation of a New Snow Parameterization. *Mon. Wea. Rev., 136*(12), 5095-5115. doi:10.1175/2008mwr2387.1

Tomasi, E., Giovannini, L., Zardi, D., & Franceschi, M. d. (2017). Optimization of Noah and Noah_MP WRF Land Surface Schemes in Snow-Melting Conditions over Complex Terrain. *Mon. Wea. Rev., 145*(12), 4727-4745. doi:10.1175/mwr-d-16-0408.1

Ulmer, F.-G., & Balss, U. (2016). Spin-up time research on the weather research and forecasting model for atmospheric delay mitigations of electromagnetic waves. *Journal of Applied Remote Sensing, 1-12*, 12. doi:10.1117/1.JRS.10.016027

UNESCO. (2017). Hydro-meteorological hazards. Disaster Risk Reduction. Retrieved from http://www.unesco.org/new/en/natural-sciences/special-themes/disaster-risk-reduction/natural-hazards/hydro-meteorological-hazards/

USGS. (2020). What are the two types of floods? Water. Retrieved from https://www.usgs.gov/faqs/what-are-two-types-floods?qt-news_science_products=0#qt-news_science_products

Varlas, G., Anagnostou, M., Spyrou, C., Papadopoulos, A., Kalogiros, J., Mentzafou, A., . . . Katsafados, P. (2018). A Multi-Platform Hydrometeorological Analysis of the Flash Flood Event of 15 November 2017 in Attica, Greece. *Remote Sensing, 11*, 45. doi:10.3390/rs11010045

Vergara, H., Hong, Y., Gourley, J. J., Anagnostou, E. N., Maggioni, V., Stampoulis, D., & Kirstetter, P.-E. (2014). Effects of resolution of satellite-based rainfall estimates on hydrologic modeling skill at different scales. *Journal of Hydrometeorology, 15*(2), 593-613. doi:10.1175/JHM-D-12-0113.1

Vincendon, B., & Amengual, A. (2017). Flash-flood forecasting in two Spanish Mediterranean catchments: a comparison of distinct hydrometeorological ensemble prediction strategies. *Hydrol. Earth Syst. Sci. Discuss., 2017*, 1-38. doi:10.5194/hess-2017-427

Vionnet, V., Fortin, V., Gaborit, E., Roy, G., Abrahamowicz, M., Gasset, N., & Pomeroy, J. W. (2019). High-resolution hydrometeorological modelling of the June 2013 flood in southern Alberta, Canada. *Hydrol. Earth Syst. Sci. Discuss., 2019*, 1-36. doi:10.5194/hess-2019-152

Vu, M. T., Raghavan, V. S., & Liong, S. Y. (2015). Ensemble Climate Projection for Hydro-Meteorological Drought over a river basin in Central Highland, Vietnam. *KSCE Journal of Civil Engineering, 19*(2), 427-433. doi:10.1007/s12205-015-0506-x

Wan, H., Zhong, Z., Yang, X., & Li, X. (2015). Ensembles to model the impact of urbanization for a summertime rainstorm process in Yangtze River Delta, China. *Met. Apps, 22*(1), 105-112. doi:10.1002/met.1360

Wang, H., & Chen, Y. (2019). Identifying Key Hydrological Processes in Highly Urbanized Watersheds for Flood Forecasting with a Distributed Hydrological Model. *Water, 11*(8), 1641. doi:10.3390/w11081641

Wang, W. and D. O. Gill. (2012). "WRF nesting." Retrieved 16 July 2019, from https://ruc.noaa.gov/wrf/wrf-chem/wrf_tutorial_2012_brazil/WRF_nesting.pdf.

Wee, T.-K., Kuo, Y.-H., Lee, D.-K., Liu, Z., Wang, W., & Chen, S.-Y. (2012). Two Overlooked Biases of the Advanced Research WRF (ARW) Model in Geopotential Height and Temperature. *Mon. Wea. Rev., 140*(12), 3907-3918. doi:10.1175/mwr-d-12-00045.1

Wehbe, Y., Temimi, M., Weston, M., Chaouch, N., Branch, O., Schwitalla, T., . . . Al Mandous, A. (2019). Analysis of an extreme weather event in a hyper-arid region using WRF-Hydro coupling, station, and satellite data. *Nat. Hazards Earth Syst. Sci., 19*(6), 1129-1149. doi:10.5194/nhess-19-1129-2019

Whitaker, J. S., & Hamill, T. M. (2002). Ensemble Data Assimilation without Perturbed Observations. *Mon. Wea. Rev., 130*(7), 1913-1924. doi:10.1175/1520-0493(2002)130<1913:Edawpo>2.0.Co;2

Wicht, M., & Osińska-Skotak, K. (2016). Identifying urban areas prone to flash floods using GIS – preliminary results. *Hydrology and Earth System Sciences Discussions*, 1-22. doi:10.5194/hess-2016-518

Winter, B., Schneeberger, K., Dung, N. V., Huttenlau, M., Achleitner, S., Stötter, J., . . . Vorogushyn, S. (2019). A continuous modelling approach for design flood estimation on sub-daily time scale. *Hydrological Sciences Journal, 64*(5), 539-554. doi:10.1080/02626667.2019.1593419

Wood, E., Luo, L., Schaake, J., Buizza, R., Hall, A., & Franz, K. (2006). Implementation Plan for the Hydrological Ensemble Prediction Experiment (HEPEX).

World Meteorological Organization. (2008). *Guide to Hydrological Practices Volume I: Hydrology – From Measurement to Hydrological Information* (Vol. 168).

World Meteorological Organization. (2012). *Guidelines on Ensemble Prediction Systems and Forecasting*. In. Swizerland:

World Meteorological Organization. (2019). Flash Flood Guidance System with Global Coverage (FFGS). Retrieved from https://public.wmo.int/en/projects/ffgs

Yáñez-Morroni, G., Gironás, J., Caneo, M., Delgado, R., & Garreaud, R. (2018). Using the Weather Research and Forecasting (WRF) Model for Precipitation Forecasting in an Andean Region with Complex Topography. *Atmosphere, 9*(8), 304. doi:10.3390/atmos9080304

Yang, J., Wang, Z.-H., Georgescu, M., Chen, F., & Tewari, M. (2016). Assessing the Impact of Enhanced Hydrological Processes on Urban Hydrometeorology with Application to Two Cities in Contrasting Climates. *J. Hydrometeor., 17*(4), 1031-1047. doi:10.1175/jhm-d-15-0112.1

Yang, L., Smith, J. A., Baeck, M. L., & Zhang, Y. (2016). Flash flooding in small urban watersheds: Storm event hydrologic response. *Water Resour. Res., 52*(6), 4571-4589. doi:10.1002/2015wr018326

Yi, L., Zhang, W., & Wang, K. (2018). Evaluation of Heavy Precipitation Simulated by the WRF Model Using 4D-Var Data Assimilation with TRMM 3B42 and GPM IMERG over the Huaihe River Basin, China. *Remote Sens., 10*(4), 646. doi:10.3390/rs10040646

Zanchetta, A. D. L., & Coulibaly, P. (2020). Recent Advances in Real-Time Pluvial Flash Flood Forecasting. *Water, 12*(2), 570. doi:10.3390/w12020570

Zehe, E., Ehret, U., Pfister, L., Blume, T., Schröder, B., Westhoff, M., . . . Kleidon, A. (2014). HESS Opinions: From response units to functional units: a thermodynamic reinterpretation of the HRU concept to link spatial organization and functioning of intermediate scale catchments. *Hydrology and Earth System Sciences, 18*(11), 4635-4655. doi:10.5194/hess-18-4635-2014

Zhang, G., Cook, K., & Vizy, E. (2016). The Diurnal Cycle of Warm Season Rainfall over West Africa. Part II: Convection-permitting Simulations. *Journal of Climate, 29*. doi:10.1175/JCLI-D-15-0875.1

Zhang, J., Murch, R. R., Ross, M. A., Ganguly, A. R., & Nachabe, M. (2008). Evaluation of Statistical Rainfall Disaggregation Methods Using Rain-Gauge Information for West-Central Florida. *Journal of Hydrologic Engineering, 13*(12), 1158-1169. doi:10.1061/(ASCE)1084-0699(2008)13:12(1158)

Zhang, W., Villarini, G., Vecchi, G., & Smith, J. (2018). Urbanization exacerbated the rainfall and flooding caused by hurricane Harvey in Houston. *Nature, 563*. doi:10.1038/s41586-018-0676-z

Zhao, W. (2013). Study of the Radiation and Energy Balances Reproduced by WRF Using 10-year (2001-2010) Observations at Cabauw. (MSc), Wageningen University, Retrieved from http://edepot.wur.nl/332361

Zhu, K., & Xue, M. (2016). Evaluation of WRF-based convection-permitting multi-physics ensemble forecasts over China for an extreme rainfall event on 21 July 2012 in Beijing. *Adv. Atmos. Sci. 33*(11), 1240-1258. doi:10.1007/s00376-016-6202-z

Someday the stranger in the corner wins the game, and gets the crown, and gets the girl, the Holy Grail ♪ The Rasmus – Holy Grail.